Nitroxides in Polymer Chemistry and Biochemistry

A thesis submitted for the degree of Doctor of Philosophy
of the Australian National University

Jennifer Louise Hodgson

December 2009

THE AUSTRALIAN NATIONAL UNIVERSITY

Declaration

This thesis presents my own original work and, to the best of my knowledge, contains no material written or published by any other person, except where due reference has been made. This work has not been previously submitted for any other degree or diploma at any university or other institution.

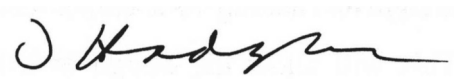

Jennifer L. Hodgson

December 2009

"By the time I was old enough and became a pilot, things had changed…The record-setting flights…across the oceans, over the poles, and to the corners of Earth, had all been accomplished. And I resented that…I was disappointed by the wrinkle in history that had brought me along one generation late. I had missed all the great times and adventures in flight."

-Neil Armstrong

(quoted by James R. Hansen in *First Man* (2005))

Acknowledgments

I am grateful to my supervisor Associate Professor Michelle Coote who, despite the arrival of two children since the commencement of this work, has tirelessly provided me with support and guidance.

I am indebted to Associate Professor Steven Bottle for many comments and suggestions on protection of biological systems using nitroixdes, and to James Blinco for the experimentally determined oxidation potentials of nitroxide radicals. My thanks also go to Professor Mark Gordon for hosting me in Ames, Iowa, to Dr Mike Schmidt for technical help during my visit, and to Luke Roskop for teaching me how to perform multireference calculations. I gratefully acknowledge useful discussions on the structure reactivity trends of nitroxides and alkoxyamines with both Dr Sylvain Marque and Professor Krzysztof Matyjaszewski.

Many thanks are also due to members of the Coote research group who have assisted me with various aspects of this work. Dr Mansoor Namazian helped me set up a thermodynamic cycle to calculate the electrode potentials of nitroxides. David Brittain had the long task of updating old submission scripts to be compatible with the Altix® 3700 Bx2 cluster. Dr Ching Yeh (Leaf) Lin provided the electron affinities of alkyl radicals and wrote me a thermochemistry program for charged species. I am grateful to Dr Katya Izgorodina and Junming Ho, for assisting me through many helpful discussions.

I acknowledge the receipt of an Australian Postgraduate Award, additional funding from the ARC Centre of Excellence for Free Radical Chemistry and Biotechnology, and the award, from the Polymer Division of the Royal Australian Chemical Institute (RACI), of the O'Donnell Young Scientist Prize, which funded my visit to the US. I am grateful to the ANU Supercomputing Facility (ANUSF) and the Australian Partnership for Advanced Computing (APAC) for generous allocations of computer time on the Altix® 3700 Bx2 and Linux Cluster.

Finally, I would like to thank my parents, Margaret and Bob, and my friends David Pinkerton and Amy Sullivan for their assistance with proof-reading this thesis, and for their continuous support during my degree.

Abstract

In this thesis, computational quantum chemistry has been used to study the reactions undergone by nitroxide free radicals in a variety of chemical and biochemical applications, with a view to providing a better understanding of the mechanisms involved and the relationships between structure and reactivity. Using new computational quantum chemical methodologies for the chemically accurate study of reactions involving nitroxide radicals, developed as part of this work, the following key results have been achieved.

Substituent effects on the oxidation and reduction potentials of nitroxide radicals have been modelled and used to evaluate the various mechanisms by which nitroxide antioxidants protect against oxidative damage in biological systems. A clear correlation between the reduction potentials of nitroxides and literature experimental protection data was observed. On this basis it was concluded that nitroxide protection against H_2O_2 mediated oxidative damage occurs primarily through the reduction-based dismutation of superoxide in a cycle mimicking that of superoxide dismutase, as well as other mechanisms that disrupt the Fenton reaction and detoxify damaging radical species. This has led to the prediction of more successful protecting agents.

Substituent effects on the equilibrium constant of the trapping/dissociation reaction of nitroxide radicals with alkyl polymeric radicals, which forms the control reaction of nitroxide mediated polymerisation, were quantified. A new equation, describing the equilibrium constant in terms of easily computed parameters representing the polar, steric and radical stability factors of each of the radicals, is presented. The equation was used to explain the success of a recently reported indoline-type nitroxide control agent for the polymerisation of methyl methacrylate.

The full mechanism of the Denisov cycle for the protection of polymer coatings against photo-oxidative damage using nitroxide stabilising agents has been elucidated from the dozen different reaction pathways and over 30 individual reactions previously suggested in the literature. Several new intermediate species in the cycle have been postulated and the final products have been determined. This work will assist in the design of new and improved hindered amine light stabilisers for surface coatings.

Table of Contents

Acknowledgements		iv
Abstract		v
Table of Contents		vi
List of Abbreviations		viii
Chapter 1	**Introduction**	1
	1.1 Background	
	1.2 Research objectives	
	1.3 Publications	
	1.4 References	
Chapter 2	**Theoretical methods**	9
	2.1 Introduction	
	2.2 Electronic structure information	
	2.3 Reaction thermodynamics and kinetics	
	2.4 Molecular properties	
	2.5 Computational resources	
	2.6 References	
Chapter 3	**Assessment of Computational Procedures**	41
	3.1 Introduction	
	3.2 Geometry optimisations	
	3.3 Gas-phase single-point energies	
	3.4 Free energies of solvation	
	3.5 Conclusions	
	3.6 References	
Chapter 4	**Biological Protection Mechanisms**	63
	4.1 Introduction	
	4.2 Literature review	
	4.3 Electrode potentials of nitroxides	
	4.4 Biological protection using nitroxides	
	4.5 Conclusions	
	4.6 References	

Chapter 5 **Structure Reactivity Trends in Nitroxide Mediated Polymerisation** 105

5.1 Introduction

5.2 Literature review

5.3 Thermodynamics of the control reaction of NMP

5.4 A new equation for the equilibrium constant

5.5 Conclusions and outlook

5.6 References

Chapter 6 **Mechanism of the Denisov Cycle** 143

6.1 Introduction

6.2 Literature review

6.3 Mechanisms of the Denisov cycle

6.4 Conclusions

6.5 References

Chapter 7 **Conclusions** 167

7.1 Introduction

7.2 Achievements of this thesis

7.3 Future outlook

Appendix **Computational Data** 173

A.1 Free energy components of species

A.2 GAUSSIAN archive files

List of Abbreviations

ATRP	atom transfer radical polymerisation
B1B95	a DFT method
B3-LYP	a DFT method
B3P86	a DFT method
B-LYP	a DFT method
BMK	a DFT method
CBS	a family of composite *ab initio* methods
CC	coupled cluster (theory)
CI	configuration interaction (theory)
CPCM	conductor polarisable continuum model
DBN	a nitroxide radical (see Table 1.1)
DFT	density functional theory
DMINO	a nitroxide radical (see Table 1.1)
DPAIO	a nitroxide radical (see Table 5.7)
EA	electron affinity
G*n*	a family of composite *ab initio* methods of order *n*
HALS	hindered amine light stabiliser
HF	Hartree-Fock (theory)
HLC	higher-level correction
IE	ionisation energy
KMLYP	a DFT method
MAD	mean average deviation
Mb	myoglobin
MC-QDP*n*	multiconfigurational quasidegenerate perturbation theory of order *n*
MCSCF	multiconfigurational (or multireference) self-consistent field
MMA	methyl methacrylate
MP*n*	Møller-Plesset perturbation theory of order *n*
MPW1B95	a DFT method
MPWB1K	a DFT method
MPWPW91	a DFT method
MRCI	multireference configuration interaction

NBO	natural bond orbital (analysis)
NMP	nitroxide mediated polymerisation
ONIOM	multi-layered approximation method
PBE	a DFT method
PCM	polarisable continuum model
PDI	polydispersity index
PES	potential energy surface
PROXYL	a nitroxide radical (see Table 1.1)
RAFT	reversible addition fragmentation chain transfer
RSE	radical stabilisation energy
SCE	saturated calomel reference electrode
SCF	self-consistent field
SG1	a nitroxide radical (see Table 1.1)
SHE	standard hydrogen electrode
SO	spin-orbit correction
SOD	superoxide dismutase
*t*BB	*tert*-butyl benzene
t-Bu	*tert*-butyl
TEMPO	a nitroxide radical (see Table 1.1)
TIPNO	a nitroxide radical (see Table 1.1)
TMAO	a nitroxide radical (see Table 1.1)
TMIO	a nitroxide radical (see Table 1.1)
TMOZO	a nitroxide radical (see Table 1.1)
W*n*	a family of composite *ab initio* methods of order *n*
ZPE	zero-point vibrational energy

Chapter 1.

Introduction

1.1 Background 2
1.2 Research objectives 3
1.3 Publications 5
1.4 References 6

1.1 Background

Although many radicals are highly reactive species with short lifetimes, some of the most useful radicals are relatively stable and can have lifetimes up to the order of months.[1] One such class of radicals is the nitroxides, containing the functional moiety of an oxygen-centred radical directly bound to a nitrogen centre. The simplest nitroxide $H_2NO^{\bullet}$ is a very reactive species. However, bulky, sterically hindered nitroxides, substituted at the nitrogen with tertiary alkyl groups (see Figure 1.1), are stable, persistent radicals, commonly used in a number of chemical and biomedical applications. Common cyclic nitroxides, such as the nitroxide derivatives of piperidine, pyrrolidine and isoindoline, have lifetimes of around 15 hours to several days at concentrations of 10^{-4} molL^{-1} in a degassed solution at 120 ºC.[2]

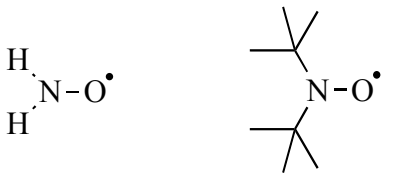

nitroxide di-*tert*-butyl nitroxide

Figure 1.1 Nitroxide radicals

Due to their relative stabilities, many reactions can be performed in the presence of a nitroxide radical moiety. This has allowed the use of nitroxides as spin probes, giving characteristic signals readily detected by electron paramagnetic resonance (EPR) spectroscopy.[3] The development of "profluorescent" nitroxide probes has provided another method for the study of reactions involving free radical and redox species.[4,5] The coupling of nitroxide species with other radicals has also provided a mechanistic probe for the evaluation of the kinetic parameters of radical reactions.[6]

Apart from their stability, other nitroxides have desirable features making them useful reagents. They are able to be reversibly oxidised to their respective oxoammonium cations and reduced to hydroxylamines with relative ease, and to

scavenge other radical species and undergo transfer reactions with non-radical species, Nitroxide radicals have also proved to be relatively non-cytotoxic in biological systems.[7]

Technological applications of nitroxide radicals include uses in the biomedical field, chemical synthesis, and materials chemistry. They are used as spin labels,[8] antioxidants,[9] initiators and control agents in free radical polymerisation processes,[10,11] UV stabilisers in polymer coatings[12] and building blocks for molecular-based magnetic materials.[13] Recently, nitroxides have been utilised as electrode materials in stable secondary batteries.[14]

Computational quantum chemistry provides a method for the study of the mechanisms, kinetics and thermodynamics of chemical reactions. It is being increasingly used in conjunction with experimental studies both to interpret results, and to predict properties that are difficult to measure and/or the outcomes of reactions in which expensive or dangerous reagents limit the availability of experimental data. Computational chemistry complements experiment by offering advantages such as the ability to study directly the individual reactions within complex processes like polymerisation reaction sequences, or within complex chemical or biological environments. It can also be used to predict side reactions that may interfere with a mechanistic process. In this project, various theoretical and computational chemistry techniques were applied to the study of reactions and the prediction of properties of nitroxide radicals.

1.2 Research objectives

The broad objective of this work was the study of the actions of nitroxides in different applications, using computational quantum chemical methodologies. This involved the identification of theoretical methods suitable for the study of nitroxide radicals and the determinations of the redox properties, reaction thermodynamics and kinetics of their reactions. Structure reactivity effects within and between the different classes of nitoxides were then analysed. A large number of different cyclic and acyclic nitroxide species were investigated, with the main structural classes shown in Table 1.1.

Table 1.1 Structural classes of nitroxide radicals

Family	Structure of parent (unsubstituted) nitroxide	Chemical name	Common acronym
Six-membered cyclic			
piperidine	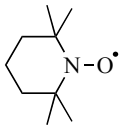	2,2,6,6-tetramethyl-piperidin-1-yloxyl	TEMPO
azaphenalene	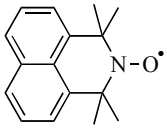	1,1,3,3-tetramethyl-2,3-dihydro-2-azaphenalene-2-yloxyl	TMAO
Five-membered cyclic			
pyrrolidine	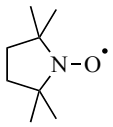	2,2,5,5-tetramethyl-pyrrolidin-1-yloxyl	PROXYL
oxazolidine	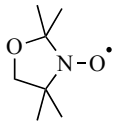	2,2,5,5-tetramethyl-3-oxazolidin-1-yloxyl	TMOZO
indoline	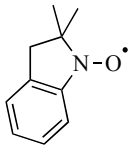	2,2-dimethyl-indolin-1-yloxyl	DMINO
isoindoline	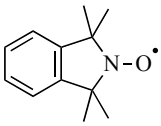	1,1,3,3-tetramethyl-isoindolin-2-yloxyl	TMIO
Acyclic	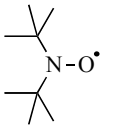	di-*tert*-butyl nitroxide	DBN
	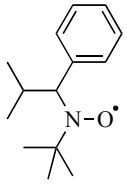	*tert*-butyl-[2-methyl-1-phenylpropyl] nitroxide	TIPNO
	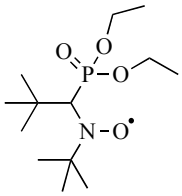	*tert*-butyl-[1-diethphosphono-2,2-dimethylpropyl] nitroxide	SG1

This thesis contains a series of investigations of nitroxide radicals in chemical and biochemical applications. Three main applications were studied; (1) the use of nitroxide antioxidants in the protection against oxidative damage in biological systems, (2) structure reactivity trends in the thermodynamics of the control reaction of nitroxide mediated polymerisation (NMP), and (3) the use of nitroxides as stabilising agents for the protection of polymer coatings against photo-oxidative damage through the Denisov cycle. Detailed reviews of current literature in these areas are provided at the beginnings of the relevant chapters.

1.3 Publications

Parts of the work described in this thesis have been published. For other parts, manuscripts are in advanced stages of preparation.

Chapter 3

Should Contemporary Density Functional Theory Methods Be Used to Study the Thermodynamics of Radical Reactions?
Izgorodina, E. I.; Brittain, D. R. B.; Hodgson, J. L.; Krenske, E. H.; Lin, C. Y.; Namazian, M.; Coote, M. L.
J. Phys. Chem. A **2007**, *111*, 10754-10768.

A Comparison of G3 and G4 Theories for Radical Addition and Abstraction Reactions
Lin, C. Y.; Hodgson, J. L.; Namazian, M.; Coote, M. L.
J. Phys. Chem. A **2009**, *113*, 3690-3697.

Prediction of Equilibrium Constants for the Control Reaction for Nitroxide Mediated Polymerisation
Hodgson, J. L.; Coote, M. L.
in preparation (to be submitted to *J. Chem. Theory Comp.*)

Chapter 4

One-Electron Oxidation and Reduction Potentials of Nitroxide Antioxidants: A Theoretical Study
Hodgson, J. L.; Namazian, M.; Bottle, S. E.; Coote, M. L.
J. Phys. Chem. A **2007**, *111*, 13595-13605.

Experimental and Theoretical Studies of the Redox Potentials of Cyclic Nitroxides

Blinco, J. P.; Hodgson, J. L.; Morrow, B. J.; Walker, J. R.; Will, G. D.; Coote, M. L.; Bottle, S. E.

J. Org. Chem. **2008**, *73*, 6763-6771.

Investigation of Protection Mechanisms of Nitroxides in Biological Systems

Hodgson, J. L.; Bottle, S. E.; Coote, M. L.

in preparation (to be submitted to *Theor. Chem. Acc.*)

Chapter 5

Substituent Effects on the Homolysis of Alkoxyamines and the Implications for NMP

Hodgson, J. L.; Coote, M. L.

Abstracts of Papers, 236th ACS National Meeting, Philadelphia, PA, United States, August 17-21, 2008.

Polymer Preprints **2008**, 49, 285-286.

Substituent Effects on the Alkyl Radical Affinities of Nitroxides: A Theoretical Study

Hodgson, J. L.; Lin, C. Y.; Marque, S. R. A.; Matyjaszewski, K.; Coote, M. L.

in preparation (to be submitted to *Macromol.*)

Chapter 6

Clarifying the Mechanism of the Denisov cycle: How do Hindered Amine Light Stabilisers Protect Polymer Coatings from Photo-oxidative Degradation?

Hodgson, J. L.; Coote, M. L.

in preparation (to be submitted to *J. Am. Chem. Soc.*)

Comparison of the Rates of NO-C and N-OC Bond Homolysis of Alkoxyamines: A Theoretical Study

Hodgson, J. L.; Roskop, L.; Gordon, M. S.; Coote, M. L.

in preparation (to be submitted to *J. Phys. Chem. A*)

1.4 References

(1) Parsons, A. F. *An Introduction to Free Radical Chemistry*; Blackwell Science: Oxford, 2000.

(2) Marque, S. R. A.; Le Mercier, C.; Tordo, P.; Fischer, H. *Macromol.* **2000**, *33*, 4402.

(3) See for example: Yan, G.-P.; Bischa, D.; Bottle, S. E. *Free Rad. Biol. Med.* **2007**, *43*, 111.

(4) Blough, N. V.; Simpson, D. J. *J. Am. Chem. Soc.* **1988**, *110*, 1915.

(5) Micallef, A. S.; Blinco, J. P.; George, D. A.; Reid, D. A.; Rizzardo, E.; Thang, S. H.; Bottle, S. E. *Polym. Degrad. Stab.* **2005**, *89*, 427.

(6) Beckwith, A. L. J.; Bowry, V. W.; Moad, G. *J. Org. Chem.* **1988**, *53*, 1632.

(7) (a) Swartz, H. M.; Santjurc, M.; Kocherginsky, N. Toxicity and the Use of Nitroxides as Drugs, In *Nitroxide Spin Labels, Reactions in Biology and Chemistry,* Kocherginsky, N. and Swartz, H. M., Eds. CRC Press Inc.: Boca Raton, 1995, pp. 175-198. (b) Damiani, E.; Greci, L.; Hrelia, P. *Free Rad. Biol. Med.* **2000**, *28*, 330.

(8) Swartz, H. M.; Santjurc, M.; Kocherginsky, N. *Nitroxide Spin Labels, Reactions in Biology and Chemistry*; CRC Press Inc.: Boca Raton, FL, 1995.

(9) Soule, B. P.; Hyodo, F.; Matsumoto, K.; Simone, N. L.; Cook, J. A.; Krishna, M. C.; Mitchell, J. B. *Free Rad. Biol. Med.* **2007**, *42*, 1632.

(10) Rizzardo, E. *Chem. Aust.* **1987**, *54*, 32.

(11) Georges, M. K.; Veregin, R. P. N.; Kazmaier, P. M.; Hamer, G. K. *Macromol.* **1993**, *26*, 2987.

(12) Allen, N. S. *Chem. Soc. Rev.* **1986**, *15*, 373.

(13) Rassat, A. *Pure Appl. Chem.* **1990**, *62*, 223.

(14) (a) Hintermann, T.; Nesvadba, P.; Frey, M. International Patent No. WO2008110466 A1, 2008; pp 55. (b) Nesvadba, P.; Bugnon Folger, L.; Hintermann, T. International Patent No. WO2008155247 A1, 2008; pp 58.

Chapter 2.

Theoretical Methods

2.1 Introduction 10

2.2 Electronic structure information 11

2.2.1 Numerical solutions to the Schrödinger equation 11

2.2.2 Molecular orbital methods 12

2.2.3 Density functional theory 15

2.2.4 Composite *ab initio* methods 16

2.2.5 ONIOM approximation for large systems 19

2.2.6 Multireference methods 20

2.2.7 Solvent effects 22

2.3 Reaction thermodynamics and kinetics 23

2.3.1 Reaction surfaces 23

2.3.2 Reaction free energies 24

2.3.3 Solvation free energies 27

2.3.4 Equilibrium constants of reactions 28

2.3.5 Reaction barriers and tunnelling corrections 29

2.4 Molecular properties 30

2.4.1 Ionisation energies and electron affinities of radicals 31

2.4.2 Electrode potentials of nitroxide radicals 31

2.4.3 Charge and spin orbital calculations 35

2.4.4 Radical stabilisation energies 35

2.5 Computational resources 36

2.5.1 Software 36

2.5.2 Hardware 36

2.6 References 36

2.1 Introduction

Computational quantum chemistry provides a method for the study of structures, energies and other properties in chemical systems, leading to information about the mechanisms, thermodynamics and kinetics of reactions. With increases in computer power and the ongoing design of more efficient algorithms, it is becoming increasingly common to carry out theoretical chemistry calculations alongside experiments in order to interpret experimental results and predict properties that are difficult to measure.

In its simplest form, quantum chemistry involves considering individual molecules as groups of particles that can be treated using quantum mechanical equations, which treat particles as waves. The energy of a system is found from the solutions to the Schrödinger equation. However, exact solutions are only available for one or two particle systems.[1] The solving of other systems requires the use of various approximations and, in most cases, computers to calculate the solutions. If solutions are generated without any reference to experimental data, using only the laws of quantum mechanics and the fundamental constants of nature, they are known as *ab initio* (Latin for "from the beginning") methods. Calculations using such methods can become very computationally expensive when the more sophisticated methods are used for larger chemical systems. Economical procedures for the treatment of reactions in this work are identified in Chapter 3.

This chapter provides a brief overview of the mathematical and quantum mechanical basis of the theoretical methods implemented in this work. More detailed discussions of these and other methods can be found in various textbooks on quantum and computational chemistry.[1-4] Methods for the calculation of the reaction pathways, thermodynamics and kinetics of chemical reactions are also discussed, with a focus on the special techniques that were adapted for this study.

2.2 Electronic structure information

2.2.1 Numerical solutions to the Schrödinger equation

The time-independent Schrödinger equation[5] is shown in Equation (2.1). It gives the total energy, E, of a system (such as a molecule) in terms of the molecular wavefunction, Ψ, which describes the position of all the electrons and nuclei in the molecule, and the Hamiltonian operator, $\mathbf{H}$.

$$\mathbf{H}\Psi = E\Psi \tag{2.1}$$

The Hamiltonian operator is made up of contributions to the kinetic energies of electrons and nuclei and the various potential energies, including the attraction of the electrons and the nuclei as well as the electron-electron and nuclear-nuclear repulsions. It can be simplified by the assumption that, as the masses of nuclei are much greater than electron masses, the nuclei move much more slowly and are approximately stationary with respect to the electrons. This is known as the Born-Oppenheimer approximation,[6] and gives the electronic Schrödinger equation. Although the Born-Oppenheimer approximation allows for considerable simplification, the electronic Schrödinger equation still has no analytical solution except for a one-electron system. Further approximations must be made in order to obtain numerical solutions. In theory these results can approach the exact solution, although in practice they would require prohibitively large computing times.

The level of theory used for a computational chemistry calculation consists of the size of the basis set and the type of method, and is commonly written using the notation “method / basis set”. When the level of theory used for the calculation of the single-point energy is different from the level used for the optimisation of the molecular geometry the notation used is “energy method / energy basis set // geometry method / geometry basis set”.

A basis set is a set of functions representing molecular orbitals, which in turn are usually described as a linear combination of known atomic orbitals. Increasing the size and scope of a basis set allows for systematic improvement in the resulting solution, with an infinite basis set of basis functions being a representation of real orbitals. The most common basis functions are the gaussian-type orbitals, which

depend upon the exponential of the radial distance squared.[7] In this work, the Pople basis sets are primarily used. They follow a standard nomenclature in which the notation 6-31G means that six primitive gaussians are used for each core orbital and two functions containing three and one primitives are used for each valence orbital. The basis set 6-31G is known as a valence double-zeta basis set. The basis set 6-311G is a triple-zeta basis set, with six primitive gaussians used for each core orbital and three functions containing three, one and one primitives used for each of the valence orbitals. Pople basis sets can be further extended by the addition of diffuse (+) and polarisation functions. For example, the notation 6-311+G(3df,2p) means that the 6-311G basis is used with the addition of diffuse (*s*- and *p*-) functions on heavy (non-hydrogen) atoms, three sets of *d*-functions and one set of *f*-functions on heavy atoms, and two sets of *p*-functions on hydrogen atoms.

In this work the correlation-consistent (or Dunning) basis sets[8] were also assessed for use in nitroxide-type reactions (see Chapter 3). These basis sets were designed with the aim of recovering the correlation energy of the valence electrons. The smallest correlation-consistent basis set is the correlation-consistent polarised valence double-zeta (cc-pVDZ) basis set. The next smallest is cc-pVTZ, which has one extra set of functions for orbital angular momentum.

2.2.2 Molecular orbital methods

Having obtained expressions for describing the molecular orbitals in the basis set, these orbitals are combined by a normalised function to form the wavefunction. This is known as the "method" of a calculation. Hartree-Fock (HF) theory[9,10] gives the simplest wavefunction that satisfies the antisymmetry requirement and the Pauli exclusion principle.[11] It is based on the molecular orbital approximation to the electronic Schrödinger equation, which assumes that the motion of each electron is independent, allowing the system to be expressed in terms of one electron wavefunctions. HF theory does not provide an accurate description of the system as it does not take account of correlation in the motion between electrons. However, it does provide a useful approximation of the system energy. Methods for dealing with electron correlation are discussed below.

For closed-shell species a restricted Hartree-Fock (RHF) solution is made up of spatial molecular orbitals containing two electrons, one of α and one of β spin. A restricted open-shell Hartree-Fock (ROHF) solution is similar but includes one molecular orbital containing only one electron representing a single unpaired electron in, for example, a radical species. Another way to consider open-shell systems is through the use of an unrestricted Hartree-Fock (UHF) wavefunction, which allows two paired electrons to be in different spatial orbitals. This makes it possible for an unpaired electron to interact differently with the α– and β–electrons. The resulting wavefunction may include contributions from higher-lying states of the molecule. This added flexibility provides a weak form of electron correlation. All calculations on radicals in this work were performed with an unrestricted wave function except in cases designated with an "R" prefix where a restricted open-shell wave function was used.

As discussed above, in Hartree-Fock theory each electron sees all the other electrons as an average field, and therefore direct electron correlation is not taken into account. Although the contribution of electron correlation to the total energy is often small it can play an important part in chemical processes. The methods for dealing with electron correlation used in this work are the configuration interaction (CI), coupled cluster (CC) and Møller-Plesset (MP) perturbation theory methods. The relationship between basis set and electron correlation method is summarised in the Pople diagram,[3] shown in Figure 2.1.

Configuration interaction (CI) methods involve the excitation of electrons from occupied to virtual orbitals. If a single electron is promoted, a singly excited configuration results. If two electrons are promoted this gives rise to a doubly excited configuration. These excitations are abbreviated as singles (S), doubles (D), triples (T) and so on. The full configuration interaction method (FCI) contains contributions from all possible excited states of the electrons within the limits of the basis set used. In the limit of an infinite basis set, the FCI method gives the exact solution to the time-independent, Schrödinger equation under the Born-Oppenheimer approximation (see Figure 2.1). In practice, and in view of the large computational cost of FCI, the series is often truncated at the CISD level.

The common CI methods, with S, D or SD excitations, are not size consistent, meaning that relative errors in the calculations do not increase more or less in proportion with the size of the system. For example, this means that a pair of systems, far apart enough to be non-interacting, shows different results when they are treated individually to when they are treated as a whole. The quadratic configuration interaction (QCI) family of methods[12] overcome, problems with size consistency through the addition of various terms to the CISD wavefunction. A QCISD wavefunction contains contributions from single and double as well as some quadruple excitations.

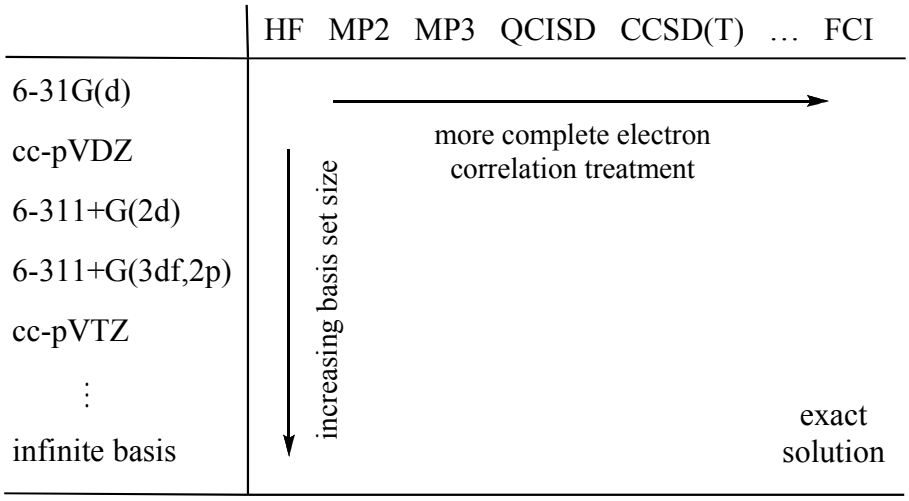

Figure 2.1 Pople diagram showing the hierarchy of *ab initio* methods

In the coupled cluster (CC)-methods,[13] the HF wavefunction is corrected using a cluster operator which takes the form of a Taylor-series expansion. The series is commonly truncated at the coupled cluster doubles (CCD) or coupled cluster singles doubles (CCSD) point. The method CCSD(T) includes a perturbative correction for triples, and provides a good approximation to the full CI wavefunction.

Electron correlation can also be accounted for using perturbation theory, the most common form being Møller-Plesset (MP) perturbation theory[14] in which the Hamiltonian is written as a sum of the Hartree-Fock Hamiltonian and a perturbation. The wavefunction and energy can then be expanded as a Taylor series, truncated to

various levels to give the MP*n* series, with the theoretical MP∞ system giving the exact solution. In practice, MP2, MP3 and MP4 levels are often utilised. The MP2 method gives the first contribution to the correlation energy. MP2 energies usually contain most of the correlation energy, and often provide the most economical way of computing electron correlation. However, they are not as accurate as the CI methods.

2.2.3 Density functional theory

Density functional theory (DFT) methods provide another approach to solving the time-independent electronic Schrödinger equation. They rest on the proof, by Hohenberg and Kohn,[15] that the ground state electronic energy is determined completely by the electron density (ρ), and can therefore be expressed by a unique functional showing the relationship between energy and density. This functional, expressed in three spatial dimensions, presents a much simpler problem than the direct determination of the wavefunction. Unfortunately, the Hohenberg-Kohn theorem merely proves the existence of such a functional and gives no clues as to the form it may take. In practice, approximate functionals are used, introducing errors into the calculation. Trial functionals are typically fitted to experimental results in order to determine their parameters. Therefore, there remains debate about whether DFT methods can be truly labelled as *ab initio*.

A functional describing the energy of a system in terms of electron density, assuming the Born-Oppenheimer approximation, can be divided into parts representing the kinetic energy due to motion of electrons, the potential energy of nuclei-electron attraction, and other terms describing interactions between the electrons. The kinetic energy and the potential energies for nuclei-electron attraction and electron-electron repulsion correspond to the classical energy of the charge distribution. The task of DFT methods, therefore, is to provide terms of the functional describing the remaining electron interactions; the exchange term, arising from the anti-symmetry of the wavefunction, and the dynamic electron correlation energy term.

In their simplest form, functionals assume a uniform electron gas. Improvements have come from including dependence upon the density and also the gradient of the density in the description of the exchange and correlation terms. This approach leads to functions known as pure functionals. Another common class of

methods is the hybrid functionals. These methods include additional contributions to the exchange functional from both the exact Hartree-Fock exchange and a density functional exchange term.

Work on the development of successful functionals is ongoing. A large variety of functionals are easily available through their implementation into quantum chemistry software such as the GAUSSIAN[16] system of programs. The various DFT methods assessed for their performance in nitroxide reactions in this work include the traditional pure functionals, PBE[17] and B-LYP,[18] the widely used hybrid three-parameter functionals, B3-LYP[19] and B3P86,[19,20] and a number of relatively new functionals, including KMLYP,[21] B1B95,[22] MPWPW91,[23] MPW1B95,[24] BB1K,[25] MPW1K,[26] MPWB1K[24] and BMK.[27] More details on each of these methods can be found in the literature references.

The computational cost of DFT methods is significantly less than any of the other methods that take electron correlation into account. However, they are typically highly dependent upon empirical parameters and can fail spectacularly when applied to systems beyond those to which they were fitted. Generally, DFT methods are useful for the calculation of molecular geometries, which include large cancellations of errors, and can often provide economical energies when applied cautiously. Currently available DFT methods have been shown to fail at providing an accurate description of the energetics of radical reactions when compared to higher levels of theory (see Chapter 3.3).[28]

2.2.4 Composite *ab initio* methods

Ab initio methods range from the simplest HF method with a minimal basis set all the way up to the most accurate methods for the treatment of electron correlation with very large basis sets. In general, as the accuracy of the method improves, the computational expense of the calculation grows dramatically. When performing calculations, a balance must be reached between the desired accuracy and computational cost.

While some properties, such as geometry optimisations and frequency calculations, are often fairly insensitive to the level of theory used for a calculation, the total gas-phase energy of the system is not. Therefore, very high levels of theory

are often required to achieve the desired "chemical accuracy" in which calculated energies differ by less that 1 kcalmol^{-1} (4 kJmol^{-1}) from experimental values. Typically SD(T) levels of electron correlation in conjunction with triple-zeta basis sets are required to achieve these levels of accuracy. Composite *ab initio* procedures have been shown to offer chemical accuracy at much lower computational expense. They seek to approximate calculations with high levels of electron correlation and large basis sets using a series of lower-cost calculations in conjunction with additivity and/or extrapolation routines. Among the most common composite methods are the G*n* family of methods,[29] the CBS methods[30] and the W*n* methods.[31]

The G*n* methods approximate CCSD(T) or QCISD(T) calculations, performed with a triple-zeta basis set, via a series of additivity approximations carried out at lower levels of theory, usually the MP2 level, or combinations of MP2 with MP3 or MP4. The CBS and W*n* methods both feature extrapolation to the infinite basis set limit. In the CBS procedures this is performed at the MP2 level of theory using pair natural orbital energies, and the results are then corrected to the CCSD(T) level via a series of additivity approximations. In the W*n* methods, extrapolation to the infinite basis set limit is carried out using coupled cluster theory with correlation-consistent basis sets. Additional corrections for relativistic effects, core correlation and spin orbit corrections are also included. Not surprisingly, the W*n* methods are generally more accurate than the CBS or G*n* methods, but are also considerably more computationally expensive. Their use is therefore limited to very small systems of up to six or seven non-hydrogen atoms.

The GAUSSIAN[16] system of programs has incorporated into it several common composite methods, including various G*n* methods, CBS-QB3[32] and W1U,[33] allowing users to perform calculations at these levels using a single keyword. Other composite methods can be utilised by running the component calculations for geometry optimisations, frequencies and various single-point energies separately and then combining them using the relevant formulae described in literature references.

One of the lowest cost G*n* methods, G3(MP2)-RAD,[34] was used primarily in this work. The G3(MP2)-RAD method approximates (U)RCCSD(T) with the triple-zeta basis set G3MP2large. This is done through the sum of the corresponding

(U)RCCSD(T)/6-31G(d) calculation and a basis set correction term, obtained as the difference of the corresponding calculations at the R(O)MP2/G3MP2large and R(O)MP2/6-31G(d) levels of theory, as shown in Equation (2.2). An example calculation for the G3(MP2)-RAD energy of a methyl radical is shown in Table 2.1.

$$\begin{aligned} E_{\mathrm{G3(MP2)-RAD}} = & E_{\mathrm{URCCSD(T)/6-31G(d)}} \\ & + E_{\mathrm{ROMP2/G3MP2large}} - E_{\mathrm{ROMP2/6-31G(d)}} \\ & + SO + HLC \end{aligned} \tag{2.2}$$

Table 2.1 Calculation of the G3(MP2)-RAD energy (in Hartrees) of $^{\bullet}CH_3$

Protocol from G3(MP2)-RAD	Energy component	Energy
E(*ZPE*) from B3-LYP/6-31G(d) optimised structure		0.02984
Scaling factor		0.98060
Scaled *ZPE*	**E(*ZPE*)**	0.02926
(U)RCCSD(T)/6-31G(d)	**E(CC)**	-39.69103
R(O)MP2/G3MP2large	**E($MP2_{large}$)**	-39.73047
R(O)MP2/6-31G(d)	**E($MP2_{small}$)**	-36.66850
number of α valence electrons (n_α)		4
number of β valence electrons (n_β)		3
$HLC = 1/1000 \times (-An_\alpha - B(n_\alpha - n_\alpha))$	**E(*HLC*)**	-0.03221
spin-orbit correction	**E(*SO*)**	0.00000
E(CC) + E($MP2_{large}$) - E($MP2_{small}$) + E(*HLC*) + E(*SO*)	**G3(MP2)-RAD electronic energy**	-39.78520
E(CC) + E($MP2_{large}$) - E($MP2_{small}$) + E(*HLC*) + E(*SO*) + E(*ZPE*)	**G3(MP2)-RAD energy at 0 K**	-39.75594

Additional corrections required in the G3(MP2)-RAD energy are the first-order spin-orbit correction (*SO*) and the higher-level correction (*HLC*) term. The *SO* correction is zero except for certain atoms and diatomic molecules, and is taken from experiment where available. The *HLC* term for G*n* theory is an empirical correction, calculated using Equation (2.3), as a function of the number of α-spin (n_α) and β-spin (n_β) valence electrons. The parameters *A*, *B*, *C* and *D* are obtained by fitting G*n* determined parameters to a large test of experimental data. For G3(MP2)-RAD, the values (in mHartrees) are A = 9.413, B = 3.969, C = 9.438, and D = 1.888. The *HLC*

cancels entirely from many reaction energies, and for these cases the G*n* calculation is truly *ab initio* in nature.

$$\begin{aligned} HLC_{molecule} &= -An_{\beta} - B\left(n_{\alpha} - n_{\beta}\right) \\ HLC_{atom} &= -Cn_{\beta} - D\left(n_{\alpha} - n_{\beta}\right) \end{aligned} \tag{2.3}$$

2.2.5 ONIOM approximation for large systems

Due to limitations in computational resources it is sometimes not possible even to use the composite methods described above for single-point energy calculations. Rather than sacrificing accuracy by using a lower level of theory, a multi-layer ONIOM-type method[35] can be utilised. This type of approach (originally known as IMOMO) was introduced by Morokuma and coworkers and has been shown to be suitable for the calculation for radical reactions.[28,36] In an ONIOM approximation the molecule is broken up, with only an active core calculated at a high level of theory such as a G*n*-type method, while the substituent effects are estimated at a lower level such as MP2. This approximation is exact if the low level of theory measures the substituent effect accurately.

The first step of an ONIOM calculation is the selection of the core, which usually includes the reaction centre and substituents up to at least the α-position. The rest of the chemical system makes up the outer section. For reactions in this study, the primary contributions to the size of the reaction species come from the bulky, cyclic nitroxide molecules. Therefore, it was usually the nitroxide itself that was truncated to a smaller core species. In forming the core section, the removed substituents were replaced with hydrogen atoms in order to maintain the correct valency. The core therefore provided a good model of the chemical reaction. For smaller cyclic nitroxide reactions, the basic ring structure could be included in the core, however for larger systems it became necessary to truncate the system further to the small nitroxide species di-methyl nitroxide $(CH_3)_2NO^{\bullet}$, as shown in Figure 2.2.

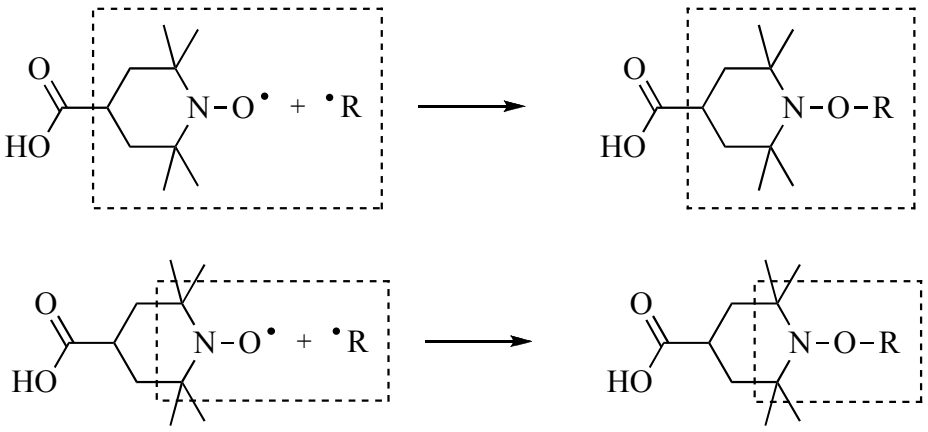

Figure 2.2 ONIOM cores for the addition of a carbon-centred radical R• to a substituted six-membered piperidine-type nitroxide

In order find an ONIOM energy of each species in a reaction, the geometries of full and core reactions are optimised. The energy of the core is calculated at a high level of theory and also at a lower level of theory, while the full system is calculated only at the lower level. The ONIOM energy of the full reaction is the sum of the high-level energy for the core system and the substituent effect of the outer section at the lower level of theory. The substituent effect is found from the difference between the low level energy of the full system and the low level energy of the core system, as shown in Equation (2.4).

$$E_{\text{ONIOM}}^{\text{full system}} = E_{\text{high level}}^{\text{core}} + E_{\text{low level}}^{\text{full system}} - E_{\text{low level}}^{\text{core}} \quad (2.4)$$

2.2.6 Multireference methods

Multireference or multiconfiguational self-consistent field (MCSCF) methods are used when it becomes necessary to include contributions from certain excited states into the ground state wavefunction. This is often required when near-degeneracy of some molecular orbitals means that allowing partial occupancy gives a better description of the system. These methods are well suited to problems like the dissociation of a bond into two open-shell (radical) species,[37] and allow the mapping of the potential energy surface (PES) between the closed-shell reactant species and the radical products.

Multiconfigurational wavefunctions account for non-ground state molecular orbitals through the inclusion of electron excitations to specific “active” orbitals contained in the “active space”, as shown in Figure 2.3. In a FORS-MCSCF (or CAS-SCF) calculation all possible configurations of the active electrons in the active orbitals are included. The common notation for such calculations is FORS-MCSCF(a,b), where a is the number of active electrons and b is the number of active orbitals. In the case where the active space includes all molecular orbitals, the MCSCF wavefunction is equivalent to a full configuration interaction (FCI) calculation. The effects of dynamic electron correlation are often accounted for by multireference configuration interaction (MRCI) or by a perturbative treatment. In this work, multiconfigurational quasidegenerate perturbation theory terminated at the second order (MC-QDP2) was utilised.

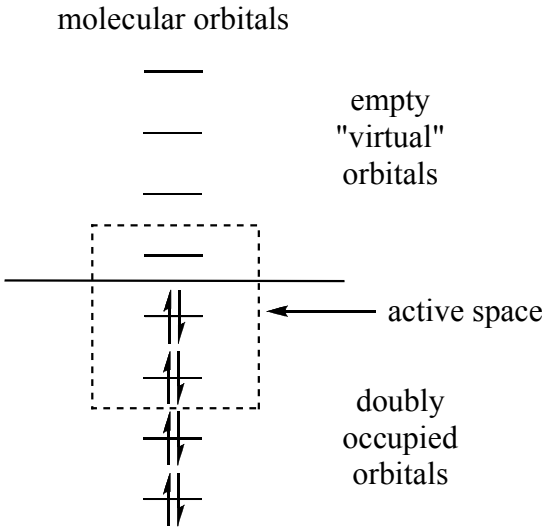

Figure 2.3 Molecular orbitals of a molecule, showing the occupied and virtual orbitals, and the active space

The need for multireference treatment of a particular chemical system can be determined by use of the T_1 diagnostic implemented into the GAUSSIAN 03[16] software package. The T_1 value is calculated as the Euclidian norm of the vector of the t_1 amplitudes in a closed-shell coupled cluster singles and doubles (CCSD) wavefunction. These amplitudes are known to be closely related to the coefficients of

singly-excited configurations in CI theory, which allow molecular orbital relaxation to occur.[38] Therefore, the T_1 value shows the reliability of results obtained from a single reference-based electron correlation procedure. A large T_1 value, of greater than 0.02, indicates the need for multireference treatment.[38]

2.2.7 Solvent effects

Calculations of chemical reactions in the gas phase are useful to computational chemists as they involve only the modelling of molecules involved in the reaction and often compare very well with experimental models. However, in some cases, such as reactions involving highly polar or charged species, the solvent medium can have a large effect on the stability of molecules and on the kinetic and thermodynamic parameters of the reaction. In order to obtain a good model for a solution phase reaction it often becomes necessary to compute the effect of the solvent molecules surrounding the reacting species.

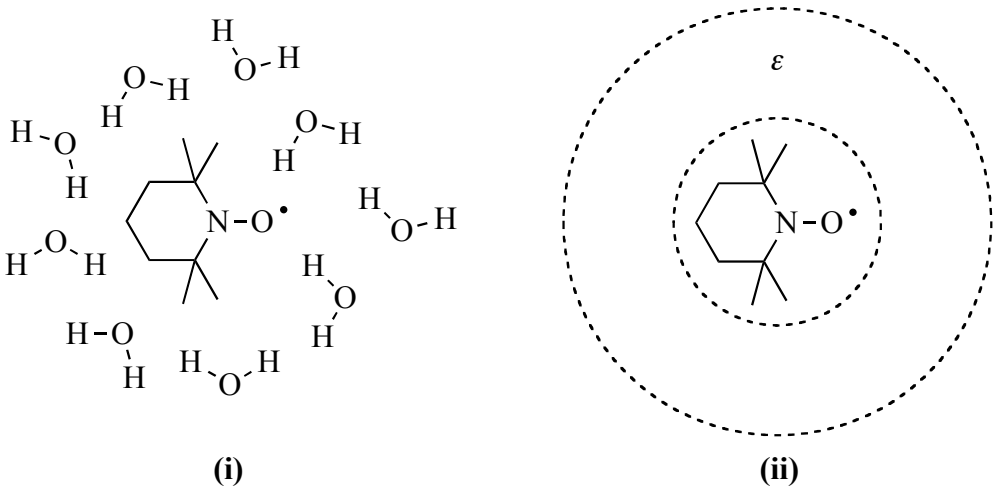

Figure 2.4 Examples of calculations of a nitroxide radical in aqueous solvent using (i) explicit solvent molecules and (ii) a dielectric field

Ideally, solvent effects should be measured by surrounding a molecule with many individual solvent molecules, as shown in Figure 2.4(i). However, in practice this technique is not often feasible as it leads to very large calculation systems. Instead, common solvent calculation methods involve estimating the effects of solvent

molecules by a dielectric field, ε, surrounding the calculated species, as shown in Figure 2.4(ii). As discussed further in Chapter 2.3.3, these methods are typically parameterised at low levels of theory and care must be taken in their implementation.

2.3 Reaction thermodynamics and kinetics

2.3.1 Reaction surfaces

From a theoretical point of view, a chemical reaction can be thought of as set of nuclei moving on a potential energy surface (PES) along which are the solutions to the electronic Schrödinger equation. For the purposes of most computational studies however, it is unnecessary (and even impractical) to calculate the full PES. Instead, it is often sufficient to locate only the stationary points on the surface. The stationary points of most use to chemists are local minima, corresponding to equilibrium structures, and first-order saddle points, corresponding to transition state structures. Equilibrium structures are identified as having no negative eigenvalues of the Hessian, while first-order saddle points have one negative eigenvalue (corresponding to one imaginary frequency).

The enthalpy of a chemical reaction is the difference in energies between the ground state minimum-energy structures of the product and reactant species. In order to determine the energies of these individual molecules accurately, the geometries of their equilibrium structures must first be optimised. In this work, the efficient geometry optimisation techniques implemented into the GAUSSIAN 03[16] and GAMESS[39] programs were utilised, allowing stationary points to be located and verified through further calculation of second derivatives.

In principle, any molecule will exist as an ensemble of its conformers, non-superimposable structures differing by hindered internal rotations about one or more bonds. The set of conformers, known as the "conformational space", can grow rapidly with the size of the molecule. The enthalpy of the reaction is calculated using the lowest energy conformers of the reactant and product species. While in reality it is likely that the molecule exists as an ensemble of several low-lying conformations, for thermochemical purposes performing calculations on the conformer of lowest energy

(the global minimum structure) is usually sufficient. Those conformations with similar energies yield similar results, while conformations with much higher energies will not contribute significantly. In this work, the lowest energy conformations of molecules were located through exhaustive systematic screening of the conformational space. Where relevant, calculations on molecules were performed in the highest possible symmetry state.

2.3.2 Reaction free energies

The Gibbs free energy of an individual molecule in the gas phase, G_{gas}, is found from its enthalpy, H_{gas}, and entropy, S_{gas}, through Equation (2.5), where T is the temperature expressed in Kelvin.

$$G_{gas} = H_{gas} - TS_{gas} \tag{2.5}$$

In this work, terms for the enthalpy and entropy were found using statistical thermodynamics[40] of an ideal gas, under the rigid rotor, harmonic oscillator approximation.[41] The enthalpy term is made up of the electronic energy, the scaled zero-point vibrational energy (*ZPE*) associated with the geometry of the molecule, and a temperature correction term, T_c, to correct from 0 K to the desired temperature, as shown in Equation (2.6).

$$H_{gas} = E^{o}_{gas} + ZPE + T_c \tag{2.6}$$

Zero-point energy and temperature correction terms are found from the sum of the vibrational frequencies of the molecule, ν_i, through Equations (2.7) and (2.8), in which h is Planck's constant (6.62607×10^{-34} Js), R is the ideal gas constant (8.3143 $Jmol^{-1}K^{-1}$) and k_B is Boltzmann's constant (1.38065×10^{-23} $Jmolecule^{-1}K^{-1}$). Scaling factors for zero-point energies often differ and care must be taken to use factors appropriate for the level of theory.[42] In Equation (2.8), the first term represents the vibrational contribution to the thermal correction, while the second term is the sum of the translational, rotational and electronic contributions.

$$ZPE = \frac{hR}{2k_{\mathbf{B}}} \sum_i \nu_i \tag{2.7}$$

$$T_c = \frac{hR}{k_B}\sum_i \frac{\nu_i}{\exp\left(h\nu_i / k_B T\right) - 1} + 4RT \tag{2.8}$$

The entropy of a system is calculated from the vibrational (S_{vib}), translational (S_{trans}), rotational (S_{rot}), and electronic (S_{elec}) contributions to the entropies of the individual species, as shown in Equation (2.9). These individual contributions to the entropy are expressed in Equations (2.10) to (2.14), in which M is the molecular mass of the species, and T and P are the corresponding reference temperature and pressure. I is the principal moment of inertia of a linear molecule, while I_x, I_y, and I_z are the principal moments of inertia about the x, y, and z axes respectively for a non-linear molecule. σ_r is the symmetry number of the molecule, which counts its number of symmetry equivalent forms, and ω_0 is the electronic spin multiplicity of the molecules (ω_0 = 1 for singlet species, 2 for doublet species, etc).

$$S = S_{vib} + S_{trans} + S_{rot} + S_{elec} \tag{2.9}$$

$$S_{vib} = R\sum_i \left(\frac{h\nu_i / k_B}{\exp\left(h\nu_i / k_B T\right) - 1} - \ln\left(1 - \exp\left(-h\nu_i / k_B T\right)\right) \right) \tag{2.10}$$

$$S_{trans} = R\left(\ln\left(\left(\frac{2\pi M k_B T}{h^2} \right)^{3/2} \frac{k_B T}{P} \right) + \frac{5}{2} \right) \tag{2.11}$$

$$S_{rot,linear} = R\left(\ln\left(\frac{1}{\sigma_r}\left(\frac{T}{\Theta_r} \right) \right) + 1 \right), \text{ where } \Theta_r = \frac{h^2}{8\pi^2 I k_B} \tag{2.12}$$

$$S_{rot,nonlinear} = R\left(\ln\left(\frac{\pi^{1/2}}{\sigma_r}\left(\frac{T^{3/2}}{\left(\Theta_{r,x}\Theta_{r,y}\Theta_{r,z}\right)^{1/2}} \right) \right) + \frac{3}{2} \right), \text{ where } \Theta_{r,i} = \frac{h^2}{8\pi^2 I_i k_B} \tag{2.13}$$

$$S_{elec} = R\ln\left(\omega_0\right) \tag{2.14}$$

It should be noted that the equations for finding H and S shown above are entirely equivalent to formulae found using molecular partition functions, Q, which were designed to serve as a bridge between the quantum mechanical states of a system and its thermodynamic properties. The partition function of a system with g_i degenerate states is given by Equation (2.15), where the values ξ_i are the energy levels

of the system. The enthalpy and entropy of a system in terms of the partition functions are shown in Equations (2.16) and (2.17).[40e]

$$Q = \sum_i g_i \exp\left(-\frac{\xi_i}{k_B T}\right) \tag{2.15}$$

$$H = k_B T V \left(\frac{\partial \ln Q}{\partial V}\right)_T - \left(\frac{\partial \ln Q}{\partial \gamma}\right)_V \tag{2.16}$$

$$S = k_B \ln Q - \left(\frac{\partial \ln Q}{\partial \gamma}\right)_V, \text{ where } \gamma = \frac{1}{k_B T} \tag{2.17}$$

The free energy change that occurs during a reaction is found from the difference in the individual free energies of the product and reactant species. Since the levels of theory used to correct for the effects of a solvent medium are typically small basis set HF or B3-LYP calculations and are parameterised against free energies of solvation, they should not be used to calculate the full solution phase energy of a molecule. The free energy change of a reaction in solution can be found most accurately by the use of a thermodynamic cycle, as demonstrated in Scheme 2.1. This method also has the advantage of being adaptable to the use of experimental free energies in solution for cases (such as H^+ and H_3O^+) where the calculation of values is not straightforward.

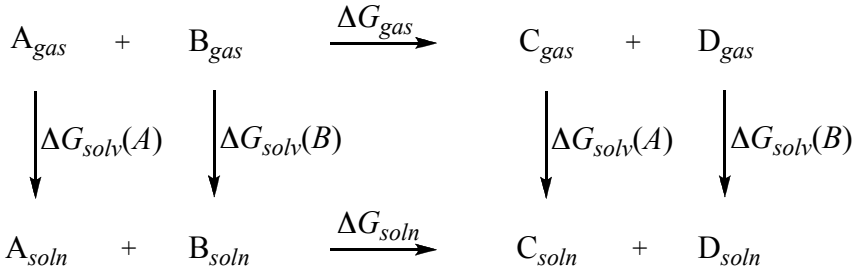

Scheme 2.1 Thermodynamic cycle used to calculate the free energy change for a reaction in solution

In Scheme 2.1, ΔG_{gas} is the gas-phase free energy change of the reaction, which is calculated separately at a high level of theory as the difference between the sum of

the gas-phase free energies of the products *C* and *D*, and the reactants, *A* and *B*. The ΔG_{solv} terms are the individual free energies of solvation of species which, when added to the gas-phase free energies, give the free energies of species in solution. The value of ΔG_{soln} therefore expresses the solution-phase free energy change of the reaction and is found from Equation (2.18). The correction term $\Delta G^{1\text{atm}\rightarrow 1\text{M}}$ is added to Equation (2.18) to take account of the change from the gas-phase standard state for an ideal gas (typically one atmosphere) to a concentration of one molar in solution.

$$\Delta G_{soln} = \Delta G_{gas} + \Delta G_{solv} + \Delta G^{1\text{atm}\rightarrow 1\text{M}} \tag{2.18}$$

The change of state correction term, $\Delta G^{1\text{atm}\rightarrow 1\text{M}}$, is found from Equation (2.19) where *R* is the ideal gas constant, *T* is the reaction temperature and *P* is the standard pressure of one atmosphere (101.325 kPa). The term Δn is the change in the number of moles of solvated species in the reaction. For example, the combination of two radical species in a reaction of the form $A^{\bullet} + B^{\bullet} \rightarrow A\text{–}B$ has $\Delta n = -1$, while the reverse dissociation reaction has $\Delta n = 1$. When calculations involve a free electron in oxidation or reduction type processes, the electron convention of "Fermi-Dirac electron energetics"[43] is used, and the electron is not counted toward Δn. Therefore, for example, an oxidation half reaction such as $A^{\bullet} \rightarrow A^{+} + e^{-}$ has $\Delta n = 0$.

$$\Delta G^{1\text{atm}\rightarrow 1\text{M}} = \Delta n \ln\left(\frac{RT}{P}\right) \tag{2.19}$$

2.3.3 Solvation free energies

In this work, a common method for calculating solution free energies known as the polarisable continuum model (PCM) was utilised. In this representation, a series of overlapping spheres makes up the solute cavity containing a dielectric field, used to represent the effects of the solvent molecules (as shown in Figure 2.4(ii)). The calculation includes terms for non-electrostatic contributions of the solvent, such as dispersion, repulsion and cavitation.

The polarised continuum models PCM[44] and CPCM[45] are implemented as keywords into the GAUSSIAN 03[16] software package, and give outputs of the free energy of a species calculated in solution medium. As discussed in Chapter 2.3.2, the low-level methods used for these calculations are not sufficient to describe the gas-

phase component of the calculation. Therefore, the free energy of solvation, ΔG_{solv}, (measuring the stabilising or destabilising effect of the solvent) must be extracted from the PCM calculation. This term is then added to the independently calculated high-level gas-phase free energy using a thermodynamic cycle to give the total free energy of a species in solution (see Scheme 2.1). Often ΔG_{solv} is calculated from the output of a single calculation in solution, estimated as the difference between $\langle \psi(\varepsilon) | \mathbf{H} | \psi(\varepsilon) \rangle$ (where $\psi(\varepsilon)$ is the wavefunction in the presence of the solvent field) and the total free energy of the solute in solution. However, it is more rigorous to calculate ΔG_{solv} as the difference of the gas and solution-phase free energies at the same level of theory.[46] To this end, the SCFVAC keyword, implemented into the GAUSSIAN 03[16] software package, is used to perform an additional gas-phase calculation, to find $\langle \psi(0) | \mathbf{H} | \psi(0) \rangle$ (where $\psi(0)$ is the wavefunction in the gas phase). The free energy of solvation calculated using the SCFVAC keyword differs from the value estimated using a single solution phase calculation by a small solute polarisation term.

2.3.4 Equilibrium constants of reactions

The equilibrium constant of a reaction at temperature T is related to the Gibbs free energy change of the reaction through Equation (2.20), in which R is the ideal gas constant.

$$K = \exp\left(\frac{-\Delta G}{RT}\right) \tag{2.20}$$

For reactions calculated in a solution, the free energy ΔG already includes a change of state term, which accounts for a transformation to standard concentration. For reactions in the gas phase, where the free energy is taken as ΔG_{gas}, a factor representing the standard unit of concentration is required, leading to the gas-phase equilibrium constant shown in Equation (2.21). This represents the equivalent of the addition of the term $\Delta G^{1\text{atm}\rightarrow 1\text{M}}$ to the free energy.

$$K_{gas} = \left(\frac{P}{RT}\right)^{\Delta n} \exp\left(\frac{-\Delta G_{gas}}{RT}\right) \tag{2.21}$$

2.3.5 Reaction barriers and tunnelling corrections

The barrier of a chemical reaction is defined as the difference in energies between the transition state and the reactant species. The free energy of activation for a reaction $\Delta G^{\ddagger}$ is found from Equation (2.22). In transition-state theory,[41,47] the rate coefficient at the temperature T is found from Equation (2.23), in which κ is the tunnelling correction factor, h is Planck's constant, k_B is Boltzmann's constant and R is the ideal gas constant. When calculation of the rate constant is performed in the gas phase, the term $\left(P/RT\right)^{1-m}$, where m is the molecularity of the reaction, is also required to account for the addition of the term $\Delta G^{1\text{atm}\rightarrow 1\text{M}}$ to the free energy. The effective free energy barrier including tunnelling, $\Delta G_{eff}^{\ddagger}$, can be found from Equations (2.24). In this work, transition state structures were optimised as first-order saddle points (having one imaginary frequency), and were verified by intrinsic reaction coordinate (IRC) calculations mapping the potential energy surface on either side of the optimised structure.

$$\Delta G^{\ddagger} = \Delta H^{\ddagger} - T\Delta S^{\ddagger} \tag{2.22}$$

$$k = \kappa \frac{k_B T}{h} \exp\left(\frac{-\Delta G^{\ddagger}}{RT}\right) \tag{2.23}$$

$$\Delta G_{eff}^{\ddagger} = \Delta G^{\ddagger} - RT\ln(\kappa) \tag{2.24}$$

The tunnelling coefficient, κ, measures the effect of quantum mechanical tunnelling through the reaction barrier on the rate of the reaction. When a transition state involves the transfer of atoms other than hydrogen or deuterium the extent of tunnelling is small. However, when a transition state involves transfer of these species the wavelength of the atom is large enough, due to its small mass, to allow measurable tunnelling through the barrier. In this work, the effect of quantum mechanical tunnelling was calculated using the Eckart method,[48] giving a simple approximation to the full minimum energy path and generally recognised as one of the more accurate one-dimensional methods.[49] The use of a multi-dimensional method was not practical for the large systems in this work.

In the Eckart method, the change in potential energy, $V(x)$, along the minimum energy path is described by the Eckart function[50] shown in Equation (2.25), where A and B are defined in terms of the forward and reverse reaction barriers, V_f and V_r for an exothermic reaction. The parameter Δ is chosen to give the most appropriate fit to the minimum energy path, primarily near the transition structure where tunnelling is most important. In this work, Δ was calculated using Equation (2.26), where ν_{imag} is the imaginary frequency, i is the imaginary unit ($i^2 = -1$) and c is the speed of light.

$$V(x) = \frac{Ay}{(1+y)^2} + \frac{By}{(1+y)^2}$$
$$\text{where } y = \exp\left(\frac{x}{\Delta}\right),\ A = \left(\sqrt{V_f} + \sqrt{V_r}\right)^2 \text{ and } B = V_f - V_r \tag{2.25}$$

$$\Delta = \frac{i}{2\pi c \nu_{imag}} \sqrt{\frac{\left(B^2 - A^2\right)^2}{8A^3}} \tag{2.26}$$

The permeability of the reaction barrier, $G(W)$, can then be written as a function of the energy W, as shown in Equation (2.27). The Eckart tunnelling correction factor, κ, is obtained by numerical integration of $G(W)$ over a Boltzmann distribution of energies,[51b] as shown in Equation (2.28). In this work integrations were performed using a Microsoft® Excel® spreadsheet.

$$G(W) = 1 - \frac{\cosh(\alpha - \beta) + \cosh(\delta)}{\cosh(\alpha + \beta) + \cosh(\delta)}$$
$$\text{where } \alpha = \frac{4\pi^2\Delta}{h}\sqrt{2W},\ \beta = \frac{4\pi^2\Delta}{h}\sqrt{2(W-B)} \text{ and } \delta = \frac{4\pi^2\Delta}{h}\sqrt{2A - \frac{h^2}{16\pi^2\Delta^2}} \tag{2.27}$$

$$\kappa = \frac{\exp\left(V_f / k_B T\right)}{k_B T} \int_0^\infty G(W) \exp\left(\frac{-W}{k_B T}\right) dW \tag{2.28}$$

2.4 Molecular properties

As well as allowing for the study of the mechanisms, kinetics and thermodynamics of chemical reactions, computational quantum chemistry also provides access to other properties of molecules. These properties can assist in the interpretation of both theoretical and experimental results. In this work, ionisation

energies, electron affinities and other redox properties, charge and spin density distributions and radical stabilisation energies were used to understand the actions of nitroxides and related molecules.

2.4.1 Ionisation energies and electron affinities of radicals

The first ionisation energy (*IE*) measures the ease with which a single electron is removed from a molecule. The first electron affinity (*EA*) measures the ease of adding an electron. The ionisation energies and electron affinities of radical species $R^{\bullet}$ are calculated as the enthalpies of Reactions (2.29) and (2.30), respectively. *IEs* and *EAs* are typically measured in electron volts (eV).

$$R^{\bullet} \longrightarrow R^{+} + e^{-} \qquad (2.29)$$

$$R^{-} \longrightarrow R^{\bullet} + e^{-} \qquad (2.30)$$

Vertical *IEs* and *EAs* measure the change in energy between the lowest energy state of a molecule and its cationic or anionic form, frozen in the same geometry. These types of calculations are useful for comparisons of related molecules, being a reflection of the abilities of substituents to stabilise the anionic or cationic forms of the molecule. They reflect the stability of charge-transfer configurations of bonds and transition state structures. Vertical *IEs* and *EAs* are therefore an effective tool to determine the polarity of substituent groups.

Adiabatic *IEs* and *EAs* measure the change in energy between the lowest energy state of a molecule and the lowest energy state of its cationic or anionic form. These calculations involve the re-optimisation of the geometries of the positively and negatively charged molecules. Adiabatic *IEs* and *EAs* are utilised as half-reactions in the calculation of electrode potentials.

2.4.2 Electrode potentials of nitroxide radicals

Oxidation and reduction potentials are another measure of the ease with which electrons are added to or removed from a molecule, with values calculated relative to a reference electrode. In this work, electrode potentials of nitroxide radicals were determined in order to better understand their actions as protecting agents against oxidative damage in biological systems.

Nitroxide radicals undergo a simple reversible one-electron oxidation to the corresponding oxoammonium cation. The reduction of a nitroxide is a more complex, irreversible process, known to produce a hydroxylamine, but with some debate over the mechanism by which this occurs. Scheme 2.2 shows products of oxidation and reduction reactions upon a nitroxide radical.

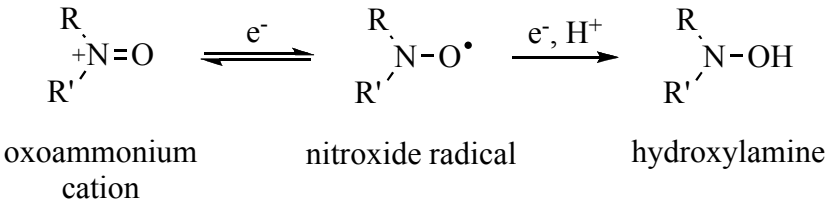

Scheme 2.2 Oxidation and reduction reactions of a nitroxide radical

Two different methodological approaches can be used for the calculation of redox potentials in solution.[52] One method is to use an isodesmic reaction in order to calculate the Gibbs free energy of the reaction relative to a reference system. Results for this method have been shown to be somewhat dependant upon the reference molecule used,[53] limiting their predictive power. A second approach, in which electrons and protons are used explicitly as the reference system for the reactions, was used in this study.

The formal oxidation potential of a nitroxide radical is calculated, relative to the standard hydrogen electrode (SHE), through the free energy of Reaction (2.31). This can be written in terms of the two half-reactions shown in Reactions (2.32) and (2.33).

$$RR'NO^{\bullet}_{soln} + H^{+}_{soln} \longrightarrow RR'N^{+}{=}O_{soln} + \tfrac{1}{2}H_{2\ gas} \qquad (2.31)$$

$$RR'NO^{\bullet}_{soln} \longrightarrow RR'N^{+}{=}O_{soln} + e^{-}_{gas} \qquad (2.32)$$

$$H^{+}_{soln} + e^{-}_{gas} \longrightarrow \tfrac{1}{2}H_{2\ gas} \qquad (2.33)$$

The free energy change of Reaction (2.31), $\Delta G_{\mathrm{Rx}(2.31)}$, is the sum of the free energies of Reactions (2.32) and (2.33), $\Delta G_{\mathrm{Rx}(2.32)}$ and $\Delta G_{\mathrm{Rx}(2.33)}$, as shown in Equation

(2.34). The value for $\Delta G_{Rx(2.32)}$ is calculated using a thermodynamic cycle (see Scheme 2.1) in which the free energy change in solution is found from Equation (2.18). Since calculation of the free energy of H^+ is not straightforward, an experimental value for $\Delta G_{Rx(2.33)}$ must be used. The value for $\Delta G_{Rx(2.33)}$, is reported to be -4.36 eV in water and -4.52 eV in acetonitrile.[54]

$$\Delta G_{Rx(2.31)} = \Delta G_{Rx(2.32)} + \Delta G_{Rx(2.33)} \tag{2.34}$$

The formal oxidation potential, E^o_{ox}, is obtained using Equation (2.35),[55] where n is the number of electrons transferred (in this case n = 1), and F is the Faraday constant (96485.3383 coulombs/mole):

$$\Delta G_{Rx\ (2.31)} = nFE^o_{ox} \tag{2.35}$$

As noted above, the mechanism for reduction leading to a hydroxylamine is more complicated than a simple one-electron transfer reaction. Fish *et al*[56] have suggested a reaction scheme for the reduction to a hydroxylamine in an aqueous medium. Reduction occurs as a three-step process, with one-electron reduction to the anionic form of the nitroxide followed by two reversible protonation steps, shown in Scheme 2.3. Thus for comparison with experimental values, the acid dissociation constants of these protonation steps, K_1 and K_2, need to be determined, as well as the formal potential of the electron transfer process, E^o_{red}.

$$RR'NO^{\bullet}_{aq} + e^-_{gas} \overset{E^o_{red}}{\rightleftharpoons} RR'NO^-_{aq} \tag{2.36}$$

$$RR'NO^-_{aq} + H^+_{aq} \overset{1/K_2}{\rightleftharpoons} RR'NOH_{aq} \tag{2.37}$$

$$RR'NOH_{aq} + H^+_{aq} \overset{1/K_1}{\rightleftharpoons} RR'\overset{H}{\underset{OH}{N^+}}_{aq} \tag{2.38}$$

Scheme 2.3 Suggested multi-step mechanism for the reduction of nitroxides[56]

Experimentally determination of the reduction potential of a nitroxide radical gives the half-wave potential, $E_{1/2}$, rather than the standard formal reduction potential, E^o_{red}. In a previous study, Kato *et al*[57] investigated the relationship between the formal potential, E^o_{red}, and the acid dissociation constants, K_1 and K_2, found from Reactions (2.37) and (2.38), for a range of pH values. These workers determined an equation for the half-wave potential, $E_{1/2}$, shown in Equation (2.39). This relationship was also subsequently reported by Israeli *et al*.[58]

$$E_{1/2} = E^o_{red} - \frac{RT}{F}\ln(K_1K_2) + \frac{RT}{F}\ln(K_1K_2 + K_1[H^+] + [H^+]^2) \qquad (2.39)$$

In the present work, the half-wave potentials of several relatively small nitroxide species were compared directly with experimental data using Equation (2.39), and are discussed in Chapter 3.4. In order to perform these comparisons, K_1 and K_2 were found from Reactions (2.37) and (2.38) using the method of Liptak and Shields,[59] which incorporate experimental values of H^+; a gas-phase energy of -6.28 kcalmol^{-1}, and a free energy of solvation in an aqueous medium of -264.61 kcalmol^{-1}.

In this work, formal reduction potentials, E^o_{red}, with respect to the SHE were used in the determination of structure reactivity trends of nitroxide radicals. In a similar manner to the calculation of the oxidation potential, the formal reduction potential is calculated from the free energy change of Reaction (2.40), made up of the two half reactions shown in Reaction (2.41) and (2.42). E^o_{red} is then found using Equations (2.43) and (2.44).

$$RR'NO^{\bullet}_{soln} + \tfrac{1}{2}H_{2\,gas} \longrightarrow RR'NO^-_{soln} + H^+_{soln} \qquad (2.40)$$

$$RR'NO^{\bullet}_{soln} + e^-_{gas} \longrightarrow RR'NO^-_{soln} \qquad (2.41)$$

$$\tfrac{1}{2}H_{2\,gas} \longrightarrow H^+_{soln} + e^-_{gas} \qquad (2.42)$$

$$\Delta G_{\mathrm{Rx\,(2.40)}} = \Delta G_{\mathrm{Rx\,(2.41)}} + \Delta G_{\mathrm{Rx\,(2.42)}} \qquad (2.43)$$

$$\Delta G_{\mathrm{Rx\,(2.40)}} = -nFE^o_{red} \qquad (2.44)$$

2.4.3 Charge and spin orbital calculations

Calculation of the ground state wavefunction of a molecular system leads to information about the distribution of electrons within the molecule. By the appropriate division of molecular volume, electrons can be "assigned" to the different nuclei and the distribution of charge and spin density within a molecule determined. This leads to a computationally created "Lewis structure" of the molecule.

Common methods for the determination of charge and spin density distributions include the Mulliken population analysis,[3] and the natural bond orbital (NBO) analysis.[60] Both of these methods were utilised in this work. The Mulliken population analysis is performed by default when calculations are run using the GAUSSIAN 03[16] software package. The more rigorous NBO-type analysis was originally designed as a technique for studying the hybridisation and covalency effects in molecular wavefunctions by giving pictures of localised bonds and lone pairs.[60] The calculation of an NBO analysis comprises a sequence of transformations of the input basis set to various localised basis sets. These steps are automated by the NBO v3.1 program,[61] which is attached to the GAUSSIAN 03[16] software package.

2.4.4 Radical stabilisation energies

The thermodynamic stability of a carbon-centred radical $R^{\bullet}$ can be quantified as its radical stabilisation energy, *RSE*, which is defined as the enthalpy of the isodesmic Reaction (2.45).[62]

$$R^{\bullet} + CH_4 \longrightarrow R-H + {}^{\bullet}CH_3 \qquad (2.45)$$

Reaction (2.45) compares the energy of the radical with the reference methyl radical, using the corresponding alkanes to balance the reaction. The radical $R^{\bullet}$ is said to be "more stable" (relative to ${}^{\bullet}CH_3$) if the *RSE* is positive, and "less stable" if it is negative. In order for the isodesmic reaction to give good values of radical stability, the contributions of the closed-shell species on the reaction thermodynamics must be minor. While it is well known that Reaction (2.45) successfully compares the true stabilities of carbon-centred radicals, this description may not be valid for other radical systems.[63] The use of *RSE* in the determination of radical stability is discussed further in Chapter 5.4.1

2.5 Computational resources

2.5.1 Software

Ab initio molecular orbital and density functional calculations in this work were carried out using the software packages GAUSSIAN 03,[16] and MOLPRO 2000.6,[64] and GAMESS.[39] Visualisation of molecules and initial structure design was performed using the programs MOLDEN 4.4,[65] Molecule v1.3.5,[66] and MacMolPlt v7.2.1.[67]

The calculation of entropies and temperature corrections was performed using a program to extract thermochemical information from a GAUSSIAN output file, written in the programming language Perl, by Dr Rodolfo Gomez-Balderas and updated to allow the calculations of charged species by Dr Ching Yeh (Leaf) Lin. Also used in this work was a program for the generation of MOLPRO input files, written by Dr Anthony Scott. A program controlling the submission and collection of calculation jobs to the various supercomputers utilised in this work was written by Dr Anthony Scott and updated by David Brittain. Eckart tunnelling coefficients[51] were calculated using a Microsoft® Excel® spreadsheet designed by Associate Professor Michelle Coote. The multiparameter fittings of molecular data, described in Chapter 5.3, were performed using linear regression techniques integrated into Microsoft® Excel®.

2.5.2 Hardware

The bulk of calculations in this work were performed using the National Computational Infrastructure (NCI) National Facility (NF) SGI® Altix® 3700 Bx2 cluster owned by the Australian Partnership for Advanced Computing (APAC). Simple calculations such as geometry optimisation of small systems were run on the APAC Linux Cluster. Some short running GAMESS[39] calculations as well as all data processing was performed on a Mac OS X v10.5.6 workstation.

2.6 References

(1) Jensen, F. *Introduction to Computational Chemistry*; John Wiley & Sons: Chichester, 1999 and references within.

(2) Szabo, A.; Ostlund, N. S. *Modern Quantum Chemistry: Introduction to Advanced Electronic Structure Theory*; Macmillan: New York, 1982.

(3) Hehre, W. J.; Radom, L.; Schleyer, P. V. R.; Pople, J. A. *Ab Initio Molecular Orbital Theory*; Wiley: New York, 1986.

(4) Levine, I. N. *Quantum Chemistry*, 4th ed.; Prentice-Hall: Englewood Cliffs, 1991.

(5) Schrödinger, E. *Phys. Rev.* **1926**, *28*, 1049.

(6) Born, M.; Oppenheimer, J. R. *Ann. Physik* **1927**, *84*, 457.

(7) Boys, S. F. *Proc. Roy. Soc. London A* **1950**, *26*, 57.

(8) (a) Dunning, T. H. *J. Chem. Phys.* **1989**, *90*, 1007. (b) Kendell, R. A.; Dunning, T. H.; Harrison, R. J. *J. Chem. Phys.* **1992**, *96*, 6796. (c) Woon, D. E.; Dunning, T. H. *J. Chem. Phys.* **1993**, *98*, 1358.

(9) (a) Hartree, D. R. *Proc. Cam. Phil. Soc.* **1928**, *24*, 89. (b) Hartree, D. R. *Proc. Cam. Phil. Soc.* **1928**, *24*, 111. (c) Hartree, D. R. *Proc. Cam. Phil. Soc.* **1928**, *24*, 246.

(10) Fock, V. Z. *Z. Physik* **1930**, *61*, 126.

(11) Pauli, W. *Z. Physik* **1925**, *31*, 765.

(12) Pople, J. A.; Head-Gordon, M.; Raghavachari, K. *J. Chem. Phys.* **1987**, *87*, 5968.

(13) (a) Cizek, J. *Advan. Chem. Phys.* **1969**, *14*, 35. (b) Cizek, *J. Int. J. Quant. Chem.* **1969**, *3*, 149. (c) Cizek, J. *J. Chem. Phys.* **1966**, *45*, 4256.

(14) Møller, C.; Plesset, M. S. *Phys. Rev.* **1934**, *46*, 618.

(15) Hohenberg, P.; Kohn, W. *Phys. Rev. B* **1964**, *136*, 864.

(16) Frisch, M. J.; Trucks, G. W.; Schlegel, H. B.; Scuseria, G. E.; Robb, M. A.; Cheeseman, J. R.; Montgomery Jr., J. A.; Vreven, T.; Kudin, K. N.; Burant, J. C.; Millam, J. M.; Iyengar, S. S.; Tomasi, J.; Barone, V.; Mennucci, B.; Cossi, M.; Scalmani, G.; Rega, N.; Petersson, G. A.; Nakatsuji, H.; Hada, M.; Ehara, M.; Toyota, K.; Fukuda, R.; Hasegawa, J.; Ishida, M.; Nakajima, T.; Honda, Y.; Kitao, O.; Nakai, H.; Klene, M.; Li, X.; Knox, J. E.; Hratchian, H. P.; Cross, J. B.; Adamo, C.; Jaramillo, J.; Gomperts, R.; Stratmann, R. E.; Yazyev, O.; Austin, A. J.; Cammi, R.; Pomelli, C.; Ochterski, J. W.; Ayala, P. Y.; Morokuma, K.; Voth, G. A.; Salvador, P.; Dannenberg, J. J.; Zakrzewski, V. G.; Dapprich, S.; Daniels, A. D.; Strain, M. C.; Farkas, O.; Malick, D. K.; Rabuck, A. D.; Raghavachari, K.; Foresman, J. B.; Ortiz, J. V.; Cui, Q.; Baboul, A. G.; Clifford, S.; Cioslowski, J.; Stefanov, B. B.; Liu, G.; Liashenko, A.; Piskorz, P.; Komaromi, I.; Martin, R. L.; Fox, D. J.; Keith, T.; Al-Laham, M. A.; Peng, C. Y.; Nanayakkara, A.; Challacombe, M.; Gill, P. M. W.; Johnson, B.; Chen, W.; Wong, M. W.; Gonzalez, C.; Pople, J. A. *Gaussian 03, Revision B.03*; Gaussian, Inc.: Pittsburgh PA, 2003.

(17) Perdew, J. P.; Burke, K.; Ernzerhof, M. *Phys. Rev. Lett.* **1996**, *77*, 3865.

(18) (a) Becke, A. D. *Phys. Rev. A* **1988**, *38*, 3098. (b) Lee, C.; Yang, W.; Parr, R. G. *Phys. Rev. B* **1988**, *37*, 785.

(19) Becke, A. D. *J. Chem. Phys.* **1993**, *98*, 5648.

(20) Perdew, J. P. *Phys. Rev. B* **1986**, *33*, 8822.

(21) Kang, J. K.; Musgrave, C. B. *J. Chem. Phys.* **2001**, *115*, 11040.

(22) Zhao, Y.; Pu, J.; Lynch, B. J.; Truhlar, D. G. *Phys. Chem. Chem. Phys.* **2004**, *6*, 673.

(23) Adamo, C.; Barone, V. *J. Chem. Phys.* **1998**, *108*, 664.

(24) Zhao, Y.; Truhlar, D. G. *J. Phys. Chem. A* **2004**, *108*, 6908.

(25) Zhao, Y.; Lynch, B. J.; Truhlar, D. G. *J. Phys. Chem. A* **2004**, *108*, 2715.

(26) Lynch, B. J.; Fast, P. L.; Harris, M.; Truhlar, D. G. *J. Phys. Chem. A* **2000**, *104*, 4811.

(27) Boese, A. D.; Martin, J. M. L. *J. Chem. Phys.* **2004**, *121*, 3405.

(28) Izgorodina, E. I.; Coote, M. L.; Radom, L. *J. Phys. Chem. A* **2005**, *109*, 7558.

(29) (a) Pople, J. A.; Head-Gordon, M.; Fox, D. J.; Raghavachari, K.; Curtiss, L. A. *J. Chem. Phys.* **1989**, *90*, 5622. (b) Curtiss, L. A.; Jones, C.; Trucks, G. W.; Raghavachari, K.; Pople, J. A. *J. Chem. Phys.* **1990**, *93*, 2537. (c) Curtiss, L. A.; Raghavachari, K.; Trucks, G. W.; Pople, J. A. *J. Chem. Phys.* **1991**, *94*, 7221. (d) Curtiss, L. A.; Raghavachari, K.; Redfern, P. C.; Rassolov, V.; Pople, J. A. *J. Chem. Phys.* **1998**, *109*, 7764. (e) Curtiss, L. A.; Redfern, P. C.; Raghavachari, K.; Pople, J. A. *J. Chem. Phys.* **2001**, *114*, 108. (f) Curtiss, L. A.; Redfern, P. C.; Raghavachari, K. J. *Chem. Phys.* **2007**, *126*, 084108.

(30) Montgomery Jr., J. A.; Frisch, M. J.; Ochterski, J.; Petersson, G. A. *J. Chem. Phys.* **1999**, *110*, 2822.

(31) Martin, J. M. L.; Parthiban, S., In *Quantum Mechanical Prediction of Thermochemical Data*, Cioslowski, J., Ed. Kluwer-Academic: Dordrecht, The Netherlands, 2001; pp 31–65.

(32) Montgomery Jr., J. A.; Frisch, M. J.; Ochterski, J. W.; Petersson, G. A. *J. Chem. Phys.* **2000**, *112*, 6532.

(33) Martin, J. M. L.; de Oliveira, G. J. *J. Chem. Phys.* **1999**, *111*, 1843.

(34) Henry, D. J.; Sullivan, M. B.; Radom, L. *J. Chem. Phys.* **2003**, *118*, 4849.

(35) Humbel, S.; Sieber, S.; Morokuma, K. *J. Chem. Phys.* **1996**, *105*, 1959.

36) Izgorodina, E. I.; Coote, M. L. *J. Phys. Chem. A* **2006**, *110*, 2486.

(37) Schmidt, M. W.; Gordon, M. S. *Ann. Rev. Phys. Chem.* **1998**, *49*, 233.

(38) Lee, T. J.; Taylor, P. R. *Int. J. Quant. Chem. Symp.* **1989**, *23*, 199.

(39) Schmidt, M. W.; Baldridge, K. K.; Boatz, J. A.; Elbert, S. T.; Gordon, M. S.; Jensen, J. H.; Koseki, S.; Matsunaga, N.; Nguyen, K. A.; Su, S.; Windus, T. L.; Dupuis, M.; Montgomery, J. A. *J. Comp. Chem.* **1993**, *14*, 1347.

(40) See for example: (a) Benson, S. W. *Thermochemical Kinetics*: John Wiley & Sons: New York, 1976. (b) McQuarrie, D. A. *Statistical Mechanics*; Harper & Row: New York, 1976. (c) Gilbert, R. G.; Smith, S. C. *Theory of Unimolecular and Recombination Reactions*; Blackwell Scientific: Oxford, 1990. (d) Steinfeld, J. I.; Francisco, J. S.; Hase, W. L. *Chemical Kinetics and Dynamics*; Prentice Hall: Englewood Cliffs, N. J., 1999. (e) Atkins, P. W. *Physical Chemistry*, 6th ed.; W. H. Freeman & Co.: San Francisco, 2000.

(41) These formulae are also summarised in: Coote, M. L. Computational Chemistry for Free-Radical Polymerization, In *Encyclopedia of Polymer Science and Technology;* 3rd Ed. Kroschwitz, J. I., Ed; John Wiley & Sons: New York, 2004, Volume 9, pp. 319–371.

(42) (a) Pople, J. A.; Scott, A. P.; Wong, M. W.; Radom, L. *Isr. J. Chem.* **1993**, *33*, 345. (b) Scott, A. P.; Radom, L. *J. Phys. Chem.* **1996**, *100*, 16502.

(43) Bartmess, J. E. *J. Phys. Chem.* **1994**, *98*, 6420.

(44) (a) Cancès, M. T.; Mennucci, B.; Tomasi, J. *J. Chem. Phys.* **1997**, *107*, 3032. (b) Cossi, M.; Barone, V.; Mennucci, B.; Tomasi, J. *Chem. Phys. Lett.* **1998**, *286*, 253. (c) Mennucci, B.; Tomasi, J. *J. Chem. Phys.* **1997**, *106*, 5151.

(45) (a) Barone, V.; Cossi, M. *J. Phys. Chem. A* **1998**, *102*, 1995. (b) Cossi, M.; Rega, N.; Scalmani, G.; Barone, V. *J. Comp. Chem.* **2003**, *24*, 669.

(46) Frisch, A.; Frisch, M. J.; Trucks, G. W. *Gaussian 03 User's Reference*; Gaussian, Inc.: Wallingford, CT, 2003.

(47) Eyring, H. *J. Chem. Phys.* **1935**, *3*, 107.

(48) Coote, M. L.; Collins, M. A.; Radom, L. *Mol. Phys.* **2003**, *101*, 1329.

(49) Bell, R. P. *The Tunnel Effect in Chemistry*; Chapman and Hall: London, 1980.

(50) Eckart, C. *Phys. Rev.* **1930**, *35*, 1303.

(51) (a) Eckart, C. *Phys. Rev.* **1930**, *35*, 1303. (b) Bell, R. P. *The Tunnel Effect in Chemistry*; Chapman and Hall: London, 1980.

(52) See for example: Namazian, M.; Almodarresieh, H. A.; Noorbala, M. R.; Zare, H. R. *Chem. Phys. Lett.* **2004**, *396*, 424.

(53) Wass, J. R. T. J.; Ahlberg, E.; Panas, I.; Schiffrin, D. J. *J. Phys. Chem. A* **2006**, *110*, 2005.

(54) Winget, P.; Cramer, C. J.; Truhlar, D. G. *Theor. Chem. Acc.* **2004**, *112*, 217.

(55) Fu, Y.; Yu, H.-Z.; Wang, Y.-M.; Guo, Q.-X. *J. Am. Chem. Soc.* **2005**, *127*, 7227.

(56) Fish, J. R.; Swarts, S. G.; Sevilla, M. D.; Malinski, T. *J. Phys. Chem.* **1988**, *92*, 3745.

(57) Kato, Y.; Shimizu, Y.; Yijing, L.; Unoura, K.; Utsumi, H.; Ogata, T. *Electrochim. Acta* **1995**, *40*, 2799.

(58) Israeli, A.; Patt, M.; Oron, M.; Samuni, A.; Kohen, R.; Goldstein, S. *Free Radical Biol. Med.* **2005**, *38*, 317.

(59) Liptak, M. D.; Shields, G. C. *J. Am. Chem. Soc.* **2001**, *123*, 7314.

(60) Foster, J. P.; Weinhold, F. *J. Am. Chem. Soc.* **1980**, *102*, 7211.

(61) Glendening, E. D.; Reed, A. E.; Carpenter, J. E.; Weinhold, F. NBO Version3.1.

(62) Benson, S. W. *Thermochemical Kinetics. Methods for the Estimation of Thermochemical Data and Rate Parameters*; John Wiley & Sons: New York, 1976.

(63) Coote, M. L.; Dickerson, A. B. *Aust. J. Chem.* **2008**, *61*, 163.

(64) Werner, H.-J.; Knowles, P. J.; Amos, R. D.; Bernhardsson, A.; Berning, A.; Celani, P.; Cooper, D. L.; Deegan, M. J. O.; Dobbyn, A. J.; Eckert, F.; Hampel, C.; Hetzer, G.; Korona, T.; Lindh, R.; Lloyd, A. W.; McNicholas, S. J.; Manby, F. R.; Meyer, W.; Mura, M. E.; Nicklass, A.; Palmieri, P.; Pitzer, R.; Rauhut, G.; Schütz, M.; Stoll, H.; Stone, A. J.; Tarroni, R.; Thorsteinsson, T. MOLPRO 2000.6; University of Birmingham: Birmingham, 1999.

(65) Schaftenaar, G. MOLDEN 4.4, 1991.

(66) Van Eikema Hommes, N. J. R. Molecule for Macintosh v1.3.5, 1998.

(67) Bode, B. M.; Gordon, M. S. *J. Mol. Graph. Model.* **1998**, *16*, 133.

Chapter 3.

Assessment of Computational Procedures

3.1 Introduction 42
3.2 Geometry optimisations 42
3.3 Gas-phase single-point energies 44
3.4 Free energies of solvation 52
3.5 Conclusions 59
3.6 References 59

3.1 Introduction

The choice of theoretical procedures to be used during a computational quantum chemical study is a balance between accuracy and (computational) expense, with the performance of different methods being dependant upon the type of reaction and the property being calculated. Before beginning this work it was therefore necessary to identify suitable low-cost procedures to model reactions in this study, which can be quite large, especially when they involve polymeric species and larger nitroxide agents.

There is a significant overlap in the chemistry of nitroxide free radicals in biological, polymerisation and industrial applications, with these very different utilisations involving similar chemical reactions. Nitroxide reactions fall into three categories; redox reactions involving either the oxidation or reduction of a nitroxide radical, trapping reactions of radical species by nitroxides and subsequent decomposition reactions, and transfer reactions involving various radicals and closed-shell species.

In this chapter, the performance of a variety of levels of theory is assessed for calculations of molecular geometries, single-point energies, and solvation effects, on redox and trapping reactions of nitroxides. These assessment studies were carried out using reactions of some of the smaller nitroxides and reactant species used later in this work as examples. The results were compared with high-level benchmarking calculations and, where possible, experimental results. Further descriptions of the various levels of theory and methods of calculation can be found in Chapter 2.

3.2 Geometry optimisations

In this study, potential errors in the geometries of molecules could lead to errors when they are incorporated into the further calculations of molecular properties, reaction kinetics and thermodynamics. Therefore, it was necessary to establish whether differences in the procedure used to optimise molecular geometries will have any significant effect on subsequent calculations of nitroxide systems and reactions. To this end, single-point energies in the gas phase were calculated at a consistent level

of theory (QCISD/6-31G(d)) for various optimised geometries of neutral, positively and negatively charged nitroxides and their corresponding methoxyamines. These energies were used to calculate adiabatic ionisation energies (*IEs*), adiabatic electron affinities (*EAs*) and methyl trapping enthalpies, shown in Tables 3.1 and 3.2. Optimisations were performed using a range of levels of theory including the computationally lower cost Hartree-Fock and density functional theory (DFT) methods through to more demanding MP2 and QCISD calculations, with both small and larger basis sets. The results were benchmarked against the high-level QCISD/6-31G(d) method.

Table 3.1 Effect of the level of theory used for geometry optimisation on the adiabatic ionisation energy (*IE*) and electron affinity (*EA*) (at 0 K) of nitroxides[a]

Level of Theory	*IE* (eV)			*EA* (eV)		
			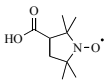			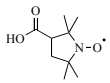
HF/6-31G(d)	6.45	6.51	6.62	-0.63	-0.60	-0.53
HF/6-311+G(2d)	6.48	6.54	6.65	-0.64	-0.62	-0.55
HF/6-311+G(3df,2p)	6.48	6.54	6.66	-0.64	-0.62	-0.55
B3-LYP/6-31G(d)	6.39	6.45	6.56	-0.62	-0.59	-0.52
B3-LYP/cc-pVDZ	6.39	6.46	6.57	-0.62	-0.60	-0.52
B3-LYP/6-311+G(2d)	6.40	6.46	6.57	-0.63	-0.61	-0.53
B3-LYP/6-311+G(3df,2p)	6.40	6.46	6.57	-0.63	-0.61	-0.53
B3-LYP/cc-pVTZ	6.40	6.46	6.57	-0.62	-0.59	-0.52
MP2/6-31G(d)	6.41	6.47	6.59	-0.61	-0.58	-0.51
MP2/6-311+G(d)	6.40	6.45	6.57	-0.63	-0.60	-0.53
MP2/6-311+G(3df,2p)	6.40	6.46	-	-0.61	-0.59	-
QCISD/6-31G(d)	6.39	6.45	-	-0.62	-0.59	-

[a]QCISD/6-31G(d) values for species optimised using various wavefunctions and basis sets.

In line with previous studies showing that low cost methods perform very well in geometry optimisations of nitroxides,[1] all of the lower cost methods yielded reasonably accurate geometries for the calculation of nitroxide reactions, though there are some minor differences amongst the methods used. The DFT method B3-LYP/6-

31G(d) appears to offer the best compromise between accuracy and computational cost for both the redox and trapping reactions. The *IEs* and *EAs*, calculated from geometries optimised at the B3-LYP/6-31G(d) level, show a difference of less than 0.004 eV (0.4 $kJmol^{-1}$) from the corresponding benchmark values, while the methyl trapping enthalpies show a difference of less than 0.3 $kJmol^{-1}$. Thus, B3-LYP/6-31G(d) was adopted for the determination of the geometries of molecules in this work.

Table 3.2 Effect of the level of theory used for geometry optimisation on the gas-phase enthalpy of trapping (at 0 K) of methyl radical by nitroxides[a]

Level of Theory	Enthalpy of trapping ($kJmol^{-1}$)		
			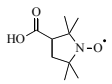
HF/6-31G(d)	-200.2	-206.3	-200.0
HF/6-311+G(2d)	-200.6	-206.3	-200.1
HF/6-311+G(3df,2p)	-200.5	-206.2	-199.9
B3-LYP/6-31G(d)	-202.9	-208.4	-202.3
B3-LYP/cc-pVDZ	-203.2	-208.7	-202.4
B3-LYP/6-311+G(2d)	-203.0	-208.5	-202.3
B3-LYP/6-311+G(3df,2p)	-203.0	-208.5	-202.3
B3-LYP/cc-pVTZ	-203.0	-208.4	-202.2
MP2/6-31G(d)	-203.6	-209.3	-202.7
MP2/6-311+G(d)	-204.0	-209.8	-203.0
MP2/6-311+G(3df,2p)	-	-210.0	-
QCISD/6-31G(d)	-202.9	-208.6	-

[a]QCISD/6-31G(d) values for species optimised using various wavefunctions and basis sets.

3.3 Gas-phase single-point energies

In order to identify an appropriate method for the calculations of gas-phase single-point energies, various nitroxide reactions were assessed for a wide variety of levels of theory. Adiabatic ionisation energies (*IEs*) and electron affinities (*EAs*) for several nitroxide radicals, as well as enthalpies of various alkyl radical trappings by

the six-membered piperidine-type nitroxide 2,2,6,6-tetramethyl-piperidin-1-yloxyl (TEMPO), were calculated at different levels of theory, using species optimised at the B3-LYP/6-31G(d) level. The results are shown in Tables 3.3 to 3.5. The methods of calculation assessed include various DFT methods, relatively low-cost MP2 methods, and several computationally expensive high-level composite methods such as CBS-QB3[2] and methods from the G3 family.[3,4] Since the accuracy of G3 methods is dependent upon the specific method used and also the system examined, several different G3 methods were assessed, including methods using the "X" and "RAD" variation as well as the "MP2" approximation. Calculations were also performed using versions of the ONIOM approximation method[5] (described in Chapter 2.2.5) at different levels of theory, in order to examine its suitability for the calculation of reactions involving large nitroxide radical species. The results shown in Table 3.5 have been incorporated into a collaborative work, with colleagues in the Coote research group, on the use of DFT methods in studies of the thermodynamics of a wide range of radical reactions. This work was recently published in the *Journal of Physical Chemistry A*.[6]

The adiabatic *IEs* of several common nitroxides are shown in Table 3.3 and their corresponding *EAs* are shown in Table 3.4. Experimental *IEs* are available for di-*tert*-butyl nitroxide (DBN) as well as for 2,2,6,6-tetramethyl-piperidin-1-yloxyl (TEMPO),[7] however the temperature at which these experiments were carried out is unclear. The results may therefore deviate from the 0 K values calculated in the present work by a small thermal correction. Taking this into consideration, calculations performed at the highest levels of theory compare reasonably well with experimental data.

The adiabatic *IEs* and *EAs* shown in Table 3.3 and 3.4 were benchmarked against the highest calculated level, G3X. The composite G3 and CBS-QB3 methods all produced accurate *IEs* and *EAs* with respect to the benchmark value. Mean absolute deviations (MADs) for the calculation of *IEs* and *EAs* are up to 0.03 eV (2.9 $kJmol^{-1}$), with only slightly higher values for the calculation of *EAs* at the CBS-QB3 level. The method G3(MP2)-RAD was selected as an appropriate high-level method to use for reactions throughout this work because it is the lowest-cost G3 method that includes the "RAD" variant, especially designed to deal with open-shell species.[4] Gas-

phase enthalpies of trapping of various alkyl radicals by the six-membered piperidine-type nitroxide 2,2,6,6-tetramethyl-piperidin-1-yloxyl (TEMPO) (see Table 3.5) were therefore benchmarked against the G3(MP2)-RAD level of theory.

Table 3.3 Effect of the level of theory used for single-point energies on the adiabatic ionisation energy (at 0 K) of nitroxides[a]

Level of Theory	*IE* (eV)						MAD[b] (eV)
			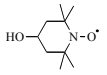		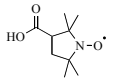		
B3-LYP/6-311+G(3df,2p)	6.91	6.97	7.07	7.36	7.15	7.28	0.11
MPW1B95/6-311+G(3df,2p)	6.80	6.86	6.96	7.24	7.01	7.15	0.01
MPW1K/6-311+G(3df,2p)	7.04	7.10	7.20	7.50	7.27	7.41	0.24
MPWB1K/6-311+G(3df,2p)	6.89	6.95	7.04	7.34	7.10	7.25	0.08
RMP2/6-311+G(3df,2p)	6.70	6.76	6.85	7.09	6.94	7.08	0.12
ONIOM (B3-LYP)[c]	6.72	6.78	6.88	7.16	6.95	7.09	0.09
ONIOM (RMP2)[c]	6.90	6.96	7.04	7.28	7.13	7.27	0.08
UCBS-QB3	6.83	6.89	6.98	7.25	7.03	7.17	0.01
CBS-QB3	6.83	6.90	6.99	7.26	7.04	7.18	0.02
G3(MP2)	6.83	6.90	6.99	7.26	7.04	7.17	0.02
G3X(MP2)	6.82	6.89	6.99	7.25	7.03	7.16	0.01
G3(MP2)-RAD	6.85	6.91	7.01	7.27	7.06	7.19	0.03
G3X(MP2)-RAD	6.85	6.91	7.01	7.27	7.06	7.19	0.03
G3	6.81	6.88	6.98	7.24	-	7.16	0.00
G3X	6.81	6.88	6.97	7.24	-	7.15	0
Experimental[c]	6.77	6.73	-	-	-	-	0.10

[a]Calculated on species optimised at the B3-LYP/6-31G(d) level. [b]Mean absolute deviation from the benchmark G3X value. [c]Found using G3(MP2)-RAD core systems $(CH_3)_2NO^{\bullet}$, and $(CH_3)_2NO^{-}$, with the full system calculated at the stated level with a 6-311+G(3df,2p) basis set. [c]Reported by Morishima *et al.*[7]

The use of various low-cost DFT and MP2 procedures in the calculation of *IEs*, *EAs* and trapping enthalpies was examined with a view to finding a suitable method to use for larger systems for which G3(MP2)-RAD calculations are impractical. In the past, single-point energies calculated using either DFT[8-10] or MP2[11] procedures have been adopted as low-cost methods for calculating electrode

potentials. From Table 3.3 it is seen that the DFT methods MPW1B95 and MPWB1K produce *IEs* very close to the benchmark G3X values. The MAD of the MPW1B95 *IE* values from the benchmark G3X values is only 0.01 eV (1.0 $kJmol^{-1}$). However, this same method produces *EAs* with large differences from the G3X values, showing an MAD of 0.36 eV (35 $kJmol^{-1}$). In general, the DFT and RMP2 methods fail to reproduce the benchmark *IE* and *EA* values. The trapping enthalpies shown in Table 3.5 also show large and unpredictable deviations for a wide range of DFT methods, with MADs over 25 $kJmol^{-1}$, and in some cases over 80 $kJmol^{-1}$. The RMP2 method gives better results, but the enthalpy values still differ from the benchmark values by an average of 8.0 $kJmol^{-1}$. It is therefore clear that the DFT and RMP2 methods assessed are not suitable as an accurate low-cost methods for reactions in this study.

It has previously been shown that an ONIOM method can been used to approximate G3(MP2)-RAD energies of radical reactions at a much lower computational cost.[12] To test the accuracy of this approach for nitroxide reactions, *IEs*, *EAs* and trapping enthalpies of nitroxides were also calculated using a version of ONIOM. In this approach the full reaction system was calculated using a method such as B3-LYP, BMK or RMP2 with a large 6-311+G(3df,2p) basis set, while only a core reaction system was calculated at G3(MP2)-RAD. The core system was set up to include substituents up to the β-position in the nitroxide, so that in the core the nitroxide was represented by the small species di-methyl nitroxide, $(CH_3)_2NO^{\bullet}$. In all reactions studied, the results obtained using an ONIOM method show excellent agreement with the G3(MP2)-RAD value. The best results were obtained with the substituent effect measured using RMP2/6-311+G(3df,2p) (see Tables 3.2 to 3.5). In this case, the MADs, relative to full G3(MP2)-RAD calculations, are only 0.05 eV (4.8 $kJmol^{-1}$) for *IEs*, 0.03 eV (2.9 $kJmol^{-1}$) for *EAs* and 4.7 $kJmol^{-1}$ for alkyl radical trapping enthalpies. Therefore, when the computational cost of G3(MP2)-RAD becomes excessive, it is expected that an ONIOM approximation, in which the full nitroxide system is represented by di-methyl nitroxide, will still give a reasonable approximation to the full G3(MP2)-RAD calculated energy.

Table 3.4 Effect of the level of theory used for single-point energies on the adiabatic electron affinity (at 0 K) of nitroxides[a]

Level of Theory	*EA* (eV)						MAD[b] (eV)
			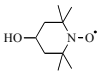		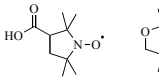		
B3-LYP/6-311+G(3df,2p)	0.29	0.31	0.49	0.71	0.44	0.41	0.26
MPW1B95/6-311+G(3df,2p)	0.16	0.22	0.39	0.62	0.32	0.29	0.36
MPW1K/6-311+G(3df,2p)	0.08	0.12	0.29	0.53	0.21	0.21	0.46
MPWB1K/6-311+G(3df,2p)	0.09	0.15	0.32	0.56	0.23	0.22	0.43
RMP2/6-311+G(3df,2p)	0.41	0.46	0.65	0.88	0.51	0.51	0.12
ONIOM (B3-LYP)[c]	0.48	0.50	0.67	0.90	0.63	0.60	0.07
ONIOM (RMP2)[c]	0.48	0.54	0.73	0.96	0.59	0.58	0.04
UCBS-QB3	0.48	0.52	0.69	0.91	0.59	0.60	0.06
CBS-QB3	0.47	0.51	0.69	0.90	0.59	0.59	0.07
G3(MP2)	0.55	0.59	0.77	0.98	0.68	0.67	0.01
G3X(MP2)	0.55	0.59	0.77	0.98	0.68	0.67	0.01
G3(MP2)-RAD	0.52	0.56	0.74	0.95	0.63	0.63	0.02
G3X(MP2)-RAD	0.52	0.56	0.74	0.96	0.64	0.64	0.02
G3	0.53	0.57	0.75	0.96	-	0.66	0.00
G3X	0.53	0.58	0.76	0.97	-	0.66	0

[a]Calculated on species optimised at the B3-LYP/6-31G(d) level. [b]Mean absolute deviation from the benchmark G3X value. [c]Found using G3(MP2)-RAD core systems $(CH_3)_2NO^{\bullet}$, and $(CH_3)_2NO^{-}$, with the full system calculated at the stated level with a 6-311+G(3df,2p) basis set.

While an ONIOM approximation using a di-methyl nitroxide core provides a good estimation of a G3(MP2)-RAD calculation, it is expected that treating the entire ring structure of the nitroxide system as a complete functional group and including it intact in the core reaction will give an even better approximation. Thus, this method was applied where possible throughout this work. A di-methyl nitroxide core was used when the computational cost of including the entire unsubstituted nitroxide ring structure in the core was too large.

Table 3.5 Effect of the level of theory used for single-point energies on the gas-phase enthalpy of trapping[a] (0 K, kJmol^{-1}) of various alkyl radicals by TEMPO[b]

Level of Theory	Enthalpy of trapping (kJmol^{-1})							MAD[c] (kJmol^{-1})
	$\cdot CH_3$							
RHF	-108.0	-118.0	-119.0	-96.9	-64.8	-129.9	-88.8	99.3
PBE	-165.0	-164.3	-164.9	-144.6	-115.8	-174.9	-105.4	55.1
B-LYP	-140.6	-138.9	-139.1	-116.2	-85.1	-146.9	-76.6	82.5
B3-YP	-151.0	-151.9	-152.6	-130.8	-101.0	-161.1	-93.3	68.4
B3P86	-167.9	-168.9	-169.8	-149.5	-121.1	-180.4	-111.9	50.2
KMLYP	-126.5	-130.6	-133.2	-112.9	-88.0	-144.4	-80.7	86.3
B1B95	-173.7	-174.4	-175.3	-155.1	-125.8	-183.2	-116.8	45.2
MPWPW91	-155.7	-154.5	-155.0	-133.3	-102.9	-164.9	-94.7	65.7
MPW1B95	-181.4	-183.1	-184.0	-165.1	-137.3	-192.3	-126.8	35.8
BB1K	-176.7	-179.2	-180.2	-160.7	-132.0	-188.9	-123.6	39.9
MPW1K	-159.1	-162.7	-163.9	-143.2	-113.7	-175.2	-108.5	56.4
MPWB1K	-182.9	-186.1	-187.2	-168.7	-141.2	-196.1	-131.5	32.4
BMK	-185.8	-190.1	-191.3	-174.7	-149.9	-198.4	-140.9	27.1
RMP2	-203.9	-219.8	-222.6	-216.5	-201.5	-229.6	-182.6	8.0
ONIOM (B3-LYP)[d]	-188.0	-199.7	-201.6	-192.1	-177.4	-213.9	-160.1	12.6
ONIOM (BMK)[d]	-194.4	-206.2	-208.2	-198.8	-181.9	-218.8	-167.1	6.5
ONIOM (RMP2)[d]	-193.2	-207.5	-210.1	-202.8	-186.4	-218.1	-169.9	4.7
G3(MP2)-RAD	-197.8	-211.8	-214.4	-207.1	-192.0	-223.3	-174.3	0

[a]Calculated with 6-311+G(3df,2p) basis sets (except at the G3(MP2)-RAD level), for species optimised at the B3-LYP/6-31G(d) level. [b]2,2,6,6-tetramethyl-piperidin-1-yloxyl. [c]Mean absolute deviation from the benchmark G3(MP2)-RAD value. [d]Found using G3(MP2)-RAD core systems with $(CH_3)_2NO^{\bullet}$ used in place of TEMPO, with the full system calculated at the stated level with a 6-311+G(3df,2p) basis set.

There are very limited experimental data for the gas-phase trapping of radical species by nitroxide radicals. However, experimental heats of formation are available in literature sources for the individual reactants and products that make up some small trapping reactions of oxygen and nitrogen-centred radicals.[13] These allowed the gas-phase trapping enthalpies of the reactions to be determined. The calculated and experimental enthalpies are shown in Table 3.6. Since these reactions involve small species, the experimental values could be compared with the very high-level method W1U.[14]

Enthalpies calculated using the recently reported G4[15] method were also determined and are included in Table 3.6 for completeness. Studies, performed with colleagues in the Coote research group and related to this work, have shown that this method does not offer significant improvement over the various G3 methods for radical addition and abstraction reactions. These results were recently published in the *Journal of Physical Chemistry A*.[16]

Reactions examined in Table 3.6 include the small nitroxide trapping reaction of $H_2NO^{\bullet}$ and $^{\bullet}CH_3$ as well as trapping reactions of similar small oxygen and nitrogen-centred radicals. Enthalpies, calculated using the highest theoretical method assessed W1U, show an MAD from experimental values of 4.3 kJmol^{-1}. The respective MAD for the G3(MP2)-RAD values is only marginally larger, at 6.3 kJmol^{-1}. Moreover, for the trapping reaction of a methyl radical by the oxygen-centred radical $H_3CO^{\bullet}$ (which is most relevant to the present work), the two G3 methods show the smallest deviations from the experiment values. G3(MP2)-RAD is capable of reproducing gas-phase experimental results to within 5 kJmol^{-1} for the studied reactions, and thus achieves chemical accuracy. This method was therefore adopted as an accurate method with which to calculate gas-phase energies throughout this work.

Table 3.6 Calculated[a] and experimental[b] enthalpies (298 K) for gas-phase radical trapping reactions

Reaction	Enthalpy of trapping (kJmol^{-1})					
	CBS-QB3	G3(MP2)-RAD	G3X	G4	W1U	Experimental
$H_2N^{\bullet} + {}^{\bullet}H \rightarrow NH_3$	-447.8	-443.0	-438.8	-441.4	-447.9	-454.3
$H_2N^{\bullet} + {}^{\bullet}CH_3 \rightarrow H_2NCH_3$	-357.0	-346.8	-348.5	-350.1	-354.8	-359.9
$H_3CO^{\bullet} + {}^{\bullet}H \rightarrow CH_3OH$	-437.9	-435.9	-430.3	-431.5	-438.4	-436.0
$H_3CO^{\bullet} + {}^{\bullet}CH_3 \rightarrow H_3COCH_3$	-356.3	-347.5	-348.5	-347.1	-351.5	-348.1
$H_2NO^{\bullet} + {}^{\bullet}CH_3 \rightarrow H_2NOCH_3$	-240.1	-237.4	-237.0	-235.3	-237.6	-
MAD[c] (kJmol^{-1})	4.8	6.3	8.2	7.0	4.3	0

[a]Calculated at various levels of theory using literature recommended geometries. [b]Found from experimental gas-phase heats of formation.[13] [c]Mean absolute deviation from experimental values.

Reactions involving the combination of two radical species are expected to be very fast and essentially barrierless. The single-reference methods used for other reactions in this work are likely to be inadequate when studying the transition state structures and reaction pathways of the trapping reactions of nitroxides with other radical species and the dissociation of the products back to radical species. In order to calculate the full reaction pathway of the trapping reaction, a multireference treatment is required. Therefore, multiconfigurational self-consistent field (MCSCF) wavefunctions were constructed and used to calculate the energies along the path of the trapping reaction between the nitroxide species 2,2,6,6-tetramethyl-piperidin-1-yloxyl (TEMPO) and the isopropyl radical species $^{\bullet}CH(CH_3)_2$.

Figure 3.1 shows the reaction pathway of the trapping reaction of the isopropyl radical by TEMPO as well as the trapping of the same radical by the ONIOM core species $(CH_3)_2NO^{\bullet}$. The active space used for both reactions includes eight active electrons and five active orbitals, consisting of the σ-bonding and σ* anti-bonding orbitals of the forming bond as well as the lone pair orbitals on the nitrogen and oxygen atoms. The inclusion of lone pairs in the active space has previously been shown to be necessary in these types of calculations.[17] Single-point energies along the path were calculated at the MC-QDP2/6-31G(d)//FORS-MCSCF(8,5)/6-31G(d) level. This level of theory is a multiconfigurational quasidegenerate second order perturbative treatment on orbitals initially optimised using a multiconfigurational, self-consistent wavefunction of the fully optimised reaction space type.

The reaction surface of the trapping reaction shown in Figure 3.1 is a smooth curve, as expected, with no enthalpic barrier. A free energy barrier exists due to the effects of entropy, occurring at around 1.8Å separation for both TEMPO and the smaller nitroxide. Although the kinetic parameters of the reaction require multireference treatment, single-reference methods may be suitable for calculations of the thermodynamic parameters of these types of trapping reactions. This is because energies of only the reactant and product species are required. The T_1 diagnostic value[18] for the TEMPO–$CH(CH_3)_2$ alkoxyamine is 0.0051, indicating that ground-state alkoxyamine does not require multireference treatment. The trioxide-type species TEMPO–$OOCH(CH_3)_2$ formed from the combination of TEMPO and an isopropyl

peroxyl radical has a T_1 diagnostic value of 0.0076, showing that this species may also be treated with single-reference methods.

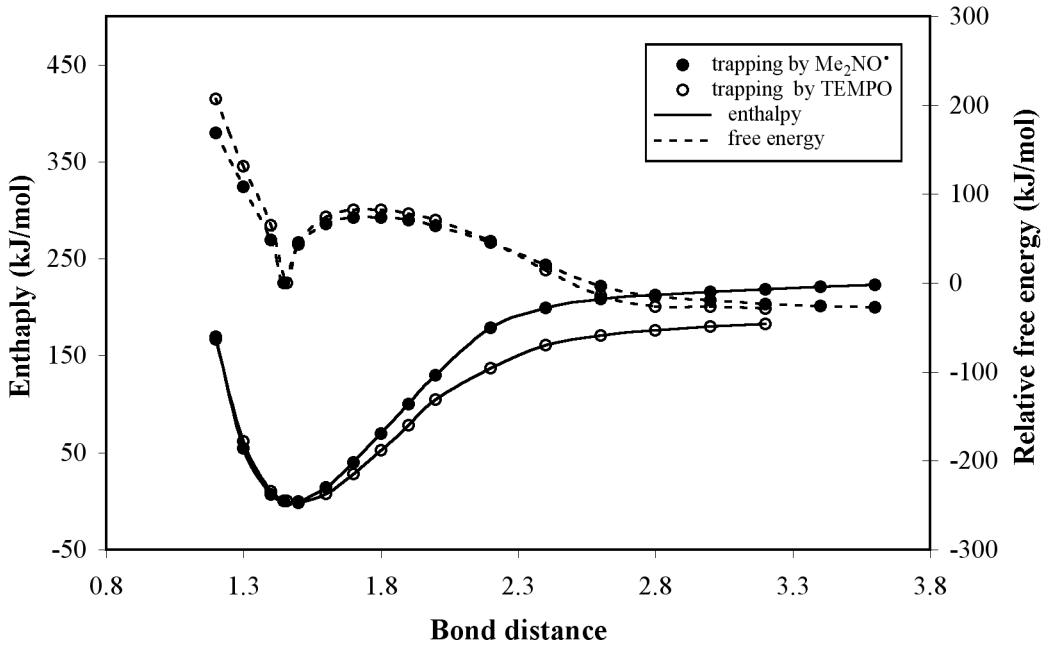

Figure 3.1 Energy surface for the addition of nitroxide to $^{\bullet}CH(CH_3)_2$

3.4 Free energies of solvation

The free energy of solvation, ΔG_{solv}, quantifies the free energy difference between a gas-phase system and the same system in a solvent medium caused by the stabilising or destabilising effect of solvent molecules. The value of ΔG_{solv} is calculated separately and added to the total gas-phase free energy when a calculation is performed in solution. Although it is possible to directly calculate total free energies in solution, as discussed in Chapter 2.3.2, this method generally gives poor results.

In order to assess the level of theory used to calculate free energies of solvation for nitroxide species in this work, calculated thermodynamic parameters of nitroxide reactions were compared with the experimental values found in literature sources. Oxidation potentials of common nitroxide radicals have previously been experimentally measured,[19,20] and are shown along with calculated values in Table

3.7. In order to make direct comparisons to the experimental values, oxidation potentials were calculated relative to the standard hydrogen electrode (SHE) in an aqueous medium as described in Chapter 2.4.2. The solution phase free energy of the H^+ half-reaction was taken as the experimental value -4.36 eV.[9] For the nitroxide half-reaction, gas-phase energies were calculated at the G3(MP2)-RAD//B3-LYP/6-31G(d) level and added to free energies of solvation calculated using different levels of theory, basis sets and solvation models. Since the accuracy of the gas-phase calculation has been separately validated, it was expected that any differences in the oxidation potentials would be caused by differences in the free energies of solvation.

Table 3.7 Effect of the level of theory used for free energies of solvation on the oxidation potentials (vs. SHE in water, 298 K) of nitroxides[a]

Solvation model[b]	Method	Basis set	Oxidation potential E^o_{ox} (V)					MAD[c] (V)
				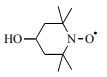		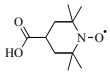	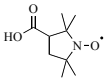	
PCM	HF	6-31G(d)	0.784	0.773	0.896	0.781	0.886	0.032
		6-311+G(3df,2p)	0.808	0.786	0.891	0.789	0.909	0.038
	B3-LYP	6-31G(d)	0.794	0.781	0.940	0.813	0.928	0.037
		6-311+G(3df,2p)	0.820	0.799	0.940	0.813	0.953	0.044
PCM[† d]	B3-LYP	6-31G(d)	0.762	0.756	0.946	0.794	0.910	0.034
CPCM	HF	6-31G(d)	0.784	0.772	0.894	0.780	0.895	0.034
		6-311+G(3df,2p)	0.808	0.784	0.892	0.784	0.911	0.039
	B3-LYP	6-31G(d)	0.794	0.779	0.935	0.810	0.927	0.036
		6-311+G(3df,2p)	0.821	0.799	0.940	0.810	0.954	0.044
Experimental[e]			0.740	0.825	0.918	0.805	0.870	0

[a]Incorporating gas-phase G3(MP2)-RAD//B3-LYP/6-31G(d) gas-phase energies. [b]Calculated using the united atom topological model with the recommended optimisation of radii ie. UAHF and UAKS keywords for the Hartree-Fock and B3-LYP methods, respectively.[21] [c]Mean absolute deviation from experimental values. [d]Calculated using the SCFVAC keyword[21] in GAUSSIAN 03.[22] [e]Reported by Goldstein *et al*[19] and Israeli *et al*[20].

Two methods of calculating solvation effects were assessed; the polarised continuum models PCM[23] and CPCM.[24] During the solvation energy calculations the molecular structures were re-optimised in an aqueous medium as implemented in the

GAUSSIAN 03[22] software package. The recommended radii were used for these calculations, with the united atom topological model, applied on radii optimised for the HF/6-31G(d) and PBE0/6-31G(d) levels of theory, used for the Hartree-Fock and B3-LYP methods respectively.[21] Previous calculations of reduction potentials of various nitrogen oxides, performed using similar methods, have been found to correlate with experimental data and to exhibit an average error of 0.12 V for both the PCM and CPCM methods.[25]

As Table 3.7 shows, calculated oxidation potentials vary only a small amount when different methods of calculating solvation energy are used. The MADs of the calculated potentials from the experimental values are between 0.032 V (3.1 $kJmol^{-1}$) and 0.044 V (4.2 $kJmol^{-1}$). The level of theory, basis set and solvation model have very little effect on the value of the free energy of solvation. As such, the method chosen for use in this work appeared to be fairly arbitrary. A PCM solvation model was chosen as it has previously been found to produce a lower maximum deviation from experimental data than that found using CPCM, for a range of nitrogen oxides.[25] As geometries are re-optimised during the solvation energy calculation, a B3-LYP level was chosen as it was shown in Chapter 3.2 to be a reliable method for geometry optimisations (see Tables 3.1 and 3.2). Notably, the use of a larger basis set actually increases the MAD, probably due to the fact that the (semi-empirical) solvation models are parameterised to the 6-31G(d) basis set.

During calculations using polarisable continuum model methods, the total free energy of a molecule in solution is determined. As discussed in Chapter 2.3.2, the low-level methods used for these calculations are not sufficient to describe the gas-phase component of the calculation. Therefore, in this work, the free energy of solvation of each molecule (measuring the stabilising or destabilising effect of the solvent) was extracted from the PCM calculation and added to an independently calculated high-level gas-phase free energy. Two estimates of the solvation energy were assessed, a simplified approximation obtained from a single calculation of the free energy in solution as described in Chapter 2.3.3, and the true solvating energy obtained using an SCFVAC keyword[21] during the GAUSSIAN 03[22] calculation. Using the SCFVAC keyword allows for the direct determination of the free energy of solvation through a second gas-phase calculation, so that the solvation energy is

calculated as the difference of the gas and solution phase free energies at the same level of theory.[21] As shown in Table 3.7, the MAD of the oxidation potential of nitroxides from experimental values is only slightly lowered when the SCFVAC keyword is used. Although the extra term generated by the SCFVAC keyword does not play a large role in the calculation, it was included in calculations performed in this work for completeness. Therefore, the PCM method at the B3-LYP/6-31G(d) level, using an SCFVAC keyword in the GAUSSIAN calculation, is a suitable method for the calculation of free energies of solvation for nitroxide radicals and related species.

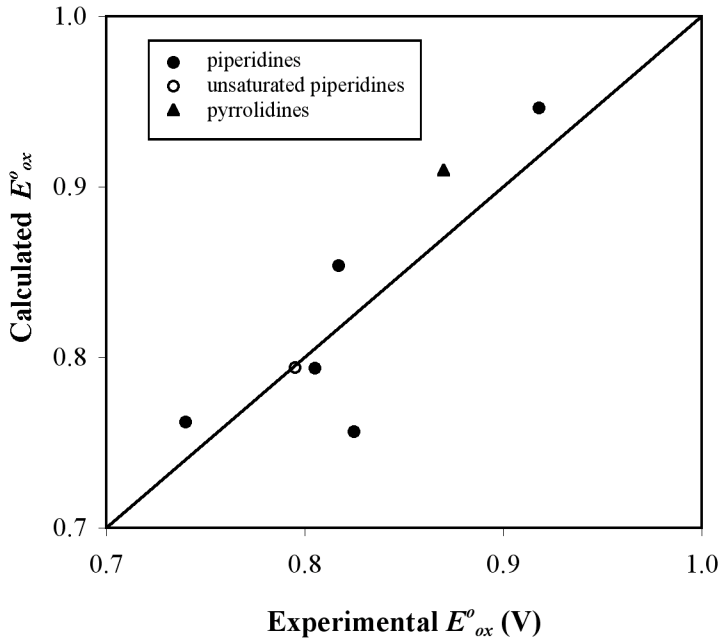

Figure 3.2 Correlation (R^2 = 0.745) between experimental and calculated oxidation potentials of nitroxides

In this work, oxidation potentials of nitroxide radicals were calculated using G3(MP2)-RAD//B3-LYP/6-31G(d) gas-phase energies and PCM free energies of solvation at the B3-LYP/6-31G(d) level. Figure 3.2 shows the correlation between the calculated and experimental[19,20] oxidation potentials of some common nitroxide radicals. As well as those assessed in Table 3.7, results for two additional piperidine derivatives are shown, one with a charged ammonio (H_3N^+) group at the 4-position

and one showing unsaturation in the six-membered ring (labelled **13** and **14** in Table 4.1). The calculated values compare well with experimental results. The one outlying point, for the species 4-hydroxy-2,2,6,6-tetramethyl-piperidin-1-yloxyl (4-hydroxy-TEMPO), shows a difference from experiment of 0.069 V (6.6 kJmol^{-1}). The other nitroxide species show an MAD of 0.023 V (2.2 kJmol^{-1}) from the experimental results, with a maximum deviation of 0.040 V (3.8 kJmol^{-1}).

Nitroxide reduction is a more complex process than oxidation. The addition of an electron and a proton to a nitroxide radical produces a hydroxylamine species, as shown in Scheme 2.2 in Chapter 2.4.2. The multi-step reaction mechanism, shown in Scheme 2.3, was previously suggested for this process.[26] In this mechanism, the reduction half-wave potential is determined from the formal reduction potential, E^o_{red}, and the acid dissociation constants, K_1 and K_2, of two subsequent protonation steps through Equation (2.39).[27] Therefore, a full systematic examination of the effects of the level of theory used to calculate solvation free energies in the determination of reduction potentials is not feasible.

Half-wave reduction potentials, comparable to experimental values were calculated for both TEMPO and 4-hydroxy-TEMPO, using appropriate methods identified during the assessment of the calculation of oxidation potentials. The formal reduction potentials, E^o_{red}, were calculated for the nitroxide half-reaction using the methods described in Chapter 2.4.2. Solution-phase free energies for the protonation Reactions (2.37) and (2.38) were obtained using the same theoretical methods (G3(MP2)-RAD//B3-LYP/6-31G(d) gas-phase energies and PCM solvation free energies at the B3-LYP/6-31G(d) level) and transformed to acid dissociation constants, K_1 and K_2, using the method of Liptak and Shields.[28] This method incorporates experimental values of H^+, a gas-phase energy of -6.28 kcalmol^{-1}, and a free energy of solvation of -264.61 kcalmol^{-1}.

Using the determined values of E^o_{red}, K_1 and K_2, the half-wave potentials of TEMPO and 4-hydroxy-TEMPO were calculated using Equation (2.39), at room temperature and pH 7 ($[H^+] = 10^{-7}$), to be -0.031 and -0.011 V respectively when calibrated against a saturated calomel reference electrode (SCE). These values show agreement to within 0.010 V (1.0 kJmol^{-1}) with the reported experimental values for

the same species, -0.037 and -0.016 V.[27] A subsequent study reported the half-wave potentials of reduction for the same species versus the standard hydrogen electrode (SHE).[20] Using Equation (2.39), calculated half-wave potentials (again at room temperature and pH 7) versus SHE of TEMPO and 4-hydroxy-TEMPO were found to be 0.213 and 0.233 V, respectively. These values are in good agreement with the corresponding experimental values (estimated from Figure 6 in the literature reference[20] to be approximately 0.2 V in each case).

In the previous sections, reliable methods were identified for the determination of geometries, gas-phase single-point energies and free energies of solvation for nitroxide species. To verify the robustness of these methods, additional comparisons

Table 3.8 Calculated[a] and experimental[b] equilibrium constants (at 393 K) for radical trapping reactions by nitroxide radicals in solution

Nitroxide	Radical	$k_{c,393,t\mathrm{BB}}$ ($\mathrm{Lmol^{-1}s^{-1}}$)	$k_{d,393,t\mathrm{BB}}$ ($\mathrm{s^{-1}}$)	Experimental $K_{393}=k_c/k_d$	Calculated $K_{393,\mathrm{toluene}}$ ($\mathrm{Lmol^{-1}}$)
		2.1×10^{8}	1.9×10^{-4}	1.1×10^{12}	4.1×10^{11}
		3.5×10^{8}	1.1×10^{-5}	3.2×10^{13}	7.8×10^{12}
		2.5×10^{8}	5.2×10^{-4}	4.8×10^{11}	2.6×10^{11}
		5.5×10^{7}	8.5×10^{-2}	6.5×10^{8}	4.5×10^{9}
		2.3×10^{9} [d]	8.1×10^{-8}	2.8×10^{16}	3.0×10^{15}
		5.9×10^{8}	2.2×10^{-2}	2.7×10^{10}	4.4×10^{10}
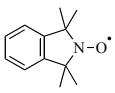		1.5×10^{8} [e]	2.2×10^{-4}	6.8×10^{11}	2.3×10^{10}
		1.5×10^{8}	4.1×10^{-2}	3.7×10^{9}	3.0×10^{9}

[a]Found using ONIOM approximated G3(MP2)-RAD//B3-LYP/6-31G(d) gas-phase energies using core systems of $(CH_3)_2NO^{\bullet}$ (with the full system calculated at the RMP2/ 6-311+G(3df,2p) level) and PCM solvation energies at the B3-LYP/6-31G(d) level. [b]As reported by Fischer, Marque and coworkers.[29-31] [c]Experimental and calculated values determined in acetonitrile. [d]Determined at 297 K. [e]Determined at 293 K.

of nitroxide reactions with experimental results were conducted. The solution-phase equilibrium constants for radical trapping reactions of a range of carbon-centred radicals by nitroxides were calculated and compared with available experimental data.[29-31] The results are shown in Table 3.8 and plotted in Figure 3.3. The experimental equilibrium constant, $K = k_c/k_d$, was obtained by combining independently measured values of the rate coefficients for the forward, k_c, and reverse, k_d, trapping reactions. Since the experimental measurements were performed at 393 K in *tert*-butyl benzene (*t*BB), the *ab initio* equilibrium constants were also calculated at 393 K from the solution-phase reaction free energies of the individual species determined in the closely related solvent toluene.

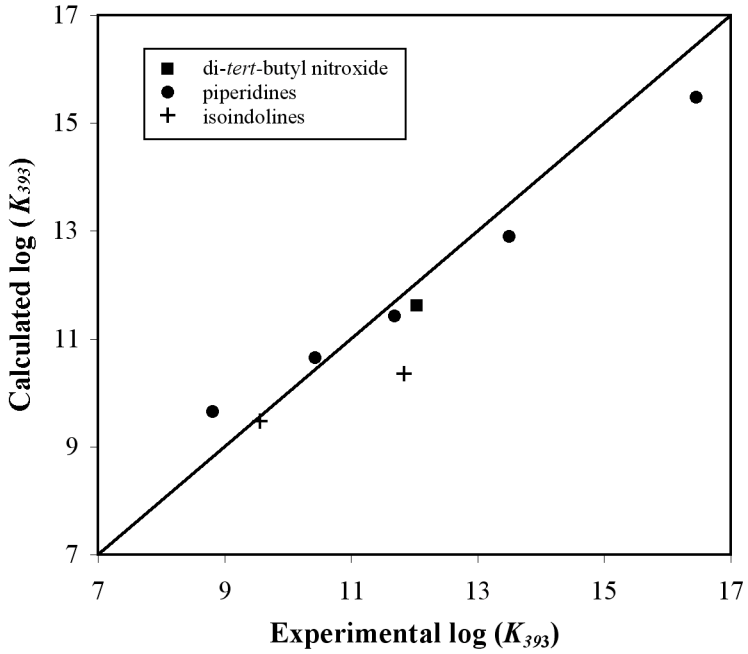

Figure 3.3 Correlation (R^2 = 0.933) between experimental and calculated equilibrium constants for nitroxide trapping of alkyl radicals

Table 3.8 and Figure 3.3 show the agreement between calculated equilibrium constants of the trapping of alkyl radicals by nitroxides, and the experimentally determined values. The differences are generally within half an order of magnitude, although larger variations are seen for species for which the only available experimental combination rate coefficients were measured at lower temperatures than

those at which polymerisation reactions are typically carried out. The calculated values for the nitroxide species show an MAD from the experimental results corresponding to 4.6 kJmol^{-1} in free energy. The maximum deviation is observed for the trapping of the phenylethyl radical, $^{\bullet}CH(CH_3)Ph$, by the five-membered isoindoline derivative 1,1,3,3-tetramethylisoindolin-2-yloxyl (TMIO). The calculated value for this reaction shows a deviation from experiment corresponding to 11.1 kJmol^{-1} in free energy.

3.5 Conclusions

A series of assessment studies were used to determine appropriate levels for the calculation of the nitroxide reactions in this work. It was determined that G3(MP2)-RAD//B3-LYP/6-31G(d) is an appropriate level of theory for the calculation of gas-phase nitroxide reactions and molecular properties, with an ONIOM approximation (in which the full system is calculated at the RMP2/6-311+G(3df,2p) level of theory) providing good results for large systems. The full reaction pathway for the combination of two radical species can be plotted from points calculated at the MC-QDP2/6-31G(d)//FORS-MCSCF/6-31G(d) level of theory, using an active space made up of the bonding and anti-bonding orbitals and adjacent lone pairs. However, it was found that in order to determine thermodynamics parameters of these types of reactions, single reference methods are appropriate. For reactions calculated in solution, the effects of the solvent medium are well described by a PCM method at the B3-LYP/6-31G(d) level using the SCFVAC keyword in the GAUSSIAN calculation. Using the methods determined in this chapter, deviations between calculated values of nitroxide-based reactions and available experimental results are around 5 kJmol^{-1}. Based on this, chemical accuracy is achieved.

3.6 References

(1) Siri, D.; Gaudel-Siri, A.; Tordo, P. *J. Mol. Struct. (Theochem)* **2002**, *582*, 171.

(2) Montgomery Jr., J. A.; Frisch, M. J.; Ochterski, J. W.; Petersson, G. A. *J. Chem. Phys*. **2000**, *112*, 6532.

(3) Curtiss, L. A.; Raghavachari, K. *Theor. Chem. Acc*. **2002**, *108*, 61.

(4) Henry, D. J.; Sullivan, M. B.; Radom, L. *J. Chem. Phys*. **2003**, *118*, 4849.

(5) Humbel, S.; Sieber, S.; Morokuma, K. *J. Chem. Phys.* **1996**, *105*, 1959.

(6) Izgorodina, E. I.; Brittain, D. B. R.; Hodgson, J. L.; Krenske, E. H.; Lin, C. Y.; Namazian, M.; Coote, M. L. *J. Phys. Chem. A* **2007**, *111*, 10754.

(7) Morishima, I.; Yoshikawa, K.; Yonezawa, T.; Matsumoto, H. *Chem. Phys. Lett.* **1972**, *16*, 336.

(8) Fu, Y.; Yu, H.-Z.; Wang, Y.-M.; Guo, Q.-X. *J. Am. Chem. Soc.* **2005**, *127*, 7227.

(9) Winget, P.; Cramer, C. J.; Truhlar, D. G. *Theor. Chem. Acc.* **2004**, *112*, 217.

(10) Patterson, E. V.; Cramer, C. J.; Truhlar, D. G. *J. Am. Chem. Soc.* **2001**, *123*, 2025.

(11) Namazian, M.; Siahrostami, S.; Noorbala, M. R.; Coote, M. L. *J. Mol. Struct. (Theochem)* **2006**, *759*, 245.

(12) Izgorodina, E. I.; Coote, M. L. *J. Phys. Chem. A* **2006**, *110*, 2486.

(13) Afeefy, H. Y.; Liebman, J. F.; Stein, S. E. "Neutral Thermochemical Data", In *NIST Chemistry WebBook, NIST Standard Reference Database Number 69*, Linstrom P. J. and Mallard, W. G., Eds. National Institute of Standards and Technology: Gaithersburg, http://webbook.nist.gov, (retrieved 26 October, 2007).

(14) Martin, J. M. L.; de Oliveira, G. J. *J. Chem. Phys.* **1999**, *111*, 1843.

(15) Curtiss, L. A.; Redfern, P. C.; Raghavachari, K. *J. Chem. Phys.* **2007**, *126*, 084108.

(16) Lin, C. Y.; Hodgson, J. L.; Namazian, M.; Coote, M. L. *J. Phys. Chem. A* **2009**, *113*.

(17) Kutateladze, A. G. *J. Am. Chem. Soc.* **2001**, *123*, 9279.

(18) Lee, T. J.; Taylor, P. R. *Int. J. Quant. Chem. Symp.* **1989**, *23*, 199.

(19) Goldstein, S.; Samuni, A.; Hideg, K.; Merenyi, G. *J. Phys. Chem. A* **2006**, *110*, 3679.

(20) Israeli, A.; Patt, M.; Oron, M.; Samuni, A.; Kohen, R.; Goldstein, S. *Free Radical Biol. Med.* **2005**, *38*, 317.

(21) Frisch, A.; Frisch, M. J.; Trucks, G. W. *Gaussian 03 User's Reference*; Gaussian, Inc.: Wallingford, CT, 2003.

(22) Frisch, M. J.; Trucks, G. W.; Schlegel, H. B.; Scuseria, G. E.; Robb, M. A.; Cheeseman, J. R.; Montgomery Jr., J. A.; Vreven, T.; Kudin, K. N.; Burant, J. C.; Millam, J. M.; Iyengar, S. S.; Tomasi, J.; Barone, V.; Mennucci, B.; Cossi, M.; Scalmani, G.; Rega, N.; Petersson, G. A.; Nakatsuji, H.; Hada, M.; Ehara, M.; Toyota, K.; Fukuda, R.; Hasegawa, J.; Ishida, M.; Nakajima, T.; Honda, Y.; Kitao, O.; Nakai, H.; Klene, M.; Li, X.; Knox, J. E.; Hratchian, H. P.; Cross, J. B.; Adamo, C.; Jaramillo, J.; Gomperts, R.; Stratmann, R. E.; Yazyev, O.; Austin, A. J.; Cammi, R.; Pomelli, C.; Ochterski, J. W.; Ayala, P. Y.; Morokuma, K.; Voth, G. A.; Salvador, P.; Dannenberg, J. J.; Zakrzewski, V. G.; Dapprich, S.; Daniels, A. D.; Strain, M. C.; Farkas, O.; Malick, D. K.; Rabuck, A. D.; Raghavachari, K.; Foresman, J. B.; Ortiz, J. V.; Cui, Q.; Baboul, A. G.; Clifford, S.; Cioslowski, J.; Stefanov, B. B.; Liu, G.; Liashenko, A.; Piskorz, P.; Komaromi, I.; Martin, R. L.; Fox, D. J.; Keith, T.; Al-Laham, M. A.; Peng, C. Y.; Nanayakkara, A.; Challacombe, M.; Gill, P. M. W.; Johnson, B.; Chen, W.; Wong, M. W.; Gonzalez, C.; Pople, J. A. *Gaussian 03, Revision B.03*; Gaussian, Inc.: Pittsburgh PA, 2003.

(23) (a) Cancès, M. T.; Mennucci, B.; Tomasi, J. *J. Chem. Phys.* **1997**, *107*, 3032. (b) Cossi, M.; Barone, V.; Mennucci, B.; Tomasi, J. *Chem. Phys. Lett.* **1998**, *286*, 253. (c) Mennucci, B.; Tomasi, J. *J. Chem. Phys.* **1997**, *106*, 5151.

(24) (a) Barone, V.; Cossi, M. *J. Phys. Chem. A* **1998**, *102*, 1995. (b) Cossi, M.; Rega, N.; Scalmani, G.; Barone, V. *J. Comp. Chem.* **2003**, *24*, 669.

(25) Dutton, A. S.; Fukuto, J. M.; Houk, K. N. *Inorg. Chem.* **2005**, *44*, 4024.

(26) Fish, J. R.; Swarts, S. G.; Sevilla, M. D.; Malinski, T. *J. Phys. Chem.* **1988**, *92*, 3745.

(27) Kato, Y.; Shimizu, Y.; Yijing, L.; Unoura, K.; Utsumi, H.; Ogata, T. *Electrochim. Acta* **1995**, *40*, 2799.

(28) Liptak, M. D.; Shields, G. C. *J. Am. Chem. Soc.* **2001**, *123*, 7314.

(29) Sobek, J.; Martschke, R.; Fischer, H. *J. Am. Chem. Soc.* **2001**, *123*, 2849.

(30) Fischer, H.; Marque, S. R. A.; Nesvadba, P. *Helvetica Chimica Acta* **2006**, *89*, 2330.

(31) Marque, S. R. A.; Le Mercier, C.; Tordo, P.; Fischer, H. *Macromol.* **2000**, *33*, 4402.

Chapter 4.

Biological Protection Mechanisms

4.1 Introduction 64
4.2 Literature review 64
4.2.1 Superoxide dismutase mimic activity 66
4.2.2 Inhibition of the Fenton reaction 68
4.2.3 Inhibition of lipid peroxidation 70
4.2.4 Enhancement of catalase-like activity of heme proteins 72
4.2.5 Detoxification of semiquinones 74
4.2.6 Protection against radiation-induced damage 75
4.3 Electrode potentials of nitroxides 77
4.3.1 Oxidation and reduction potentials of nitroxides 78
4.3.2 Comparison of oxidation potentials to experimental values 85
4.4 Biological protection using nitroxides 88
4.4.1 Superoxide dismutase mimicking mechanisms 88
4.4.2 Reduction-based protection mechanisms 91
4.4.3 Oxidation-based protection mechanisms 93
4.4.4 Scavenging mechanisms 93
4.4.5 Experimental protection data 94
4.5 Conclusions 99
4.6 References 100

4.1 Introduction

The protection against oxidative damage afforded by nitroxides in biological systems has been previously well documented. In this chapter, the reactions through which such protection occurs will be investigated, and attempts will be made to determine which out of a range of nitroxides should be the more effective protecting agents. Even a cursory examination of literature on this subject reveals a wide range of damaging free radical and other species against which nitroxides are said to protect, and a variety of different mechanisms by which protection is suggested to occur. Therefore, any investigation into the actions of nitroxides in biological systems will first require an extensive literature survey. Until recently, such a review had not been attempted, however, soon after the completion of the literature review for this work, a review covering these areas was published in the journal *Free Radical Biology & Medicine*.[1] This review supports the conclusions of the literature review, conducted as part of this work, which is presented in this chapter.

4.2 Literature review

Many free radicals are highly reactive species able to cause damage in biological systems via various different mechanisms. Reactive oxygen species such as superoxide, hydrogen peroxide and hydroxyl radicals exert cytotoxicity by the oxidation of biomolecules, damaging critical cellular components. Hydroxyl, alkoxyl, and peroxyl radicals have been reported to cause damage to DNA by cleaving the phosphodiester backbone and leading to single and double breaks, and have also been shown to oxidise DNA bases giving highly mutagenic products.[2,3] The superoxide radical anion ($O_2^{\bullet -}$) shows little reactivity towards DNA bases, being a poor oxidant at physiological pH,[4] however in its conjugate acid form ($HOO^{\bullet}$) it is thought to cause DNA strand-nicking through the 5′-hydrogen atom abstraction from the deoxyribose ring.[5] Reactive oxygen species are also known to damage various lipids through the initiation and mediation of lipid peroxidation,[6] and are responsible for the inactivity of certain enzymes,[7] catalases,[8] and peroxidases.[9]

Reactive oxygen species causing damage to biological systems are usually detoxified by antioxidants already present for this purpose. Enzymatic antioxidants

consume reactive oxygen species in a catalytic fashion. These include superoxide dismutase (SOD), which dismutes $O_2^{\bullet -}$ into H_2O_2 and O_2,[10] catalases, which dismute H_2O_2 into water and O_2, and various peroxidases, including glutathione peroxidase, which reduce H_2O_2 into water.[11] Non-ezymatic antioxidants such as α-tocopherol (vitamin E) detoxify radicals by hydrogen atom donation.[12] In some cases however, the actions of enzymatic and non-ezymatic antioxidants may be inadequate, causing an excess of reactive oxygen species and a state of "oxidative stress". This imbalance may be caused by ionising radiation, or by medical conditions such as ataxia-telangiectasia, in which the gene responsible for sensing oxidative damage to DNA and subsequent activation of a signalling network leading to repair of the damage, is absent.[13] In these cases, supplementary antioxidants may be necessary in order to minimise biological damage.

Nitroxide radicals, stabilised by bulky substituents, are persistent in tissues and in the circulatory system, and have been shown to be effective against a wide range of types of oxidative damage in various experimental models. This is due to the many desirable features they possess including the ability to be reversibly oxidised to their respective oxoammonium cations and reduced to hydroxylamines with relative ease, and the ability to scavenge a wide range of reactive species. They are capable of penetrating through membranes into cellular compartments and have also proved to be relatively non-cytotoxic.[14] Studies have shown that nitroxides attenuate oxidative damage in a variety of experimental models including cells,[15] xenobiotics toxicity,[16] lipid peroxidation in liver microsomes,[17] intestinal and gastric lesions,[18] experimental pancreatitis,[19] thymocyte apoptosis,[20] hyperoxia-induced brain damage,[21] and closed-head injury induced by mechanical trauma.[22]

In this review of current literature, the main sources of oxidative stress will be examined and the effectiveness of nitroxides in protecting from damage through various mechanisms will be discussed. Protection mechanisms involving nitroxides include catalytic removal of superoxide by SOD-mimicking activity, prevention of the Fenton reaction, inhibition of lipid peroxidation, improvement of the catalase-like activity of hemeproteins, detoxifcation of xenobiotic-derived semiquinones, and protection from ionising radiation-induced oxidative damage.

4.2.1 Superoxide dismutase mimic activity

The reactive oxygen species superoxide ($O_2^{\bullet -}$) is generated by a variety of metabolic processes in the presence of oxygen. It can act both as an oxidant and a reductant, and can give rise to other dangerous reactive oxygen species. The toxic effects of superoxide, as well as its dismutation catalysed by the metal-containing enzymatic antioxidants known as superoxide dismutases (SODs), have been known for some time.[10]

Superoxide and its conjugate acid ($HOO^{\bullet}$), with a pK_a of 4.7, undergo spontaneous dismutations as shown in Reactions (4.1) to (4.3).[23] The rates of Reactions (4.1) and (4.2) are fast (around 1×10^5 and 1×10^8 $Lmol^{-1}s^{-1}$ respectively), while Reaction (4.3) occurs with a much slower rate (< 0.3 $Lmol^{-1}s^{-1}$). Spontaneous dismutation occurs most rapidly at pH 4.7, decreasing as the pH is raised.[10b]

$$HOO^{\bullet} + HOO^{\bullet} \longrightarrow H_2O_2 + O_2 \quad (4.1)$$

$$HOO^{\bullet} + O_2^{\bullet -} + H^+ \longrightarrow H_2O_2 + O_2 \quad (4.2)$$

$$2O_2^{\bullet -} + 2H^+ \longrightarrow H_2O_2 + O_2 \quad (4.3)$$

Superoxide dismutases (SODs) contain a transition metal ion (Mt^n) that undergoes alternate reduction and re-oxidation reactions, catalysing Reaction (4.3). A range of different SODs, incorporating manganese, iron, copper and zinc, have all been shown to catalyse Reaction (4.3) through two half-reactions, shown in Reactions (4.4) and (4.5), with comparable efficiencies.

$$Mt^nSOD + O_2^{\bullet -} \longrightarrow Mt^{n-1}SOD + O_2 \quad (4.4)$$

$$Mt^{n-1}SOD + O_2^{\bullet -} + 2H^+ \longrightarrow Mt^nSOD + H_2O_2 \quad (4.5)$$

The dismutation half-reactions occur with fast rates. For example, the copper-containing dismutation reaction shows rate constants of around 1×10^9 $Lmol^{-1}s^{-1}$ at room temperature for Reactions (4.4) and (4.5), and has proved to be insensitive to pH over a wide range.[10b] SOD activity has long been known to be abundant in a wide variety of mammalian organisms,[10a] and is thought to play a significant role in protection of the organism against the damaging effects of the superoxide radical. However, as native SOD is a relatively large molecule, it does not easily cross cell

membranes, complicating attempts to increase its intracellular concentrations. Therefore, compounds showing SOD-like activity, but with lower molecular weights and increased membrane permeability, have been sought. The antioxidant activity of nitroxides in protection against oxidative damage has been found to be linked, at least in part, to their ability to catalyse the dismutation of superoxide in SOD-mimicking reactions, with the added desirable feature that nitroxides act without the need for transition metals.[15]

Nitroxide radicals are well known to undergo one-electron oxidation and reduction reactions, by various chemical and electrochemical means, to yield their respective oxoammonium cations or hydroxylamines (see Scheme 2.2 in Chapter 2.4.2). Oxidation is kinetically and thermodynamically reversible, while reduction is an irreversible process due to protonation of the anionic species to form the hydroxylamine. Re-oxidation of hydroxylamines occurs at a higher potential than that of the initial reduction, showing that it is not an exact reversal of the reduction process.[24] The oxazolidine-type nitroxide 2-ethyl-2,5,5-trimethyl-3-oxazolidine-1-oxyl has been shown to be reduced, in the presence of superoxide, to its corresponding hydroxylamine with a rate constant strongly dependent upon pH (attributable to the different reactivities of $O_2^{\bullet -}$ and $HOO^{\bullet}$).[25] The hydroxylamine then reduces superoxide to hydrogen peroxide.[26] Therefore, oxazolidine-type nitroxides mimic the reactions undergone by native SODs by catalysing Reaction (4.3), through Reactions (4.6) and (4.7).

$$RR'NO^{\bullet} + O_2^{\bullet -} + H^+ \longrightarrow RR'NOH + O_2 \qquad (4.6)$$

$$RR'NOH + O_2^{\bullet -} + H^+ \longrightarrow RR'NO^{\bullet} + H_2O_2 \qquad (4.7)$$

In contrast, piperidine derivatives such as 2,2,6,6,-tetramethylpiperidin-1-yloxyl (TEMPO, **2**) show no significant decrease in EPR signal when exposed to superoxide, suggesting either that they lack SOD-like activity, or that any hydroxylamine formed is re-oxidised very rapidly.[15] However, only a slow rate constant of 4×10^2 $Lmol^{-1}s^{-1}$ was observed for the reaction of 4-hydroxy-TEMPOH (the hydroxylamine form of nitroxide **6**) with $O_2^{\bullet -}$. Based on these observations, dismutation involving a nitroxide/oxoammonium cation couple, shown in Reaction (4.8) and (4.9), was proposed.[27] The rate constant of dismutation was found to

increase with the concentration of H^+, indicating that protonated superoxide ($HOO^\bullet$) oxidises the nitroxide.[28]

$$RR'NO^\bullet + HOO^\bullet + H^+ \longrightarrow RR'N^+=O + H_2O_2 \quad (4.8)$$

$$RR'N^+=O + O_2^{\bullet -} \longrightarrow RR'NO^\bullet + O_2 \quad (4.9)$$

The dismutation of superoxide via Reactions (4.8) and (4.9) has been shown to have a rate of 1.2×10^5 $Lmol^{-1}s^{-1}$,[27] around two orders of magnitude faster than the catalytic cycle described in Reactions (4.6) and (4.7).[15] The restoration of a piperidine-type nitroxide via Reaction (4.9) occurs so quickly that no accumulation of the oxoammonium cation is detectable.[28] Although the SOD-mimetic activity of nitroxides is several orders of magnitude lower at physiological pH than that of native SODs, their lower molecular weights facilitate increased intracellular concentrations, allowing effective dismutation of superoxide and protection against oxidative damage.

A possible complication to the dismutation model described above is the reduction of molecular oxygen in the presence of hydroxylamines, which actually increases the concentration of superoxide. This reaction has not been investigated experimentally. However, it has been noted that the corresponding hydroxylamine of an isoindoline-type nitroxide provides less protection against DNA strand breaks with increasing concentrations, possibly due to this oxidation reaction.[29]

$$RR'NOH + O_2 \longrightarrow RR'NO^\bullet + HOO^\bullet \quad (4.10)$$

4.2.2 Inhibition of the Fenton reaction

Early experiments showed that nitroxide derivatives of oxazolidine and piperidine afford cellular protection from hypoxanthine/xanthine oxidase (HX/XO), forming an $O_2^{\bullet -}$ flux, and also from H_2O_2-induced damage. However, it was shown that nitroxides do not exhibit catalase-like activity, showing no direct reaction with H_2O_2. Experiments conducted in an hypoxic environment, to limit the chance of superoxide production, showed that nitroxides protect against H_2O_2 cytotoxicity even under these conditions. Therefore, a second mechanism of protection was inferred in which nitroxides inhibit the Fenton reaction by accepting electrons from ferrous ions, preventing the intracellular reduction of H_2O_2 to produce highly toxic hydroxyl radicals.[15,30]

Hydroxyl radicals are produced from superoxide in the presence of both hydrogen peroxide and transition metal ions, in the immediate vicinity of biological targets. The production requires the binding of the metal ions to the biomolecule (for example DNA) as shown in Reaction (4.11).[31] Therefore, the location of oxidative attack is most likely to be at or near the site of metal binding. In the metal-catalysed Haber-Weiss mechanism, superoxide radicals react neither with the biological target nor with H_2O_2, instead reducing either bound iron (Fe^{3+}) or copper (Cu^{2+}) transition metal ions or metal-ligand chelates (Fe^{3+}-L or Cu^{2+}-L) as shown in Reaction (4.12). The bound reduced metal ion can generate hyroxyl radicals, or higher oxidation states of the metal, through the formation of a transient peroxo complex, via the Fenton reaction shown in Reactions (4.13) to (4.15).[32]

$$\text{DNA} + Fe^{3+} \rightleftharpoons \text{DNA-}Fe^{3+} \quad (4.11)$$

$$\text{DNA-}Fe^{3+} + O_2^{\bullet -} \rightleftharpoons \text{DNA-}Fe^{2+} + O_2 \quad (4.12)$$

$$\text{DNA-}Fe^{2+} + H_2O_2 \longrightarrow \text{DNA-}Fe^{2+}\text{-}H_2O_2 \quad (4.13)$$

$$\text{DNA-}Fe^{2+}\text{-}H_2O_2 \longrightarrow \text{DNA-}Fe^{3+} + {}^{\bullet}OH + {}^{-}OH \quad (4.14)$$

$$\text{DNA-}Fe^{2+}\text{-}H_2O_2 \rightleftharpoons \text{DNA-}Fe^{4+} + 2\,{}^{-}OH \quad (4.15)$$

As the generation of hydroxyl radicals occurs near the target molecules for oxidative damage, this mechanism has a high damaging efficiency. It has been observed that known $^{\bullet}OH$ scavengers often exhibit little protection.[33] Therefore, the protection demonstrated by nitroxides is probably not due to radical scavenging. Nitroxide radicals are instead thought to inhibit the production of damaging hydroxyl radicals by maintaining the transition metal ion in an oxidised state and thereby preventing the Fenton reaction. Initial experiments showed that when an oxazolidine-type nitroxide was incubated with Fe^{2+} in the presence of DNA, the species DNA-Fe^{3+} was formed, providing evidence for Reaction (4.16).[15]

$$RR'NO^{\bullet} + \text{DNA-}Fe^{2+} + H^{+} \rightleftharpoons RR'NOH + \text{DNA-}Fe^{3+} \quad (4.16)$$

Reaction (4.16) is thought be responsible for the protection seen for nitroxides against oxidative damage to DNA causing single and double strand breaks. Various nitroxides protect against damage caused in the presence of both copper and iron ions.

However, protection becomes negligible at high concentrations of metals ions and also when H_2O_2 is added to the incubation mixture, due to the high efficiency of the "site-specific" damage.[29]

As well as the antioxidant effect of nitroxides shown in Reaction (4.16), it has also been suggested that they may demonstrate a potential pro-oxidant effect, acting as reductants and facilitating metal-catalysed DNA breakage, as shown in Reaction (4.17). This reaction would only occur in the absence of common reductants and so is not likely in tissues, where sufficient reducing equivalents are present.[34]

$$RR'NO^{\bullet} + DNA\text{-}Fe^{3+} \rightleftharpoons RR'N^{+}=O + DNA\text{-}Fe^{2+} \qquad (4.17)$$

When the pH, temperature, and presence of buffers and ligands are modelled to physiological conditions, the equilibrium of Reaction (4.16) is shifted to the right. The presence of ^{-}OH catalyses the oxidation of iron, further shifting the equilibrium to the right.[35] It was observed that piperidine-type nitroxides undergo Reaction (4.16) more readily and may therefore be more effective protectors than pyrrolidine-type nitroxides.[35]

4.2.3 Inhibition of lipid peroxidation

Lipids are oxidised by molecular oxygen in a free-radical chain-reaction known as lipid peroxidation. This process produces dangerous products known to cause cell injuries and has been linked to a variety of pathological events such as cancers and even aging.[36] The main steps in the sequence of lipid peroxidation are shown in Reactions (4.18) to (4.25).[36] The initiation step occurs when a carbon-centred lipid radical ($L^{\bullet}$) is formed by the attack of a free radical species ($X^{\bullet}$), often a reactive oxygen species, as shown in Reaction (4.18). The initial lesion is then propagated by a reaction with oxygen, shown in Reaction (4.19). The peroxyl radical product goes on to cause the oxidation of many more lipids, as shown in Reaction (4.20) to (4.22), until oxygen is depleted.

$$LH + X^{\bullet} \longrightarrow L^{\bullet} + XH \qquad (4.18)$$

$$L^{\bullet} + O_2 \longrightarrow LOO^{\bullet} \qquad (4.19)$$

$$LOO^{\bullet} + LH \longrightarrow L^{\bullet} + LOOH \qquad (4.20)$$

$$LOOH \rightleftharpoons LO^{\bullet} + {}^{\bullet}OH \quad (4.21)$$

$$LO^{\bullet} + LH \longrightarrow L^{\bullet} + LOH \quad (4.22)$$

The termination of lipid peroxidation occurs through the combination of free radicals to form stable non-radical products, as shown in Reactions (4.23) to (4.25) Trapping can occur between lipid radicals and lipid peroxyl radicals, or with other radical scavengers.

$$L^{\bullet} + L^{\bullet} \longrightarrow LL \quad (4.23)$$

$$LOO^{\bullet} + LOO^{\bullet} \longrightarrow LOOL + O_2 \quad (4.24)$$

$$LOO^{\bullet} + L^{\bullet} \longrightarrow LOOL \quad (4.25)$$

Lipid peroxidation may be inhibited by either "preventative" or "chain-breaking" antioxidants. Preventative antioxidants deactivate the radical species ($X^{\bullet}$) or its precursors, and thereby suppress the rate of chain initiation. Chain-breaking antioxidants interfere with the propagation of the peroxidation, by reacting with the formed radical species in termination reactions.[36] Nitroxides have been found to act as both preventative and chain-breaking antioxidants, inhibiting lipid peroxidation at all stages.[37,38]

Initiation of lipid peroxidation occurs through reactive oxygen species such as superoxide or hydroxyl radicals. Reactions to produce these species include the reduction of molecular oxygen to superoxide by heme proteins such as cytochrome P450 reductase,[39] and the production of hydroxyl radicals via the Fenton reaction. The interference in the Fenton reaction by nitroxides is discussed in Chapter 4.2.2, and is thought to contribute to the slowing of the initiation of lipid peroxidation. Nitroxides also interact with the redox-active iron metal site of cytochrome P450, keeping it in the ferric (Fe^{3+}) state and preventing the auto-oxidation reaction.[40] The observation that piperidine nitroxides are more efficient inhibitors than oxazolidine nitroxides is thought to be due to differences in their reactions with cytochrome P450, in turn caused by the difference in lipophilicity between the nitroxides,[38a] and differences in their ring structure.[40]

Hydroxylamine, produced when a nitroxide oxidises Fe^{2+} to Fe^{3+}, has been suggested to act as a chain-breaking antioxidant, slowing the propagation of peroxidation through hydrogen-donation reactions to lipid radicals, lipid peroxides and lipid alkoxides, as shown in Reaction (4.26) to (4.28).[1,17] It has recently been observed that hydroxylamines undergo reactions with peroxyl radicals with rates slightly less than 10^5 $Lmol^{-1}s^{-1}$.[41] Oxazolidine-type nitroxides, being more lipophilic than piperidine nitroxides, are also thought to inhibit lipid peroxidation through radical trapping reactions with the nitroxides themselves, as shown in Reaction (4.29).[17]

$$RR'NOH + L^{\bullet} \longrightarrow LH + RR'NO^{\bullet} \quad (4.26)$$

$$RR'NOH + LO^{\bullet} \longrightarrow LOH + RR'NO^{\bullet} \quad (4.27)$$

$$RR'NOH + LOO^{\bullet} \longrightarrow LOOH + RR'NO^{\bullet} \quad (4.28)$$

$$RR'NO^{\bullet} + L^{\bullet} \longrightarrow RR'NOL \quad (4.29)$$

4.2.4 Enhancement of catalase-like activity of heme proteins

Myoglobin (Mb), the major heme protein in muscle tissue, is involved in the storage and delivery of oxygen by shuttling between oxymyoglobin ($MbFe^{2+}$-O_2) and myoglobin. However, oxymyoglobin is also involved in a catalase-like cycle for the dismutation of hydrogen peroxide, a species capable of generating potentially harmful reactive oxygen species. Oxymyoglobin can undergo oxidation to yield the aquo complex metmyoglobin ($MbFe^{3+}$) and superoxide, as shown in Reaction (4.30).[42]

$$MbFe^{2+}\text{-}O_2 \longrightarrow MbFe^{3+} + O_2^{\bullet -} \quad (4.30)$$

The reaction between hydrogen peroxide and metmyoglobin produces a two-electron oxidation product, $^{\bullet +}MbFe^{4+}=O$, as shown in Reaction (4.31). One reducing equivalent comes from the heme ion giving an Fe^{4+} state, while the other has been shown to reside on the globin, existing as a transient radical located on an aromatic amino acid residue.[43] The peroxide bond splits and water is released with one oxygen atom remaining bound to iron as the oxoferryl complex $Fe^{4+}=O$,[44] thought to have a lifetime of minutes or even hours.[45] The mechanism for the peroxide bond cleavage is not known.

$$MbFe^{3+} + H_2O_2 \longrightarrow {}^{\bullet+}MbFe^{4+}{=}O + H_2O \qquad (4.31)$$

The mechanism for the decay of the globin radical is also not conclusively known. It is thought that, in the absence of other reductants, the globin radical may oxidise hydrogen peroxide, as shown in Reaction (4.32). However, there is no direct evidence for this reaction. The resulting species oxoferrylmyoglobin ($MbFe^{4+}$=O) can be reduced to metmyoglobin by a further reaction shown in Reaction (4.33), thus completing the cycle of hydrogen peroxide dismutation.[46] Alternatively, the decay of the globin radical may occur by another mechanism, leaving the oxoferrylmyoglobin species to be reduced by a reaction with hydrogen peroxide, as shown in Reaction (4.34).[46] The structures of the various myoglobin intermediates are shown in Figure 4.1.

$${}^{\bullet+}MbFe^{4+}{=}O + H_2O_2 \longrightarrow MbFe^{4+}{=}O + O_2^{\bullet-} + 2H^+ \qquad (4.32)$$

$$MbFe^{4+}{=}O + O_2^{\bullet-} + 2H^+ \longrightarrow MbFe^{3+} + O_2 + H_2O \qquad (4.33)$$

$$MbFe^{4+}{=}O + H_2O_2 \longrightarrow MbFe^{3+} + O_2^{\bullet-} + 2H^+ \qquad (4.34)$$

Both the globin radical and the oxoferryl species mentioned above have been proposed to cause oxidative damage to biological components by initiating free radical-mediated reactions.[47] Oxoferrylmyoglobin is a strong oxidant capable of inflicting significant damage by oxidising biological targets such as unsaturated fatty acids and membrane lipoproteins.[43b,48] It can also be converted to an oxidase capable of generating additional hydrogen peroxide.[49]

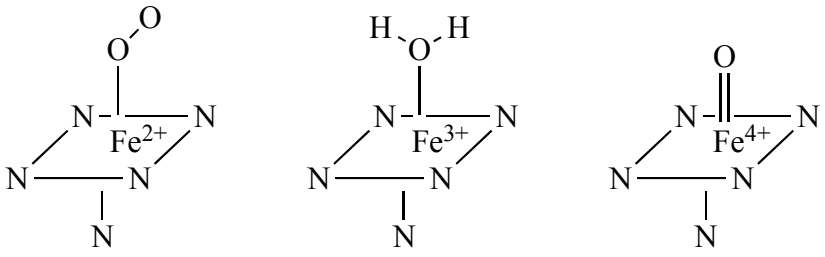

oxymyoglobin ($MbFe^{2+}$-O_2) | aquo metmyoglobin ($MbFe^{3+}$) | oxoferrylmyoglobin ($MbFe^{4+}$=O)

Figure 4.1 Structures of myoglobin intermediates around the iron centre[50]

Nitroxides have been found to play a role enhancing the catalase-like activity of metmyoglobin.[46] The nitroxide reacts with the damaging species oxoferrylmyoglobin, as shown in Reaction (4.35), reducing it back to metmyoglobin faster than its reaction with hydrogen peroxide, the rate-limiting step in the catalytic cycle described above. This produces an oxoammonium cation, which can then generate oxygen by oxidising superoxide, regenerating the nitroxide, as shown in Reaction (4.9). The overall rate of hydrogen peroxide dismutation by metmyoglobin increases by about four to six fold with the introduction of 4-hydroxy-2,2,6,6,-tetramethylpiperidin-1-yloxyl (4-hydroxy-TEMPO, **6**) into the system.[46]

$$RR'NO^{\bullet} + MbFe^{4+}{=}O + 2H^{+} \longrightarrow RR'N^{+}{=}O + MbFe^{3+} + H_2O \quad (4.35)$$

4.2.5 Detoxification of semiquinones

Naphthoquinone (Q) and its derivatives such as juglone (5-hydroxy-1,4-naphthoquinone) and menadione (2-methyl-1,1-naphthoquinone), as well as the related quinone streptonigrin (a derivative of quinoline-5,8-dione), show toxicity that is dependent upon their bioreduction to semiquinone radicals ($Q^{\bullet -}$), shown in Reaction (4.36). This is thought to be caused by reduced transition metal ions or thiol reducing agents such as glutathione.[51] The toxicity of naphthoquinones is caused through the generation of superoxide, hydroxyl radicals and other reactive oxygen species, as shown in Reaction (4.37) and (4.38).[52] The semiquinone radicals themselves are also thought to exert cytotoxicity independently of oxygen species.[53]

$$Q + Fe^{2+} \longrightarrow Q^{\bullet -} + Fe^{3+} \quad (4.36)$$

$$Q^{\bullet -} + O_2 \longrightarrow Q + O_2^{\bullet -} \quad (4.37)$$

$$Q^{\bullet -} + H_2O_2 \longrightarrow Q + {}^{\bullet}OH + {}^{-}OH \quad (4.38)$$

Nitroxide radicals protect against naphthoquinone toxicity by several different mechanisms. These include the oxidation of reduced metals such as Fe^{2+} and Cu^{+}, which prevents the reduction of naphthoquinone to semiquinone radicals, and the dismutation of intracellular superoxide, in reactions discussed in Chapters 4.2.2 and 4.2.1. Additionally, the protective effect of nitroxides is also thought to be attributable to a direct oxidation of the semiquinone radical,[52,53] as shown in Reaction (4.39).

$$RR'NO^{\bullet} + Q^{\bullet -} + H^{+} \rightleftharpoons RR'NOH + Q \quad (4.39)$$

4.2.6 Protection against radiation-induced damage

As well as protecting against superoxide and hydrogen peroxide-mediated oxidative damage, it has been found that nitroxide radicals provide protection against oxidative stress caused by exposure to ionising radiation.[54] The high energy of ionising radiation is greater than bond energies of many molecules and results in the cleavage of molecular bonds, forming radical species. Since water is the main component in living tissue, the radiolysis of water is thought to be the dominant reaction of this type. Many different reactions are thought to be involved in the ionisation of water,[55] however it was demonstrated that the process produces hydrated electrons (e^-_{aq}).[56] Since known hydroxyl radical scavengers have been shown to protect cells,[57] it is thought that oxidative damage is caused primarily through the production of hydroxyl radicals.

$$H_2O \xrightarrow{h\nu} {}^{\bullet}OH + e^-_{aq} + H^+ \quad (4.40)$$

Hydroxyl radicals are not the sole cause of radiobiological damage to cells as they have only very short lifespans of the order of nanoseconds.[55] Radical intermediates ($X^{\bullet}$) with significantly longer lifespans, in the microsecond range, are produced by reactions with hydroxyl radicals and contribute to the damage. The nature of $X^{\bullet}$ is not entirely clear. It may take the form of an OH-adduct radical,[58] or a diradical species.[59]

$${}^{\bullet}OH + XH \longrightarrow X^{\bullet} + H_2O \quad (4.41)$$

Cell membranes, enzymes, and other proteins are targets in radiation-induced cytotoxicity. However, the crucial target is thought to be DNA,[60] which undergoes double-strand breaks when exposed to radiation.[61] DNA ionisation occurs through hydrogen abstraction by either direct ionisation, hydroxyl radicals or, more commonly, secondary radicals.[62] The DNA radical can react with oxygen to form a peroxyl radical, as shown in Reaction (4.43), however subsequent strand breakage has been shown to occur without this step.[63]

$$X^{\bullet} + DNA\text{-}H \longrightarrow XH + DNA^{\bullet} \quad (4.42)$$

$$DNA^{\bullet} + O_2 \longrightarrow DNA\text{-}OO^{\bullet} \quad (4.43)$$

Nitroxides radicals have been shown to provide radioprotection to cells,[54] with the suggested protection mechanisms involving oxidation reactions of the nitroxide and its corresponding hydroxylamine shown in Reactions (4.44) to (4.47).[1,64] However, these reactions have been discredited by many observations. It was observed that hydroxylamines, similarly to other reducing agents such as vitamins C and E, do not protect against radiation-induced damage, except in cases when the hydroxylamines have a propensity to undergo spontaneous oxidation back to nitroxides.[64] Also, the protection caused by nitroxides probably occurs via different mechanisms than their actions as superoxide dismutase mimics or as oxidisers of redox-active transition metal ions, since other species with these properties show poor radioprotective activity.

$$RR'NO^{\bullet} + X^{\bullet} + H^{+} \longrightarrow RR'N^{+}{=}O + XH \quad (4.44)$$

$$RR'NOH + X^{\bullet} \longrightarrow RR'NO^{\bullet} + XH \quad (4.45)$$

$$RR'NO^{\bullet} + DNA^{\bullet} + H^{+} \longrightarrow RR'N^{+}{=}O + DNA\text{-}H \quad (4.46)$$

$$RR'NOH + DNA^{\bullet} \longrightarrow RR'NO^{\bullet} + DNA\text{-}H \quad (4.47)$$

It was found that although nitroxides show higher reactivities towards hydroxyl radicals than hydroxylamines, their radioprotection is probably not related to the scavenging of $^{\bullet}OH$. Instead, nitroxides were shown to detoxify some OH-derived secondary radicals, as shown in Reaction (4.48), whereas hydroxylamines are essentially unreactive with these species. Electron paramagnetic resonance (EPR) studies confirmed a mechanism in which the nitroxide acts as an oxidant of the secondary radical while correspondingly undergoing a reduction to a hydroxylamine.[58] Scavenging reactions between nitroxides and $X^{\bullet}$ or ionised DNA, as shown in Reactions (4.49) and (4.50), have also been suggested but not observed conclusively.[29,64]

$RR'NO^{\bullet}$ +  $\longrightarrow$ $RR'NOH$ + 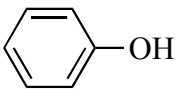 (4.48)

$$RR'NO^{\bullet} + X^{\bullet} \longrightarrow RR'NO\text{-}X \quad (4.49)$$

$$RR'NO^{\bullet} + DNA^{\bullet} \longrightarrow RR'NO\text{-}DNA \quad (4.50)$$

Reactions between nitroxides and alkyl peroxyl radicals have been the focus of previous studies. However, there is not complete agreement on the issue, with several authors considering these reactions unlikely to occur.[29,65] Suggested mechanisms involve the initial reaction of nitroxide with alkyl peroxyl radicals such as *tert*-butyl peroxyl to give a transient intermediate of the form RR′NO–O–O–*t*-Bu, with subsequent decomposition.[66] However the mechanism occurs, recent studies have shown that nitroxides do react directly with peroxyl radicals,[41,63] with spectrophotometric analysis showing subsequent production of oxoammonium cations. It was also observed that hydroxylamines show no reaction with peroxyl radicals, further confirming a reaction in which the nitroxide is oxidised while the peroxyl radical is reduced.[41] Therefore, the reaction of a nitroxide with the alkyl peroxyl radical DNA-OO$^{\bullet}$, shown in Reaction (4.51) may contribute to protection from damage caused by ionising radiation.

$$RR'NO^{\bullet} + DNA\text{-}OO^{\bullet} + H^{+} \longrightarrow RR'N^{+}{=}O + DNA\text{-}OOH \quad (4.51)$$

4.3 Electrode potentials of nitroxides

As the literature review presented in Chapter 4.2 reveals, nitroxide free radicals are extremely diverse protecting agents against oxidative damage in biological systems. They are effective against damage mediated by superoxide and hydrogen peroxide, as well as exposure to ionising radiation. Due to the complexity of the damage and protection mechanisms, it is not immediately clear how a nitroxide may be designed in order to exploit its ability to protect against oxidative damage. In the previous section, the individual reactions undergone by nitroxides as part of the protection mechanisms were discussed. It is clear that, although they also undergo radical scavenging reactions and their corresponding hydroxylamines undergo hydrogen donation reactions, by far the most common protection reactions involve either the oxidation of nitroxides to oxoammonium cations or their reduction to hydroxyamines. Indeed, it has previously been suggested that the biological activity of

nitroxides may be linked to their rates of electron transfer and redox potentials. For six-membered cyclic nitroxides a direct correlation between oxidation potential and ability to protect from H_2O_2-induced oxidative damage has been observed.[64] That this trend is not repeated for the case of five-membered nitroxides is not surprising because, as the literature review of protection methods suggests, biological protection by nitroxides is a complex process. Nonetheless, an understanding of the effects of the structure and substitution of nitroxides on electrode potentials is expected to assist in the determination of the roles they play in biological systems, and may eventually aid in the design of an optimal target for synthetic efforts.

4.3.1 Oxidation and reduction potentials of nitroxides

Using the reliable computational method identified in Chapter 3, the oxidation and reduction potentials of a large number of sterically hindered, stable nitroxide radicals were calculated. These results have recently been published in the *Journal of Physical Chemistry A*.[67] Electrode potentials were calculated relative to the standard hydrogen electrode (SHE) in an aqueous medium. Calculated species include di-*tert*-butyl nitroxide (DBN, **1**) as well as various five- and six-membered cyclic nitroxides; a large number of substituted derivatives of piperidine, pyrrolidine, oxazolidine, isoindoline, and azaphenalene-like nitroxides. The calculated and experimental oxidation and reduction potentials are shown in Table 4.1.

Table 4.1 Calculated electrode potentials (298 K) of nitroxides versus the SHE in water[a]

Nitroxide	Structure	E^o_{ox} (V)	E^o_{red} (V)	Nitroxide	Structure	E^o_{ox} (V)	E^o_{red} (V)
1		0.697	-1.553	**35**[b]	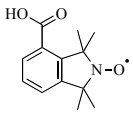	1.016	-1.697
2		0.762	-1.483	**36**[b]	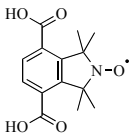	1.023	-2.331
3	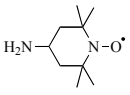	0.704	-1.455	**37**[b]	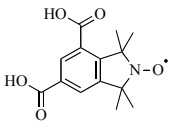	1.072	-1.755

4	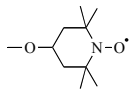	0.780	-1.436	**38**[b]	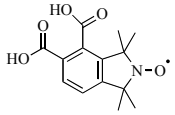	1.107	-1.617
5	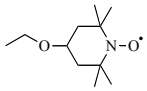	0.783	-1.441	**39**[b]	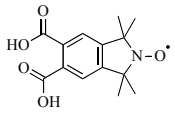	1.057	-1.424
6	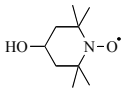	0.756	-1.414	**40**[b]	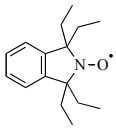	0.972	-1.912
7	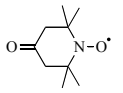	0.946	-1.255	**41**[b]	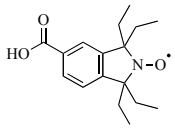	1.024	-1.936
8	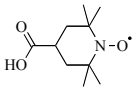	0.794	-1.388	**42**[b]	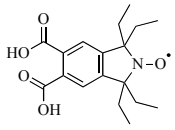	1.105	-1.876
9	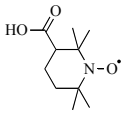	0.879	-1.348	**43**[b]	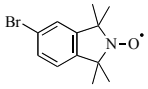	1.028	-1.487
10[b]	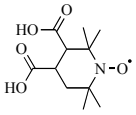	0.914	-1.270	**44**[b]	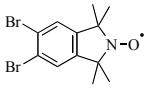	1.052	-1.442
11[b]	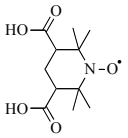	1.016	-1.217	**45**[b]	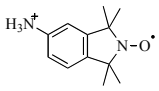	1.100	-1.758
12[b]	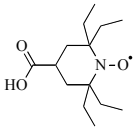	0.741	-1.783	**46**[b]	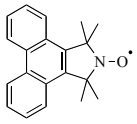	1.033	-1.544
13	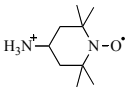	0.854	-1.315	**47**	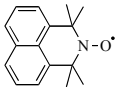	0.469	-1.336
14		0.794	-1.480	**48**[b]	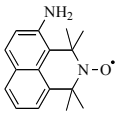	0.387	-1.318
15		0.764	-1.621	**49**[b]	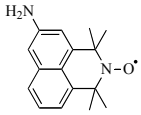	0.440	-1.347
16	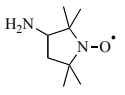	0.730	-1.591	**50**[b]	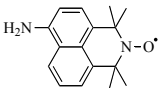	0.359	-1.369
17	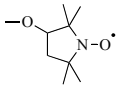	0.727	-1.553	**51**[b]	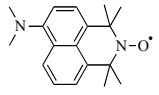	0.507	-1.361

18	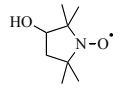	0.719	-1.598	**52**[b]	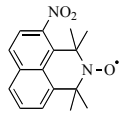	0.575	-1.450
19	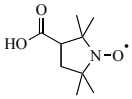	0.910	-1.505	**53**[b]	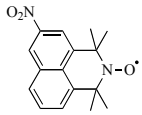	0.555	-2.237
20[b]	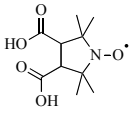	0.997	-1.396	**54**[b]	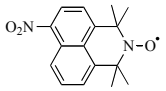	0.514	-2.343
21[b]	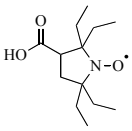	0.765	-1.723	**55**[b]	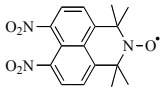	0.592	-1.675
22	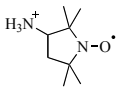	1.044	-	**56**[b]	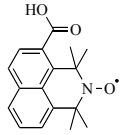	0.481	-1.313
23		0.922	-1.507	**57**[b]	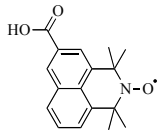	0.530	-1.391
24	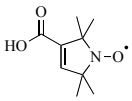	1.069	-1.450	**58**[b]	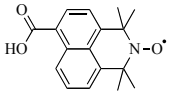	0.513	-1.356
25[b]	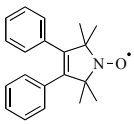	0.972	-1.476	**59**[b]	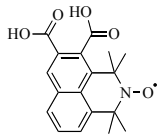	0.486	-1.328
26		1.023	-1.350	**60**[b]	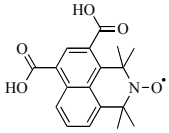	0.527	-1.475
27	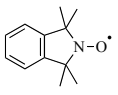	1.000	-1.505	**61**[b]	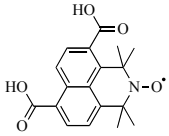	0.511	-1.792
28[b]	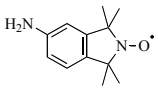	0.942	-1.526	**62**[b]	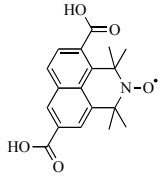	0.554	-1.543
29[b]	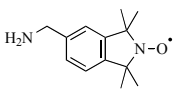	0.965	-1.498	**63**[b]	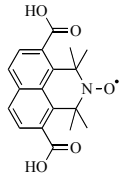	0.510	-1.226

30[b]	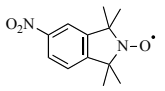	1.084	-1.828	**64**[b]	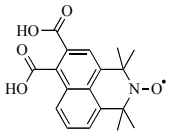	0.619	-1.402
31[b]	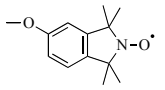	0.974	-1.544	**65**[b]	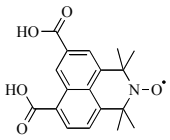	0.593	-1.468
32[b]	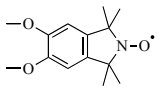	0.953	-1.587	**66**[b]	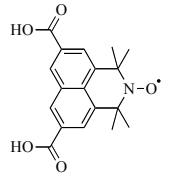	0.601	-1.384
33[b]	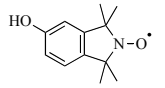	0.971	-1.516	**67**[b]	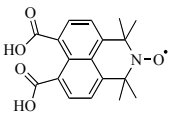	0.541	-1.329
34[b]	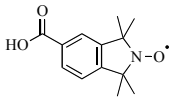	1.056	-1.537				

[a]Found from G3(MP2)-RAD//B3-LYP/6-31G(d) gas-phase energies and PCM solvation energies at the B3-LYP/6-31G(d) level. [a]ONIOM approximation using the parent (H-substituted) nitroxides as the core systems (with the full system calculated at the RMP2/ 6-311+G(3df,2p) level).

The oxidation potentials (E^o_{ox}) and reduction potentials (E^o_{red}) of many nitroxide radicals are shown in Table 4.1, and are plotted against each other in Figure 4.2. Species with lower oxidation potentials are more easily oxidised, while species with less negative reduction potentials are more easily reduced. The order for increasing favourability of the oxidation potentials of the parent (H-substituted) nitroxides is: TMOZO (**26**), TMIO (**27**), PROXYL (**15**), TEMPO (**2**), DBN (**1**), TMAO (**47**). In general, the lowest oxidation potentials are seen for the azaphenalene derivatives centred around 0.51 V, and the highest for the isoindoline derivatives centred around 1.00 V. Piperidine and pyrrolidine derivatives both show oxidation potentials centred around 0.83 V. The order of increasing favourability of the reduction potentials of the parent compounds is not the inverse of the oxidation results, instead it is: PROXYL (**15**), DBN (**1**), TMIO (**27**), TEMPO (**2**), TMOZO (**26**), TMAO (**47**). In general, the five-membered cyclic pyrrolidine and isoindoline derivatives have reduction potentials centred around -1.57 V, while the six-membered cyclic piperidine and azaphenalene derivatives have reduction potentials around 0.20 V less negative, centred at -1.37 V.

The oxazolidine derivative TMOZO (**26**) is easily reduced, but not easily oxidised. This is due to a electronegative heterocyclic oxygen, which stabilises the negative charge over the ring when the anion is formed, but destabilises the positive charge when the cation is formed. This is consistent with the observation that the very similar species 2-ethyl-2,5,5-trimethyl-3-oxazolidin-1-yloxyl undergoes reduction to the corresponding hydroxylamine, with the reduced species then being re-oxidised back to the nitroxide radical. This cycle, mimicking the actions of SOD,[25] is shown in Reactions (4.6) and (4.7) of Chapter 4.2.1. In contrast, nitroxides such as the piperidine derivatives in this study are thought to undergo oxidation to the corresponding oxoammonium cation, with the oxidised species then undergoing reduction, as seen in Reactions (4.8) and (4.9).[27]

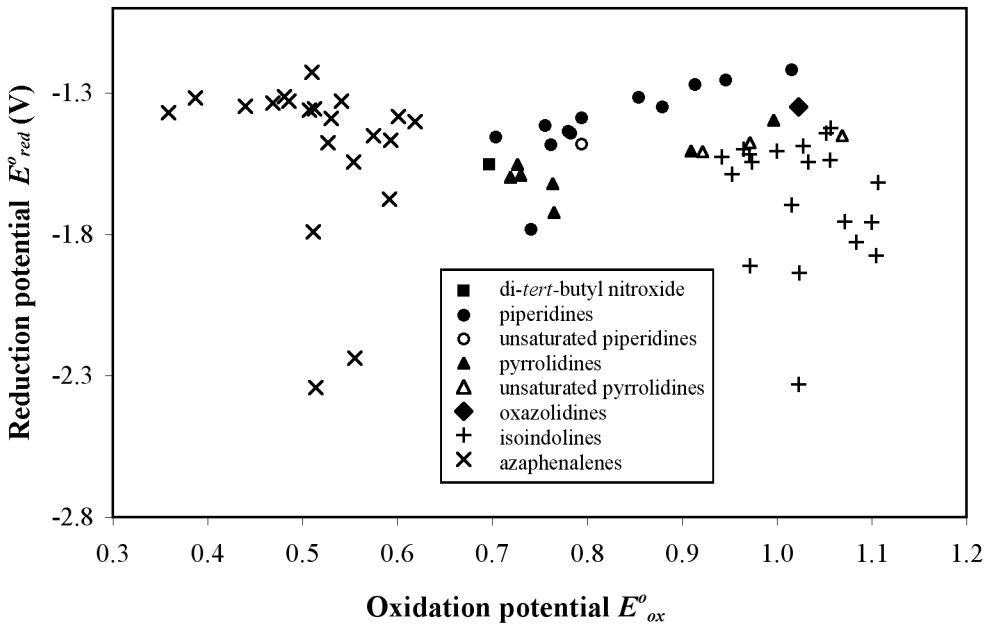

Figure 4.2 Oxidation and reduction potentials (V) for nitroxide derivatives

Excepting TMOZO (**26**), the nitroxides in this study have only cyclic carbon atoms, apart from the nitroxide moiety itself. For these species, the ability to be oxidised or reduced appears to be related to the flexibility of the ring structure, which determines how easily the anion is pyramidalised and the cation is planarised at the nitrogen centre. The non-cyclic species DBN (**1**) can be planarised easily, but steric

hindrance between the methyl groups causes the pyramidal anion to be of higher energy. Therefore DBN shows a low oxidation potential, but quite a negative reduction potential. All other things being equal, piperidine and pyrrolidine rings are relatively flexible, with out of plane motion that has been studied using quantum mechanical methods.[68] Piperidine derivatives are more easily reduced since they are more easily pyramidalised around the nitrogen centre in the anionic form, while five-membered pyrrolidine derivatives are held in a more planar conformation due to ring strain. The similar oxidation potentials seen for both the piperidine and pyrrolidine derivatives indicate that they are both relatively easy to planarise in the cationic form. On the other hand, the five-membered ring in the isoindoline derivatives is held quite rigid by the presence of an aromatic ring, leading to higher oxidative potentials and more negative reductive potentials for these species. This is also demonstrated through the observation that the isotropic electron paramagnetic resonance (EPR) spectra of the TMIO family of radicals have linewidths much smaller then those of the TEMPO family of radicals.[69,70] Despite the presence of two fused aromatic rings, the six-membered ring in azaphenalene is quite flexible around the nitrogen centre, showing similar steric characteristics to TEMPO-like nitroxides in the vicinity of the nitroxide group. This is confirmed by the EPR spectrum of TMAO (**47**), which shows broader lines than the spectra of the TMIO family.[71]

Azaphenalene derivatives show markedly lower oxidation potentials than piperidines due to resonance contribution from the delocalisation of the positive charge into the naphthalene ring as shown in Reaction (4.52). These resonance structures are supported by the calculated distribution of charge within the cationic parent azaphenalene derivative, shown in Figure 4.3. A similar effect may also be expected to occur for the isoindoline derivatives, however delocalisation does not occur for these species because it involves a loss of aromatisation. The azaphenalene cation retains aromatic character in one ring, increasing the favourability of delocalisation.

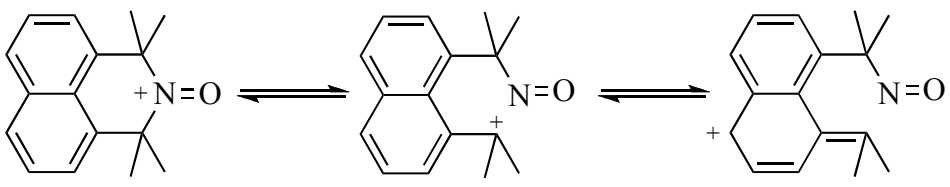

(4.52)

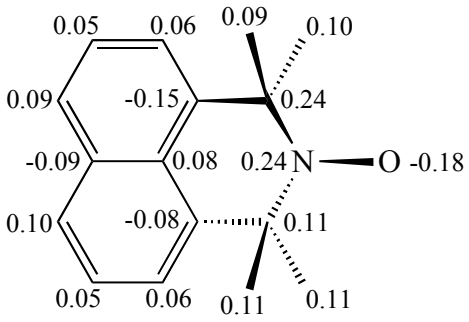

Figure 4.3 Distribution of charge within the azaphenalene oxoammonium cation

Large discrepancies between the theoretical and experimental oxidation potentials of azaphenalenes, discussed in section 4.3.2, indicate that it is likely that oxidation involves additional processes, which are not taken into account by the theoretical model. In fact, the oxidation potentials may actually be much higher than the theoretical calculations suggest.

Structural and substitution effects cause changes in the oxidation and reduction potentials within a family of nitroxides. Replacing the four methyl groups in α-positions to the nitrogen centre of the parent structures with ethyl groups causes only a small reduction in the oxidation potentials, but has a large effect on reduction, making it far less favourable (by up to 0.40 V). The presence of unsaturation in the six-membered TEMPO ring has only a small effect. However, for the five-membered PROXYL ring system there is a large increase in oxidation potential, of around 0.16 V, and a small decrease of reduction potential with the substitution of a double bond into the ring, for both the H and COOH substituted species.

For all of the different types of ring structures studied, trends in the oxidation and reduction potentials within a family correspond with the electron donating and accepting abilities of the ring substituents. The piperidine and pyrrolidine derivatives show oxidation potentials that increase with substituents in the order NH_2, OH, OCH_3, COOH, NH_3^+, while the reduction potentials become less negative with the same substituents. As expected, the increase in electron density around the ring from donating substituents stabilises the positive charge in the oxidised species. Substituents with a greater electron accepting ability stabilise the negative charge in the reduced ring. These effects can be relatively small, especially when the

substitution is in the same ring position. For instance, in the sequence of TEMPO radicals substituted in the 4-position with neutral substituents (H, NH_2, OH, OCH_3, OCH_2CH_3 and COOH), the oxidation potentials vary by only 0.09 V. However, this result is not repeated in the case of a similar sequence for PROXYL radicals substituted in the 3-position with neutral substituents. These values show only a 0.05 V variation in oxidation potentials for substituents H, NH_2, OH,and OCH_3, and then a large jump of around 0.18 V to the COOH substituted species.

Substituent effects in the isoindoline and azaphenalene derivatives largely follow electronegativity trends, with, for example, NH_2 stabilising the cation and lowering the oxidation potential, and COOH stabilising the anion and making reduction more favourable. For these species, the effects of the positions of electron withdrawing and electron donating substituents around the ring are shown to significantly affect the electrode potentials. This is possibly due to the way in which charge can be delocalised around the ring structures via hyperconjugation. The presence of electron withdrawing groups around the ring, accepting large proportions of negative charge, as well as other factors such as steric bulk may also complicate these effects. Overall, the electrode potentials of the nitroxides can be, in some cases, quite sensitive to substituents around the ring and care must be taken in the design of new targets for synthetic efforts. Substituents chosen to affect other properties of a nitroxide such as its solubility or binding may also compromise antioxidant ability.

4.3.2 Comparison of oxidation potentials to experimental values

In Chapter 3.4, oxidation potentials of several nitroxide radicals were calculated and compared with experimental values in an aqueous medium. The mean absolute deviation (MAD) of the calculated potentials from experimental values was 0.023 V (2.2 $kJmol^{-1}$). To further verify the calculation methods used, the oxidation potentials of a variety of nitroxide species were recalculated in acetonitrile. These values were then directly compared with experimental values measured by colleagues at the Queensland University of Technology, with the collaborative results published in the *Journal of Organic Chemistry*.[24] The experimental potentials were determined by cyclic voltammetry with the use of platinum and Ag/AgCl electrodes. The collected cyclic voltammograms for oxidation showed that all the measured nitroxides

underwent a one-electron oxidation corresponding to the formation of an oxoammonium cation. The recorded peak separation values approached the theoretical Nernstian value, indicating that the oxidations are kinetically reversible and, except when an amino functionality is present, also thermodynamically reversible. A second oxidation wave was observed for the amino substituted structures (**3**, **28**, **50** and **51**), most likely caused by the oxidation of that group. Similar oxidations have been previously observed for other amino substituted species.[72] The robustness of the nitroxide/oxoammonium cation couple was confirmed by cycling of the parent (H-substituted) structures more than 100 times each.

Experimental reduction potentials of nitroxides were also measured by cyclic voltammetry, where possible. The voltammograms showed a broad, irreversible cathodic peak corresponding to the reduction of the nitroxide moiety to a hydroxylamine, initially formed as the non-protonated anionic species. Re-oxidation was observed at a much higher potential than the initial reduction, reflecting the oxidation of the hydroxylamine rather than the exact reversal of the reduction process. The complexity of reduction made estimating E^{o}_{red} values for these measurements impractical, as only the cathodic and anodic peak potentials could be determined. Since there is currently no published formula describing the calculation of irreversible half-wave potentials for nitroxides in acetonitrile, a comparison with theoretical values was not possible.

In order to directly compare the theoretical and experimental oxidation potentials, the experimental values were corrected to the standard hydrogen electrode (SHE) using standard conversion constants.[73] The calculated and experimental oxidation potentials, as well as the differences between them, are shown in Table 4.2. From this data it is seen that the correlation between theory experimental is very high for the pyrroline, piperidine, and isoindoline ring classes. For these species, the mean absolute deviation (MAD) of the theoretical values from the experimental values is only 0.05 V. Slightly higher differences occur for species substituted by an amine group, since the irreversible oxidation of the amine group affects the experimental results. While there is excellent agreement between theory and experiment for the other classes of nitroxide studied, the azaphenalenes show much larger differences,

with an MAD of 0.60 V, with the experimental oxidation potentials being systematically 0.50–0.70 V higher than the theoretical values.

Table 4.2 Calculated and experimental oxidation potentials (298 K) of nitroxides versus the SHE in acetonitrile[a]

Nitroxide	Calculated E^o_{ox} (V)	Experimental E^o_{ox} (V)	Difference (V)
2	0.807	0.850	0.043
3	0.795	1.063	0.268
6	0.836	0.877	0.041
8	0.895	0.924	0.029
19	0.971	0.976	0.005
25[b]	0.967	1.091	0.124
27	0.999	1.045	0.046
28[b]	0.920	0.990	0.070
30[b]	1.142	1.148	0.006
31[b]	0.972	1.030	0.058
32[b]	0.957	1.007	0.050
33[b]	0.980	1.023	0.043
34[b]	1.080	1.095	0.015
39[b]	1.167	1.123	-0.044
40[b]	0.972	1.003	0.031
43[b]	1.061	1.099	0.038
44[b]	1.112	1.130	0.018
45[b]	1.042	1.067	0.025
46	0.474	1.010	0.536
50[b]	0.341	1.102	0.761
51[b]	0.474	1.182	0.708
54[b]	0.572	1.096	0.524
55[b]	0.705	1.175	0.470

[a]Found from G3(MP2)-RAD//B3-LYP/6-31G(d) gas-phase energies and PCM solvation energies at the B3-LYP/6-31G(d) level. [a]ONIOM approximation using the parent (H-substituted) nitroxides as the core systems (with the full system calculated at the RMP2/ 6-311+G(3df,2p) level).

The source of the unprecedented differences between the theoretical and experimental oxidation potentials of azaphenalenes is not immediately clear. The level of error is an order of magnitude higher than that observed for other species both in

acetonitrile and in water. This result is therefore inconsistent with the generally good agreement between theory and experiment for other nitroxides, and would seem to suggest that the error does not arise in the electronic structure calculations themselves. Instead, the one-electron oxidation might involve additional processes, which are not being taken into account by the theoretical model. For example, if the azaphenalenes were to form complexes through π-stacking, this could lead to the experimentally observed oxidation potential being higher than the calculated formal one-electron oxidation potential as this would limit the concentration of free nitroxide available for oxidation. The azaphenalene nitroxides have only recently been synthesised and experimental data on their properties are limited.[71] However, there is currently no indication that they should behave any differently to the piperidine-like nitroxides, and the discrepancy between theory and measurement is puzzling. Further studies are required to explore the origin of this intriguing result.

Whatever the reason for the discrepancy between theory and experiment, it is clear that in practice the oxidation potentials of azaphenalenes are higher than those predicted and, in the experimental model used for this collaborative study, are closer in value to those of the isoindoline derivatives. It is therefore likely that the piperidine derivatives will be more useful nitroxides than the azaphenalenes in the protection of biological systems from oxidative damage caused by reactive oxygen species.

4.4 Biological protection using nitroxides

Having studied the structure-reactivity relationships of the electrode potentials of nitroxides, it is now possible to use the protection mechanisms suggested in the literature to interpret experimentally observed protecting abilities and identify better protecting agents.

4.4.1 Superoxide dismutase mimicking mechanisms

The reactions of nitroxides and their oxidised and reduced forms with superoxide are shown in Reactions (4.6) to (4.10) in Chapter 4.2.1. In Reactions (4.6) and (4.7) the nitroxide mimics the action of native superoxide dismutase (SOD), undergoing reduction and re-oxidation with the catalytic removal of superoxide. Reactions (4.8) and (4.9) show a similar cycle with a nitroxide/oxoammonium cation

couple. A possible side reaction is shown in Reaction (4.10), in which hydroxylamine reduces dioxygen to form the conjugate acid of the damaging superoxide species. The free energies of Reactions (4.6) to (4.10) for various nitroxide protecting agents are shown in Table 4.3. Just as for the calculation of electrode potentials, the inclusion of a solvation system into the reactions is important, as the presence of the solvent helps to stabilise the charged species. Due to the previous difficulties encountered in the calculations of the azaphenalene-type nitroxides, these new compounds were omitted from the investigation.

Table 4.3 Calculated free energies ($kJmol^{-1}$ at 298 K) in water of the SOD-mimicking reactions for selected nitroxide species[a]

Nitroxide	Reaction (4.6)	Reaction (4.7)	Reaction (4.8)	Reaction (4.9)	Reaction (4.10)
1	-85.4	-125.1	-75.2	-94.9	45.1
2	-88.2	-122.2	-68.9	-101.2	47.9
3	-88.7	-121.7	-74.5	-95.6	48.4
5	-89.3	-121.2	-66.8	-103.3	48.9
6	-90.0	-120.4	-69.4	-100.7	49.7
7	-97.4	-113.0	-51.1	-119.0	57.1
9	-93.8	-116.6	-57.6	-112.5	53.5
10[b]	-95.4	-115.1	-55.1	-115.0	55.0
11[b]	-98.2	-112.3	-45.2	-124.9	57.8
15	-73.0	-137.5	-68.7	-101.4	32.6
16	-73.0	-137.4	-72.0	-98.1	32.7
17	-78.6	-131.9	-72.3	-97.8	38.2
18	-74.4	-136.0	-73.1	-97.0	34.1
19	-74.7	-135.8	-54.6	-115.5	34.4
20[b]	-80.0	-130.5	-47.4	-122.7	39.6
24	-79.1	-131.3	-39.3	-130.9	38.8
26	-85.0	-125.4	-43.7	-126.4	44.7
27	-78.1	-132.4	-45.9	-124.2	37.8
34[b]	-78.9	-131.6	-40.6	-129.6	38.5
39[b]	-88.6	-121.8	-40.5	-129.7	48.3

[a]Found from G3(MP2)-RAD//B3-LYP/6-31G(d) gas-phase energies and PCM solvation energies at the B3-LYP/6-31G(d) level. [a]ONIOM approximation using the parent (H-substituted) nitroxides as the core systems (with the full system calculated at the RMP2/ 6-311+G(3df,2p) level).

From Table 4.3 it is observed that Reactions (4.6) to (4.9) are thermodynamically favourable. The trend in exothermicities generally follows that expected on the basis of the calculated electrode potentials, with easier to reduce nitroxides showing greater exothermicities for Reaction (4.6), and easier to oxidise nitroxides showing greater exothermicities for Reaction (4.8). The side Reaction (4.10) shows positive enthalpies for all the nitroxide species, with the five-membered cyclic nitroxides having lower enthalpies than the six-membered cyclic nitroxides. Therefore, although this reaction is more likely to affect protection by pyrrolidine and isoindoline nitroxides, it is not expected to interfere with the reduction-based SOD-mimicking reaction, in an aqueous environment.

Although the trend of exothermicities of Reaction (4.6) follows, in general, the reduction potentials of the nitroxides, the correlation is not exact due to the effects of the addition of a proton during the reaction. It is interesting to note that even though the reduction of nitroxides was observed to be an irreversible process, Reaction (4.7) shows opposite favourabilities to Reaction (4.6), indicating that a nitroxide is formed through the oxidation of a hydroxylamine. In all cases, the re-oxidation of the hydroxylamine, Reaction (4.7), is the more thermodynamically favourable reaction. Therefore, in order to optimise the cycle, it is necessary to optimise the reduction of the nitroxide in Reaction (4.6). The results of Chapter 4.3 can be used to determine nitroxides with the most favourable reduction potentials, which should show the greatest propensity to undergo Reaction (4.6). The six-membered piperidine and azaphenalene derivatives are the easiest species in this study to reduce, however they show a wide spread of, and in the case of azaphenalenes unclear, oxidation potentials (see Figure 4.2). It is also expected that nitroxides with higher (less favourable) oxidation potentials may be more successful, as this will minimise the probability of any oxidation-based side reactions. Therefore, species selected on the basis of their reduction (and oxidation) potentials to be most useful are the dicarboxy-substituted piperidine, pyrrolidine and isoindoline derivatives (**10**, **11**, **20** and **39**), as well as 4-oxo-TEMPO (**7**) and the ozazolidine derivative TMOZO (**26)**. From Table 4.3 it is seen that these species show a good balance of exothermicities between Reactions (4.6) and (4.7). With the greatest exothermicities for Reaction (4.6), species **7**, **10** and

11 are expected to be the most successful nitroxides to optimise the reduction-based SOD-mimicking cycle through Reactions (4.6) and (4.7).

The exothermicities of Reaction (4.8) closely follow the trend in oxidation potentials of the nitroxides, with Reaction (4.9) showing the opposite trend in favourabilities. As for the case of the reduction-based cycle, the oxidation-based SOD-mimicking cyclic shows larger exothermicities for the re-reduction reaction and therefore, in order to optimise this cycle, it is necessary to optimise the oxidation of the nitroxide in Reaction (4.8). The species showing the lowest oxidation potentials in this study are di-*tert*-butyl nitroxide (**1**), the amino-substituted piperidine and pyrrolidine deriviatives (**3** and **16**), as well as the hydroxy and methoxy-subsituted pyrrolidines (**17** and **18**). As expected, these species show a good balance of exothermicities through the cycle of Reactions (4.8) and (4.9) and are expected to be desirable nitroxides for protection via this cycle. However, since experimental observations showed that the amino-subsituted nitroxides undergo irreversible oxidation at the amino group as well as the reversible oxidation of the nitroxide moiety (see Chapter 4.3.2),[24] these species may not be suitable for use in biological protection. Indeed, it has been observed that 4-amino-TEMPO (**3**) shows poor protection against DNA breakage and H_2O_2-induced damage, which can not be attributed entirely to a pro-oxidative effect,[34] and may instead be due to irreversible oxidation of the amino group. Species **1**, **17** and **18** are therefore expected to be the most successful nitroxides to optimise the oxidation-based SOD-mimicking cycle through Reactions (4.8) and (4.9).

4.4.2 Reduction-based protection mechanisms

As well as the dismutation of intracellular superoxide in a SOD-mimicking cycle, nitroxides are also thought to take part in several other protective mechanisms based on the reduction of a nitroxide, previously discussed in Chapter 4.2. The first of these is the inhibition of the production of damaging hydroxyl radicals by the maintenance of biomolecule-bound transition metal ions in an oxidised state, thereby preventing the Fenton reaction, as shown in Reaction (4.16). As well, the donation of hydrogen from hydroxylamine to lipid radicals, peroxides and alkoxides, inhibiting lipid peroxidation (Reactions (4.26) to (4.28)) has been suggested. Additionally,

protection may occur through the direct oxidation of the semiquinone radical, a damaging species in its own right that is also able to produce superoxide and hydroxyl radicals (Reaction (4.39)). Finally, protection may also occur through the oxidation of $^{\bullet}OH$-derived secondary radicals. These radicals, produced as a result of radiation-induced damage, would otherwise go on to abstract hydrogen from DNA causing strand breaks (Reaction (4.48)).

Apart from the lipid peroxidation inhibition reactions involving hydroxylamines, the protection reactions listed above can all be optimised for nitroxides in the same way as Reaction (4.6), with nitroxides showing greater propensity towards reduction expected to be better protecting agents. In addition, choosing nitroxides with higher oxidation potentials will reduce the chances of oxidation side reactions such as Reaction (4.17), in which the nitroxide acts as a pro-oxidant, facilitating metal-catalysed DNA breakage through the Fenton reaction. Therefore, as above, the species **7**, **10** and **11** are expected to be most effective in the protection of H_2O_2-induced oxidative damage through the oxidation of transition metal ions and semiquinone radicals.

The protection against radiation-induced damage is complex, and it is not clear whether a protecting agent should be a good oxidant, reductant, scavenger or some combination of these. If all of the Reactions (4.48) to (4.51) contribute to protection, then TEMPO, PROXYL and their hydroxy, methoxy, and ethoxy-substituted derivatives (**2**, **4**, **5**, **6**, **15**, **17**, **18**) are expected to provide the most successful protection. These species are the most easily oxidised and reduced species in the study, as well as being known radical scavengers. However, in a recent study of the effects of nitroxide radicals in the treatment the genetic disease ataxia telangiectasia, for which patients show hypersensitivity to ionising radiation, the carboxyl-substituted cyclic nitroxides, especially 4-carboxy-TMIO (**34**), were shown to be most successful.[74] This result could suggest that the reduction of nitroxide, shown in Reaction (4.48), is the dominant protection mechanism.

Reactions involving hydrogen donation from hydroxylamines to radical species are claimed to be chain-breaking steps in the inhibition of lipid peroxidation by nitroxides. Although, these reactions cannot be considered to be simply the re-

oxidation of a reduced nitroxide, the reaction thermodynamics can be calculated using the same methods used in the previous section to investigate the related Reaction (4.7). Calculations on Reactions (4.26) to (4.28), with the lipid radical modelled using the small secondary radical $L^{\bullet} = {}^{\bullet}CH(CH_3)_2$, are exothermic in water, with free energies of reactions for the hydroxylamine TEMPOH (the hydroxylamine form of nitroxide **2**) of -100.4 $kJmol^{-1}$ for Reaction (4.26), -157.1 $kJmol^{-1}$ for Reaction (4.27) and -120.1 $kJmol^{-1}$ for Reaction (4.28). It is therefore likely that these reactions could contribute to the inhibition of lipid peroxidation.

4.4.3 Oxidation-based protection mechanisms

As well as the oxidation-based nitroxide cycle for the dismutation of intracellular superoxide, two other reactions have been proposed in which the protection demonstrated by a nitroxide agent is based on its success as a reducing agent. These are the removal of the damaging species $MbFe^{4+}=O$ through Reaction (4.35) and the detoxification of a DNA-peroxyl radical through Reaction (4.51). It has been seen that the rate of removal of H_2O_2 is increased by about four to six times when 4-hydroxy-TEMPO (**6**), one of the more easily oxidised nitroxides in this study, is introduced. This rate could theoretically be increased by the use of an even more easily oxidised nitroxide agent, such as di-*tert*-butyl nitroxide (**1**) or the hydroxy or methoxy-subsituted pyrrolidines (**17** and **18**). As discussed above, amino-substituted nitroxides should be avoided due to side reactions.

It has also been suggested that the reduction of a DNA-peroxyl radical by a nitroxide may contribute to the protection of biological systems from radiation-induced damage. This reaction, in which the nitroxide and peroxyl radicals combine to form a trioxide species, with subsequent decomposition and electron transfer to the charged species shown in Reaction (4.51), is also important for the protection of polymer coatings from photo-oxidative damage in industrial applications. This mechanism is discussed further in Chapter 6.

4.4.4 Scavenging mechanisms

Other previously suggested protection mechanisms are the radical scavenging reactions, Reactions (4.29), (4.49) and (4.50). Combination reactions of nitroxides

with carbon-centred radicals are known to be fast. At high temperatures, these reactions are reversible and form the basis of nitroxide mediated polymerisation (NMP). It is therefore likely that radical scavenging reactions forming alkoxyamines occur in biological systems, and contribute to protection from radiation-induced oxidative damage and lipid peroxidation. With measured trapping reaction rates of around 10^8 $Lmol^{-1}s^{-1}$, these reactions may be faster than the dismutation of superoxide. The trapping reactions of carbon-centred radicals by nitroxides will be discussed further, and investigated for both a variety of nitroxides and a variety of alkyl polymeric radicals, in Chapter 5.

4.4.5 Experimental protection data

In the above sections, predictions of the protecting abilities of nitroxide agents against oxidative damage in biological systems were made. This theoretical data can be compared with published experimental work by Krishna *et al.*[64] These workers exposed Chinese hamster V79 cells to either H_2O_2 at fixed concentration or to ionising radiation, and determined "protection factors" by monitoring the viability of cells after exposure. The experimental protection factors of piperidine and pyrrolidine-type nitroxides are shown in Table 4.4, and are compared with free energies of Reactions (4.6) and (4.8), shown in Table 4.3, with the results shown in Figures 4.4 to 4.8.

Table 4.4 Experimentally determined protection factors of nitroxide species[a]

Nitroxide	H_2O_2 protection factor	Radiation protection factor
2	3.5	4.20
3	2.8	18.5
5	1.9	-
6	2.5	5.10
7	1.1	7.10
15	0.9	4.60
16	1.1	12.9
18	1.4	2.90
19	1.0	-
24	1.0	-

[a]As reported by Krishna *et al.*[64]

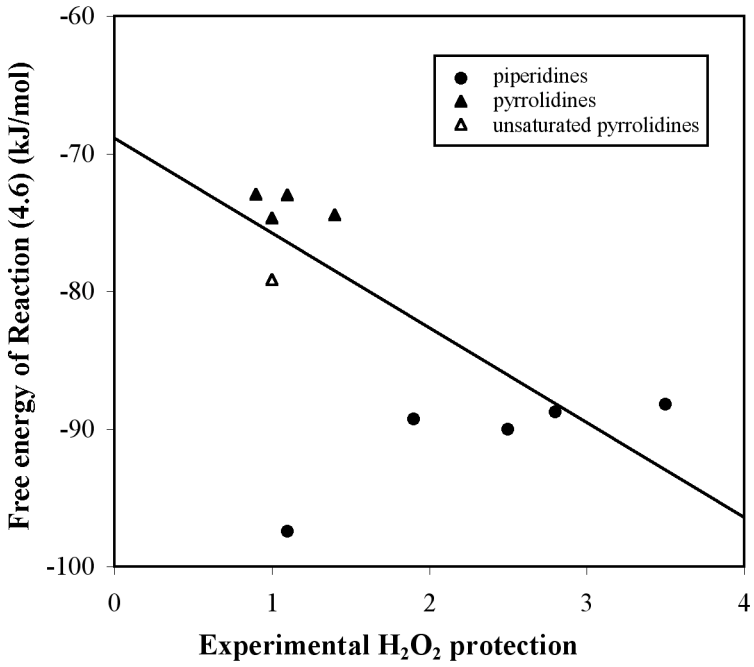

Figure 4.4 Correlation ($R^2 = 0.711$) between experimental H_2O_2 protection factors and the free energies of Reaction (4.6)

From Figure 4.4 it is seen that there is quite good correlation between the free energies of Reaction (4.6) and the H_2O_2 protection factors. A fair amount of scatter is seen, probably due to the competing effects of nitroxide metabolism, the cycling and slow consumption of the nitroxide driven by cellular reductases. The H_2O_2 protection factors of the piperidine nitroxides are higher than those of the pyrrolidine nitroxides, as would be expected on the basis of their reduction potentials (see Figure 4.2). Exceptions are the TEMPO species 4-oxo-TEMPO (**7**) and to a lesser extent 4-ethoxy-TEMPO (**5**). The reasons for the underperformance in protection observed for these species is unclear. It is possible that piperidine nitroixides with oxygen-type substituents at the 4-position may display lower solubilities or cell permeabilities, or may undergo side reactions involving the substituent group. Since, apart from nitroxide **7**, the experimental values generally follow the trends expected for reduction based-protection (shown as a linear trend line in Figure 4.4), it is probable that more easily reduced species will show greater protection. It is therefore expected that the dicarboxy-substituted TEMPO derivatives **10** and **11** will show even greater protection than the species examined in the experimental study.

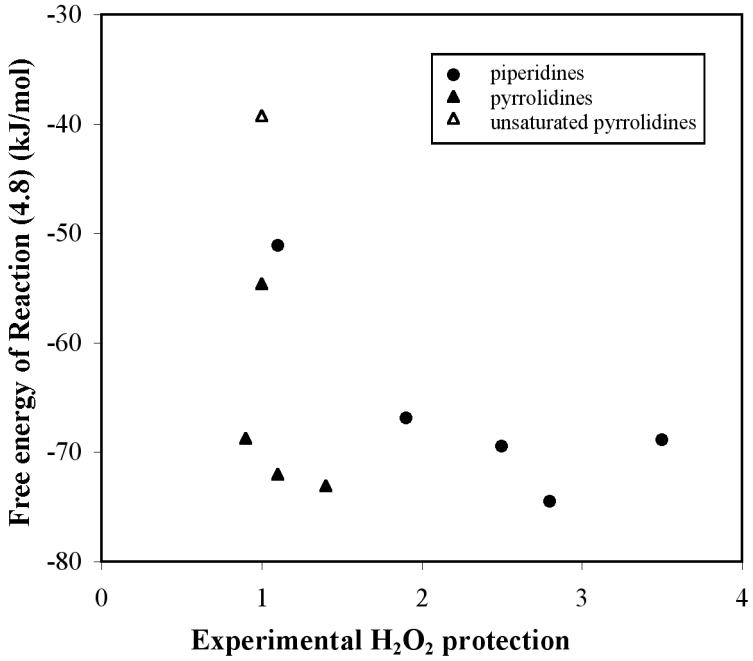

Figure 4.5 Correlation ($R^2 = 0.011$) between experimental H_2O_2 protection factors and the free energies of Reaction (4.8)

As noted in previous investigations, the oxidation potentials of six-membered ring nitroxides show some correlation between protection from H_2O_2-induced cytotoxicity.[64] However, in general it is seen from Figure 4.5 that there is no correlation between the free energies of Reaction (4.8) and the H_2O_2 protection factors. A previously suggested mechanism for protection is of a dismutation cycle based on oxidation for the piperidine nitroxides (see Chapter 4.2.1).[27] However, at least for this particular experimental system, the primary mechanisms for protection by piperidine and pyrrolidine-type nitroxides against H_2O_2-induced damage appear to be reduction-based reactions. These include the SOD-mimicking dismutation of superoxide, and the oxidation of transition metal ions, semiquinones and other damaging radical species. It is noted that a high protection factor is seen for the amino-substituted nitroxide **3**, indicating that the previously observed irreversible oxidation of the amino group does not occur, further supporting a reduction-based protection mechanism.

From Figures 4.6, 4.7 and 4.8 it is seen that the protection from radiation-induced damage does not correlate with either oxidising or reducing ability, or with

radical scavenging ability (as seen from a comparison with the enthalpies of methyl trapping taken from Table 5.1). It is noted that the amino-substituted piperidine and pyrrolidine derivatives show by far the greatest protecting abilities, higher than would be expected on the basis of their oxidation and reduction potentials and radical trapping abilities. With the limited number of data points available, it is not possible to draw solid conclusions about the nature of protection from radiation-induced damage. However, the lack of correlation to any one of the three protection mechanisms previously suggested may indicate that a combination of two or more of these mechanisms provides the overall protection observed. It is also possible that the effects of differing solubilities of the nitroxide species further complicate the results. In order to determine the contribution of each of the mechanisms, further experimental studies are required.

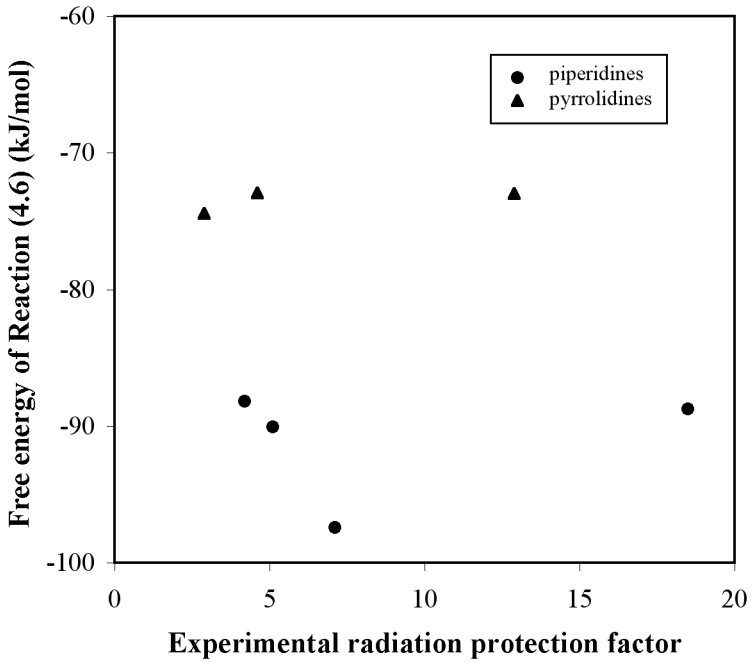

Figure 4.6 Correlation (R^2 = 0.260) between experimental radiation protection factors and the free energies of Reaction (4.6)

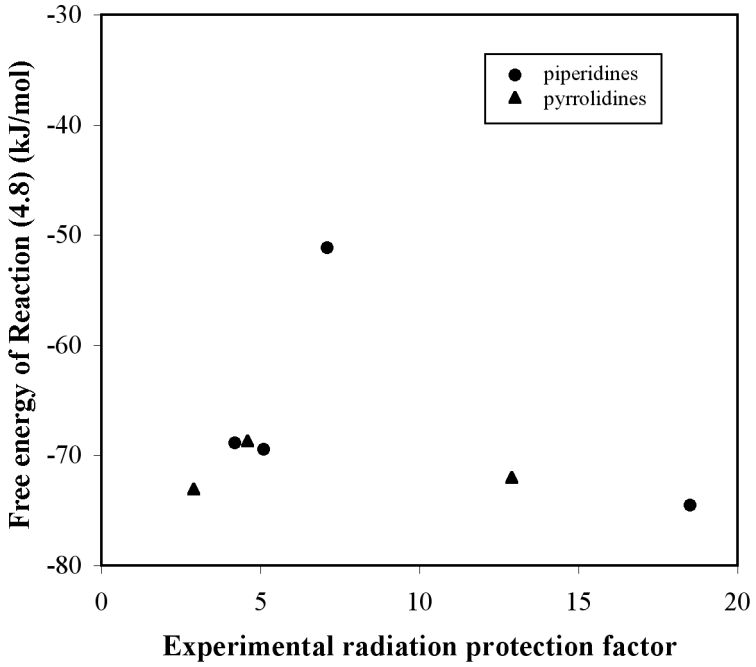

Figure 4.7 Correlation (R^2 = 0.063) between experimental radiation protection factors and the free energies of Reaction (4.8)

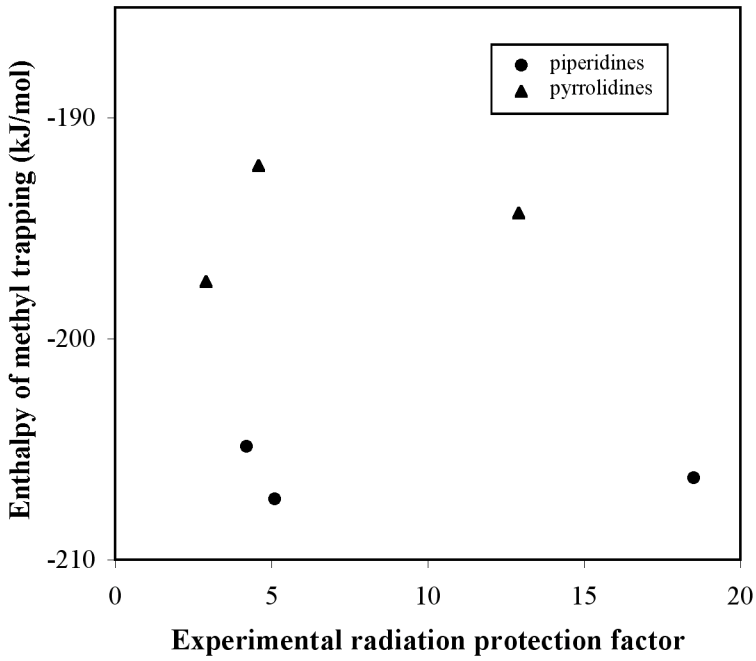

Figure 4.8 Correlation (R^2 = 0.035) between experimental radiation protection factors and the enthalpy of methyl radical trapping (see Table 5.1)

4.5 Conclusions

Nitroxide free radicals have been shown to be extremely diverse protecting agents against oxidative damage in biological systems, effective against hydrogen peroxide induced oxidative damage as well as exposure to ionising radiation. The mechanisms of oxidative damage and protection are very complex. Protection mechanisms involve radical scavenging reactions and, more commonly, oxidation reactions of nitroxides to oxoammonium cations or reductions of nitroxides to hydroxyamines (see Scheme 2.2 in Chapter 2.4.2). Since the biological activities of nitroxides are clearly linked to their rates of electron transfer and redox potentials, a study of the electrode potentials of a wide range of cyclic nitroxide species was completed in order to provide insight into their protecting abilities.

The oxidation and reduction potentials of nitroxide radicals are strongly affected by their ring size and structure. Six-membered piperidine and azaphenalene-type nitroxides are easier to reduce than the less flexible five-membered pyrrolidine and isoindoline-type nitroxides. Nitroxides showing the lowest oxidation potentials are the piperidine and pyrrolidine-type nitroxides, while the isoindoline nitroxides show the highest. Within a family of nitroxides, variation of the ring substituents alters the electrode potentials in a manner expected on the basis of electronegativity considerations. Thus, electron withdrawing subsitutent groups act to stabilise the anionic form of the nitroxide, making reduction more favourable, while electron donating groups stabilise the cationic form, lowering the oxidation potential. For example, substitution of carboxy groups around the ring structure significantly increases the oxidation potential and lowers the reduction potential. The placement of substituents around the ring was found to cause significant changes in the electrode potentials, due to both the effects of resonance and steric bulk. A comparison of the calculated oxidation potentials with experimental results showed good agreement for all the nitroxide species except the azaphenalene class, which were found to show unprecedented (order of magnitude higher) differences. It is thought that the one-electron oxidation for these species might involve additional or alternative processes, not taken into account by the theoretical model.

Using experimental protection data, it was shown that protection against H_2O_2-mediated oxidative damage is dependent upon the ease of reduction of the nitroxide agent. In this case protection occurs through reactions such as the SOD-mimicking dismutation of superoxide, as well as the oxidation of transition metal ions, semiquinones and other damaging radical species. Therefore, applying the calculated trends in electrode potentials with the literature protection mechanisms, it is concluded that the six-membered piperidine nitroxides are likely to be most successful in protection against H_2O_2-induced damage. For the most successful protection, the reduction of the nitroxide should be enhanced but the oxidation limited, in order to avoid possible damaging side reactions. Therefore, the dicarboxyl-substituted piperidine species 3,4-dicarboxy-TEMPO (**10**) and 3,5-dicarboxy-TEMPO (**11**) are expected to be the most desirable nitroxide species to optimise protection against H_2O_2- induced damage. The protection against radiation-induced oxidative damage was found to be more complex. This process is likely to involve several different nitroxide reactions, with further experimental data being needed to determine the relative importance of each.

4.6 References

(1) Soule, B. P.; Hyodo, F.; Matsumoto, K.; Simone, N. L.; Cook, J. A.; Krishna, M. C.; Mitchell, J. B. *Free Rad. Biol. Med.* **2007**, *42*, 1632.

(2) McBride, T. J.; Preston, B. D.; Loeb, L. A. *Biochemistry* **1991**, *30*, 207.

(3) Valentine, M. R.; Rodriguez, H.; Termini, J. *Biochemistry* **1998**, *37*, 7030.

(4) Bielski, B. H. J. *Photochem. Photobiol* **1978**, *28*, 645.

(5) Dix, T. A.; Hess, K. M.; Medina, M. A.; Sullivan, R. W.; Tilly, S. L.; Webb, T. L. L. *Biochemistry* **1996**, *35*, 4578.

(6) Porter, N. A.; Caldwell, S. E.; Mills, K. A. *Lipids* **1995**, *30*, 277.

(7) Lin, W. S.; Armstrong, D. A.; Lal, M. *Int. J. Radiat. Biol.* **1978**, *33*, 231.

(8) Kono, Y.; Fridovich, I. *J. Biol. Chem.* **1983**, *258*, 13646.

(9) Okajima, T.; Yamazaki, I. *Biochim. Biophys. Acta* **1972**, *284*, 355.

(10) (a) McCord, J.; Fridovich, I. *J. Biol. Chem.* **1969**, *244*, 6049. (b) Fridovich, I. *J. Biol. Chem.* **1989**, *264*, 7761.

(11) (a) Starke, P. E.; Farber, J. L. *J. Biol. Chem.* **1985**, *260*, 86. (b) Loewen, P. *J. Bacteriol.* **1984**, *157*, 622.

(12) Halliwell, B.; Gutteridge, J. M. C. *Free Radicals in Biology and Medicine*; pp 210. Clarendon Press: 1989.

(13) (a) Rotman, G.; Shiloh, Y. *BioEssays* **1997**, *19*, 911. (b) Rotman, G.; Shiloh, Y. *Oncogene* **1999**, *18*, 6135.

(14) (a) Swartz, H. M.; Santjurc, M.; Kocherginsky, N. Toxicity and the Use of Nitroxides as Drugs, In *Nitroxide Spin Labels, Reactions in Biology and Chemistry,* Kocherginsky, N. and Swartz, H. M., Eds. CRC Press Inc.: Boca Raton, 1995, pp. 175-198. (b) Damiani, E.; Greci, L.; Hrelia, P. *Free Rad. Biol. Med.* **2000**, *28*, 330.

(15) Mitchell, J. B.; Samuni, A.; Krishna, M. C.; DeGraff, W.; Ahn, M. S.; Samuni, U.; Russo, A. *Biochemistry* **1990**, *29*, 2802.

(16) Konovalova, N. P.; Diatchkovskaya, R. F.; Volkova, L. M.; Varfolomeev, V. N. *Anticancer Drugs* **1991**, *2*, 591.

(17) Miura, Y.; Utsumi, H.; Hamada, A. *Arch. Biochem. Biophys* **1993**, *300*, 148.

(18) Rachmilewitz, D.; Karmeli, F.; Okon, E.; Samuni, A. *Gut* **1994**, *35*, 1181.

(19) Sledzinski, Z.; Wozniak, M.; Antosiewicz, J.; Lezoche, E.; Familiari, M.; Bertoli, E.; Greci, L.; Brunelli, A.; Mazera, N.; Wajda, Z. *Int. J. Pancreatol.* **1995**, *18*, 153.

(20) Slater, A. F.; Nobel, C. S.; Maellaro, E.; Bustamante, J.; Kinland, M.; Orrenius, S. *Biochem. J.* **1995**, *306*, 771.

(21) Howard, B. J.; Yatin, S.; Hensley, K.; Allen, K. L.; Kelly, J. P.; Carney, J.; Butterfield, D. A. *J. Neurochem.* **1996**, *67*, 2045.

(22) Beit-Yannai, E.; Zhang, R.; Trembovler, V.; Samuni, A.; Shohami, E. *Brain Res.* **1996**, *717*, 22.

(23) Bielski, B. H. J.; Arudi, R. L. *Anal. Biochem.* **1983**, *133*, 170.

(24) Blinco, J. P.; Hodgson, J. L.; Morrow, B. J.; Walker, J. R.; Will, G. D.; Coote, M. L.; Bottle, S. E. *J. Org. Chem.* **2008**, *73*, 6763.

(25) Samuni, A.; Krishna, M. C.; Riesz, P.; Finkelstein, E.; Russo, A. *J. Biol. Chem.* **1988**, *263*, 17921.

(26) Rosen, G. M.; Finkelstein, E.; Rauckman, E. J. *Arch. Biochem. Biophys* **1982**, *215*, 367.

(27) Krishna, M. C.; Grahame, D. A.; Samuni, A.; Mitchell, J. B.; Russo, A. *Proc. Natl. Acad. Sci. U.S.A.* **1992**, *89*, 5537.

(28) Krishna, M. C.; Russo, A.; Mitchell, J. B.; Goldstein, S.; Dafni, H.; Samuni, A. *J. Biol. Chem.* **1996**, *271*, 26026.

(29) Damiani, E.; Kalinska, B.; Canapa, A.; Canestrari, S.; Wozniak, M.; Olmo, E.; Greci, L. *Free Rad. Biol. Med.* **2000**, *28*, 1257.

(30) Samuni, A.; Godinger, D.; Aronovitch, J.; Russo, A.; Mitchell, J. B. *Biochemistry* **1991**, *30*, 555.

(31) Samuni, A.; Chevion, M.; Czapski, G. *J. Biol. Chem.* **1981**, *256*, 12632.

(32) Masarwa, M.; Cohen, H.; Meyerstein, D.; Hickman, D. L.; Bakac, A.; Espenson, J. H. *J. Am. Chem. Soc.* **1988**, *110*, 4293.

(33) Samuni, A.; Aronovitch, J.; Godinger, D.; Chevion, M.; Czapski, G. *Eur. J. Biochem.* **1983**, *137*, 119.

(34) Aronovitch, Y.; Godinger, D.; Israeli, A.; Krishna, M. C.; Samuni, A.; Goldstein, S. *Free Rad. Biol. Med.* **2007**, *42*, 1317.

(35) Bar-On, P.; Mohsen, M.; Zhang, R.; Feigin, E.; Chevion, M.; Samuni, A. *J. Am. Chem. Soc.* **1999**, *121*, 8070.

(36) See for example: Niki, E. *Chem. Phys. Lipids* **1987**, *44*, 227 and references therein.

(37) Weil, J. T.; Van der Veen, J.; Olcott, H. S. *Nature* **1968**, *219*, 168.

(38) (a) Nilsson, U. A.; Olsson, L.-I.; Carlin, G.; Bylund-Fellenius, A.-C. *J. Biol. Chem.* **1989**, *264*, 11131. (b) Nilsson, U. A.; Carlin, G.; Bylund-Fellenius, A.-C. *Chem.-Biol. Interact.* **1990**, *74*, 1155.

(39) Svingen, B. A.; Buege, J. A.; O'Neal, F. O.; Aust, S. D. *J. Biol. Chem.* **1979**, *254*, 5892.

(40) Rosen, G. M.; Rauckman, E. J.; Hanck, K. W. *Toxicol. Lett.* **1977**, *1*, 71.

(41) Goldstein, S.; Samuni, A. *J. Phys. Chem. A* **2007**, *111*, 1066.

(42) Tajima, G.; Shikama, K. *J. Biol. Chem.* **1987**, *262*, 12603.

(43) (a) Catalano, C. E.; Choe, Y. S.; Ortiz de Montellano, P. R. *J. Biol. Chem.* **1989**, *264*, 10534. (b) Ortiz de Montellano, P. R.; Catalano, C. E. *J. Biol. Chem.* **1985**, *260*, 9265.

(44) Chance, M.; Powers, L.; Kumar, C.; Chance, B. *Biochemistry* **1986**, *25*, 1259.

(45) (a) Choe, Y. S.; Rao, S. I.; Ortiz de Montellano, P. R. *Arch. Biochem. Biophys* **1995**, *314*, 126. (b) Giulivi, C.; Cadenas, E. *Methods Enzymol.* **1994**, *233*, 189.

(46) Krishna, M. C.; Samuni, A.; Taira, J.; Goldstein, S.; Mitchell, J. B.; Russo, A. *J. Biol. Chem.* **1996**, *271*, 26018.

(47) Tew, D.; Ortiz de Montellano, P. R. *J. Biol. Chem.* **1988**, *263*, 17880.

(48) (a) Keilin, D.; Hartree, E. F. *Nature* **1950**, *166*, 513. (b) Turner, J. J. O.; Rice-Evans, C. A.; Davies, M. J.; Newman, E. S. R. *Biochem. J.* **1991**, *277*, 833. (c) Rao, S. I.; Wilks, A.; Hamberg, M.; Ortiz de Montellano, P. R. *J. Biol. Chem.* **1994**, *2669*, 7210.

(49) Osawa, Y.; Korzekwa, K. *Proc. Natl. Acad. Sci. U.S.A.* **1991**, *88*, 7081.

(50) Powers, L.; Sessler, J.; Woolery, C.; Chance, B. *Biochemistry* **1984**, *3*, 239.

(51) (a) Monks, T. J.; Walker, S. E.; Flynn, L. M.; Conti, C. J.; DiGiovanni, J. *Carcinogenesis* **1990**, *11*, 1795. (b) Nutter, L. M.; Ngo, E. O.; Fisher, G. R.; Gutierrez, P. L. *J. Biol. Chem.* **1992**, *267*, 2474. (c) Lowen, J. W. *Mol. Cell Biochem.* **1983**, *55*, 17.

(52) Krishna, M. C.; Halevy, R. F.; Zhang, R.; Gutierrez, P. L.; Samuni, A. *Free Rad. Biol. Med.* **1994**, *17*, 379.

(53) Zhang, R.; Hirsch, O.; Mohsen, M.; Samuni, A. *Arch. Biochem. Biophys.* **1994**, *312*, 385.

(54) Mitchell, J. B.; DeGraff, W.; Kaufman, D.; Krishna, M. C.; Samuni, A.; Finkelstein, E.; Ahn, M. S.; Hahn, S. M.; Gamson, J.; Russo, A. *Arch. Biochem. Biophys* **1991**, *289*, 62.

(55) See for example: Yamaguchi, H.; Uchihori, Y.; Yasuda, N.; Takada, M.; Kitamura, H. *J. Radiat. Res.* **2005**, *46*, 333 and references therein.

(56) Hart, E. J.; Boag, J. W. *J. Am. Chem. Soc.* **1962**, *84*, 4090.

(57) Roots, R.; Okada, S. *Int. J. Radiat. Biol.* **1972**, *21*, 329.

(58) Samuni, A.; Goldstein, S.; Russo, A.; Micthell, J. B.; Krishna, M. C.; Neta, P. *J. Am. Chem. Soc.* **2002**, *124*, 8719.

(59) Milligan, J. R.; Ng, J. Y.; Wu, C. C.; Aguilera, J. A.; Fahey, R. C.; Ward, J. F. *Radiat. Res*. **1995**, *143*, 273.

(60) Painter, R. B. The Role of DNA Damage and Repair in Cell Killing Induced by Ionising Radiation. In *Radiation Biology in Cancer Research*, Meyn, R. E. and Withers, H. R., Eds., Raven Press: New York, 1979, pp. 59-68.

(61) Bryant, P. E. *Int. J. Radiat. Biol.* **1985**, *48*, 55.

(62) Ward, J. F. *Int. J. Radiat. Biol.* **1994**, *66*, 427.

(63) Offer, T.; Samuni, A. *Free Rad. Biol. Med*. **2002**, *32*, 872.

(64) Krishna, M. C.; DeGraff, W.; Hankovszky, O. H.; Sár, C. P.; Kálai, T.; Jekó, J.; Russo, A.; Mitchell, J. B.; Hideg, K. *J. Med. Chem.* **1998**, *41*, 3477.

(65) (a) Blough, N. V. *Environ. Sci. Technol.* **1988**, *22*, 77. (b) Brownlie, I. T.; Ingold, K. U. *Can. J. Chem.* **1967**, *45*, 2427.

(66) Barton, D. H. R.; Le Gloahec, V. N.; Smith, J. *Tetrahedron Lett.* **1998**, *39*, 7483.

(67) Hodgson, J. L.; Namazian, M.; Bottle, S. E.; Coote, M. L. *J. Phys. Chem. A* **2007**, *111*, 13595.

(68) Siri, D.; Gaudel-Siri, A.; Tordo, P. *J. Mol. Struct. (Theochem)* **2002**, *582*, 171.

(69) Bolton, R.; Gillies, D. G.; Sutcliffe, L. H.; Wu, X. *J. Chem. Soc., Perkin Trans. 2* **1993**, *11*, 2049.

(70) Shen, J.; Bottle, S.; Khan, N.; Grinberg, O.; Reid, D.; Micallef, A.; Shartz, H. *Appl. Magn. Reson.* **2002**, *22*, 357.

(71) Blinco, J. P.; McMurtrie, J. C.; Bottle, S. E. *Angew. Chem*. **2007**, 4638.

(72) Korbi, B. H.; Tapsoba, I.; Benkhoud, M. L.; Boujlel, K. *J. Electroanal. Chem.* **2004**, *571*, 241.

(73) Pavlishchuk, V. V.; Addison, A. W. *Inorg. Chim. Acta.* **2000**, *298*, 97.

(74) Hosokawa, K.; Phillip, C.; Lavin, M. F.; Bottle, S. E. *Free Rad. Biol. Med.* **2004**, *37*, 946.

Chapter 5.

Structure Reactivity Trends in Nitroxide Mediated Polymerisation

5.1 Introduction 106
5.2 Literature review 106
5.2.1 Controlled radical polymerisation 107
5.2.2 Nitroxide mediated polymerisation (NMP) 109
5.2.3 Prediction of rate constants for the control reaction of NMP 110
5.2.4 Nitroxide mediated polymerisation of methyl methacrylate 112
5.3 Thermodynamics of the control reaction of NMP 114
5.3.1 Nitroxide substituent effects 114
5.3.2 Polymer substituent effects 118
5.4 A new equation for the equilibrium constant 120
5.4.1 Fitting parameters for nitroxides 121
5.4.2 Fitting parameters for alkyl radicals 125
5.4.3 Equation for K_{eq} 128
5.4.4 Relationship between kinetics and thermodynamics 132
5.4.5 Control of methyl methacrylate polymerisation 136
5.5 Conclusions and outlook 139
5.6 References 140

5.1 Introduction

Computational quantum chemistry excels as a resource for polymer chemists because it allows individual reactions making up complex processes such as polymerisation to be studied and optimised separately. In this chapter, the thermodynamics of the controlling step of the nitroxide mediated polymerisation (NMP) process will be examined using high-level computational techniques, for a variety of different monomers and controlling agents. The effects of different controlling agents on the polymerisation of various monomers will be quantified in terms of easily computed parameters representing the polar, steric and radical stability factors of both the nitroxide and the polymeric radical. A new equation, approximating the equilibrium constant of the trapping reaction in terms of these parameters will then be used to examine the polymerisation of methyl methacrylate.

5.2 Literature review

Developed in the early 20th century, radical polymerisation has become an increasingly popular method to produce polymers, due to its simplicity and robustness. It is used in industrial applications to produce millions of tons of homo- and copolymers each year.[1] Radical polymerisation processes include four main types of reactions; initiation, propagation, radical transfer and termination steps. These are shown in Scheme 5.1.

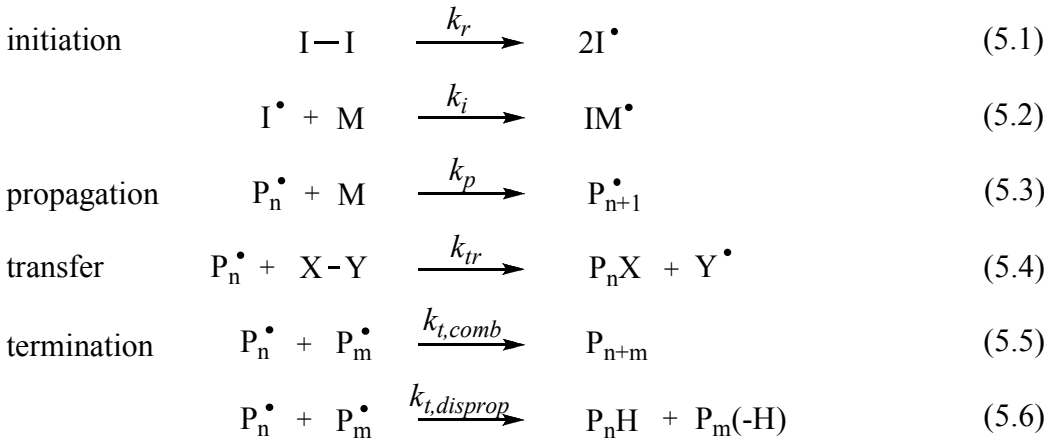

Scheme 5.1 Reactions making up a generic radical polymerisation process

5.2.1 Controlled radical polymerisation

Radical polymerisations involve a variety of transfer and termination reactions undergone at random by highly reactive radical species. Therefore, polymers produced using radical methods typically show a broad distribution of molecular weights and often have complex architectures. The polydispersity index (PDI), which decreases towards unity as the polymer chains approaches a uniform chain length, is typically higher than 2.0 for uncontrolled radical polymerisations. Over the past two decades, there has been an increasing demand for more well-defined materials. This has lead to an increase in the research of "pseudo-living" or "controlled" radical polymerisations in which the chain growth occurs in a regular and controlled fashion with a minimum of transfer and termination reactions, giving PDIs of 1.0–1.2 (see Figure 5.1).

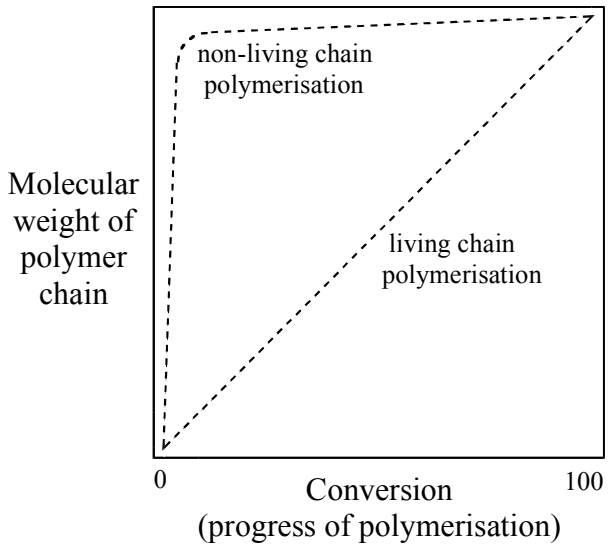

Figure 5.1 Molecular weight development of living verses non-living chain polymerisation

Controlled radical polymerisation involves the introduction of a controlling agent, which undergoes a reversible trapping reaction with the propagating radical, converting it to a dormant form. Only small amounts of the propagating radical are present at any one time and, due to the excess of monomer present, propagation

reactions become much more likely than termination reactions between two propagating radical chains. The polymer chain is therefore grown in a regular, controlled manner and shows a well-defined structure with less chain branching or premature termination.

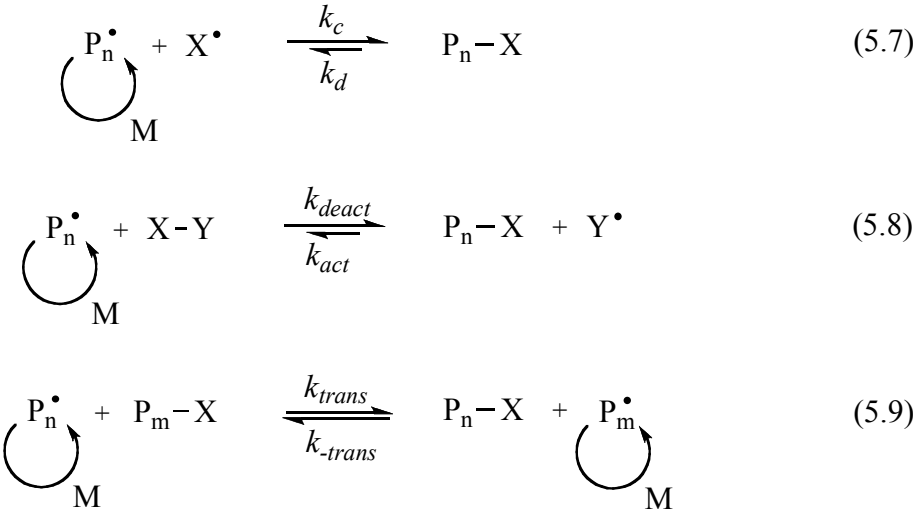

Figure 5.2 Generic controlling reactions for radical polymerisation

Three generic types of radical polymerisation controlling reactions are shown in Scheme 5.2. The focus of this work is the controlled radical polymerisation process using nitroxide radicals, known as nitroxide mediated polymerisation (NMP). Nitroxide radicals undergo a trapping and dissociation-type controlling reaction as shown in Reaction (5.7), in which the propagating radical is trapped in a dormant alkoxyamine form. Other trapping agents such as nitrogen,[2] sulfur,[3] selenium,[4] and carbon-centred radicals,[5] as well as other oxygen-centred radicals[6] and even metal complexes[7] have been described as control agents utilising a trapping reaction. However, these alternative agents display a poor degree of control, and larger polydispersities than those observed for nitroxide agents.[1]

Other important examples of controlling reactions for radical polymerisation processes are shown in Reactions (5.8) and (5.9). Reaction (5.8) shows a method of control utilising a transfer reaction. Commonly, this reaction involves the transfer of a halide (usually Cl, Br or I) between the propagating radical chain and a transition

metal complex of copper or iron, in a process known as atom transfer radical polymerisation (ATRP).[8] Reaction (5.9) shows a method of control utilising a reversible chain transfer step. The most common polymerisation that uses this controlling reaction is reversible addition fragmentation chain transfer (RAFT) polymerisation.[9] RAFT agents typically take the form of thiocarbonyl compounds such as dithioesters, xanthates or dithiocarbamates.[1]

5.2.2 Nitroxide mediated polymerisation (NMP)

Nitroxide mediated polymerisation (NMP) is a radical polymerisation process in which polymer chain growth is controlled by the reversible trapping reaction shown in Reaction (5.10). The growing polymer radical is trapped by a nitroxide radical species to form a dormant alkoxyamine.

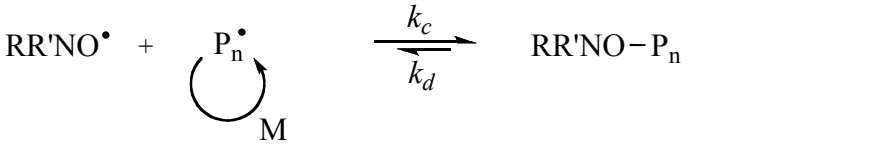

(5.10)

The effect of a nitroxide radical on a polymerisation process was first described as an inhibition reaction, rather than a method of control.[10] The introduction of nitroxide radicals as control agents appeared in the 1980s. Early studies revealed that polymers and copolymers with predictable molecular masses and relatively narrow molecular weight distributions can be prepared with the simple step of addition of a nitroxide to the polymerisation medium.[11-13] Initial investigations showed that homopolymerisations of styrene and acrylates could be controlled by the nitroxide species di-*tert*-butyl nitroxide (**1**)[12] and piperidine-like nitroxides such as 2,2,6,6,-tetramethylpiperidin-1-yloxyl (TEMPO, **2**),[13] however with further study it became clear that controlled polymerisation was limited to these monomers only.

Despite decades of investigation, NMP remains at the forefront of current research with ongoing efforts to expand the scope of the process to new monomers and copolymerisation reactions. Several workers have been able to overcome limitations in the scope of NMP through the identification of other nitroxide species able to polymerise a wider range of monomers. The most success has come from the development of β-H nitroxides such as *tert*-butyl-[2-methyl-1-phenylpropyl] nitroxide (TIPNO, **68**)[14,15] and *tert*-butyl-[1-diethylphosphono-2,2-dimethylpropy)] nitroxide

(SG1, **69**).[16] These species have been shown to control the polymerisation of styrenes, alkyl acrylates, acrylamides, acrylonitrile and dienes,[15] but have had limited success in the control of methacrylate derivatives.

5.2.3 Prediction of rate constants for the control reaction of NMP

Reaction (5.10) shows the rate constants for the coupling of a nitroxide controlling agent with an alkyl polymeric radical, k_c, and the dissociation of the formed alkoxyamine, k_d, making up the controlling reaction of NMP. In this work the equilibrium constant of the control reaction is defined as $K = k_c/k_d$. The rate constants k_c and k_d, and their relationship described by K, are important parameters in determining the success of the control reaction and therefore the properties of the polymer produced. If K is too small, not enough of the growing polymer will be trapped at any one time to afford control, resulting in polymers with high polydispersity indices (PDIs). On the other hand, if K is too large, too much of the growing polymer will remain trapped in a dormant form and the polymerisation will occur sluggishly, also resulting in poor control.

The prediction of rate and equilibrium constants via theoretical methods allows for the optimisation of the control reaction and the identification of targets for experimental study. In 1996, the equilibrium constant for the successfully controlled polymerisation of styrene in the presence of TEMPO (**2**) was determined to be approximately 10^{11} $Lmol^{-1}$ at 393 K, using electron spin resonance (ESR) data[17] and the Predici® simulations package.[18] Subsequent kinetic analyses by Souaille and Fischer for generic living polymerisations controlled by a reversible trapping reaction showed that for efficient control, the equilibrium constant, K, should vary roughly from 10^7 to 10^{11} $Lmol^{-1}$.[19,20]

Several investigators have performed kinetic studies on the factors affecting the combination and dissociation rate constants, k_c and k_d, for a range of nitroxides and alkyl radical species. It was observed that the energy of activation and deactivation of the control reaction was affected by the structure of the nitroxide radical including its ring size, steric bulk, potential for intramolecular hydrogen bonding and the polar effects from groups attached to the ring.[21,22] These effects have been quantified using parameters such as bond dissociation energies, radical

stabilisation, polar, and steric factors.[23] Equations to predict combination and dissociation rate constants for the reaction between a nitroxide radical and the styrene unimeric radical, $^{\bullet}CH(CH_3)Ph$, have been determined and are shown in Equations (5.11) and (5.12). In these equations, k_c and k_d are expressed in terms of the Hammett parameter for polar/inductive field (σ_I)[24] and the Taft parameter for steric effects (E_s)[25], for substituents on the nitroxide.[26,27]

$$\log\left(k_c\right) = 0.57\sigma_I + 0.40E_s + 9.86 \tag{5.11}$$

$$\log\left(k_d\right) = -3.07\sigma_I - 0.88E_s - 5.88 \tag{5.12}$$

Separately, the stability, polarity and steric bulk of the leaving alkyl radical were found to affect the rate of the dissociation reaction in a similar way.[21] The dissociation rate constant can be expressed in terms of the Charton parameters for polar/inductive field (σ_U)[24] and steric effects (υ)[28], as well as a parameter quantifying the radical stability (σ_{RS}), a normalised version of the values determined by Rüchardt *et al*.[29] Equations (5.13) and (5.14) give the homolysis rate constants for TEMPO (**2**) and SG1 (**68**) type alkoxyamines, respectively.[30]

$$\log\left(k_d/k_{d,0}\right) = 13.6\sigma_U + 6.6\upsilon + 13.7\sigma_{RS} \tag{5.13}$$

$$\log\left(k_d/k_{d,0}\right) = 19.5\sigma_U + 7.0\upsilon + 15.3\sigma_{RS} \tag{5.14}$$

Although successful, the equations determined previously to describe the combination and dissociation reactions of nitroxides and alkyl radicals are not general. They describe the rate constants of the reactions for the variation of either the nitroxide radical or the alkyl radical separately, but are not applicable for the variation of both. They also use various experimentally determined parameters instead of a standard set of parameters. In many cases, these are not available in the literature and must be estimated by additivity approximations. For example, the Taft steric constant, E_s, of an unusual substituent group can be estimated as a linear combination of individual known parameters for parts of the group, using equation coefficients determined by Fujita and coworkers.[31]

Another issue that may affect the success of the current set of equations is the use of a unimeric model polymer radical to represent the full propagating radical. It

has been shown recently in a theoretical study of the polymerisation of methyl methacrylate (MMA) using the control agent SG1 (**68**), that the penultimate monomer unit has a large effect on the rate constants. Calculations performed using only the unimeric radical were found to underestimate the dissociation rate constant and overestimate the combination rate constant by well over an order of magnitude in each case.[32,33] Penultimate unit effects are also known to be large in calculations of the propagation rates for copolymerisation reactions[34] and the rates of controlling reactions for ATRP[35] and RAFT-type[36] polymerisations.

The design of an equation, generalised for all nitroxide controlling agents and monomers, suitable for the use of larger model radicals where necessary, and made up of easily computed parameters calculable for any species, would be advantageous. In this work, such an equation will be determined using a multiparameter analysis and will be used to examine the nitroxide-controlled polymerisation of methyl methacrylate.

5.2.4 Nitroxide mediated polymerisation of methyl methacrylate

Polymethacrylates are important industrial polymers, used in many applications including optic fibres and building and biomedical products. Many studies have been devoted to improving the controlled polymerisations of these monomers. Soon after the development of NMP it was shown that the common piperidine nitroxide TEMPO (**2**) does not control the polymerisation of methyl methacrylate (MMA). Other six-membered derivatives of TEMPO (**2**) yielded similar results, with polymerisation stopping after 30–40% conversion and showing no living character.[37] These experimental observations disagreed with a previous theoretical analysis, which showed that the homopolymerisation of MMA with TEMPO (**2**) has suitable kinetic parameters to be controlled at 393 K (120°C).[38] The lack of control has been attributed to a hydrogen transfer side reaction, leading to the formation of a hydroxylamine and an alkene species. In the literature this reaction is sometimes (incorrectly) called a disproportionation reaction. Reaction (5.15) shows the transfer occurring as an intermolecular hydrogen atom abstraction reaction between the nitroxide and the propagating radical, in a commonly described mechanism.[39] It was recently suggested that transfer occurring as an intramolecular coordinatied reaction

within the alkoxyamine species, as shown in Reaction (5.16), may offer a plausible alternative mechanism.[40]

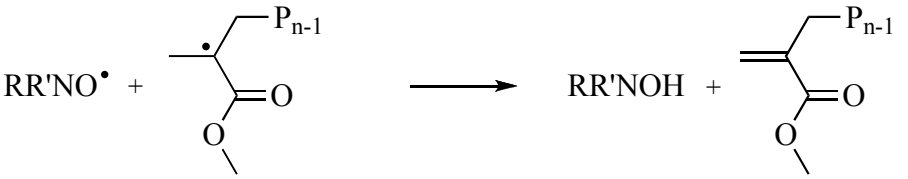

(5.15)

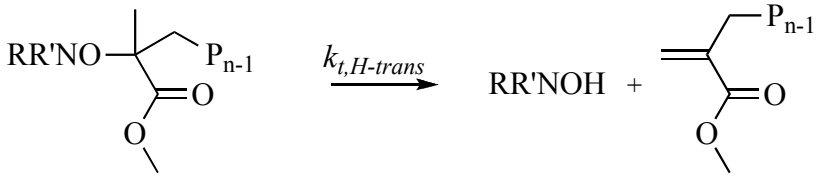

(5.16)

The hydrogen transfer side reaction occurs only to a small extent for styrene and acrylate polymerisations. However, it is dominant in the polymerisation of MMA, effectively halting the polymerisation process when a TEMPO (**2**) controlling agent is used.[39] This side reaction occurs only to a minor extent for polymerisation of MMA with SG1 (**68**) as the controlling agent, however, kinetic studies have shown that at 393 K the equilibrium constant of the trapping reaction, *K*, is too small to afford control.[41] Decreasing the polymerisation temperature to below 323 K (50°C) was found to yield only partial control at the beginning of the polymerisation process.[32] Recently, it was found that MMA-rich block copolymers can been produced via an SG1-mediated polymerisation in the presence of small amounts (4.4–8.8%) of a styrene monomer.[42] The addition of the styrene monomer drastically increases the equilibrium constant of the trapping reaction resulting in polymerisation control.

The search for nitroxides to control the homopolymerisation of MMA has been ongoing for several years and was originally one of the aims of this work. At the outset of this study, control could not be achieved using any of the nitroxide agents so far tested. However, during the course of this investigation, work with a similar aim was carried out in parallel by Tordo and co-workers. These workers have recently described the controlled polymerisation of MMA using a new indoline nitroxide species 2,2-diphenyl-3-phenyliminoindolin-1-yloxyl (DPAIO, **72**) (see Table 5.7).[43] Since this new successful nitroxide controlling agent satisfies one of the initial goals of this project it will instead be used in this work as a practical test of the equation describing *K* in terms of computationally determined parameters.

5.3 Thermodynamics of the control reaction of NMP

The thermodynamics of the control reaction of nitroxide mediated polymerisation (NMP) is the principal factor determining the extent of control and the properties of the polymer produced. By using computational quantum chemistry as a method for the calculation of thermodynamics, many different controlling agents and monomers can be investigated, with the aim of identifying suitable control agents for further experimental study. In this work, reliable methods for the determination of thermodynamic parameters will be identified, both by direct calculation and through multiparameter analysis.

5.3.1 Nitroxide substituent effects

Gas-phase thermochemical data for the trapping of methyl radical by various nitroxides is shown in Table 5.1. Although the entropies of these similar reactions show little variation, it can be seen that the enthalpies, and consequently the free energies and equilibrium constants, show larger variations. The free energies of trapping show a similar trend to the reduction potentials of the same nitroxides, calculated in Chapter 4.3.1. It is observed that the trapping of nitroxides, like their reduction, is determined by the flexibility of the nitroxide species around the nitrogen centre. That is, it is dependent upon how easily this centre can adopt a pyramidal shape upon conversion to an alkoxyamine. In general, the six-membered piperidine and azaphenalene ring-containing nitroxides are more reactive to radical addition than the five-membered pyrrolidine and isolindoline species due to the extra flexibility within the six-membered ring. Variations caused by substituents on the rings affect the reaction energies far less than the overall ring structures, and follow a trend expected on the basis of electronegativity considerations. Thus, for example, the addition of an electron donating substituent such as a carboxy group makes radical addition more favourable. Nitroxides with β-positioned ethyl rather than methyl substituents show smaller exothermicities for radical addition due to their additional steric bulk around the reaction centre.

Also shown in Table 5.1 are the β-H nitroxides TIPNO (**68**) and SG1 (**69**). These species show relatively low reactivities compared with the cyclic nitroxides

species, with TIPNO having a similar exothermicity of trapping to the five-membered pyrrolidine and isoindoline derivatives, and SG1 showing an even smaller exothermicity. The lowering in trapping favourability for the non-cyclic species (including di-*tert*-butyl nitroxide (**1**)) is due to greater steric bulk around the reaction centre. The reaction site is rendered less accessible because the β substituents are not "pinned back" by the confines of a ring structure. In contrast, the indoline-type nitroxides 2,2-dimethylindolin-yloxyl (**70**) and 2,2-diphenylindolin-yloxyl (**71**) show higher reactivities to methyl trapping than the isoindoline nitroxides due to a reduction in steric bulk around the reaction centre.

Table 5.1 Calculated[a] gas-phase thermochemical data (at 298 K) for methyl radical addition to nitroxides

Nitroxide	Structure	ΔH (kJmol^{-1})	ΔS (kJmol^{-1})	ΔG (kJmol^{-1})	K (Lmol^{-1})	log (K_{calc})
1		-198.5	-181.4	-144.5	5.0×10^{26}	26.7
2		-204.9	-178.0	-151.8	9.6×10^{27}	28.0
3	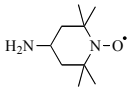	-206.3	-175.9	-153.8	2.2×10^{28}	28.3
4	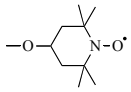	-206.1	-176.1	-153.6	2.0×10^{28}	28.3
6	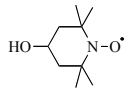	-207.2	-175.7	-154.9	3.3×10^{28}	28.5
8	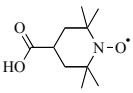	-207.6	-176.9	-154.8	3.2×10^{28}	28.5
9	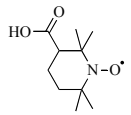	-208.3	-178.6	-155.1	3.6×10^{28}	28.6
10	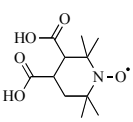	-211.0 [b]	-181.5	-156.9	7.4×10^{28}	28.9

11	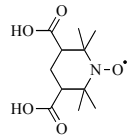	-213.0 [b]	-177.1	-160.2	2.9×10^{29}	29.5
12	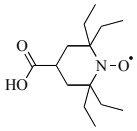	-189.1 [b]	-170.6	-138.2	4.1×10^{25}	25.6
15		-192.1	-177.4	-139.3	6.1×10^{25}	25.8
16	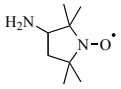	-194.3	-175.1	-142.1	1.9×10^{26}	26.3
17	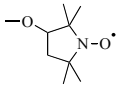	-196.2	-169.6	-145.6	8.0×10^{26}	26.9
18	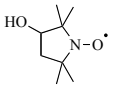	-197.4	-176.5	-144.8	5.8×10^{26}	26.8
19	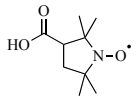	-195.0	-178.7	-141.8	1.7×10^{26}	26.2
20	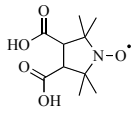	-196.9 [b]	-175.6	-144.5	5.1×10^{26}	26.7
21	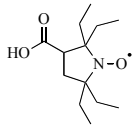	-186.6 [b]	-182.8	-132.1	3.4×10^{24}	24.5
27	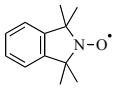	-194.5	-174.7	-142.4	2.1×10^{26}	26.3
28	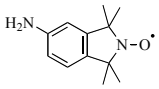	-193.3 [b]	-176.4	-140.7	1.1×10^{26}	26.0
31	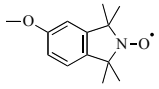	-193.6 [b]	-180.1	-139.9	7.9×10^{25}	25.9
33	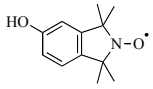	-194.2 [b]	-179.6	-140.7	1.1×10^{26}	26.0
34	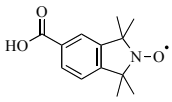	-197.2 [b]	-181.1	-143.2	3.0×10^{26}	26.5
35	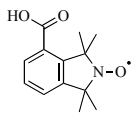	-194.3 [b]	-180.1	-140.6	1.1×10^{26}	26.0

36	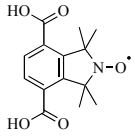	-195.0 [b]	-171.9	-143.8	3.8×10^{26}	26.6
37	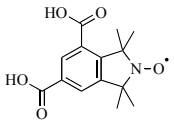	-196.5 [b]	-180.0	-142.8	2.6×10^{26}	26.4
38	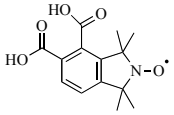	-199.6 [b]	-175.9	-147.2	1.5×10^{27}	27.2
39	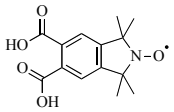	-199.6 [b]	-180.6	-145.8	8.5×10^{26}	26.9
47	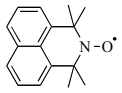	-203.6	-167.9	-153.5	1.9×10^{28}	28.3
56	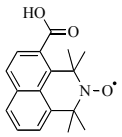	-204.0 [b]	-176.3	-151.4	8.4×10^{27}	27.9
57	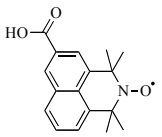	-206.2 [b]	-171.5	-155.0	3.5×10^{28}	28.5
58	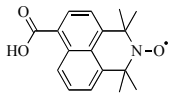	-205.5 [b]	-177.0	-152.8	1.4×10^{28}	28.2
68	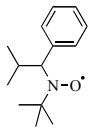	-196.3	-179.9	-142.6	2.4×10^{26}	26.4
69	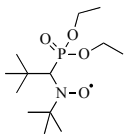	-192.9 [b]	-177.6	-140.0	8.2×10^{25}	25.9
70	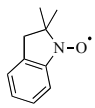	-202.3	-177.1	-149.5	3.8×10^{27}	27.6
71	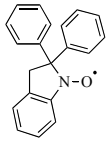	-209.2 [b]	-177.5	-156.3	5.9×10^{28}	28.8

[a]G3(MP2)-RAD//B3-LYP/6-31G(d) values except where noted. [b]ONIOM approximation including the parent (H-substituted) nitroxides and the methyl radical in the core system, with the full system calculated at the RMP2/6-311+G(3df,2p) level.

5.3.2 Polymer substituent effects

Gas-phase thermochemical data for the trapping of various radicals by the nitroxide radical TEMPO (**2**) is shown in Table 5.2. The data follow the expected trend based upon characteristics of the alkyl radicals. Figure 5.3 shows the correlation between the radical stabilisation energy of alkyl radicals (calculated from the enthalpy of Reaction (2.45) in Chapter 2.4.4, with values shown in Table 5.3) and the equilibrium constants of trapping by TEMPO (**2**). Ignoring the outlying points discussed below, fairly good correlation between log (K_{calc}) and RSE_{alkyl} is shown by the value $R^2 = 0.872$. Some scatter is seen due to the additional influence of the polar and steric properties of the radicals. In general however, it is seen that the trends in trapping depend primarily upon the radical stability, with less stable radicals showing greater favourabilities for trapping.

Table 5.2 Calculated[a] gas-phase thermochemical data (at 298 K) for alkyl radical addition to TEMPO

Radical	ΔH (kJmol^{-1})	ΔS (kJmol^{-1})	ΔG (kJmol^{-1})	K (Lmol^{-1})	log (K_{calc})
$\cdot CH_3$	-204.9	-178.0	-151.8	9.6×10^{27}	28.0
	-217.7	-209.2	-155.3	4.0×10^{28}	28.6
	-218.9	-202.2	-158.6	1.5×10^{29}	29.2
	-212.8	-223.8	-146.1	9.7×10^{26}	27.0
	-196.9	-216.6	-132.3	3.7×10^{24}	24.6
	-228.9	-202.8	-168.5	8.0×10^{30}	30.9
	-249.7	-200.1	-190.1	4.9×10^{34}	34.7
	-220.3	-215.3	-156.1	5.6×10^{28}	28.7
	-174.5	-183.7	-119.7	2.3×10^{22}	22.4
	-178.0	-210.5	-115.3	3.9×10^{21}	21.6
	-159.7[b]	-223.1	-93.1	5.1×10^{17}	17.7
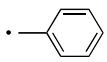	-163.8[b]	-180.5	-110.0	4.6×10^{20}	20.7
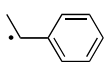	-168.9[b]	-214.3	-105.0	6.1×10^{19}	19.8

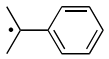	-161.3 [b]	-230.1	-92.7	4.3×10^{17}	17.6
	-187.1	-194.4	-129.1	1.0×10^{24}	24.0
	-181.5 [b]	-212.2	-118.3	1.3×10^{22}	22.1
	-168.8 [b]	-232.0	-99.7	7.1×10^{18}	18.9
	-234.7 [b]	-219.1	-169.3	1.1×10^{31}	31.1

[a]G3(MP2)-RAD//B3-LYP/6-31G(d) values except where noted. [b]ONIOM approximation including $(CH_3)_2NO^{\bullet}$ and the alkyl radical in the core system, with the full system calculated at the RMP2/6-311+G(3df,2p) level.

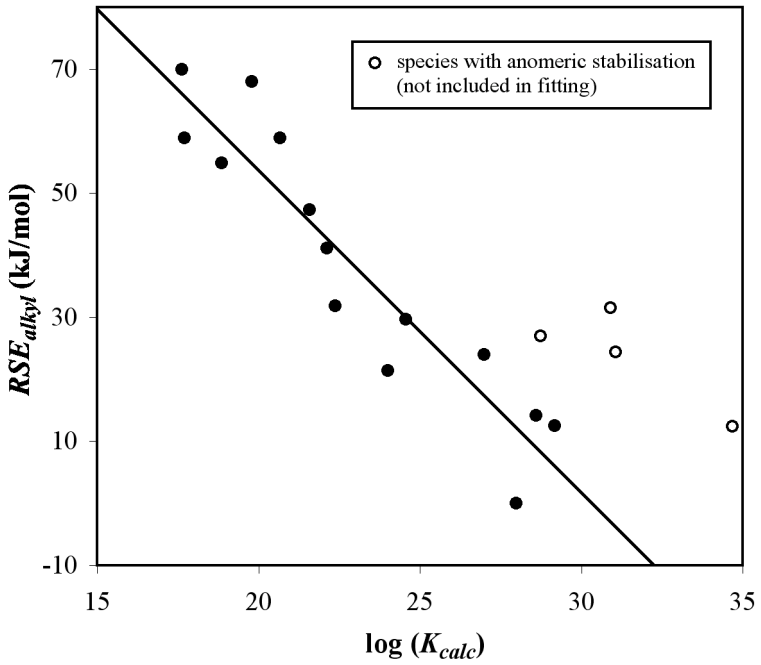

Figure 5.3 Correlation ($R^2 = 0.872$) between the directly calculated equilibrium constant for alkyl radical trapping by TEMPO (2) and RSE_{alkyl}

Greater than expected free energies of trapping are seen for the radical species $^{\bullet}CH_2OH$, $^{\bullet}CH_2F$, $^{\bullet}CH(CH_3)OC(O)CH_3$ and $^{\bullet}CH(CH_3)Cl$. These radicals, seen as outlying points in Figure 5.3, all possess a heteroatom in the position α to the radical centre. Their higher reactivity is due to anomeric stabilisation[44] of the product alkoxyamine species. This effect has been previously noted for TEMPO alkoxyamines

derived from tetrahydrofuran and triethylamine, which show higher energies of dissociation at the C–O bond than expected.[45] It has also been investigated using computational methods.[46] One of the lone pairs of the nitroxyl oxygen lies antiperiplanar to the carbon–heteroatom bond, allowing hyper-conjugation to occur between the lone pair and the σ^* anti-bonding orbital of the bond. This is illustrated in Figure 5.4 for the TEMPO–CH_2OH alkoxyamine. In this example, anomeric stabilisation results in a significant lengthening of the NOC(H_2)–OH bond while the NO–CH_2OH bond is significantly shortened and strengthened.[46]

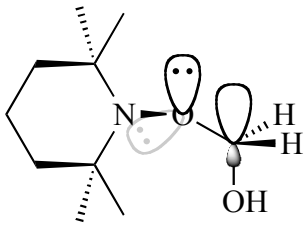

Figure 5.4 The alkoxyamine product of the reaction between TEMPO (2) and $^{\bullet}CH_2OH$, with anomeric stabilisation of the NO–C bond

5.4 A new equation for the equilibrium constant

In the previous two sections the effects of the nitroxide and the alkyl radical on the control reaction of NMP were examined separately for relatively small systems. Through an assessment study (see Chapter 3), it was determined that high-level *ab initio* methods are required for the study of nitroxide reactions. Since these methods are very computationally expensive it is not possible to calculate equilibrium constants directly for the larger systems in this study. Computational limitations mean that for these species, only the thermodynamics for addition to small radicals such as methyl are directly calculable (see Table 5.1). Similarly, when larger alkyl radical species are examined, only additions to smaller nitroxides such as TEMPO (**2**) may be calculated (see Table 5.2). In order to study a much larger range of nitroxide and alkyl radical combinations, without sacrificing a high level of theory, a multi-parameter analysis, building upon those from literature describing reaction rate constants, is

required. This gives an equation for the standard state equilibrium constant in terms of molecular parameters both of the nitroxide and the alkyl radical. It is therefore necessary to identify computational parameters to describe the effects of both the nitroxide and the alkyl radical on the thermodynamics of the trapping reaction.

5.4.1 Fitting parameters for nitroxides

In order to choose parameters to quantify the effect of the nitroxide on the thermodynamics of trapping, the isodesmic reaction shown in Reaction (5.17) is proposed. This reaction compares the energy of a nitroxide with the reference di-*tert*-butyl nitroxide (**1**), using the corresponding hydroxylamines to balance the reaction. Reaction (5.17) is similar to the reaction quantifying the standard radical stabilisation energy (*RSE*) of an alkyl radical shown in Reaction (2.45) in Chapter 2.4.4. The only difference is that the zero-point for Reaction (5.17) is systematically shifted by the reference species to a more convenient value. The enthalpy of Reaction (5.17) is therefore defined as the radical stabilisation energy of a nitroxide radical, RSE_{nxd}.

$$RR'NO^{\bullet} + (t\text{-}Bu)_2NOH \longrightarrow RR'NOH + (t\text{-}Bu_3)_2NO^{\bullet} \qquad (5.17)$$

It is well known that the isodesmic Reaction (2.45) successfully describes the true stability of an alkyl radical, with trends following those expected from considering the substitution patterns on the radical. As shown in Figure 5.5, the radical stabilisation energies of alkyl radicals, RSE_{alkyl}, (shown in Table 5.3) also correlate well with the spin densities on the radical centre, which provide a good measure of the level of delocalisation of the unpaired electron.

Despite the success of Reaction (2.45), it has been shown that using isodesmic reactions to predict radical stabilities can be problematic due to the contribution from the reference species used to balance the reaction.[47] For example, completely different trends have been observed for the same series of phosphoranyl radicals when the reference species are changed.[48] As seen in Figure 5.6, the RSE_{nxd} values of the nitroxide radicals (shown in Table 5.3) do not correlate with the trend in spin densities, nor do they follow the trend expected based upon radical delocalisation arguments. The most notable example is for the indoline nitroxides, which are expected to be more stable than the isoindoline nitroxides due to radical delocalisation

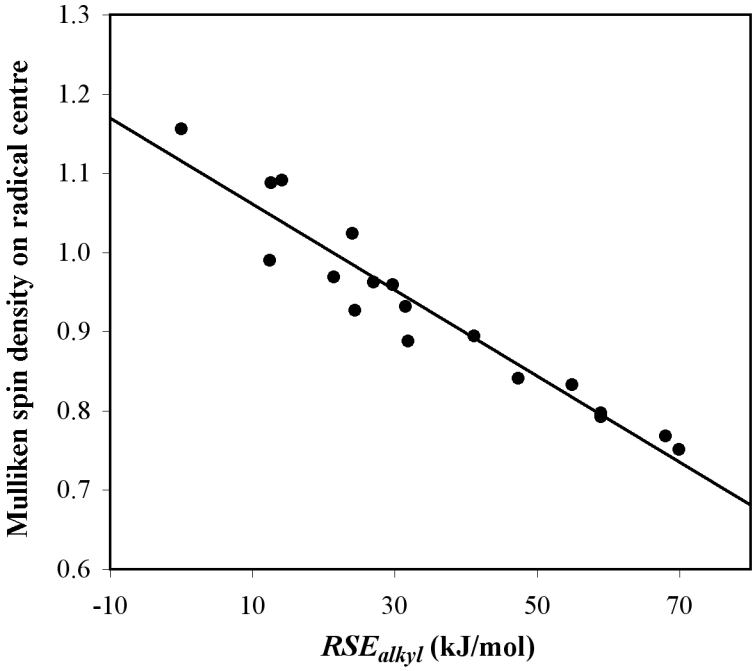

Figure 5.5 Correlation ($R^2 = 0.917$) between the RSE_{alkyl} and Mulliken spin densities on the radical centre

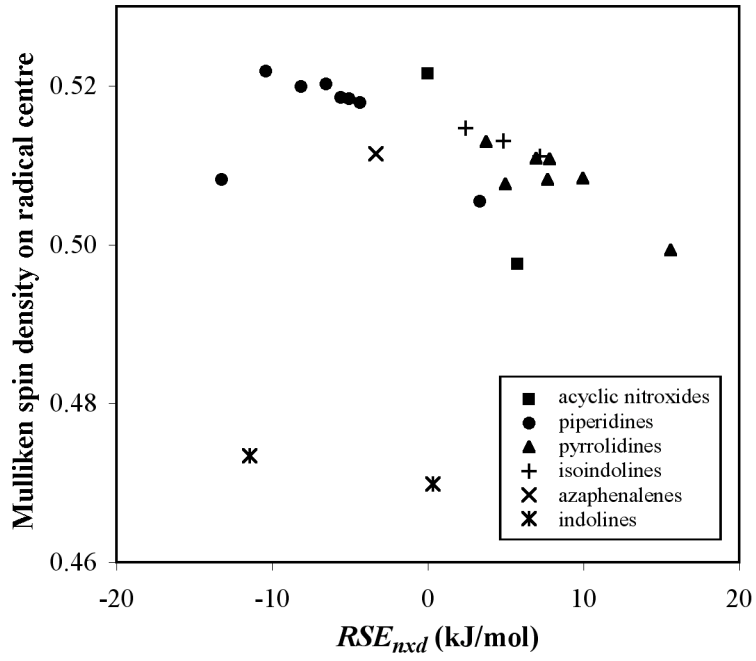

Figure 5.6 Correlation ($R^2 = 0.007$) between the RSE_{nxd} and Mulliken spin densities on the radical centre

on the phenyl ring.[43] The indolines have much lower spin densities on the oxygen radical centre than the isoindolines, indicating that radical delocalisation occurs, however the RSE_{nxd} values do not reflect this stabilisation. Therefore, RSE_{nxd} values do not measure the true stabilities of the nitroxide radicals, despite the similarity of their determination with that of RSE_{alkyl} values.

Figure 5.7 shows the correlation between the RSE_{nxd} values and the formal reduction potentials of the nitroxides, E^o_{red}, listed in Table 4.1 in Chapter 4.3.1. The E^o_{red} values are determined as the ability of a nitroxide radical to accept an electron to form the corresponding anionic species as shown in Reaction (2.36) in Chapter 2.4.2. These values are directly related to the flexibility of the ring structure of the nitroxide, which determines how easily the anion undergoes pyramidalisation at the nitrogen centre, as discussed in Chapter 4.3.1. Although the correlation seen in Figure 5.7 is to the formal reduction potential, it should be noted that the nitroxide is readily protonated in its anionic form, producing a hydroxylamine. Hence, RSE_{nxd} can therefore be considered a measure of the transformation of a nitroxide to a hydroxylamine.

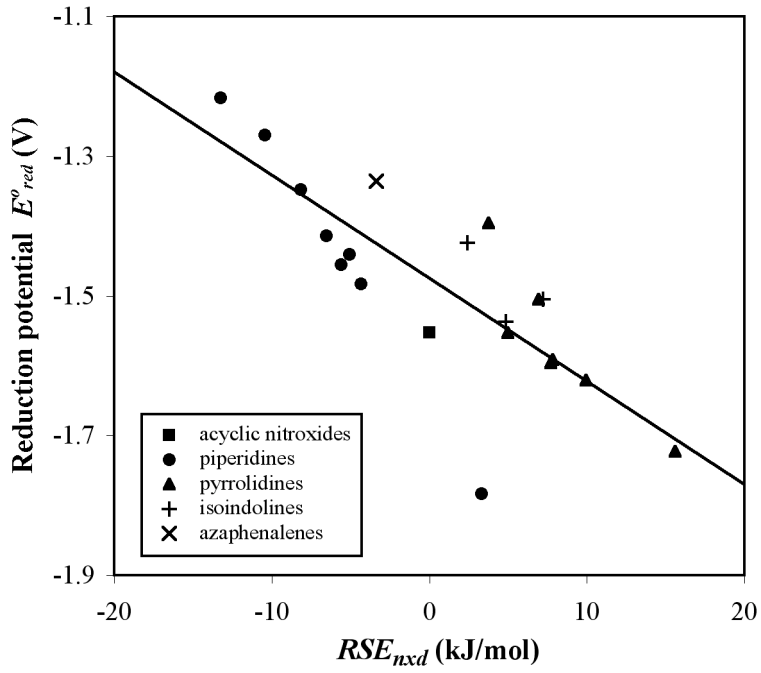

Figure 5.7 Correlation (R^2 = 0.638) between RSE_{nxd} and E^o_{red} of nitroxide radicals

Like reduction, the trapping reaction between an alkyl radical and a nitroxide also involves the pyramidalisation of the nitrogen centre in the nitroxide. Figure 5.8 shows the correlation between the logarithmic values (in base 10) of directly calculated equilibrium constants for methyl trapping, log (K_{calc}), (values shown in Table 5.1) and RSE_{nxd}, for the same species. The correlation between the values is very good, with an MAD equivalent to only 2.5 kJmol^{-1} in free energy.

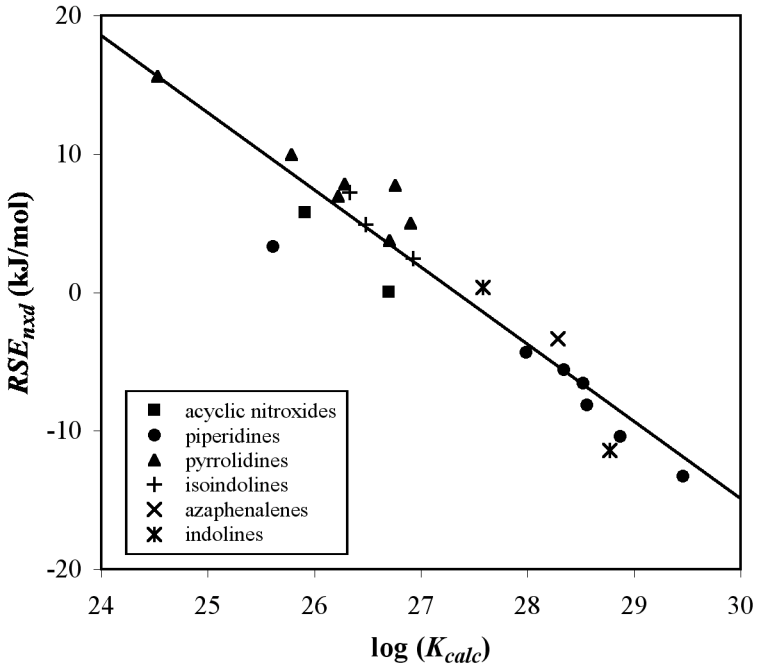

Figure 5.8 Correlation (R^2 = 0.902) between the directly calculated equilibrium constant for methyl trapping by nitroxides and RSE_{nxd}

The RSE_{nxd} parameter directly measures the hydrogen abstracting ability of nitroxides, which is primarily determined by the steric effects involved in the pyramidalisation of the nitrogen centre, with polar and radical stability effects being less significant. It correlates well with methyl radical trappings, and it is expected that it will also provide a good representation of the effect of the nitroxide on the trapping of larger alkyl radicals. The fact that only a single parameter is required to describe the nitroxide contribution to the trapping reaction is not surprising due to the similarities of these species around the reaction centre. While the alkyl radicals show

considerable variety, the nitroxides are all similarly bulky around the reaction centre, differing from each other only at the positions β to the radical. There is scope to generalise the multiparameter analysis performed in this work for the nitroxides to the study of other controlled radical polymerisation reactions such as atom transfer radical polymerisation (ATRP) and reversible addition fragmentation chain transfer (RAFT). However, in the case of a more general equation being developed, it is expected that additional parameters will need to be included to account for the large differences in the structures of these controlling agents.

5.4.2 Fitting parameters for alkyl radicals

In previous works, parameters describing the polar, steric and radical stability of alkyl radicals were found to be necessary for the description of the kinetics of the dissociation of alkoxyamines into nitroxide and alkyl radicals. From Table 5.2 it is seen that unimeric radicals representing the propagating radicals of common monomers differ greatly in structure, steric bulk and substituent groups, making them far more variable than the nitroxide controlling agents. It was found in Chapter 5.3.2 that the trend in the free energies of trapping of alkyl radicals by a constant nitroxide species depends primarily upon the radical stabilities of the alkyl radicals. However, it is expected that the addition of parameters for polar and steric effects will improve the correlation seen in Figure 5.3. Therefore, computationally based parameters quantifying the polar, steric and radical stabilisation effects from the different radicals were included in the analysis in this work.

Polar/inductive field effects on the radicals were quantified through the use of gas-phase vertical electron affinities. Values of EA_{alkyl} were calculated as the enthalpy of Reaction (2.30) in Chapter 2.4.1, measured in the standard units of electron volts (eV) with the results shown in Table 5.3.[49] The calculations were performed at the G3(MP2)-RAD(+) level of theory, which comprises standard G3(MP2)-RAD theory with extra diffuse functions added to the 6-31G(d) basis sets to provide a better description of the anionic species.

Currently there is no standard or common method to calculate the steric bulk of a molecule around a reaction centre. The isodesmic reaction shown in Reaction (5.18), in which a sterically hindered R group is compared to the same group in a non-

hindered molecule, was unsuccessful in quantifying even general steric trends. The failure of the isodesmic reaction is likely due to overwhelming polar effects in the reaction, and it is clear that Reaction (5.18) is not a suitable method for determining the effects of steric bulk on alkyl radicals. A similar approach recently proposed by Böhm and Exner,[50] using the isodesmic reaction shown in Reaction (5.19), achieves some success when calculated using low-level density functional theory methods, however it gives unsuccessful results when calculated using high-level *ab initio* methods. It has previously been shown that polar effects are underestimated by DFT methods.[51] Therefore, it is likely that the large polar effects in the isodesmic reaction are being minimised when a DFT method is used. However, basing the calculation of steric parameters on error cancellations at low levels of theory is not ideal.

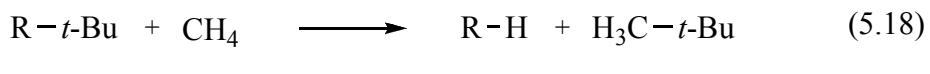

(5.18)

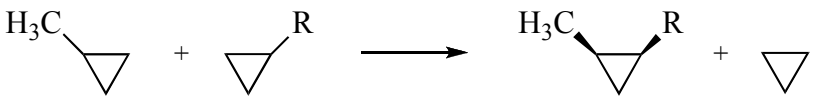

(5.19)

In the present work, a parameter to quantify steric effects is determined by the simplest possible means. The steric contribution is estimated as the radical order, called for this purpose $order_{alkyl}$, which counts the number of non-hydrogen substituents bound to the radical centre. The methyl radical is given a value of zero, primary radicals one, secondary radicals two, and tertiary radicals three. The values of $order_{alkyl}$, tabulated in Table 5.3, show a good correlation (R^2 = 0.819) with the Charton steric parameter, υ,[28] indicating their suitability to estimate the steric bulk of alkyl radicals.

As discussed in the previous section, the radical stabilisation energy of an alkyl radical, RSE_{alkyl}, is well defined as the enthalpy of the isodesmic Reaction (2.45) described in Chapter 2.4.4.[52] RSE_{alkyl} values are shown in Table 5.3. The values were found to agree with the literature values published by Zipse,[53] calculated at the same level of theory.

Figure 5.9 shows the correlation between log (K_{calc}) for the trapping of various alkyl radicals by TEMPO (**2**) (values shown in Table 5.2) and a linear combination of EA_{alkyl}, $order_{alkyl}$ and RSE_{alkyl} for the same species, fitted by linear regression. For the trapping of most of the radicals, the correlation is very good, with an MAD equivalent

to 3.5 kJmol^{-1} in free energy. Outlying points are seen for species with a heteroatom α to the alkyl radical centre due to anomeric stabilisation on the alkoxyamine species, as shown in Figure 5.4. This effect causes an underestimation in the log (*K*) values, determined by the fitted equation, by 3.4 to 6.0 orders of magnitude, corresponding to between 19.6 and 34.1 kJmol^{-1} in free energy. The anomeric effect follows electronegativity trends with stabilisation increasing with heteroatom substituents in the order: chlorine, oxygen, fluorine. It is possible that with further investigations, the effects of anomeric stabilisation could be quantified with an additional parameter in the equation. However, in the present work, due to the small number of data points of species with anomeric stability, these are not included in the fitting of equations to describe log (*K*) and remain outlying points in the comparisons with the directly calculated log (*K*) values.

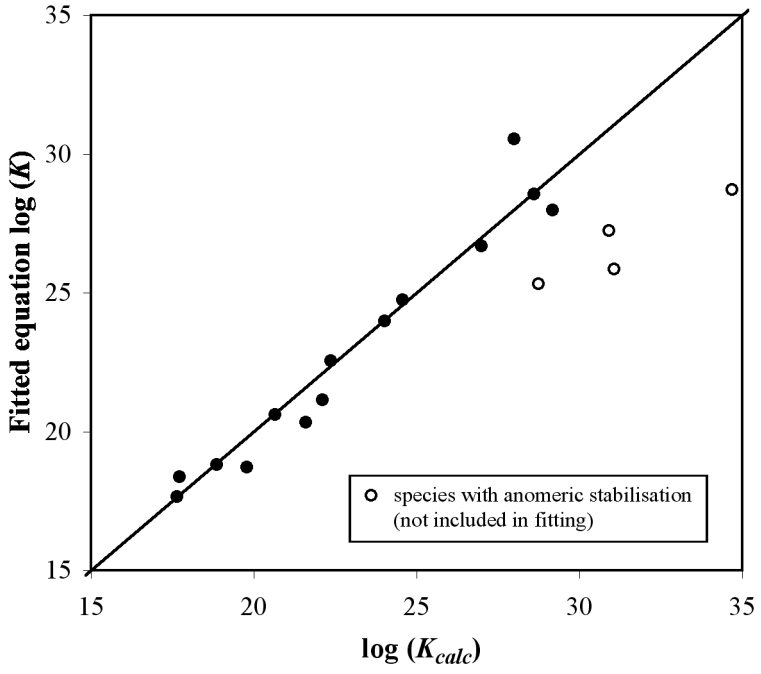

Figure 5.9 Correlation (R^2 = 0.949) between the directly calculated equilibrium constant for alkyl radical trapping by TEMPO (2) and a fitted equation for the parameters EA_{alkyl}, $order_{alkyl}$ and RSE_{alkyl}

5.4.3 Equation for K_{eq}

Computational parameters were identified, which allow the trapping reaction between nitroxide and alkyl radicals to be quantified in terms of the molecular properties of each of the radicals. These parameters measure similar properties to the experimental parameters used in previous multiparameter analyses of these reactions. However, they are more general than those used in the past, being easy and relatively cheap to calculate for any nitroxide and alkyl radical. They are useful for very large nitroxide radical species and are also adaptable to taking account of penultimate and longer chain effects, since the exchange of a dimer or longer chain radical in the place of a unimeric radical is straightforward.

The parameters RSE_{nxd}, EA_{alkyl}, $order_{alkyl}$ and RSE_{alkyl} were combined to form the equation to describe log (K) shown in Equation (5.20). Table 5.3 shows the directly calculated log (K) values, log (K_{calc}), the molecular parameters, and the log (K) values found from fitting a linear combination of the parameters, log (K_{eq}). The fitting was performed using linear regression techniques implemented into Microsoft® Excel®. Since it was found that the parameters do not accurately describe a trapping system in which anomeric stabilisation is present in the product alkoxyamine species, these systems were not included in the fitting.

Table 5.3 Calculated log (K_{calc}) values (298 K)[a], fitting parameters (0 K)[b] and log (K_{eq}) values calculated through the fitting of a new equation for different alkyl radicals and nitroxides

Nitroxide	Radical	log (K_{calc})	RSE_{nxd} (kJmol^{-1})[c]	EA_{alkyl} (eV)[d]	$order_{alkyl}$	RSE_{alkyl} (kJmol^{-1})[e]	log (K_{eq})[f]
1	·CH_3	26.7	0.0	-0.08	0	0	27.3
2	·CH_3	28.0	-4.3	-0.08	0	0	28.0
3	·CH_3	28.5	-5.6	-0.08	0	0	28.2
6	·CH_3	28.3	-6.5	-0.08	0	0	28.3
9	·CH_3	28.6	-8.2	-0.08	0	0	28.6
10	·CH_3	28.9	-10.4	-0.08	0	0	29.0
11	·CH_3	29.5	-13.3	-0.08	0	0	29.4
12	·CH_3	25.6	3.3	-0.08	0	0	26.8
15	·CH_3	25.8	9.9	-0.08	0	0	25.7

16	$\cdot CH_3$	26.3	7.8	-0.08	0	0	26.1
17	$\cdot CH_3$	26.9	5.0	-0.08	0	0	26.5
18	$\cdot CH_3$	26.8	7.7	-0.08	0	0	26.1
19	$\cdot CH_3$	26.2	6.9	-0.08	0	0	26.2
20	$\cdot CH_3$	26.7	3.8	-0.08	0	0	26.7
21	$\cdot CH_3$	24.5	15.6	-0.08	0	0	24.8
27	$\cdot CH_3$	26.3	7.2	-0.08	0	0	26.1
34	$\cdot CH_3$	26.5	4.9	-0.08	0	0	26.5
39	$\cdot CH_3$	26.9	2.4	-0.08	0	0	26.9
47	$\cdot CH_3$	28.3	-3.3	-0.08	0	0	27.8
69	$\cdot CH_3$	25.9	5.8	-0.08	0	0	26.4
70	$\cdot CH_3$	27.6	0.3	-0.08	0	0	27.2
71	$\cdot CH_3$	28.8	-11.4	-0.08	0	0	29.1
2		28.6	-4.3	-0.40	1	14.1	26.7
2		29.2	-4.3	-0.01	1	12.6	26.4
2		27.0	-4.3	-0.52	2	24.0	25.6
2		24.6	-4.3	-0.35	3	29.7	24.5
2		30.9	-4.3	-0.79	1	31.5	25.6
2		34.7	-4.3	-0.37	1	12.4	26.9
2		28.7	-4.3	0.00	2	27.0	24.6
2		22.4	-4.3	1.55	1	31.9	22.4
2		21.6	-4.3	1.27	2	47.3	20.9
2		17.7	-4.3	1.08	3	59.0	19.7
2	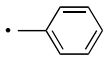	20.7	-4.3	0.88	1	59.0	20.6
2	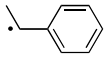	19.8	-4.3	0.82	2	68.0	19.5
2	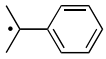	17.6	-4.3	0.77	3	69.9	19.1
2		24.0	-4.3	1.47	1	21.5	23.5
2		22.1	-4.3	1.24	2	41.2	21.6
2		18.9	-4.3	1.12	3	54.9	20.1
2		31.1	-4.3	-0.12	2	24.4	25.0

[a]See Tables 5.1 and 5.2. [b]G3(MP2)-RAD//B3-LYP/6-31G(d) values. [c]Calculated from Equation (5.17). [d]Calculated from Equation (2.30).[49] [e]Calculated from Equation (2.45). [f]Found from Equation (5.20).

Equation (5.20) shows the equilibrium constant of the trapping reaction between a nitroxide and an alkyl radical in terms of molecular parameters of the radicals involved, with the scaling factors of the parameters expressed to three significant figures. The correlation between the log (K_{eq}) values found from Equation (5.20) and the directly calculated values of log (K_{calc}) is shown in Figure 5.10. The MAD between the K_{calc} and K_{eq} values is around half an order of magnitude, corresponding to 3.1 kJmol^{-1} in free energy.

$$\log\ (K_{eq}) = -0.160 RSE_{nxd} - 1.34 EA_{alkyl} - 0.307 order_{alkyl} - 0.0982 RSE_{alkyl} + 27.2 \quad (5.20)$$

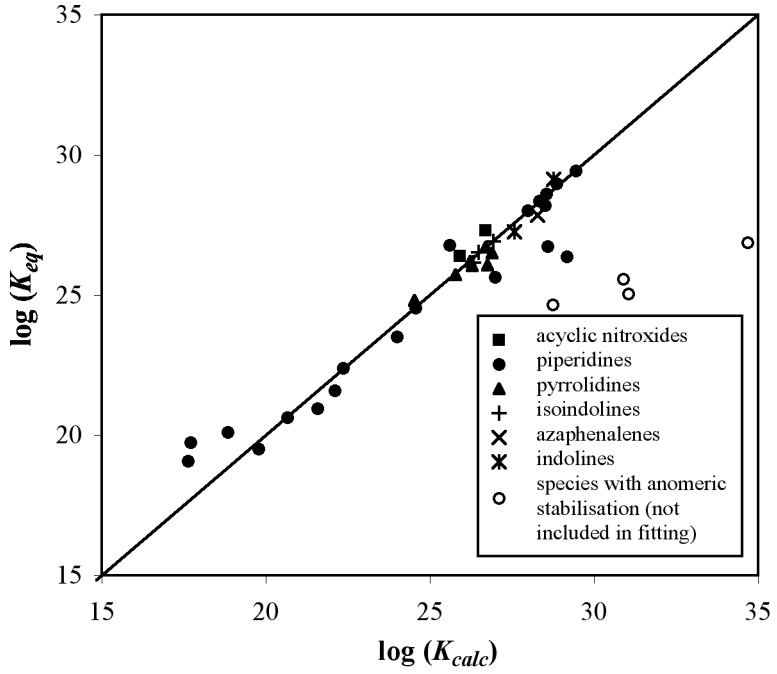

Figure 5.10 Correlation (R^2 = 0.939) between the directly calculated equilibrium constant and the fitted Equation (5.20)

Although Equation (5.20) was derived using only the fitting of methyl radicals with different nitroxides and larger alkyl radicals with TEMPO (**2**), its versatility can be shown through comparisons of some reasonably small mixed nitroxide and alkyl radical systems, for which direct calculation of the equilibrium constant is possible. Table 5.4 shows the log (K_{calc}) and log (K_{eq}) values for trapping reactions of the unimeric radicals of styrene, acrylic acid, methyl acrylate, acrylamide and methyl

methacrylate by the nitroxide species (DBN, **1**), TEMPO (**2**), PROXYL (**15**) and TMIO (**27**). The equation-calculated values show reasonably good correlation with the directly calculated values, with an MAD corresponding to 7.1 kJmol^{-1} in free energy. It is observed that Equation (5.20) performs well for the acrylic acid and acrylamide unimeric radicals, which were not included in the original fitting.

Table 5.4 Calculated log (K_{calc}) values (at 298 K)[a] and log (K_{eq}) values[b] for mixed alkyl radicals and nitroxide systems

Nitroxide	Radical	log (K_{calc})	log (K_{eq})
1	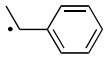	17.2	18.8
1		19.5	20.8
1		20.2	20.9
1		21.7	21.2
1		17.2	19.4
2		21.5	21.5
2		24.3	21.9
15	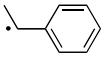	18.3	17.2
15		20.4	19.2
15		20.8	19.3
15		22.5	19.6
15		17.5	17.8
27	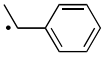	18.9	17.7
27		20.4	19.7
27		20.8	19.7

27		22.6	20.1
27		18.3	18.2

[a]ONIOM approximation of G3(MP2)-RAD//B3-LYP/6-31G(d) values including $(CH_3)_2NO^{\bullet}$ and the alkyl radical in the core system, with the full system calculated at the RMP2/6-311+G(3df,2p) level. [b]Found from Equation (5.20).

The fitted Equation (5.20) can be used to determine gas-phase equilibrium constants of the control reaction of nitroxide mediated polymerisation for large systems where direct calculation is not feasible. In its current form, Equation (5.20) is parameterised for gas-phase equilibrium constants at 298 K and therefore does not give log (*K*) values directly comparable to experimental values performed in a solvent medium. It would be relatively straightforward to re-parameterise the equation under any of the wide variety of experimental polymerisation reaction conditions found in the literature. For the present, for simplicity, the standard state equation values are useful for comparison of the relative magnitudes of *K*, which are expected to follow the same trends in different temperatures and in common polymerisation solvents.

5.4.4 Relationship between kinetics and thermodynamics

Previous equations that describe the trapping and dissociation reaction rate constants, k_c and k_d, in terms of experimentally determined parameters are shown in Equations (5.11) to (5.14). In Chapter 5.4.3, a new equation was derived to describe the ratio of these two rate constants, $K = k_c/k_d$, in terms of computed parameters. The individual rate constants can also be expressed in terms of the same parameters.

The available experimental values of k_c, at 298 K in *tert*-butyl benzene (*t*BB),[26,54] and k_d, at 393 K and in *t*BB,[27] are shown in Table 5.5. A fitting to the experimental log (k_c) and log (k_d) values was performed using the parameters for nitroxide and alkyl radicals RSE_{nxd}, EA_{alkyl}, $order_{alkyl}$ and RSE_{alkyl}. The correlation between the fitted equation values and the experimental rate constants is shown for the combination rate constant, k_c, in Figure 5.11 and for the dissociation rate constant, k_d, in Figure 5.12.

Table 5.5 Experimental[a] rate constants k_c (at 298 K in tBB) and k_d (at 393 K in tBB) and equation values[b] of log ($k_{c,eq}$)[c] and log ($k_{d,eq}$)[d]

Nitroxide	Radical	k_c ($Lmol^{-1}s^{-1}$)	log (k_c)	log ($k_{c,eq}$)	k_d (s^{-1})	log (k_d)	log ($k_{d,eq}$)
1	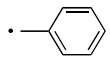	1.8×10^8	8.3	7.9	1.9×10^{-4}	-3.7	-4.6
1	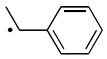	-	-	-	1.3×10^{-2}	-1.9	-2.5
2		-	-	-	6.6×10^{-12}	-11.2	-11.2
2		-	-	-	1.0×10^{-5}	-5.0	-5.0
2		-	-	-	3.4×10^{-4}	-3.5	-3.5
2		-	-	-	1.3×10^{-1}	-0.9	-1.4
2	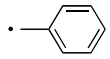	2.6×10^8	8.4	8.4	1.1×10^{-5}	-5.0	-4.9
2	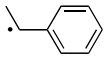	2.2×10^8	8.3	7.8	5.2×10^{-4}	-3.3	-2.9
2	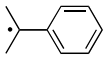	5.2×10^7	7.7	8.3	8.5×10^{-2}	-1.1	-1.2
2		2.3×10^9	9.4	9.3	8.1×10^{-8}	-7.1	-6.2
2		-	-	-	3.4×10^{-5}	-4.5	-3.8
2		6.3×10^8	8.8	7.7	2.2×10^{-2}	-1.7	-1.6
15	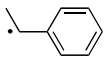	-	-	-	1.5×10^{-4}	-3.8	-1.7
27	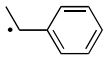	1.5×10^8	8.2	6.4	6.3×10^{-5}	-4.2	-2.0
27	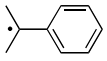	5.2×10^7	7.7	6.9	4.1×10^{-3}	-2.4	-0.3
69		-	-	-	6.5×10^{-5}	-4.2	-4.2
69		-	-	-	2.0×10^{-4}	-3.7	-4.7
69		-	-	-	2.8×10^{-3}	-2.6	-2.6
69	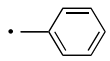	1.1×10^7	7.0	7.1	3.3×10^{-4}	-3.5	-4.1
69	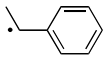	3.1×10^6	6.5	6.6	5.5×10^{-3}	-2.3	-2.1
69	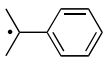	2.0×10^5	5.3	7.1	1.7	0.2	-0.4
69		8.0×10^8	8.9	8.1	3.6×10^{-6}	-5.4	-5.4

69		2.6×10^6	6.4	7.3	3.0×10^{-3}	-2.5	-3.0

[b]As reported by Fischer, Marque and coworkers.[26,27,54] [b]Found from fitting the computational parameters RSE_{nxd}, EA_{alkyl}, $order_{alkyl}$ and RSE_{alkyl}, shown in Table 5.3. [c]Found from Equation (5.21). [d]Found from Equation (5.22).

The fitted equation for the rate constant of the combination reaction is shown in Equation (5.21), with the correlation between log ($k_{c,eq}$) and the log (k_c) of the experimental rate constants shown in Figure 5.11. The experimental and equation values show an MAD of less than one order of magnitude. However, as the combination rates show little variation, all being close to 10^8 $Lmol^{-1}s^{-1}$, the correlation seen in Figure 5.11 is poor.

$$\log\ (k_{c,eq}) = -0.125RSE_{nxd} - 9.34EA_{alkyl} + 0.415order_{alkyl} - 0.172RSE_{alkyl} + 25.8 \quad (5.21)$$

It has previously been shown that the combination reaction is not a diffusion-controlled process and has rate constants around an order of magnitude slower than those of the bimolecular self-reactions of the alkyl radicals.[55] This is shown by the spread in values for the experimental rate constants. A diffusion-controlled process would lead to a relatively constant value for the combination rate constants for a specific reaction medium and temperature. Therefore, the rate constants should, in principle, be predictable by the combination of parameters shown in Reaction (5.21). However, the very fast and similar rates of these reactions lead to scatter in the experimental data, causing the equation fitting to be less successful than that of the equilibrium constant.

Values of the fitted equation for log ($k_{d,eq}$), shown in Equation (5.22), show good correlation with the experimental values, with an MAD from experimental values of just over half an order of magnitude. The coefficients for the equation for log (k_d) are not proportional to those for the equation for log (K), again indicating that the combination reaction, although fast, is not a diffusion-controlled process.

$$\log\ (k_{d,eq}) = 0.0812RSE_{nxd} + 1.35EA_{alkyl} + 1.62order_{alkyl} + 0.0560RSE_{alkyl} - 10.7 \quad (5.22)$$

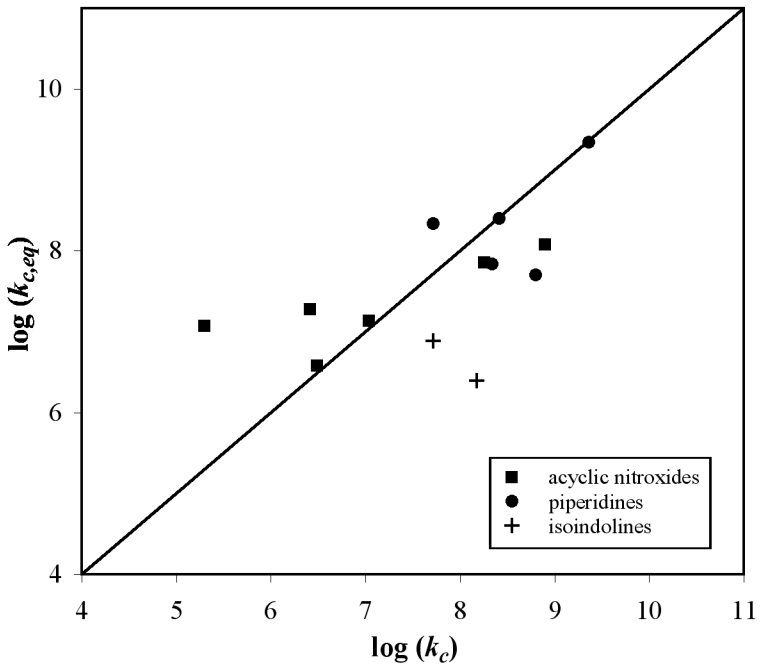

Figure 5.11 Correlation (R^2 = 0.383) between experimental combination rate constants and the fitted Equation (5.21)

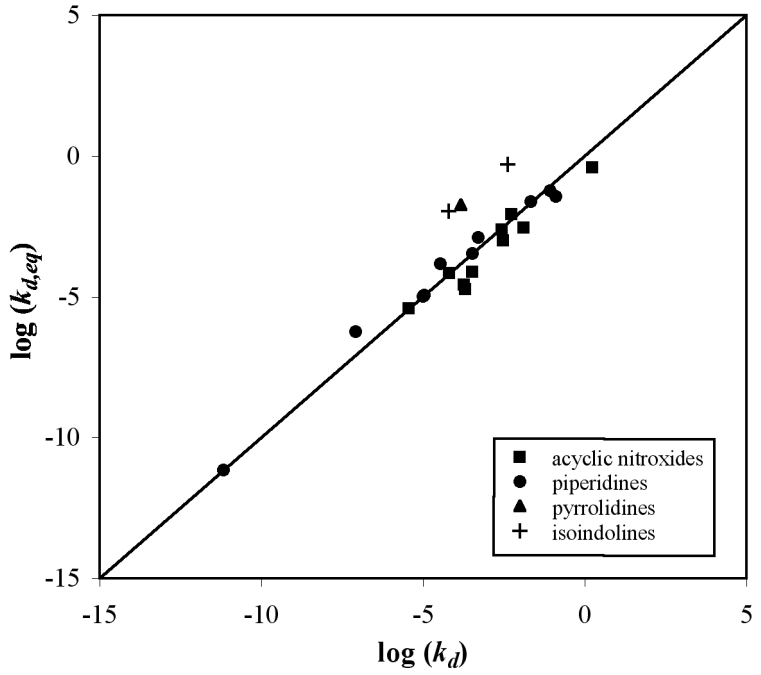

Figure 5.12 Correlation (R^2 = 0.854) between experimental dissociation rate constants and the fitted Equation (5.22)

5.4.5 Control of methyl methacrylate polymerisation

Until recently, controlled polymerisation of methyl methacrylate (MMA) could not be achieved using available nitroxide controlling agents. Kinetic studies have shown that the forward and reverse rate constants of the trapping reaction for TEMPO with the MMA propagating radical are ideal for control. However, the polymerisation process is halted by an intramolecular hydrogen transfer side reaction, occurring on the alkoxyamine, as shown in Reaction (5.16). Thermodynamic data for this side reaction, calculated for small nitroxides with the propagating methyl methacrylate radical modelled using the unimeric radical, is shown in Table 5.6.

Table 5.6 Calculated[a] gas-phase thermochemical data (at 298 K) for the hydrogen transfer side reaction.

Nitroxide	Structure	ΔH (kJmol^{-1})	ΔS (kJmol^{-1})	ΔG (kJmol^{-1})
1		46.1	198.4	-13.0
2		50.4	195.0	-7.7
15		62.5	197.3	3.7
27	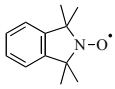	60.6	196.6	1.9

[a]ONIOM approximation of G3(MP2)-RAD//B3-LYP/6-31G(d) values including $(CH_3)_2NO^{\bullet}$ and the methyl methacrylate unimeric radical in the core system, with the full system calculated at the RMP2/6-311+G(3df,2p) level.

Table 5.6 shows that the hydrogen transfer side reaction has favourable free energy values for the six-membered TEMPO (**2**) nitroxide and also for the non-cyclic species DBN (**1**). Other six-membered nitroxides are expected to show similar free energies for this side reaction and, as previously reported,[37] the hydrogen transfer reaction will dominate in these cases. The pyrrolidine and isoindoline nitroxides PROXYL (**15**) and TMIO (**27**) show positive free energy values for the hydrogen transfer reaction, indicating that the side reaction is likely to be minimal for these five-

membered ring nitroxides. Therefore a five-membered cyclic nitroxide, showing a suitable equilibrium constant for the control reaction, may be an ideal candidate for control of the polymerisation of MMA.

Equation (5.20) can be used to determine equilibrium constants of the control reaction of nitroxide mediated polymerisation of MMA. These values cannot be directly calculated due to the large systems involved. In previous kinetic analyses, the penultimate unit of the MMA propagating radical was shown to have a large effect on the rate constants k_c and k_d.[32] Therefore, the MMA dimer, shown in Figure 5.13, is a better model for the polymeric radical chain in the calculation of log (K_{eq}).

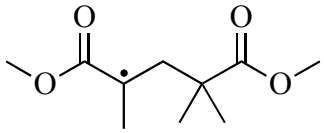

Figure 5.13 The MMA dimer radical used to model the propagating radical in polymerisation of methyl methacrylate

The parameters for the MMA dimer radical were calculated to be EA_{alkyl} = 1.35 eV and RSE_{alkyl} = 48.5 kJmol^{-1} using Equations (2.30) and (2.45), and the $order_{alkyl}$ parameter is, by definition, 3. Substituting these values, along with the RSE_{nxd} values of the individual nitroxides, into Equation (5.20), values of log (K_{eq}) were obtained and are shown in Table 5.7. The log (K_{eq}) value for the control reaction with TEMPO (**2**) was found to be 20.4. Therefore, control of polymerisation is expected to occur when the standard state log (K_{eq}) is close to this value.

Values of log (K_{eq}) for the five-membered cyclic nitroxides PROXYL (**15**) and TMIO (**27**) were found to be 18.1 and 18.6, respectively. These values are lower than the log (K_{eq}) value calculated for the β-H nitroxide SG1 (**69**), 18.8, which has previously been shown to be too low to control polymerisation.[32] Therefore, even though the pyrrolidine and isoindoline nitroxide do not undergo the hydrogen transfer side reaction, they are not expected to be suitable control agents for polymerisation, as they show equilibrium constants too low to afford control.

Table 5.7 Calculated[a] log (K_{eq}) values for nitroxide radicals with the MMA dimer

Nitroxide	Structure	log (K_{eq})
1		19.7
2		20.4
15		18.1
27	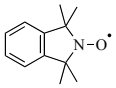	18.5
69	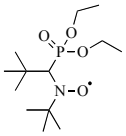	18.8
70	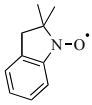	19.7
71	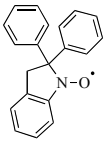	21.5
72	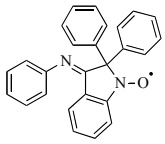	20.9

[a]Calculated from Equation (5.20) using RSE_{nxd} values shown in Table 5.3 and the values EA_{alkyl} = 1.35 eV, $order_{alkyl}$ = 3 and RSE_{alkyl} = 48.5 kJmol^{-1} for the MMA dimer.

Originally, one of the aims of this work was to identify a nitroxide controlling agent suitable for methyl methacrylate polymerisation. During the course of this study, this goal has been achieved by Tordo and co-workers, who have recently reported control of MMA polymerisation using a new indoline nitroxide species 2,2-diphenyl-3-phenyliminoindolin-1-yloxyl (DPAIO, **72**).[43] Like other five-membered cyclic nitroxides, this species undergoes a minimum of the hydrogen transfer side reaction in its trapped alkoxyamine form. However, it is seen from Table 5.7 that equilibrium constants of the trapping reactions of isoindoline derivatives (**70**, **71**, and **72**) are much higher than for pyrrolidine and isolindoline derivatives (**15** and **27**).

The recently reported indoline nitroxide DPAIO (**72**) shows a log (K_{eq}) value of 20.9, very close to that of TEMPO (**2**). This species is therefore predicted by Equation (5.20) to be a suitable controlling agent for MMA polymerisation, in agreement with the experimental finding. The 2,2-dimethyl substituted species **70** shows a lower value of log (K_{eq}) than DPAIO (**72**) because the β-methyl groups, although smaller in molecular weight than phenyl groups, cause more steric hindrance around the reaction centre. The species **71** shows a higher value of log (K_{eq}) than DPAIO (**72**) due to the lack of extra stability in the nitroxide, seen for DPAIO (**72**) through radical delocalisation on the phenylimino substiuent group.

5.5 Conclusions and outlook

The thermodynamics of the control reaction of nitroxide mediated polymerisation (NMP) have been calculated using high-level computational quantum chemistry techniques, both directly and through a fitted equation, which allows the equilibrium constant of the control reaction to be determined for large systems. The equation, shown as Equation (5.20), describes the log (K_{eq}) value of the trapping reaction between a nitroxide radical and an alkyl radical in terms of easily computed parameters designed to measure the polar, steric and radical stabilisation effects of each of the alkyl and nitroxide radicals. Testing performed on small systems showed that the equation is successful. Therefore, it can be used to predict the equilibrium constants of trapping for larger systems for which direct calculation is impractical. As a practical test, the equation for log (K_{eq}) has been used to explain the success demonstrated by the recently reported indoline-type nitroxide control agent DPAIO (**72**) for the polymerisation of methyl methacrylate.

The multiparameter analysis completed in this work shows scope for being generalised to the study of other controlled radical polymerisation reactions such as atom transfer radical polymerisation (ATRP) and reversible addition fragmentation chain transfer (RAFT). A collaborative project in this direction is currently being undertaken with members of the Coote research group, Dr Sylvain Marque of the Université de Provence and Professor Krzysztof Matyjaszewski of Carnegie Mellon University.

5.6 References

(1) Moad, G.; Solomon, D. H. *The Chemistry of Radical Polymerization*, 2nd ed.; Elsevier Ltd: Oxford, 2006.

(2) (a) Yamada, B.; Tanaka, H.; Konishi, K.; Otsu, T. *J. Macromol. Sci., Chem.* **1994**, *A31*, 351. (b) Klapper, M.; Brand, T.; Steenbock, M.; Müllen, K. *ACS Symp. Ser.* **2000**, *768*, 152.

(3) (a) Ameduri, B.; Boutevin, B.; Gramain, P. *Adv. Polym. Sci.* **1997**, *127*, 87. (b) Sebenik, A. *Prog. Polym. Sci.* **1998**, *23*, 875. (c) Otsu, T.; Matsumoto, A. *Adv. Polym. Sci.* **1998**, *136*, 75. .

(4) (a) Kwon, T. S.; Kumazawa, S.; Yokoi, T.; Kondo, S.; Kunisada, H.; Yuki, Y. *J. Macromol. Sci., Chem.* **1997**, *A34*, 1553. (b) Kwon, T. S.; Takagi, K.; Kunisada, H.; Yuki, Y. *Eur. Polym. J.* **2003**, *39*, 1437.

(5) (a) Bledzki, A.; Braun, D. *Makromol. Chem.* **1981**, *182*, 1047. (b) Roussel, J.; Boutevin, B. *Polym. Int.* **2001**, *50*, 1029.

(6) (a) Druliner, J. D. *Marcomol.* **1991**, *24*, 6079. (b) Chung, T. C.; Janvikul, W.; Lu, H. L. *J. Am. Chem. Soc.* **1996**, *118*, 705.

(7) Wayland, B. B.; Basickes, L.; Mukerjee, S.; Wei, M.; Fryd, M. *Macromol.* **1997**, *30*, 8109.

(8) (a) Kato, M.; Kamigaito, M.; Sawamoto, M.; Higashamura, T. *Macromol.* **1995**, *28*, 1721. (b) Wang, J.-S.; Matyjaszewski, K. *Macromol.* **1995**, *28*, 7901. (c) Percec, V.; Barboiu, B. *Macromol.* **1995**, *28*, 7970.

(9) Chiefari, J.; Chong, Y. K.; Ercole, F.; Krstina, J.; Jeffery, J.; Le, T. P. T.; Mayadunne, R. T. A.; Meijs, G. F.; Moad, C. L.; Moad, G.; Rizzardo, E.; Thang, S. H. *Macromol.* **1998**, *31*, 5559.

(10) Moad, G.; Rizzardo, E.; Solomon, D. H. *Poly. Bull.* **1982**, *6*, 589.

(11) Solomon, D. H.; Rizzardo, E.; Cacioli, P. U.S. Patent 4,581,429, March 27,1985.

(12) Rizzardo, E. *Chem. Aust.* **1987**, *54*, 32.

(13) Georges, M. K.; Veregin, R. P. N.; Kazmaier, P. M.; Hamer, G. K. *Macromol.* **1993**, *26*, 2987.

(14) Grimaldi, S.; Finet, J.-P.; Zeghdaoui, A.; Tordo, P.; Benoit, D.; Gnanou, Y.; Fontanille, M.; Nicol, P.; Pierson, J.-F. *Polym. Prepr.* **1997**, *38*.

(15) Benoit, D.; Chaplinski, V.; Braslau, R.; Hawker, C. J. *J. Am. Chem. Soc.* **1999**, *121*, 3904.

(16) (a) Benoit, D.; Grimaldi, S.; Finet, J.-P.; Tordo, P.; Fontanille, M.; Gnanou, Y. *Polym. Prepr.* **1997**, *38*, 729. (b) Benoit, D.; Grimaldi, S.; Robin, S.; Finet, J.-P.; Tordo, P.; Gnanou, Y. *J. Am. Chem. Soc.* **2000**, *122*, 5929.

(17) Fukuda, T.; Terauchi, T.; Goto, A.; Ohno, K.; Tsujii, Y.; Miyamoto, T.; Kobatake, S.; Yamada, B. *Macromol.* **1996**, *29*, 6393.

(18) Greszta, D.; Matyjaszewski, K. *Macromol.* **1996**, *29*, 7661.

(19) (a) Souaille, M.; Fischer, H. *Macromol.* **2000**, *33*, 7378. (b) Souaille, M.; Fischer, H. *Macromol.* **2001**, *34*, 2830. (c) Souaille, M.; Fischer, H. *Macromol.* **2002**, *35*, 248.

(20) Bertin, D.; Gigmes, D.; Marque, S. R. A.; Milardo, S.; Peri, J.; Tordo, P. *Collect. Czech. Chem. Commun.* **2004**, *69*, 2223 and references within.

(21) Marque, S. R. A.; Le Mercier, C.; Tordo, P.; Fischer, H. *Macromol.* **2000**, *33*, 4402.

(22) Marque, S. R. A.; Fischer, H.; Baier, E.; Studer, A. *J. Org. Chem.* **2001**, *66*, 1146.

(23) Fischer, H.; Kramer, A.; Marque, S. R. A.; Nesvadba, P. *Macromol.* **2005**, *38*, 9974.

(24) Hansch, C.; Leo, A.; Taft, R. W. *Chem. Rev.* **1991**, *91*, 165 and references within.

(25) Taft, R. W. *Steric Effects in Organic Chemistry*; Newman, M. S., Ed; Wiley: New York, 1956; Chapter 13.

(26) Fischer, H.; Marque, S. R. A.; Nesvadba, P. *Helvetica Chimica Acta* **2006**, *89*, 2330.

(27) Marque, S. R. A. *J. Org. Chem.* **2003**, *68*, 7582.

(28) Charton, M. *Top. Curr. Chem.* **1983**, *114*, 57.

(29) Welle, F. M.; Beckhaus, H. D.; Rüchardt, C. *J. Org. Chem.* **1997**, *62*, 552.

(30) Bertin, D.; Gigmes, D.; Marque, S. R. A.; Tordo, P. *Macromol.* **2005**, *38*, 2638.

(31) Fujita, T.; Takayama, C.; Nakajima, M. *J. Org. Chem.* **1973**, *38*, 1623.

(32) Guillaneuf, Y.; Gigmes, D.; Marque, S. R. A.; Tordo, P.; Bertin, D. *Macromol. Chem. Phys.* **2006**, *207*, 1278.

(33) Bertin, D.; Dufils, P.-E.; Durand, I.; Gigmes, D.; Giovanetti, B.; Guillaneuf, Y.; Marque, S. R. A.; Phan, T.; Tordo, P. *Macromol. Chem. Phys.* **2008**, *209*, 220.

(34) Coote, M. L.; Davis, T. P. *Prog. Polym. Sci.* **1999**, *24*, 1217.

(35) Lin, C. Y.; Coote, M. L.; Petit, A.; Richard, P.; Poli, R.; Matyjaszewski, K. *Macromol.* **2007**, *40*, 5985.

(36) Izgorodina, E. I.; Coote, M. L. *Macromol. Theory Simul.* **2006**, *15*, 394.

(37) Moad, G.; Anderson, A. G.; Ercole, F.; Johnson, C. H. J.; Krstina, J.; Moad, C. L.; Rizzardo, E.; Spurling, T. H.; Thang, S. H. *ACS Symp. Ser.* **1998**, *685*.

(38) Fischer, H. *ACS Symp. Ser.* **2003**, *854*, 10.

(39) Ananchenko, G. S.; Fischer, H. *J. Polym. Sci., Part A: Polym. Chem.* **2001**, *39*, 3604.

(40) Braslau, R. *private communication*.

(41) Ananchenko, G. S.; Souaille, M.; Fischer, H.; Le Mercier, C.; Tordo, P. *J. Polym. Sci., Part A: Polym. Chem.* **2002**, *40*, 3264.

(42) Nicolas, J.; Dire, C.; Mueller, L.; Belleney, J.; Charleux, B.; Marque, S. R. A.; Bertin, D.; Magnet, S.; Couvreur, L. *Macromol.* **2006**, *39*, 8274.

(43) Guillaneuf, Y.; Gigmes, D.; Marque, S. R. A.; Astolfi, P.; Greci, L.; Tordo, P.; Bertin, D. *Macromol.* **2007**, *40*, 3108.

(44) (a) Gorenstein, D. G. *Chem. Rev.* **1987**, *87*, 1047. (b) Juaristi, E.; Cuevas, G. *Tetrahedron* **1992**, *48*, 5019.

(45) Ciriano, M. V.; Korth, H.-G.; van Scheppingen, W. B.; Mulder, P. *J. Am. Chem. Soc.* **1999**, *121*, 6375.

(46) Gaudel-Siri, A.; Siri, D.; Tordo, P. *ChemPhysChem* **2006**, *7*, 430.

(47) Coote, M. L.; Dickerson, A. B. *Aust. J. Chem.* **2008**, *61*, 163.

(48) Hodgson, J. L.; Coote, M. L. *J. Phys. Chem. A* **2005**, *109*, 10013.

(49) Data provided by Dr Ching Yeh (Leaf) Lin, calculated as part of a larger study.

(50) Böhm, S.; Exner, O. *Org. Biomol. Chem.* **2008**, *6*, 1092.

(51) Izgorodina, E. I.; Coote, M. L.; Radom, L. *J. Phys. Chem. A* **2005**, *109*, 7558.

(52) Benson, S. W. *Thermochemical Kinetics. Methods for the Estimation of Thermochemical Data and Rate Parameters*; John Wiley & Sons: New York, 1976.

(53) Zipse, H. *Top. Curr. Chem.* **2006**, *263*, 163. In this published work the *RSE* values were calculated using the reverse of Reaction (2.45) and therefore show the opposite sign from those shown in Table 5.3.

(54) Sobek, J.; Martschke, R.; Fischer, H. *J. Am. Chem. Soc.* **2001**, *123*, 2849.

(55) Beckwith, A. L. J.; Bowry, V. W.; Ingold, K. U. *J. Am. Chem. Soc.* **1992**, *114*, 4983.

Chapter 6.

Mechanism of the Denisov Cycle

6.1 Introduction 144

6.2 Literature review 144

6.2.1 Photo-oxidative degradation of polymer coatings 144

6.2.2 Protection using stabilising agents 145

6.2.3 The Denisov cycle 146

6.2.4 Side reactions 151

6.3 Mechanisms of the Denisov cycle 153

6.3.1 Catalytic cycle 154

6.3.2 Side reactions 159

6.3.3 Trioxide reaction with a secondary alcohol 160

6.4 Conclusions 162

6.5 References 165

6.1 Introduction

Hindered amine light stabilisers (HALS) protect polymer coatings against photo-oxidative damage through the formation of nitroxide radicals, which subsequently consume damaging radical species in a process called the Denisov cycle. The exact mechanism for this process remains unclear, with a dozen different reaction pathways and over 30 individual reactions previously proposed in the literature. In this chapter, the full mechanism of the Denisov cycle will be elucidated, new intermediate species in the cycle postulated, and the final products determined. This study will assist in the design of new and improved hindered amine light stabilisers for surface coatings.

6.2 Literature review

6.2.1 Photo-oxidative degradation of polymer coatings

Polymer-coated steel products are widely used in the automotive and building industries, as well as in general household fittings and appliances. The polymer coating acts to protect the steel from corrosion as well as providing a coloured and glossy finish to the surface. Generally, polymer topcoats are constructed of polyester or acrylic polymer chains that are networked into solid three-dimensional architectures by melamine formaldehyde or urethane-type crosslinkers.[1]

During prolonged exposure to sunlight and other weathering effects, polymer coatings undergo discolouration and become brittle, developing surface cracks. Numerous studies have attempted to identify and assess the degradation processes in the types of polymers used in coated steel applications.[2] The general mechanism of the photo-oxidative degradation of polymer systems is shown in Reactions (6.1) to (6.4). Initiation is induced via the homolytic cleavage of polymeric bonds (R–R) by Norrish type I reactions, or by hydrogen abstraction by an atmospheric radical ($X^{\bullet}$) to form a polymeric radical ($R^{\bullet}$), which reacts with oxygen at a diffusion-controlled rate to form a peroxyl radical ($ROO^{\bullet}$).[3] The peroxyl radical is capable of abstracting a hydrogen atom from the polymer backbone to form a hydroperoxide (ROOH), generating further alkyl radicals ($R^{\bullet}$).[4]

$$R\text{–}R \longrightarrow R^{\bullet} + R^{\bullet} \quad (6.1)$$

$$RH + X^{\bullet} \longrightarrow R^{\bullet} + XH \quad (6.2)$$

$$R^{\bullet} + O_2 \longrightarrow ROO^{\bullet} \quad (6.3)$$

$$ROO^{\bullet} + RH \longrightarrow ROOH + R^{\bullet} \quad (6.4)$$

6.2.2 Protection using stabilising agents

Compounds including ultraviolet (UV) stabilisers are added to polymer coatings to protect the surface from light degradation. Although these additives can act through the direct absorption of UV radiation, one class of UV stabilisers, known as the hindered amine light stabilisers (HALS), are effective in the protection of polyolefins but do not absorb UV light. The mechanism by which HALS protect polyolefins has been the subject of several prior investigations. It was originally proposed that the activity of HALS was due entirely to their ability to scavenge radicals via the formation of nitroxide radicals, through a process known as the Denisov cycle.[2] More recently, other protection mechanisms which do not involve the Denisov cycle have been suggested, including the thermal regeneration of the nitroxide through the bond cleavage of alkoxyamines,[5] and the quenching of excited states of singlet oxygen, aliphatic carbonyls and aromatic hydrocarbons by hindered amines and nitroxides, thereby preventing initiation of photo-degradation.[6]

A simplified mechanism of the Denisov cycle is shown in Scheme 6.1, with the HALS depicted as the six-membered heterocyclic amine 2,2,6,6-tetramethylpiperidine. This amine is then oxidised to the corresponding nitroxide radical, 2,2,6,6-tetramethylpiperidin-1-loxyl (TEMPO), which subsequently reacts in a catalytic fashion to transform both $R^{\bullet}$ and $ROO^{\bullet}$ radicals to non-radical products. It has been observed in model systems that, after addition of the HALS, the nitroxide concentration grows (from zero) to a maximum value and then drops to level out at around 10% of the originally added HALS concentration.[7]

Although various sequences have been proposed in the literature, the mechanism of the Denisov cycle has been the subject of ongoing debate. It is now widely accepted that Scheme 6.1 does not fully describe the correct mechanism by which hindered amines and nitroxides protect materials from photo-oxidative damage.

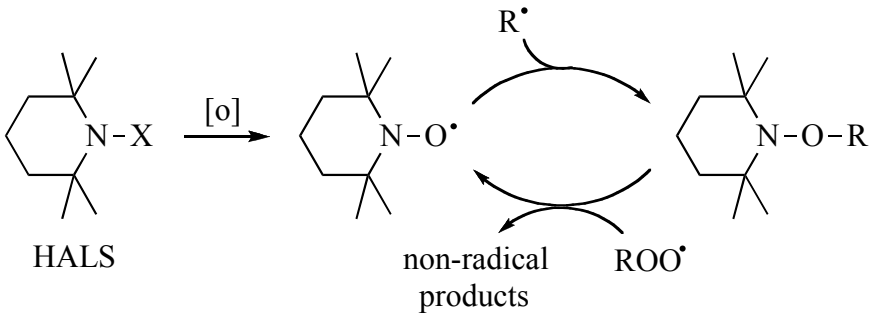

Scheme 6.1 Simplified mechanism of the Denisov cycle, showing protection using a piperidine HALS (where X is typically H or an alkyl chain)

The scheme also does not incorporate any side reactions that may account for the degradation of the protecting agent over time. There remain around a dozen different mechanistic pathways comprising over 30 individual reactions, which have been suggested to contribute to the mechanism of the Denisov cycle. Until now it has been dificult to distinguish between the various postulated mechanisms. However, due to the ease with which theoretical calculations can be used to study individual chemical reactions in such complicated reaction sequences, the various mechanisms suggested in the literature may easily be compared using computational methods in order to elucidate the most likely reaction mechanism. Previous semi-empirical and other low-level methods have been used to examine some of the possible reactions between peroxyl radicals and nitroxides[8] or alkoxyamines.[9,10] However, a full *ab initio* study has not been completed, and is described here for the first time. In this work the thermodynamics and kinetics of the reactions that comprise the Denisov cycle will be quantitatively examined using high-level computational chemistry in order to shed more light on the mechanisms of protection.

6.2.3 The Denisov cycle

Principal reactions that may contribute to the protection of polymer coatings from photo-oxidative damage, and their respective side reactions, have been described previously in the literature. These are comprehensively shown in Schemes 6.2 to 6.4, with individual reactions labelled (6.5) to (6.32). These schemes show reactions involved in the scavenging of both polymeric and peroxyl radicals by nitroxides, and

their conversion to non-radical products, with the subsequent regeneration of the nitroxide. Possible side reactions that may interfere with the catalytic cycle are also depicted.

Scheme 6.2 shows possible reactions that may contribute to the original Denisov cycle, previously summarised in Scheme 6.1. In this more detailed diagram, the nitroxide reacts with an alkyl polymeric radical, $R^{\bullet}$, generated during photo-degradation, to form an alkoxylamine. This species then goes on to react with a peroxyl radical to reform the nitroxide as well as non-radical products. The original Denisov mechanism for the reaction of the alkoxyamine and the peroxyl radical proposed that a polymeric product of the form ROOR is formed through the transition state species shown in Figure 6.1.[2] However, this product has never been detected. The transition state structure in Figure 6.1 has also been discounted by a labelling study, which indicated that the nitroxide oxygen is exchanged for one of the peroxyl oxygen atoms during the reaction.[11]

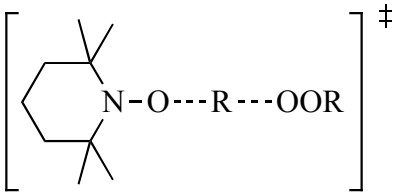

Figure 6.1 Transition state species suggested in the original Denisov cycle

The mechanism for the reaction of an alkoxyamine with a peroxyl radical has been studied using both computational and qualitative molecular orbital theory, and is now considered to proceed via a tetra-substituted nitrogen intermediate[5,11] or transition state,[9] which decomposes to form nitroxide, ketone and alcohol products as shown in Reaction (6.8) and (6.9). Two different intermediates have been postulated on the basis of semi-empirical computational studies[9,10] and molecular orbital arguments.[5] These intermediates are shown in the mechanisms described by Reactions (6.6) and (6.7). The peroxyl radical adds to the alkoxyamine to form either an intermediate made up of an aminoperoxyether and an alkoxyl radical, labelled ***A***, or an intermediate made up of a zwitterionic oxyaminoether and an alkoxyl radical,

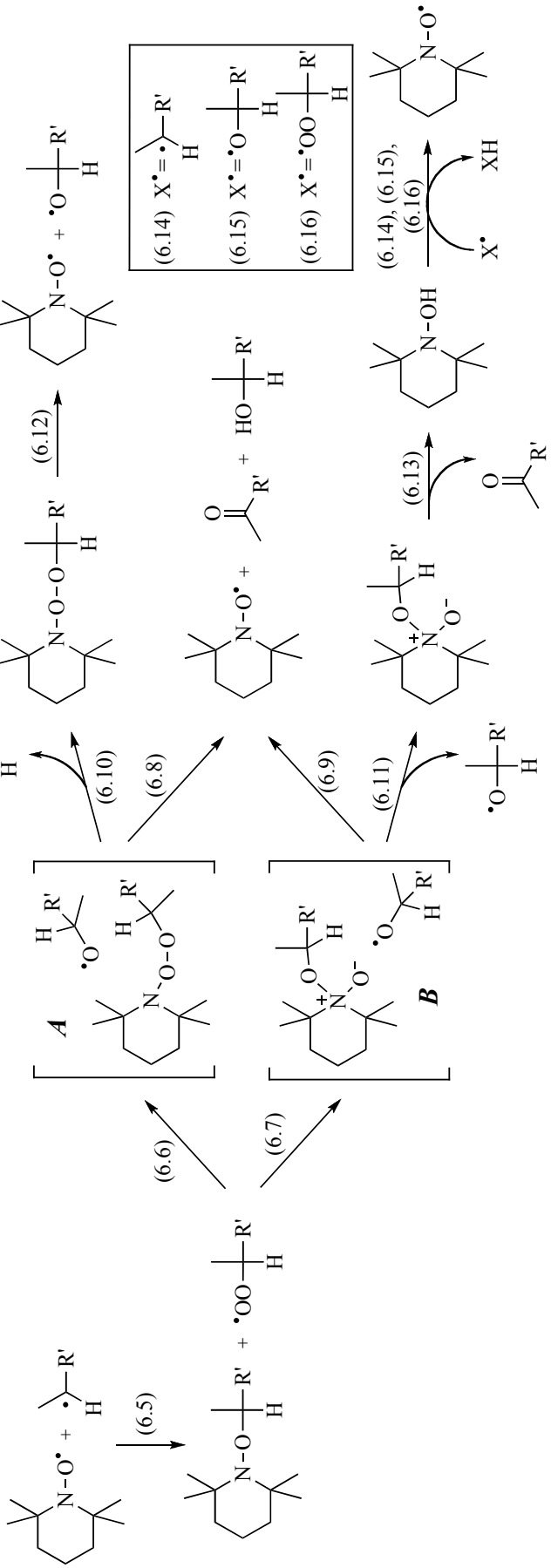

Scheme 6.2 Mechanisms for the reaction between TEMPO-alkoxyamines and a peroxyl radicals

labelled ***B***. These intermediate species have been prominent in previous literature discussions since they avoid the production of highly reactive and possibly polymer-damaging free alkoxyl radicals.[5] Although it has been suggested that Reaction (6.7) may occur via a concerted process that regenerates the nitroxide radical via a six-membered ring transition state,[9] an intrinsic reaction coordinate (IRC) calculation performed as part of a previous theoretical study found that the reaction occurs via a step-wise mechanism.[10]

Nitroxide, ketone and alcohol products are formed from intermediates ***A*** and ***B*** through the hydrogen-transfer processes shown in Reactions (6.8) and (6.9). It should be noted that, in the case that the two R' groups are not the same, different ketone and alcohol products are produced. A previous study found that, for the systems investigated, the only products observed were those reached through Reaction (6.9).[5]

It is also possible that the intermediate species ***A*** and ***B*** each dissociate forming two discrete products, an alkoxyl radical species along with aminoperoxyether and oxyaminoether-type products, respectively. The alkoxyl radical is a highly reactive species that, if formed, may contribute to the propagation of the polymer degradation process. In various works, reactions involving the degradation of the aminoperoxyether or oxyaminoether products of Reactions (6.10) and (6.11) have been postulated. The aminoperoxyether species may dissociate into the nitroxide and alkoxyl radical products shown in Reaction (6.12).[12] It has been suggested that the oxyaminoether species may undergo an intramolecular hydrogen transfer reaction to yield a hydroxylamine and a ketone as shown in Reaction (6.13).[13] In a previous study of the antioxidant activity of nitroxides in the inhibition of lipid peroxidation, it was postulated that hydroxylamines can donate hydrogen to alkyl, alkoxyl and peroxyl-type radicals forming nitroxide radicals.[14] Reactions (6.14), (6.15) and (6.16) show how hydroxylamine may detoxify alkyl and peroxyl radicals formed directly by the photo-oxidative degradation of polymer chains, as well as alkoxyl radicals formed by Reactions (6.10) and (6.11).

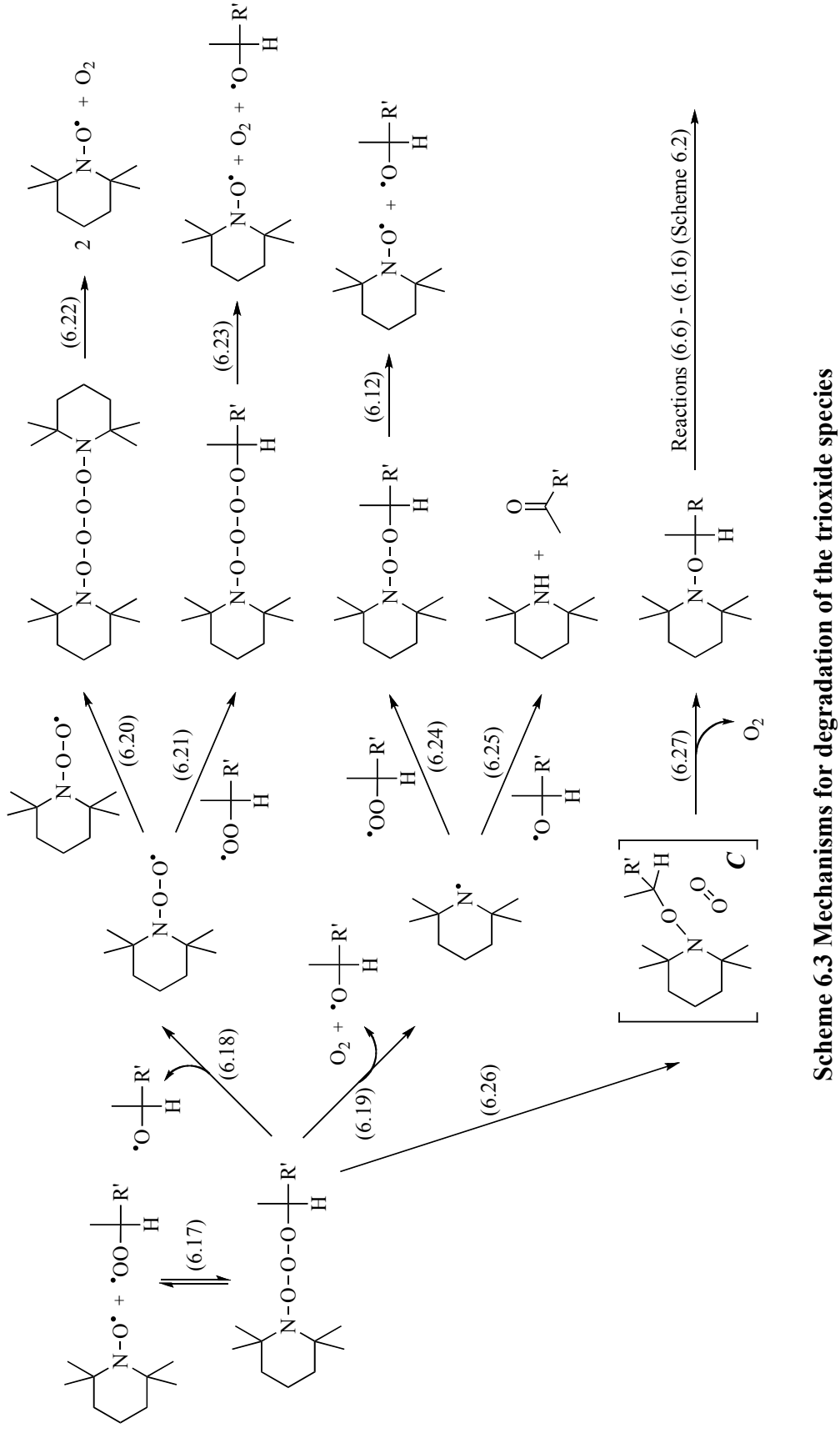

Scheme 6.3 Mechanisms for degradation of the trioxide species

6.2.4 Side reactions

The proposed Denisov cycle mechanism (Scheme 6.1) indicates that a nitroxide radical reacts with an alkyl radical $R^{\bullet}$ to form an alkoxyamine (Reaction (6.5)) that subsequently reacts with and detoxifies a peroxyl radical $ROO^{\bullet}$. However, it has been noted that while the reaction of the nitroxide and $R^{\bullet}$ is a fast reaction (exhibiting rate constants around 10^8 $Lmol^{-1}s^{-1}$) the reaction between $R^{\bullet}$ and O_2 (Reaction (6.3)) is even faster. Rate constants for the latter reaction are typically an order of magnitude higher. On kinetic grounds, for the case where $R^{\bullet}$ = benzyl, less than 10% of the alkyl radicals that appear following the initiation of photo-degradation are trapped by TEMPO,[15] and the subsequent reaction of the alkoxyamine with a peroxyl radical is expected to be slow. However, experimental consumption and regeneration of TEMPO occurs at a higher rate than this suggests, implying that nitroxides also react directly, and catalytically, with peroxyl radicals, thereby transforming them into non-radical products. While this reaction is slower than the combination of two peroxyl radicals, it is likely to be competitive due to the high concentrations of nitroxide and low concentrations of peroxyl radicals present.[15]

Scheme 6.3 is a depiction of reactions drawn from the literature that describe the combination of a nitroxide and a peroxyl radical and the subsequent decomposition of the product species. Several workers, implementing experimental and theoretical results, have suggested various conflicting mechanisms and products for these reactions. The combination of the nitroxide and the peroxyl radical, shown in Reaction (6.17), is generally agreed to give the trioxide species >N–O–O–O–R, first reported by Barton and coworkers.[12] It has been suggested that this species decomposes to radical products. Several different mechanisms for this process are listed in Scheme 6.3. It may be the case that the trioxide dissociates into either an aminoperoxyl radical and an alkoxyl radical, shown in Reaction (6.18), or an aminyl radical, dioxygen and an alkoxyl radical, shown in Reaction (6.19). Further reactions with peroxyl and other radicals go on to regenerate nitroxide radicals, as shown in Reactions (6.20) to (6.24).[12] The aminyl radical was also proposed to abstract a hydrogen atom from an alkoxyl radical and thereby form an amine and a ketone, as shown in Reaction (6.25).[12] Separately, it has been suggested that that this may occur as a concerted reaction on the trioxide itself.[15] An intramolecular transfer reaction,

shown in Reactions (6.26) and (6.27), in which oxygen is released from the trioxide to deliver an alkoxyamine, was proposed by a thermochemical study[8] and was suggested to involve an intermediate species,[15] labelled ***C***. However, this reaction is inconsistent with an experimental study in which no alkoxyamine product was detected.[12]

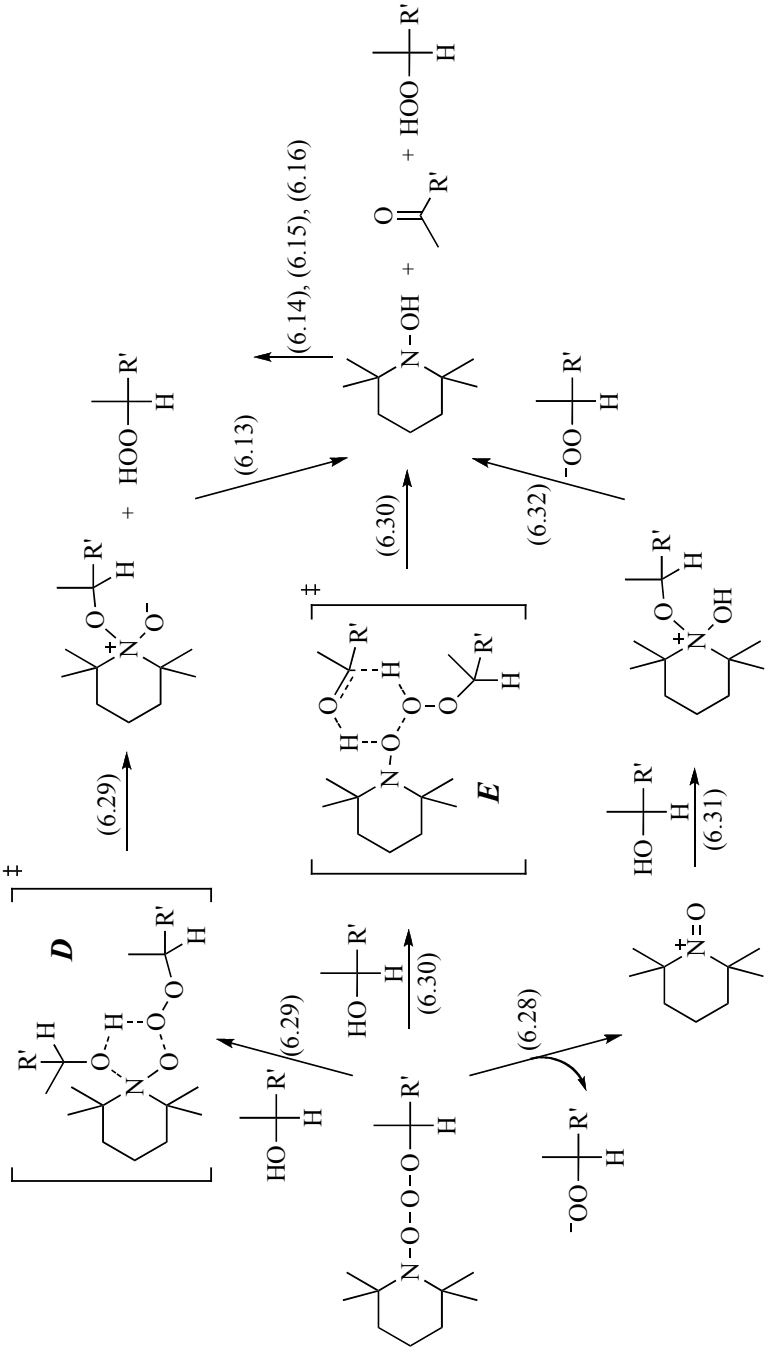

Scheme 6.4 Mechanisms for the reaction between the trioxide species and a secondary radical

More recently, it has been suggested that the decomposition of the trioxide species may occur via a reaction with a secondary alcohol, as shown in Scheme 6.4. In the case that polymer coatings are protected from photo-oxidative damage, secondary alcohol is produced as one of the major products of the reaction between an alkoxyamine and a peroxyl radical (see Reactions (6.8) and (6.9) in Scheme 6.2). The reaction between the trioxide and a secondary alcohol is reputed to proceed via the decomposition of the trioxide to the corresponding oxoammonium cation, appended by the functional group $>N^{+}=O$, and the reduced peroxyl anion ROO^{-}, shown in Reaction (6.28).[16] The oxoammonium cation then proceeds to oxidise a secondary alcohol to form a ketone and hydroperoxyalkane-type species, as well as the reduced form of the nitroxide, hydroxylamine >N–OH.[17] Two different mechanisms have been suggested for the reaction of the oxoammonium cation with an alcohol, both proceeding via a tetra-substituted nitrogen intermediate.[13,18] These reactions are shown as Reactions (6.29) and (6.31) in Scheme 6.4, along with the concerted process, labelled Reaction (6.30).

6.3 Mechanisms of the Denisov cycle

Over 30 reactions making up a dozen different mechanistic pathways are reported in the literature as contributing to the mechanism of the Denisov cycle. Theoretical calculations provide a useful method to elucidate the most likely overall mechanism. By calculating thermodynamic and kinetic favourablities, it was possible to directly compare the various individual reactions. Principal reactions and side reactions attributed in the literature to the Denisov cycle are shown in Schemes 6.2, 6.3 and 6.4, with individual reactions labelled (6.5) to (6.32). Two types of common polymer coatings agents were considered in this study, polyethylene and polyester. In order to model reactions, the unimeric radicals $R^{\bullet} = {}^{\bullet}CH(CH_3)(R')$ were chosen, as they provide primary substituent effects. The species R' = CH_3, and R' = $OCOCH_3$ were selected so as to model mid-chain polyethylene and polyester radicals respectively, by representing the most stable species formed by hydrogen abstraction from each polymer chain.[19]

Gas-phase thermodynamic parameters for reactions (6.5) to (6.32) are shown in Table 6.1. On the basis of the free energies calculated from these reactions, the thermodynamically favourable reactions were identified and gas-phase free energy barriers for these reactions calculated. The results of these calculations are shown in Table 6.2. Transition state structures were verified by their (single) imaginary frequencies and by IRC calculations in the forward and reverse directions along the reaction paths.

For work in this chapter, gas-phase reactions were considered, since they provide probably the best model of the polymer coating in a practical setting. However, as coatings may be solvated by water during weathering, the effects of an aqueous solvent on the thermodynamics of the reactions were also considered. Taking Scheme 6.4 as an example, the addition of an aqueous solvent to the calculations was found, in most cases, to cause an insignificant change to the thermodynamic results. However, for reactions involving the transfer of formal charges, the presence of an aqueous solvent provided a large stabilising effect of around 500 $kJmol^{-1}$. Therefore the free energies for reactions (6.28) and (6.32) were calculated with the free energies of solvation in a water medium included in the calculations.

6.3.1 Catalytic cycle

Reaction (6.5) in Scheme 6.2 between the nitroxide 2,2,6,6-tetramethylpiperidin-1-yloxyl (TEMPO) and a polymeric radical forms an alkoxyamine. As described in Chapter 5, reactions of TEMPO with an alkyl radical make up the control reaction of TEMPO-based nitroxide mediated polymerisation (NMP). These reactions are exothermic, having very fast rates of the order of 10^8 $Lmol^{-1}s^{-1}$.[20,21] The calculated free energies of Reaction (6.5) for the polyethylene and polyester model systems in this study, around -150 $kJmol^{-1}$, indicate that the reaction forming a TEMPO-based alkoxyamine is very favourable. This reaction, like other very fast reactions that involve the combination of two radical species, is essentially barrierless.

The mechanism of the reaction between a TEMPO-based alkoxyamine and a peroxyl radical has not been firmly elucidated in previous works. Different proposed mechanisms and products are shown in Reactions (6.6) to (6.16) in Scheme 6.2.

Table 6.1 Thermodynamics parameters (298 K) for the reactions shown in Schemes 6.2, 6.3 and 6.4[a]

Reaction	Polyethylene (R'=CH_3)			Polyester (R'=$OC(O)CH_3$)		
	ΔH (kJ mol^{-1})	ΔS (J mol^{-1} K^{-1})	ΔG (kJ mol^{-1})	ΔH (kJ mol^{-1})	ΔS (J mol^{-1} K^{-1})	ΔG (kJ mol^{-1})
(6.5)	-212.8	-223.8	-146.1	-234.7 [b]	-219.1	-169.3
(6.6)	57.2 [b]	-95.5	85.6	-36.8 [c]	-100.5	-6.8
(6.7)	-41.6 [b]	-130.9	-2.5	-99.1 [c]	-143.8	-56.2
(6.8)	-367.5 [b]	299.9	-456.9	-299.2 [c]	287.3	-384.9
(6.9)	-268.7 [b]	335.3	-368.7	-236.9 [c]	330.6	-335.4
(6.10)	-47.9 [b]	113.2	-81.6	24.4 [c]	121.9	-12.0
(6.11)	28.3 [b]	131.0	-10.8	46.3 [c]	145.5	2.9
(6.12)	60.7	187.0	5.0	11.7 [b]	189.5	-44.8
(6.13)	-141.2	198.9	-200.5	-115.4 [b]	192.1	-172.6
(6.14)	-117.9	-15.8	-113.2	-116.6	-3.9	-115.4
(6.15)	-149.5	5.4	-151.1	-162.5	-6.9	-160.4
(6.16)	-62.0	8.7	-64.6	-81.7	-3.9	-80.6
(6.17)	-12.6	-177.0	40.1	-39.4 [b]	-190.3	17.4
(6.18)	149.4	177.6	96.5	154.2 [b]	195.7	95.9
(6.19)	133.7	340.4	32.2	146.6 [b]	358.5	39.7
(6.20)	-196.1 [b]	-183.2	-141.4	-196.1 [b]	-183.2	-141.4
(6.21)	-102.1 [b]	-190.6	-45.2	-120.9 [b]	-188.5	-64.7
(6.22)	-91.1 [b]	333.6	-190.5	-91.1 [b]	333.6	-190.5
(6.23)	-49.0 [b]	341.7	-150.8	-51.3 [b]	344.3	-154.0
(6.24)	-196.7	-198.6	-137.5	-176.4 [b]	-196.5	-117.8
(6.25)	-354.5	-9.1	-351.8	-354.0 [b]	-20.7	-347.8
(6.26)	130.8 [b]	-22.5	137.5	136.3 [b]	-6.1	138.1
(6.27)	-209.7 [b]	146.6	-253.4	-226.4	146.7	-270.1
(6.28)	567.7	159.6	44.7 [d]	501.8 [b]	150.0	-6.1 [d]
(6.29)	-5.2	-24.3	2.0	-5.8 [b]	-15.9	-1.1
(6.30)	-146.4	174.6	-198.5	-121.2 [b]	176.2	-173.7
(6.31)	14.0	-198.7	73.2	9.8 [b]	-209.2	72.2
(6.32)	-727.8	213.7	-371.8 [d]	-632.9 [b]	235.3	-309.2 [d]

[a]G3(MP2)-RAD//B3-LYP/6-31G(d) values except where noted. [b]ONIOM approximation found using G3(MP2)-RAD core systems, $(CH_3)_2NO–$ in place of the TEMPO ring structure, with the full system calculated at RMP2/6-311+G(3df.2p). [c]ONIOM approximation found using G3(MP2)-RAD core systems, $(CH_3)_2NO–$ in place of the TEMPO ring structure and $R=CH_2OC(O)H$) in place of the $R=CH(CH_3)OC(O)CH_3$ polymeric fragment, with the full system calculated at RMP2/6-311+G(3df.2p). [d]Includes PCM solvation free energies at the B3-LYP/631G(d) level for an aqueous medium.

Table 6.2 Kinetics parameters (298 K) for the reactions shown in Schemes 6.2, 6.3 and 6.4[a]

Reaction	Polyethylene (R'=CH_3)			Polyester (R'=$OC(O)CH_3$)		
	$\Delta H^{\ddagger}$ (kJ mol^{-1})	$\Delta S^{\ddagger}$ (J mol^{-1} K^{-1})	$\Delta G_{eff}^{\ddagger}$ (kJ mol^{-1}) [b]	$\Delta H^{\ddagger}$ (kJ mol^{-1})	$\Delta S^{\ddagger}$ (J mol^{-1} K^{-1})	$\Delta G_{eff}^{\ddagger}$ (kJ mol^{-1}) [b]
(6.6)	234.9 [c]	-169.4	285.4	103.1 [d]	-190.1	159.1
(6.7)	108.9 [c]	-177.7	160.2	96.6 [d,e]	-199.7	154.5
(6.9)	26.6 [c]	-21.9	28.9	59.0 [d]	-49.0	70.7
(6.13)	20.3	-0.3	19.5	21.2 [c]	-6.3	21.7
(6.14) [f]	24.2 [c]	-43.1	31.5	26.1 [c]	-25.5	28.9
(6.15) [f]	3.3 [c]	-7.6	5.5		barrierless	
(6.16) [f]	25.6 [c]	-47.5	38.8	7.5 [c]	-42.9	20.2
(6.29)	54.3 [c]	-173.8	106.0	21.4 [c]	-190.0	78.1
(6.30)	99.9 [c]	-148.8	139.1	72.1 [d]	-164.2	114.1

[a]G3(MP2)-RAD//B3-LYP/6-31G(d) values except where noted. [b]Free energy barrier corrected for the effects of tunnelling. [c]ONIOM approximation found using G3(MP2)-RAD core systems, $(CH_3)_2NO–$ in place of the TEMPO ring structure, with the full system calculated at RMP2/6-311+G(3df.2p). [d]ONIOM approximation found using G3(MP2)-RAD core systems, $(CH_3)_2NO–$ in place of the TEMPO ring structure and $R=CH_2OC(O)H$) in place of the $R=CH(CH_3)OC(O)CH_3$ polymeric fragment, with the full system calculated at RMP2/6-311+G(3df.2p). [e]UMP2 calculation substituted for ROMP2 calculations in the G3(MP2)-RAD composite procedure due to convergence problems. [f]Determined in relation to the reaction going from a pre-complex species to the transition state.

In Reaction (6.6) the nitroxide and peroxyl radical form an aminoperoxylether and an alkoxyl radical via a tetrasubstituted nitrogen transition state. Reaction (6.7) is similar, but in this case the zwitterionic oxyaminoether species is formed. Calculations show that the products of Reactions (6.6) and (6.7) exist as the intermediate species ***A*** and ***B***, respectively. Examining the free energies calculated for Reactions (6.6) and (6.7), it is clear that Reaction (6.7) is thermodynamically more favourable; the formation of the intermediate exhibiting free energies of -2.5 and -56.2 $kJmol^{-1}$ for the polyethylene (R'=CH_3) and polyester radicals (R'=$OCOCH_3$) model systems respectively. The formation of intermediate ***A*** is thermodynamically unfavourable for the polyethylene system with a free energy of 85.6 $kJmol^{-1}$, but is slightly exoergic, with a free energy of -6.8 $kJmol^{-1}$, for the polyester system. An NBO population analysis on the species ***A*** and ***B*** was used to locate the charges and lone electrons within the molecules, the locations of which are shown in Scheme 6.2. It should be noted that while an

intermediate species that resembles ***B*** has been postulated previously, the negative charge and lone electron in this previous description were located on different oxygen atoms.[5,11] The spin density of the lone electron in intermediate ***B*** was found to be located entirely on the separated alkoxyl radical species instead of on the nitrogen-bound oxygen.

From the calculated kinetic data, shown in Table 6.2, it is observed that the barriers for Reaction (6.7) are similar for both polymer systems examined in this work; both free energy barriers are close to 160 $kJmol^{-1}$. Of the two barriers for Reaction (6.6), that of the polyester system is of similar magnitude at 159.1 $kJmol^{-1}$. However, the barrier for the polyethylene system, at 285.4 $kJmol^{-1}$, is much larger. The lower barrier for forming intermediate ***A*** in the case that the relevant polymer is a polyester derivative may be due to an anomeric effect of the type described in Chapter 5.3.3. This effect may stabilise the transition state structure. Along with the thermodynamic evidence, this suggests that the mechanism proceeds through intermediate ***A*** for the polyester system but does not proceed in the case of the polyethylene system.

Reactions (6.8) and (6.9) are hydrogen atom transfers within intermediates ***A*** and ***B*** that re-form the nitroxide radical and generate ketone and alcohol products. These reactions are both very exoergic and are expected to take precedence over the competing Reactions (6.10) and (6.11). If two different R' groups are present, different ketone and alcohol products will be produced by Reactions (6.8) and (6.9). For the case of polyethylene, the formation of intermediate ***A*** is thermodynamically unfavourable. The hydrogen atom transfer within intermediate ***B***, in which the alkoxyl radical abstracts a methine hydrogen atom, is consistent with previous findings. As discussed in Chapter 6.2.3, a previous study determined only products reached through Reaction (6.9).[5] However, for the polyester radical, the formation of intermediate ***A*** is thermodynamically favoured and a small contribution from Reactions (6.8) is expected. For the polymeric radicals examined in this study, this reaction gives identical products to Reaction (6.9).

A transition state structure could not be located for Reaction (6.8), specifically for the polyester model system. Due to the very high exothermicity of this reaction, it is expected that the reaction is close to barrierless and displays a fast rate. The

polyethylene and polyester systems exhibit low free energy barriers for Reactions (6.9). These barriers were calculated to be 28.9 and 70.7 kJmol^{-1}, respectively, and imply rapid rates of reaction.

Reactions (6.10) and (6.11) show the dissociation of intermediates ***A*** and ***B*** in which loss of an alkoxyl radical generates either a free aminoperoxylether or a free oxyaminoether, respectively. Intermediate ***A*** is only formed in the polyester system and, since Reaction (6.10) is thermodynamically favoured in this case (showing a free energy of -12.0 kJmol^{-1}), formation of the aminoperoxylether species is expected to occur. Due to the large negative free energy of Reaction (6.8), Reaction (6.10) is likely to take place only to a small extent. The formed aminoperoxylether species dissociates through Reaction (6.12) with a free energy of -44.8 kJmol^{-1}. In this reaction, the nitroxide and an alkoxyl radical are re-formed.

Intermediate ***B*** exhibits a thermodynamically favoured dissociation reaction for only the polyethylene system. The analogous reaction, in the polyester system, is almost thermodynamically neutral. The free energies calculated for Reaction (6.11) are -10.8 and 2.9 kJmol^{-1} respectively. Therefore, at least for polyethylene, a small amount of intermediate ***B***, will dissociate and produce the oxyaminoether species shown. Any free oxyaminoether is expected to rapidly undergo the intramolecular hydrogen transfer reaction to form hydroxylamine and ketone products, shown in Reaction (6.13). This reaction is very favourable, with free energies of -200.5 and -172.6 kJmol^{-1}, and low barriers of 19.5 and 21.7 kJmol^{-1} for the polyethylene and polyester systems. Reactions (6.14), (6.15) and (6.16) were also calculated to be thermodynamically favourable. These results indicate that the nitroxide species will likely be re-formed via these reactions. Meanwhile, various polymeric carbon and oxygen-centred radicals are consumed. Reactions (6.14), (6.15) and (6.16) were found to pass through various pre-complex species prior to the transition state. A transition state was not located for Reaction (6.15) for the polyester model system. The free energy barrier for this reaction is expected to be lower than that of the polyethylene system due to anomeric stabilisation. Therefore, since the barrier for the polyethylene model system is only 5.5 kJmol^{-1}, it is expected that Reaction (6.15), for the polyester system, is essentially barrierless.

6.3.2 Side reactions

The reaction of TEMPO with a peroxyl radical is shown as Reaction (6.17) in Scheme 6.3, and exhibits a free energy of 40.1 $kJmol^{-1}$ for the polyethylene model system and 17.4 $kJmol^{-1}$ for the polyester model system. As expected, the reaction is exothermic due to the combination of two radicals to form a closed-shell species. However, the loss of translational entropy that takes place when two molecules combine causes a positive change in the free energy of the system. Reaction (6.17) becomes slightly more favourable as the reaction temperature is lowered, with the free energies for the polyethylene and polyester systems lowering to 35.7 $kJmol^{-1}$ and 12.6 $kJmol^{-1}$ at 273 K (0 °C). While on thermodynamic grounds this reaction is not expected to proceed, experimental studies have suggested that TEMPO does react with peroxyl radicals in small amounts. These results are based on the rate of consumption of TEMPO.[12,16] A driving force for the reaction may be the consumption of the formed trioxide species. Therefore, at such high concentrations of nitroxides as are typically present in a HALS-protected polymer coating, it is expected that Reaction (6.17) may contribute to the protection process demonstrated by HALS.

The degradation of the trioxide species by various suggested mechanisms is shown in Scheme 6.3. It has been suggested that decomposition of the trioxide into radical products takes place through homolytic cleavage of the oxygen-oxygen or nitrogen-oxygen bonds, as shown in Reactions (6.18) and (6.19). Table 6.1 shows that these reactions are thermodynamically unfavourable. Calculated free energies for Reaction (6.18) are 96.5 and 95.9 $kJmol^{-1}$ for the polyethylene and polyester systems, while for the more entropically favourable Reaction (6.19) free energies of 32.2 and 39.7 $kJmol^{-1}$ were found. Based on these calculations, it is unlikely that these reactions will occur. Some reactions, drawn from the literature, suggest various other pathways for decomposition of the products of Reactions (6.18) and (6.19). These pathways are represented by Reactions (6.20) to (6.25). Although these reactions are thermodynamically favoured, the thermodynamic constraints upon Reactions (6.18) and (6.19) render these subsequent reactions unlikely.

It has also been previously suggested that the trioxide species, formed with a secondary alkylperoxyl radical, may undergo a reaction analogous to the Russell

Mechanism,[22] in which the self-reaction of two secondary alkylperoxyl radicals liberates dioxygen, alcohol and a ketone. This process would involve Reactions (6.19) and (6.25) occurring as a concerted process, with a six-membered ring transition state transferring a hydrogen atom is to the nitrogen centre.[15] Although this reaction is thermodynamically favourable, as calculated by summation of the free energies for Reactions (6.19) and (6.25), a transition state for the concerted reaction was not located. Systematic and exhaustive searching of the potential energy surface led instead to a five-membered ring transition state for a similar, but thermodynamically disfavoured, reaction. This result implies that the concerted reaction does not occur.

The decomposition of the aforementioned trioxide into oxygen and an alkoxyamine through intermediate ***C*** was found to be thermodynamically unfavourable; Reaction (6.26) exhibited free energies of 137.5 and 138.1 $kJmol^{-1}$ for the polyethylene and polyester systems. As such, it is unlikely that decomposition of the trioxide occurs via this mechanism. Notably, intermediate ***C*** was found to comprise an alkoxyamine and a dioxygen species. Conversely, the previously described intermediate was thought to comprise discrete aminyl and alkoxyl radicals with dioxygen.[15]

6.3.3 Trioxide reaction with a secondary alcohol

The reaction of the trioxide species with a secondary alcohol is thought to be preceded by an ionic fragmentation reaction that forms an oxoammonium cation and an anionic peroxyl species. This reaction is shown in Reaction (6.28). Thermodynamic parameters for the reaction, calculated on the trioxide in the gas phase, show that the reaction is extremely unfavourable. Enthalpies greater than 500 $kJmol^{-1}$ were calculated for both the polyethylene and polyester systems. However, this same calculation performed in an aqueous medium yielded free energies of 44.7 and -6.1 $kJmol^{-1}$ for the polyethylene and polyester systems respectively, due to the stabilisation of the charged species by the solvent. Reaction (6.28) is therefore only likely, at least for the polyester system, with the extra stabilisation that an aqueous solvent provides. Although it is unclear to what extent polymer surface coatings are solvated during weathering, this reaction could potentially occur if water were present. In principle, formation of an oxoammonium cation may also occur through a self-

disproportionation reaction of two nitroxide radicals. However, the gas-phase free energy calculated for this reaction was over 600 $kJmol^{-1}$ and the related free energy in an aqueous medium was calculated to be over 200 $kJmol^{-1}$. This reaction is therefore unlikely to contribute to production of oxoammonium cations. The addition of a secondary alcohol to an oxoammonium cation forming a hydroxyaminoether-type species, as illustrated in Reaction (6.31), is thermodynamically disfavoured. Free energies of 73.2 and 72.2 $kJmol^{-1}$ were calculated for the polyethylene and polyester systems. Reaction (6.31) is therefore unlikely to contribute to the overall protection mechanism, even if formation of the oxoammonium cation takes place.

The trioxide product species shown in Reaction (6.17) exhibit a considerable elongation of the >NO–OOR bond, and this indicates an increased propensity for this bond to be cleaved during an ionic fragmentation process. The >NO–OOR bond length in the trioxide is 1.82 Å for the polyethylene model system and 1.86 Å for the polyester system. The distribution of charges within the trioxide molecule was investigated using a natural bond orbital (NBO) analysis (see Chapter 2.4.3). In the ground state, the molecule was shown to contain significant charge separation, as shown in Figure 6.2, with partial positive charges of 0.23 and 0.29 on the nitroxyl fragment and -0.23 and -0.29 on the peroxyl fragment, for the polyethylene and polyester model systems respectively. Therefore, in its lowest energy state, the trioxide exists as a partially dissociated molecule. It is likely that complete electron transfer is not required for attack by the electronegative hydroxyl oxygen to take place at the positive nitrogen centre.

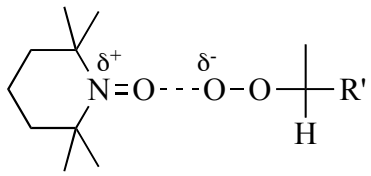

Figure 6.2 Partial positive and negative charges in the trioxide species

Reactions (6.29) and (6.30) describe the direct reaction of the trioxide with a secondary alcohol through either the five or six-membered ring transition states

labelled ***D*** and ***E***. In Reaction (6.29) the alcoholic oxygen adds to the nitrogen centre, thereby transferring a hydrogen atom to the peroxyl fragment of the trioxide and forming a hydroperoxyalkane. The formed oxyaminoether then undergoes an intramolecular hydrogen transfer Reaction (6.13) that was discussed in Chapter 6.3.1. Reaction (6.29) was found to be an almost thermoneutral reaction with calculated free energy changes of 2.0 and -1.1 $kJmol^{-1}$ for the polyethylene and polyester systems. The free energy barriers of the reactions for the polyethylene and polyester systems were found to be 106.0 and 78.1 $kJmol^{-1}$, respectively.

In Reaction (6.30) both the alcoholic hydrogen atom and hydrogen atom on the adjacent carbon group are transferred, one to the nitroxide fragment and one to the peroxyl fragment, in a concerted reaction not previously described in literature. The six-membered ring transition state structure for the reaction is labelled as intermediate ***E*** in Scheme 6.4. From Reaction (6.30), free energies of -198.5 and -173.7 $kJmol^{-1}$ and free energy barriers of 139.1 and 121.0 $kJmol^{-1}$ were calculated for the polyethylene and polyester systems respectively. It is therefore expected that Reaction (6.30) will be the dominant reaction through which the trioxide reacts with secondary alcohols. The hydroxylamine, formed through Reaction (6.30) may undergo subsequent reactions that convert it back to a nitroxide radical. These processes are described in Reactions (6.14), (6.15) and (6.16), discussed in Chapter 6.3.1.

6.4 Conclusions

The Denisov cycle describes the protection of polymer coatings from oxidative degradation caused by weathering effects, through the use of hindered amine light stabilisers (HALS). Previous mechanistic descriptions of this process have often been incomplete or inaccurate. Through prior experimental and theoretical studies, around a dozen different reaction pathways comprising over 30 individual reactions have been proposed to contribute to the overall mechanism. The high-level quantum chemical study presented in this work discriminates, for the first time, between all the suggested reactions based on calculations of their kinetic and thermodynamic parameters. This study postulates several intermediates of the polymer protection process and identifies the products of the cycle.

Predicted major products from the reactions of the nitroxide radical TEMPO with alkyl and peroxyl radicals are shown in Scheme 6.5. It was found that the dominant and catalytic mechanism of the Denisov cycle involves the addition of the nitroxide TEMPO to the polymeric radical R$^{\bullet}$ to form an alkoxyamine species, >N–OR. The alkoxyamine goes on to react with a peroxyl radical, thereby re-forming the nitroxide along with ketone and alcohol products. This process proceeds via an intermediate made up of a zwitterionic oxyaminoether and an alkoxyl radical, labelled ***B***. For polyester systems, the reaction also proceeds, to a lesser extent, through an intermediate made up of an aminoperoxyether and an alkoxyl radical. Small amounts of reactants that escape the intermediate "cage" also go on to regenerate nitroxide radicals.

A slower side reaction is the addition of TEMPO to the peroxyl radical ROO$^{\bullet}$. From this pathway, the trioxide species >N–O–O–O–R is formed. The trioxide goes on to react with the secondary alcohol product from the dominant pathway to form the reduced form of TEMPO (the hydroxylamine >N–OH), a ketone and a hydroperoxyalkane species via a concerted mechanism involving a six-membered ring transition state. The corresponding nitroxide radical is regenerated from hydrogen-transfer from the hydroxylamine to an alkyl, alkoxyl or peroxyl radical. In this way, consumption of peroxyl radicals by TEMPO also occurs in a catalytic fashion.

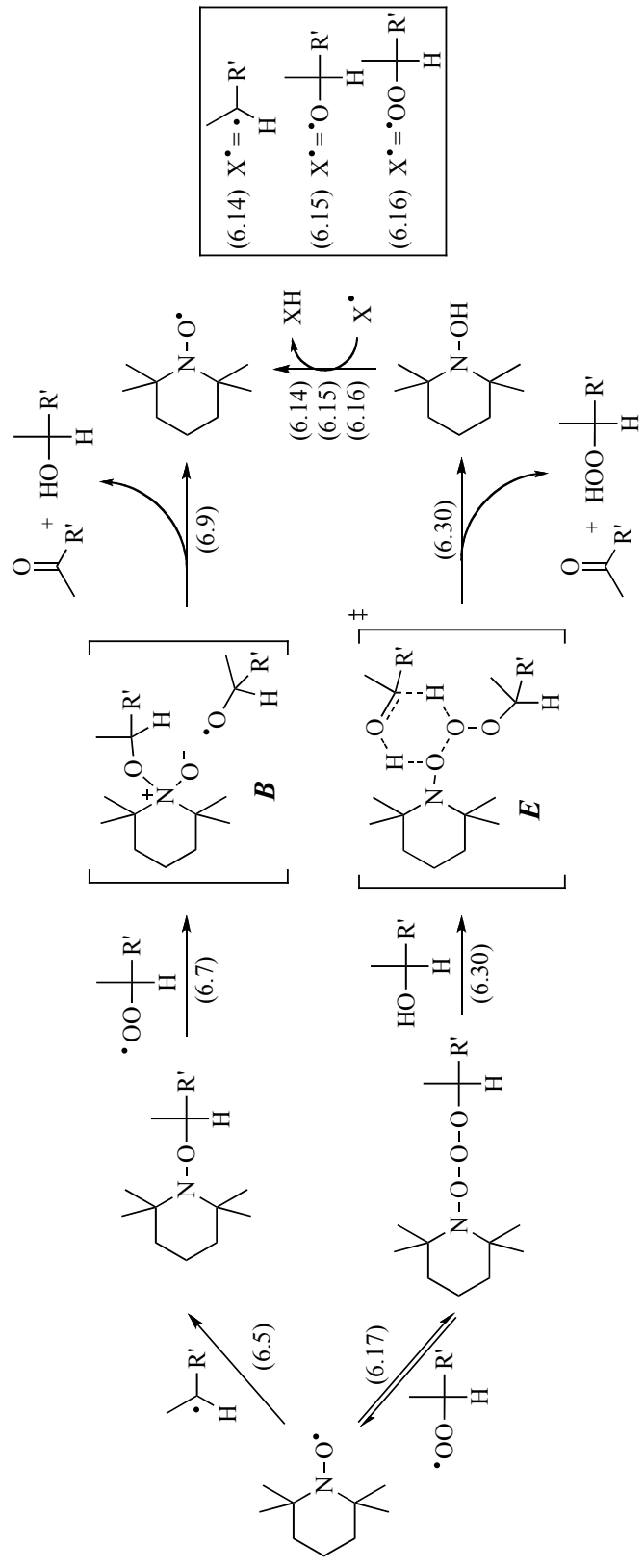

Scheme 6.5 Major products of the reactions of alkyl and peroxyl radicals with TEMPO

6.5 References

(1) Yebra, D. M.; Kill, S.; Dam-Johansen, K. *Prog. Org. Coat.* **2004**, *50*, 75.

(2) Allen, N. S. *Chem. Soc. Rev.* **1986**, *15*, 373.

(3) Denisov, E. T. *Dev. Poly. Degrad.* **1982**, *5*, 23.

(4) (a) Bolland, J. L. *Proc. Roy. Soc. London A.* **1946**, *186*, 218. (b) Bolland, J. L.; Gee, G. *Trans. Faraday Soc.* **1946**, *42*, 236. (c) Bolland, J. L.; Gee, G. *Trans. Faraday Soc.* **1946**, *42*, 244.

(5) Step, E. N.; Turro, N. J.; Klemchuk, P. P.; Gande, M. E. *Angew. Makromol. Chem.* **1995**, *232*, 65.

(6) Bortolus, P.; Camaioni, N.; Flamigni, L.; Minto, F.; Monti, S. *J. Photochem. Photobiol. A: Chem.* **1992**, *68*, 239.

(7) Pospísil, J.; Pilar, J.; Nespurek, S. *J. Vinyl Add. Tech.* **2007**, *13*, 119.

(8) Stipa, P. *J. Chem. Soc., Perkin Trans. 2* **2001**, 1793.

(9) Kysel, O.; Mach, P.; Micov, M. *Poly. Degr. and Stab.* **1993**, *40*, 31.

(10) Rossi, I.; Venturini, A.; Zedda, A. *J. Am. Chem. Soc.* **1999**, *121*, 7914.

(11) Klemchuk, P. P.; Gande, M. E.; Cordola, E. *Poly. Degr. and Stab.* **1990**, *27*, 65.

(12) Barton, D. H. R.; Le Gloahec, V. N.; Smith, J. *Tetrahedron Lett.* **1998**, *39*, 7483.

(13) Ma, Z.; Bobbitt, J. M. *J. Org. Chem.* **1991**, *56*, 6110.

(14) Miura, Y.; Utsumi, H.; Hamada, A. *Arch. Biochem. Biophys* **1993**, *300*, 148.

(15) Schwetlick, K.; Habicher, W. D. *Poly. Degr. and Stab.* **2002**, *78*, 35.

(16) Goldstein, S.; Samuni, A. *J. Phys. Chem. A* **2007**, *111*, 1066.

(17) (a) Golubev, V. A.; Zhdanov, R. I.; Gida, V. M.; Rozantsev, E. G. *Bull. Acad. Sci. U.S.S.R., Chem. Ser.* **1971**, *20*, 768. (b) Ganem, B. *J. Org. Chem.* **1975**, *40*, 1998.

(18) Semmelhack, M. F.; Schmid, C. R.; Cortés , D. A. *Tetrahedron Lett.* **1986**, *27*, 1119.

(19) (a) Lindsay Smith, J. R.; Nagatomi, E.; Stead, A.; Waddington, D. J.; Bévière, S. D. *J. Chem. Soc., Perkin Trans. 2* **2000**, 1193. (b) Lindsay Smith, J. R.; Nagatomi, E.; Waddington, D. J. *J. Chem. Soc., Perkin Trans. 2* **2000**, 2248. (c) Lindsay Smith, J. R.; Nagatomi, E.; Stead, A.; Waddington, D. J. *J. Chem. Soc., Perkin Trans. 2* **2001**, 1527.

(20) Sobek, J.; Martschke, R.; Fischer, H. *J. Am. Chem. Soc.* **2001**, *123*, 2849.

(21) Beckwith, A. L. J.; Bowry, V. W.; O'Leary, M.; Moad, G.; Rizzardo, E.; Solomon, D. H. *J. Chem. Soc., Chem. Comm.* **1986**, 1003.

(22) (a) Russell, G. A. *J. Am. Chem. Soc.* **1957**, *79*, 3871. (b) Howard, J. A.; Ingold, K. U. *J. Am. Chem. Soc.* **1968**, *90*, 1056.

Chapter 7.

Conclusions

7.1 Introduction 168

7.2 Achievements of this thesis 168

7.2.1 Assessment of computational procedures 168

7.2.2 Biological protection mechanisms 169

7.2.3 Structure reactivity trends in nitroxide mediated polymerisation 170

7.2.4 Mechanism of the Denisov cycle 170

7.3 Future outlook 171

7.1 Introduction

In this thesis, a series of investigations using computational quantum chemistry have examined the reactions undergone by nitroxide free radicals in a variety of chemical and biochemical applications. Using new computational quantum chemical methodologies for the chemically accurate study of reactions involving nitroxide radicals, developed as part of this work, the actions of nitroxides as protecting agents against oxidative damage in biological systems, as controlling agents in radical polymerisation processes, and as stabilising agents leading to protection of polymer coatings against photo-oxidative damage have all been studied. This has lead to a better understanding of the mechanisms of these processes and the relationships between structure and reactivity for a large range of nitroxide species. The main achievements of this work are summarised in this chapter.

7.2 Achievements of this thesis

7.2.1 Assessment of computational procedures

In Chapter 3, a series of assessment studies was conducted, leading to the determination of appropriate computational methods with which to conduct a study of nitroxide containing reactions. Redox and trapping reactions of various nitroxide radicals and similar species were assessed for the levels of theory used to calculated geometries, gas-phase single-point energies and free energies of solvation. Using the methods determined in this chapter, deviations between calculated values of nitroxide-based reactions and available experimental results were shown to be around 5 $kJmol^{-1}$, achieving chemical accuracy.

Assessment studies showed that G3(MP2)-RAD//B3-LYP/6-31G(d) is an appropriate level of theory for the calculation of gas-phase nitroxide reactions and molecular properties. When chemical systems become too large for such an approach, an ONIOM approximation to the G3(MP2)-RAD value, in which the full system is calculated at the RMP2/ 6-311+G(3df,2p) level of theory, was shown to provide good results. A multireference-type approach is required for the determination of the reaction pathway for the combination of two radical species, with the active space

including the bonding and anti-bonding orbitals and adjacent lone pairs. However, it was found that single reference methods are appropriate for the determination of the thermodynamic parameters of such reactions. For reactions calculated in solution, the effects of the solvent are well described by using a polarisable continuum model (PCM) method at the B3-LYP/6-31G(d) level using the SCFVAC keyword in the GAUSSIAN calculation to find the free energy of solvation of reaction species. This value is added to the gas-phase free energy in order to determine the total free energy of the species in the solution medium, via a thermodynamic cycle.

7.2.2 Biological protection mechanisms

Nitroxide radicals are effective and diverse protecting agents against a range of different types of oxidative damage in biological systems. In Chapter 4, the various mechanisms of oxidative damage and protection were compiled in an extensive literature review. The primary protection mechanisms were observed to be oxidation and reduction reactions of nitroxides as well as radical scavenging reactions.

An investigation of factors affecting the electrode potentials of a wide range of cyclic nitroxide species was then conducted in order to provide insight into their protecting abilities. The oxidation and reduction potentials of nitroxide radicals are primarily determined by the ring size and structure of the cyclic backbone. Six-membered piperidine and azaphenalene-type nitroxides are reduced more easily than the less flexible five-membered pyrrolidine and isoindoline-type nitroxides. Piperidine and pyrrolidine nitroxides are more easily oxidised than isoindoline nitroxides. Within a family of nitroxides, variation of the ring substituents alters the electrode potentials in a manner expected on the basis of electronegativity considerations. Thus, electron withdrawing subsitutent groups act to stabilise the anionic form of the nitroxide, making reduction more favourable, while electron donating groups stabilise the cation, lowering the oxidation potential. For example, substitution by carboxy groups around the ring structure significantly increases the oxidation potential while lowering the reduction potential. The placement of substituents around the ring was found to cause significant changes in the electrode potentials, due both to the effects of resonance and steric bulk. A comparison of the calculated oxidation potentials with experimental results showed good agreement for all nitroxide species except the

azaphenalene class, which showed unprecedented (order of magnitude higher) differences, possibly due to additional processes not taken into account by the theoretical model.

Using experimental protection data, it was shown that protection against H_2O_2 mediated oxidative damage is dependent upon the ease of reduction of the nitroxide agent, with protection occurring through reactions such as the superoxide dismutase (SOD) mimicking dismutation of superoxide as well as the oxidation of transition metal ions, semiquinones and other damaging radicals. From their electrode potentials, it was seen that the six-membered piperidine nitroxides are likely to be most successful in protection against H_2O_2 mediated damage. Since species should also avoid damaging side reactions caused by oxidation of the nitroxide, the dicarboxyl-substituted piperidine species are expected to be most successful. The protection against radiation induced oxidative damage was found to occur through several different mechanisms, with further experimental data being needed to determine the relative importance of each.

7.2.3 Structure reactivity trends in nitroxide mediated polymerisation

In Chapter 5, the thermodynamic parameters of the control reaction of nitroxide mediated polymerisation (NMP) were calculated for a wide range of small nitroxide species and polymeric radicals, and structure reactivity trends within the data analysed. A multiparameter analysis was then used to determine a general equation, which allows the equilibrium constant of the control reaction to be determined in terms of easily computed parameters designed to measure the polar, steric and radical stabilisation effects of each of the radicals. Testing performed on small systems showed the success of the equation and its potential for use on larger systems, for which direct computation of the equilibrium constant is impractical. As a practical test, the equation was used explain the success of a recently reported indoline-type nitroxide control agent for the polymerisation of methyl methacrylate.

7.2.4 Mechanism of the Denisov cycle

In Chapter 6, a mechanistic study was performed in order to determine the mechanism of the Denisov cycle, which describes the protection of polymer coatings

from oxidative degradation caused by weathering effects through the use of hindered amine light stabilisers (HALS). Around a dozen different reaction pathways comprising over 30 individual reactions have been suggested previously, through both experimental and theoretical studies, to contribute to the overall mechanism. For the first time, discrimination between the suggested reactions, on the basis of their kinetic and thermodynamic parameters, was made possible by the high-level quantum chemical study presented in this work. Through this study, several intermediates of the polymer protection process were postulated, and the products of the cycle identified.

The dominant and catalytic mechanism of the Denisov cycle was found to involve the addition of the nitroxide to a polymeric radical to form an alkoxyamine species. The alkoxyamine goes on to react with a peroxyl radical re-forming the nitroxide along with ketone and alcohol products via an intermediate made up of a zwitterionic oxyaminoether and an alkoxyl radical. For polyester systems, the reaction also proceeds, to a lesser extent, through an intermediate made up of an aminoperoxyether and an alkoxyl radical. Small amounts of reactants that escape the intermediate "cage" also go on to regenerate nitroxide radicals.

In a slower side reaction, the nitroxide may also react with a peroxyl radical forming a trioxide species. The trioxide goes on to react with the secondary alcohol product from the dominant pathway to form hydroxylamine, ketone and hydroperoxyalkane products via a concerted mechanism involving a six-membered ring transition state. The corresponding nitroxide radical is regenerated from hydrogen-transfer from the hydroxylamine to an alkyl, alkoxyl or peroxyl radical. In this way, consumption of peroxyl radicals by nitroxide also occurs in a catalytic fashion.

7.3 Future outlook

Nitroxide radicals are already widely utilised in a large variety of research and commercial applications. In this work, additional insights into the properties and reactivities of a large number of nitroxide species were gained, and specific advances to the field of nitroxide research made. The achievements of this work will assist to

guide future research efforts in the fields of biological protection using nitroxides, nitroxide mediated polymerisation and the protection of polymer coatings using nitroxides.

Insights into the mechanisms by which nitroxide protect against oxidative damage in biological systems gained in this work will assist in the search for more effective agents. Collaborative work in this direction is underway with members of the research team of Associate Professor Steven Bottle of the Queensland University of Technology.

An analysis of the factors effecting the trapping of alkyl radicals by nitroxides in nitroxide mediated polymerisation (NMP) completed in this work has the potential to be generalised to the study of other controlled radical polymerisation reactions such as atom transfer radical polymerisation (ATRP) and reversible addition fragmentation chain transfer (RAFT). A project in this direction is currently being undertaken by members of the Coote research group, in collaboration with Dr Sylvain Marque of the Université de Provence and Professor Krzysztof Matyjaszewski of Carnegie Mellon University.

The elucidation of the mechanism of the Denisov cycle for the protection of polymer coatings from weathering effects by nitroxide protecting agents is expected to be of great use in future studies to design better nitroxide protecting agents, which avoid any consuming side reactions. Further work in this direction is being commenced with Dr Stephen Blanksby of the University of Wollongong and Dr Philip Barker of BlueScope Steel.

Appendix.

Computational Data

A.1 Free energy components of species 174

A.1.1 Data for Chapter 4 174

A.1.2 Data for Chapter 5 188

A.1.3 Data for Chapter 6 198

A.2 GAUSSIAN archive files 204

A.2.1 Archives for Chapter 4 205

A.2.2 Archives for Chapter 5 311

A.2.3 Archives for Chapter 6 388

A.1 Free energy components of species

The principle components of the free energies of species in Chapters 4 to 6, found using G3(MP2)-RAD//B3-LYP/6-31G(d) gas-phase energies and PCM solvation energies at the B3-LYP/6-31G(d) level, are shown in Tables A.1 to A.6. The scaling factors used were 0.9806 for zero-point energies (*ZPE*), 0.9989 for temperature corrections (T_c) and 1.0015 for entropy corrections.

Nitroxide radicals in Tables A.1 to A.6 are labelled using their common acronyms (see Table 1.1) as well as their structure numbers (see Table 4.1 and 5.1). The corresponding cationic and anionic versions of the nitroxide are labelled with a + and – suffix, respectively, while hydroxylamines are labelled as nitroxideH (for example TEMPOH). Alkoxyamines are written as a combination of their radical components in the manner of nitroxide–alkyl radical (for example TEMPO–CH_3). Transition state and pre-complex species are labelled with the corresponding reaction number, with the prefix TS– or PC–, respectively.

For larger species, the gas-phase enthalpies, H^o_{gas}, were found from ONIOM approximations to G3(MP2)-RAD energies, with only an active core system calculated at the G3(MP2)-RAD level, and the substituent effects estimated at the RMP2/6-311+G(3df,2p) level. Where possible the full nitroxide ring-structure was included in the core. For very large systems the nitroxide core system was truncated to $(CH_3)_2NO^{\bullet}$.

A.1.1 Data for Chapter 4

Table A.1 Contributions to the gas-phase enthalpies (0 K) of species in Chapter 4

Species	Sym.	E^o_{gas}(RMP2) (Hartrees)	E^o_{gas}(G3(MP2)-RAD) (Hartrees)	*ZPE* (Hartrees)	H^o_{gas} (Hartrees)
DBN (**1**)	C_1	-444.64289	-445.05945	0.24965	-444.80979
DBN+	C_1	-444.39748	-444.80875	0.25057	-444.55818
DBN-	C_s	-444.65415	-445.07475	0.24603	-444.82872

DBNH	C_1	-445.25596	-445.68100	0.26131	-445.41969
TEMPO (**2**)	C_s	-482.68700	-483.12856	0.25821	-482.87034
TEMPO+	C_s	-482.43972	-482.87570	0.25948	-482.61623
TEMPO-	C_s	-482.70073	-483.14581	0.25494	-482.89087
TEMPOH	C_s	-483.30211	-483.75173	0.26984	-483.48190
4-amino-TEMPO (**3**)	C_1	-537.94553	-538.42297	0.27503	-538.14794
4-amino-TEMPO+	C_1	-537.69649	-538.16818	0.27577	-537.89240
4-amino-TEMPO-	C_1	-537.96271	-538.44368	0.27179	-538.17189
4-amino-TEMPOH	C_1	-538.56101	-539.04644	0.28647	-538.75997
4-methoxy-TEMPO (**4**)	C_1	-597.01165	-597.52536	0.29016	-597.23520
4-methoxy-TEMPO+	C_1	-596.76180	-597.26992	0.29083	-596.97909
4-methoxy-TEMPO-	C_1	-597.02968	-597.54683	0.28690	-597.25992
4-ethoxy-TEMPO (**5**)	C_1	-636.23552	-636.79230	0.31807	-636.47423
4-ethoxy-TEMPO+	C_1	-635.99149	-636.54233	0.31943	-636.22290
4-ethoxy-TEMPO-	C_1	-636.25339	-636.81362	0.31468	-636.49894
4-ethoxy-TEMPOH	C_1	-636.85086	-637.41565	0.32959	-637.08606
4-hydroxy-TEMPO (**6**)	C_s	-557.80823	-558.27898	0.26240	-558.01658
4-hydroxy-TEMPO+	C_1	-557.55715	-558.02201	0.26292	-557.75908
4-hydroxy-TEMPO-	C_s	-557.82883	-558.30284	0.25916	-558.04367
4-hydroxy-TEMPOH	C_s	-558.42432	-558.90284	0.27387	-558.62897
4-oxo-TEMPO (**7**)	C_s	-556.61153	-557.06617	0.23912	-556.82705
4-oxo-TEMPO+	C_s	-556.35139	-556.79955	0.23950	-556.56005
4-oxo-TEMPO-	C_s	-556.64078	-557.09806	0.23599	-556.86207
4-oxo-TEMPOH	C_s	-557.22989	-557.69163	0.25060	-557.44103
4-carboxy-TEMPO (**8**)	C_1	-670.98919	-671.51277	0.27278	-671.23998
4-carboxy-TEMPO+	C_1	-670.73691	-671.25460	0.27348	-670.98111
4-carboxy-TEMPO-	C_1	-671.01112	-671.53786	0.26955	-671.26831
3-carboxy-TEMPO (**9**)	C_1	-670.98643	-671.50990	0.27319	-671.23670
3-carboxy-TEMPO+	C_1	-670.73475	-671.25232	0.27400	-670.97832
3-carboxy-TEMPO-	C_1	-671.00999	-671.53662	0.26971	-671.26691
3-carboxy-TEMPOH	C_1	-671.60325	-672.13430	0.28459	-671.84971
3,4-dicarboxy-TEMPO (**10**)	C_1	-859.29033	-	0.28727	-859.52653
3,4-dicarboxy-TEMPO+	C_1	-859.03490	-	0.28804	-859.26443
3,4-dicarboxy-TEMPO-	C_1	-859.32064	-	0.28407	-859.56320
3,4-dicarboxy-TEMPOH	C_1	-859.90804	-	0.29919	-860.05848
3,5-dicarboxy-TEMPO (**11**)	C_s	-859.28492	-	0.28795	-859.52044
3,5-dicarboxy-TEMPO+	C_s	-859.02928	-	0.28827	-859.25857
3,5-dicarboxy-TEMPO-	C_s	-859.31785	-	0.28403	-859.56045

3,5-dicarboxy-TEMPOH	C_s	-859.90342	-	0.29957	-860.05347
4-carboxy-2,2,6,6-tetraethyl piperidin-1-lyoxyl (**12**)	C_1	-827.86346	-	0.38588	-828.00116
4-carboxy-2,2,6,6-tetraethyl piperidin-1-lyoxyl+	C_1	-827.62131	-	0.38622	-827.75278
4-carboxy-2,2,6,6-tetraethyl piperidin-1-lyoxyl-	C_1	-827.88412	-	0.38253	-828.02832
4-ammonio-TEMPO (**13**)	C_s	-538.29811	-538.78100	0.28915	-538.49185
4-ammonio-TEMPO+	C_s	-537.92946	-538.40404	0.28979	-538.11424
4-ammonio-TEMPO-	C_s	-538.43824	-538.92143	0.28465	-538.63678
2,2,6,6-tetramethyl-1,2,3,6-tetrahydropyridin-1-lyoxyl (**14**)	C_1	-481.46959	-481.89671	0.23434	-481.66237
2,2,6,6-tetramethyl-1,2,3,6-tetrahydropyridin-1-lyoxyl+	C_1	-481.22027	-481.64179	0.23510	-481.40669
2,2,6,6-tetramethyl-1,2,3,6-tetrahydropyridin-1-lyoxyl-	C_1	-481.48334	-481.91443	0.23105	-481.68338
PROXYL (**15**)	C_2	-443.47115	-443.86807	0.22889	-443.63917
PROXYL+	C_2	-443.22291	-443.61574	0.23016	-443.38558
PROXYL-	C_1	-443.47590	-443.87790	0.22564	-443.65226
PROXYLH	C_1	-444.07902	-444.48593	0.24065	-444.24528
3-amino-PROXYL (**16**)	C_1	-498.72919	-499.16208	0.24587	-498.91621
3-amino-PROXYL+	C_1	-498.48174	-498.90988	0.24674	-498.66314
3-amino-PROXYL-	C_1	-498.73814	-499.17602	0.24276	-498.93326
3-amino-PROXYLH	C_1	-499.33806	-499.78062	0.25749	-499.52313
3-methoxy-PROXYL (**17**)	C_1	-557.79489	-558.26347	0.26122	-558.00225
3-methoxy-PROXYL+	C_1	-557.55013	-558.01460	0.26217	-557.75243
3-methoxy-PROXYL-	C_1	-557.80274	-558.27701	0.25777	-558.01924
3-methoxy-PROXYLH	C_1	-558.40389	-558.88282	0.27257	-558.61025
3-hydroxy-PROXYL (**18**)	C_1	-518.59214	-519.01770	0.23323	-518.78448
3-hydroxy-PROXYL+	C_1	-518.34435	-518.76566	0.23428	-518.53138
3-hydroxy-PROXYL-	C_1	-518.60899	-519.03905	0.23107	-518.80798
3-hydroxy-PROXYLH	C_1	-519.20034	-519.63618	0.24474	-519.39144
3-carboxy-PROXYL (**19**)	C_1	-631.77305	-632.25187	0.24355	-632.00831
3-carboxy-PROXYL+	C_1	-631.51905	-631.99331	0.24452	-631.74878
3-carboxy-PROXYL-	C_1	-631.78880	-632.27215	0.24057	-632.03158
3-carboxy-PROXYLH	C_1	-632.38285	-632.87095	0.25539	-632.61557
3,4-dicarboxy-PROXYL (**20**)	C_1	-820.07656	-	0.25818	-820.29720
3,4-dicarboxy-PROXYL+	C_1	-819.81872	-	0.25902	-820.03396
3,4-dicarboxy-PROXYL-	C_1	-820.09951	-	0.25509	-820.32777
3,4-dicarboxy-PROXYLH	C_1	-820.68684	-	0.26998	-820.82377

3-carboxy-2,2,5,5-tetraethyl pyrrolidin-1-lyoxyl (**21**)	C_1	-788.64910	-	0.35644	-788.77149
3-carboxy-2,2,5,5-tetraethyl pyrrolidin-1-lyoxyl+	C_1	-788.40489	-	0.35713	-788.52201
3-carboxy-2,2,5,5-tetraethyl pyrrolidin-1-lyoxyl-	C_1	-788.66682	-	0.35348	-788.79668
3-ammonio-PROXYL (**22**)	C_1	-499.07845	-499.51835	0.26011	-499.25824
3-ammonio-PROXYL+	C_1	-498.69434	-499.12575	0.26071	-498.86504
2,2,5,5-tetramethyl-2,5-di hydro-1*H*-pyrrol-1-yloxy (**23**)	C_2	-442.25170	-442.63417	0.20489	-442.42928
2,2,5,5-tetramethyl-2,5-di hydro-1*H*-pyrrol-1-yloxy+	C_2	-441.99772	-442.37641	0.20592	-442.17050
2,2,5,5-tetramethyl-2,5-dihydro-1*H*-pyrrol-1-yloxy-	C_s	-442.25892	-442.64596	0.20143	-442.44454
2,2,5,5-tetramethyl-3-carboxy-2,5-dihydro-1*H*-pyrrol-1-yloxy (**24**)	C_s	-630.55787	-631.02166	0.21981	-630.80186
2,2,5,5-tetramethyl-3-carboxy-2,5-dihydro-1*H*-pyrrol-1-yloxy+	C_s	-	-630.75954	0.22063	-630.53891
2,2,5,5-tetramethyl-3-carboxy-2,5-dihydro-1*H*-pyrrol-1-yloxy-	C_1	-630.57287	-631.04112	0.21630	-630.82482
1-hydroxy-2,2,5,5-tetra methyl-3-carboxy-2,5-dihydro-1*H*-pyrrole	C_1	-631.16761	-631.64095	0.23150	-631.40945
2,2,5,5-tetramethyl-3,4-diphenyl-2,5-dihydro-1*H*-pyrrol-1-yloxy (**25**)	C_2	-903.36675	-	0.36445	-903.39923
2,2,5,5-tetramethyl-3,4-diphenyl-2,5-dihydro-1*H*-pyrrol-1-yloxy+	C_2	-903.12035	-	0.36504	-903.14814
2,2,5,5-tetramethyl-3,4-diphenyl-2,5-dihydro-1*H*-pyrrol-1-yloxy-	C_1	-903.38403	-	0.36082	-903.42521
TMOZO (**26**)	C_1	-479.35963	-479.74470	0.20482	-479.53988
TMOZO+	C_1	-479.10042	-479.48116	0.20563	-479.27553
TMOZO-	C_1	-479.37522	-479.76497	0.20184	-479.56312
TMOZOH	C_1	-479.97155	-480.36601	0.21658	-480.14943
TMIO (**27**)	C_{2v}	-595.58586	-596.08162	0.25152	-595.83010
TMIO+	C_{2v}	-595.33446	-595.82621	0.25246	-595.57375
TMIO-	C_s	-595.60050	-596.10080	0.24855	-595.85224
TMIOH	C_s	-596.19493	-596.70050	0.26325	-596.43725
5-amino-TMIO (**28**)	C_1	-650.85112	-	0.26772	-651.07916
5-amino-TMIO+	C_1	-650.60446	-	0.26804	-650.82816

5-amino-TMIO-	C_1	-650.86281	-	0.26459	-651.09851
5-aminomethyl-TMIO (**29**)	C_1	-690.06360	-	0.29646	-690.26289
5-aminomethyl-TMIO+	C_1	-689.81666	-	0.29732	-690.01108
5-aminomethyl-TMIO-	C_1	-690.08031	-	0.29323	-690.28737
5-nitro-TMIO (**30**)	C_s	-799.80981	-	0.25398	-800.05160
5-nitro-TMIO+	C_s	-799.54684	-	0.25464	-799.78394
5-nitro-TMIO-	C_1	-799.83271	-	0.25142	-800.08159
5-methoxy-TMIO (**31**)	C_s	-709.91456	-	0.28359	-710.12673
5-methoxy-TMIO+	C_s	-709.66654	-	0.28438	-709.87390
5-methoxy-TMIO-	C_1	-709.92807	-	0.28039	-710.14798
5,6-dimethoxy-TMIO (**32**)	C_2	-824.23895	-	0.31568	-824.41902
5,6-dimethoxy-TMIO+	C_s	-823.99307	-	0.31653	-824.16829
5,6-dimethoxy-TMIO-	C_1	-824.25070	-	0.31192	-824.43907
5-hydroxy-TMIO (**33**)	C_s	-670.71146	-	0.25537	-670.95185
5-hydroxy-TMIO+	C_s	-670.46166	-	0.25627	-670.69714
5-hydroxy-TMIO-	C_1	-670.72648	-	0.25219	-670.97459
5-carboxy-TMIO (**34**)	C_s	-783.89097	-	0.26613	-784.12060
5-carboxy-TMIO+	C_s	-783.63556	-	0.26689	-783.86041
5-carboxy-TMIO-	C_1	-783.91104	-	0.26314	-784.14821
5-carboxy-TMIOH	C_1	-784.50103	-	0.27795	-784.72864
4-carboxy-TMIO (**35**)	C_1	-783.88731	-	0.26670	-784.11636
4-carboxy-TMIO+	C_1	-783.63817	-	0.26746	-783.86246
4-carboxy-TMIO-	C_1	-783.89847	-	0.26328	-784.13550
4,7-dicarboxy-TMIO (**36**)	C_s	-972.18630	-	0.28163	-972.40043
4,7-dicarboxy-TMIO+	C_{2v}	-971.93958	-	0.28234	-972.14899
4,7-dicarboxy-TMIO-	C_{2v}	-972.19442	-	0.27866	-972.41606
4,6-dicarboxy-TMIO (**37**)	C_1	-972.19087	-	0.28098	-972.40565
4,6-dicarboxy-TMIO+	C_1	-971.93848	-	0.28181	-972.14841
4,6-dicarboxy-TMIO-	C_1	-972.20599	-	0.27782	-972.42847
4,5-dicarboxy-TMIO (**38**)	C_1	-972.18643	-	0.28061	-972.40159
4,5-dicarboxy-TMIO+	C_1	-971.93169	-	0.28148	-972.14196
4,5-dicarboxy-TMIO-	C_1	-972.20433	-	0.27742	-972.42721
5,6-dicarboxy-TMIO (**39**)	C_1	-972.18581	-	0.28021	-972.40136
5,6-dicarboxy-TMIO+	C_1	-971.92678	-	0.28086	-972.13766
5,6-dicarboxy-TMIO-	C_1	-972.21031	-	0.27715	-972.43345
5,6-dicarboxy-TMIOH	C_1	-972.79678	-	0.29201	-973.01034
1,1,3,3-tetraethylisoindolin-1-yloxyl (**40**)	C_1	-752.46538	-	0.36475	-752.59638

1,1,3,3-tetraethylisoindolin-1-yloxyl+	C_2	-752.22006	-	0.36516	-752.34665
1,1,3,3-tetraethylisoindolin-1-yloxyl-	C_1	-752.47733	-	0.36125	-752.61638
5-carboxy-1,1,3,3-tetraethyl isoindolin-1-yloxyl (**41**)	C_1	-940.77082	-	0.37925	-940.88733
5-carboxy-1,1,3,3-tetraethyl isoindolin-1-yloxyl+	C_1	-940.52175	-	0.37955	-940.63394
5-carboxy-1,1,3,3-tetraethyl isoindolin-1-yloxyl-	C_1	-940.78745	-	0.37601	-940.91174
5,6-dicarboxy-1,1,3,3-tetra ethylisoindolin-1-yloxyl (**42**)	C_1	-1129.06645	-	0.39354	-1129.16866
5,6-dicarboxy-1,1,3,3-tetra ethylisoindolin-1-yloxyl+	C_2	-1128.81365	-	0.39356	-1128.91184
5,6-dicarboxy-1,1,3,3-tetra ethylisoindolin-1-yloxyl-	C_1	-1129.08742	-	0.38998	-1129.19774
5-bromo-TMIO (4**3**)	C_s	-3167.53600	-	0.24156	-3167.79020
5-bromo-TMIO+	C_s	-3167.28045	-	0.24233	-3167.52986
5-bromo-TMIO-	C_1	-3167.55731	-	0.23850	-3167.81910
5,6-dibromo-TMIO (**44**)	C_2	-5739.48320	-	0.23159	-5739.74737
5,6-dibromo-TMIO+	C_2	-5739.22507	-	0.23223	-5739.48459
5,6-dibromo-TMIO-	C_s	-5739.50934	-	0.22871	-5739.78093
5-ammonio-TMIO (**45**)	C_s	-651.19099	-	0.28147	-651.40528
5-ammonio-TMIO+	C_s	-650.83956	-	0.28248	-651.04883
5-ammonio-TMIO-	C_1	-651.30462	-	0.27639	-651.52853
1,1,3,3-tetramethyl-2,3-dihydro-1*H*-dibenzo[*e*,*g*] isoindol-1-lyoxyl (**46**)	C_2	-902.21493	-	0.34438	-902.36630
1,1,3,3-tetramethyl-2,3-dihydro-1*H*-dibenzo[*e*,*g*] isoindol-1-lyoxyl+	C_2	-901.96664	-	0.34496	-902.11342
1,1,3,3-tetramethyl-2,3-dihydro-1*H*-dibenzo[*e*,*g*] isoindol-1-lyoxyl-	C_s	-902.23282	-	0.34058	-902.39254
TMAO (**47**)	C_s	-748.89162	-749.50439	0.29886	-749.20553
TMAO+	C_1	-748.64711	-749.27242	0.29998	-748.97244
TMAO-	C_s	-748.91645	-749.53363	0.29540	-749.23823
4-amino-TMAO (**48**)	C_1	-804.15192	-	0.31547	-804.44921
4-amino-TMAO+	C_1	-803.91346	-	0.31674	-804.22202
4-amino-TMAO-	C_1	-804.17821	-	0.31210	-804.48329
5-amino-TMAO (**49**)	C_1	-804.15770	-	0.31519	-804.45527
5-amino-TMAO+	C_1	-803.91659	-	0.31577	-804.22613
5-amino-TMAO-	C_1	-804.18062	-	0.31185	-804.48595

6-amino-TMAO (**50**)	C_1	-804.15718	-	0.31548	-804.45447
6-amino-TMAO+	C_1	-803.91895	-	0.31602	-804.22824
6-amino-TMAO-	C_1	-804.17985	-	0.31212	-804.48490
6-dimethylamino-TMAO (**51**)	C_1	-882.57530	-	0.37095	-882.81712
6-dimethylamino-TMAO+	C_1	-882.33560	-	0.37257	-882.58834
6-dimethylamino-TMAO-	C_1	-882.59863	-	0.36731	-882.84850
4-nitro-TMAO (**52**)	C_1	-953.10542	-	0.30129	-953.41690
4-nitro-TMAO+	C_1	-952.85460	-	0.30230	-953.17761
4-nitro-TMAO-	C_1	-953.13383	-	0.29826	-953.45275
5-nitro-TMAO (**53**)	C_1	-953.11668	-	0.30136	-953.42809
5-nitro-TMAO+	C_1	-952.86114	-	0.30204	-953.18441
5-nitro-TMAO-	C_1	-953.12394	-	0.29804	-953.44308
6-nitro-TMAO (**54**)	C_1	-953.10978	-	0.30141	-953.42114
6-nitro-TMAO+	C_1	-952.85622	-	0.30212	-953.17940
6-nitro-TMAO-	C_1	-953.11113	-	0.29797	-953.43034
6,7-dinitro-TMAO (**55**)	C_1	-1157.32366	-	0.30349	-1157.63293
6,7-dinitro-TMAO+	C_1	-1157.06068	-	0.30383	-1157.38216
6,7-dinitro-TMAO-	C_1	-1157.35882	-	0.30051	-1157.67549
4-carboxy-TMAO (**56**)	C_1	-937.18489	-	0.31343	-937.48422
4-carboxy-TMAO+	C_1	-936.94287	-	0.31484	-937.25334
4-carboxy-TMAO-	C_1	-937.21134	-	0.30991	-937.51860
5-carboxy-TMAO (**57**)	C_1	-937.19758	-	0.31351	-937.49684
5-carboxy-TMAO+	C_1	-936.94942	-	0.31429	-937.26044
5-carboxy-TMAO-	C_1	-937.22696	-	0.31040	-937.53374
6-carboxy-TMAO (**58**)	C_1	-937.19199	-	0.31360	-937.49116
6-carboxy-TMAO+	C_1	-936.94511	-	0.31446	-937.25596
6-carboxy-TMAO-	C_1	-937.22197	-	0.31023	-937.52892
4,5-dicarboxy-TMAO (**59**)	C_1	-1125.48653	-	0.32809	-1125.77120
4,5-dicarboxy-TMAO+	C_1	-1125.24212	-	0.32868	-1125.53875
4,5-dicarboxy-TMAO-	C_1	-1125.51720	-	0.32450	-1125.80988
4,6-dicarboxy-TMAO (**60**)	C_1	-1125.48407	-	0.32823	-1125.76861
4,6-dicarboxy-TMAO+	C_1	-1125.24013	-	0.32937	-1125.53606
4,6-dicarboxy-TMAO-	C_1	-1125.51050	-	0.32504	-1125.80264
4,7-dicarboxy-TMAO (**61**)	C_1	-1125.48474	-	0.32834	-1125.76917
4,7-dicarboxy-TMAO+	C_1	-1125.23986	-	0.32921	-1125.53596
4,7-dicarboxy-TMAO-	C_1	-1125.49944	-	0.32519	-1125.79143
4,8-dicarboxy-TMAO (**62**)	C_1	-1125.49069	-	0.32801	-1125.77546
4,8-dicarboxy-TMAO+	C_1	-1125.24478	-	0.32904	-1125.54104

4,8-dicarboxy-TMAO-	C_1	-1125.51596	-	0.32508	-1125.80806
4,9-dicarboxy-TMAO (**63**)	C_s	-1125.47593	-	0.32834	-1125.76036
4,9-dicarboxy-TMAO+	C_1	-1125.23247	-	0.32924	-1125.52854
4,9-dicarboxy-TMAO-	C_1	-1125.50529	-	0.32448	-1125.79798
5,6-dicarboxy-TMAO (**64**)	C_1	-1125.49220	-	0.32746	-1125.77751
5,6-dicarboxy-TMAO+	C_1	-1125.24088	-	0.32833	-1125.53785
5,6-dicarboxy-TMAO-	C_1	-1125.52425	-	0.32447	-1125.81695
5,7-dicarboxy-TMAO (**65**)	C_1	-1125.49754	-	0.32792	-1125.78239
5,7-dicarboxy-TMAO+	C_1	-1125.24704	-	0.32885	-1125.54350
5,7-dicarboxy-TMAO-	C_1	-1125.52919	-	0.32504	-1125.82133
5,8-dicarboxy-TMAO (**66**)	C_s	-1125.50232	-	0.32784	-1125.78725
5,8-dicarboxy-TMAO+	C_1	-1125.25095	-	0.32860	-1125.54766
5,8-dicarboxy-TMAO-	C_s	-1125.53612	-	0.32442	-1125.82888
6,7-dicarboxy-TMAO (**67**)	C_1	-1125.48893	-	0.32779	-1125.77390
6,7-dicarboxy-TMAO+	C_1	-1125.23918	-	0.32835	-1125.53614
6,7-dicarboxy-TMAO-	C_1	-1125.52231	-	0.32426	-1125.81523
O_2	D_h	-150.12649	-150.17181	0.00371	-150.16810
$O_2^{\bullet-}$	D_h	-150.12716	-150.18579	0.00271	-150.18308
$HOO^{\bullet}$	C_s	-150.67674	-150.75868	0.01376	-150.74492
H_2O_2	C_2	-151.32892	-151.40966	0.02575	-151.38391

Table A.2 Contributions to the solution-phase free energies (298 K) of species in Chapter 4

Species	T_c (kJ mol^{-1})	H_{gas} (kJmol^{-1})	S_{gas} (Jmol^{-1}K^{-1})	G_{gas} (kJmol^{-1})	ΔG_{solv} (water) (kJmol^{-1})	ΔG_{solvn} (aceto-nitrile) (kJmol^{-1})
DBN (**1**)	35.7	-1167812.4	450.4	-1167946.7	-6.8	-
DBN+	35.9	-1167151.6	446.1	-1167284.6	-181.0	-
DBN-	35.0	-1167862.8	437.1	-1167993.2	-231.2	-
DBNH	36.0	-1169413.4	445.6	-1169546.2	-11.0	-
TEMPO (**2**)	34.1	-1267742.0	437.7	-1267872.5	-10.4	8.5
TEMPO+	34.0	-1267074.9	432.0	-1267203.7	-184.9	-146.2
TEMPO-	33.1	-1267796.9	420.1	-1267922.1	-238.3	-
TEMPOH	34.5	-1269347.3	429.5	-1269475.3	-14.1	-
4-amino-TEMPO (**3**)	37.5	-1412869.9	461.7	-1413007.5	-31.6	1.8
4-amino-TEMPO+	37.8	-1412198.7	459.8	-1412335.8	-214.8	-157.2

4-amino-TEMPO-	36.6	-1412933.7	445.3	-1413066.4	-253.0	-
4-amino-TEMPOH	38.0	-1414476.3	454.9	-1414611.9	-34.4	-
4-methoxy-TEMPO (**4**)	41.2	-1567999.8	494.4	-1568147.2	-17.9	-
4-methoxy-TEMPO+	41.6	-1567327.0	494.1	-1567474.3	-194.9	-
4-methoxy-TEMPO-	40.2	-1568065.7	476.9	-1568207.9	-239.3	-
4-ethoxy-TEMPO (**5**)	44.8	-1671018.3	525.8	-1671175.1	-17.5	-
4-ethoxy-TEMPO+	44.3	-1670358.9	515.8	-1670512.7	-183.7	-
4-ethoxy-TEMPO-	43.9	-1671084.0	509.8	-1671236.0	-238.2	-
4-ethoxy-TEMPOH	45.2	-1672624.2	518.5	-1672778.8	-21.5	-
4-hydroxy-TEMPO (**6**)	37.2	-1465035.4	459.8	-1465172.4	-34.7	0.7
4-hydroxy-TEMPO+	37.6	-1464358.8	459.8	-1464495.9	-217.6	-159.0
4-hydroxy-TEMPO-	36.3	-1465107.3	443.8	-1465239.6	-251.8	-
4-hydroxy-TEMPOH	37.7	-1466642.7	452.9	-1466777.7	-37.9	-
4-oxo-TEMPO (**7**)	36.1	-1461913.3	457.7	-1462049.8	-22.8	-
4-oxo-TEMPO+	36.5	-1461211.9	457.9	-1461348.4	-212.2	-
4-oxo-TEMPO-	35.4	-1462006.0	442.1	-1462137.8	-234.3	-
4-oxo-TEMPOH	36.6	-1463524.8	450.7	-1463659.2	-29.2	-
4-carboxy-TEMPO (**8**)	41.8	-1762298.8	506.9	-1762449.9	-40.0	2.4
4-carboxy-TEMPO+	41.9	-1761619.0	503.2	-1761769.0	-223.7	-156.1
4-carboxy-TEMPO-	41.0	-1762373.9	492.1	-1762520.7	-256.1	-
3-carboxy-TEMPO (**9**)	41.3	-1762290.7	499.3	-1762439.6	-35.1	-
3-carboxy-TEMPO+	41.2	-1761612.4	492.7	-1761759.3	-209.9	-
3-carboxy-TEMPO-	40.6	-1762370.7	482.8	-1762514.7	-250.6	-
3-carboxy-TEMPOH	41.9	-1763899.5	493.1	-1764046.5	-40.4	-
3,4-dicarboxy-TEMPO (**10**)	49.3	-2256637.6	565.2	-2256806.1	-60.0	-
3,4-dicarboxy-TEMPO+	49.1	-2255949.6	559.1	-2256116.3	-241.0	-
3,4-dicarboxy-TEMPO-	48.5	-2256734.7	547.6	-2256898.0	-266.3	-
3,4-dicarboxy-TEMPOH	49.4	-2258034.1	553.6	-2258199.2	-65.6	-
3,5-dicarboxy-TEMPO (**11**)	48.7	-2256622.2	562.7	-2256789.9	-61.2	-
3,5-dicarboxy-TEMPO+	48.6	-2255934.8	554.6	-2256100.1	-232.3	-
3,5-dicarboxy-TEMPO-	48.5	-2256727.4	548.9	-2256891.1	-263.3	-
3,5-dicarboxy-TEMPOH	49.2	-2258021.2	553.8	-2258186.4	-66.3	-
4-carboxy-2,2,6,6-tetra ethylpiperidin-1-lyoxyl (**12**)	55.9	-2173861.2	615.0	-2174044.5	-14.2	-
4-carboxy-2,2,6,6-tetra ethylpiperidin-1-lyoxyl+	56.5	-2173208.4	616.5	-2173392.2	-174.3	-

4-carboxy-2,2,6,6-tetra ethylpiperidin-1-lyoxyl-	54.9	-2173933.5	593.7	-2174110.5	-196.8	-
4-ammonio-TEMPO (**13**)	38.3	-1413772.1	467.2	-1413911.4	-291.9	-216.8
4-ammonio-TEMPO+	38.4	-1412780.5	464.2	-1412918.9	-781.3	-659.8
4-ammonio-TEMPO-	37.8	-1414153.1	454.1	-1414288.4	-208.6	-
2,2,6,6-tetramethyl-1,2, 3,6-tetrahydropyridin-1-lyoxyl (**14**)	33.6	-1264570.9	435.6	-1264700.8	-10.5	-
2,2,6,6-tetramethyl-1,2, 3,6-tetrahydropyridin-1-lyoxyl+	33.7	-1263899.6	432.8	-1264028.6	-185.4	-
2,2,6,6-tetramethyl-1,2, 3,6-tetrahydropyridin-1-lyoxyl-	32.7	-1264627.0	419.3	-1264752.1	-237.2	-
PROXYL (**15**)	32.6	-1164742.1	426.7	-1164869.3	-11.1	-
PROXYL+	32.1	-1164076.7	414.8	-1164200.4	-185.6	-
PROXYL-	31.5	-1164777.5	413.8	-1164900.8	-243.8	-
PROXYLH	32.5	-1166333.5	418.7	-1166458.3	-13.5	-
3-amino-PROXYL (**16**)	35.7	-1309868.8	452.8	-1310003.8	-29.6	-
3-amino-PROXYL+	35.7	-1309204.4	445.0	-1309337.1	-205.2	-
3-amino-PROXYL-	34.7	-1309914.6	435.3	-1310044.3	-256.1	-
3-amino-PROXYLH	35.9	-1311462.1	442.2	-1311593.9	-30.9	-
3-methoxy-PROXYL (**17**)	38.9	-1464996.0	479.3	-1465138.9	-13.6	-
3-methoxy-PROXYL+	38.9	-1464340.1	473.6	-1464481.3	-180.4	-
3-methoxy-PROXYL-	38.1	-1465041.4	463.3	-1465179.6	-243.8	-
3-methoxy-PROXYLH	39.6	-1466591.6	474.8	-1466733.1	-16.3	-
3-hydroxy-PROXYL (**18**)	35.2	-1362033.4	449.5	-1362167.5	-30.7	-
3-hydroxy-PROXYL+	34.9	-1361369.2	439.3	-1361500.2	-207.9	-
3-hydroxy-PROXYL-	33.4	-1362097.0	425.7	-1362223.9	-240.7	-
3-hydroxy-PROXYLH	35.7	-1363626.5	442.3	-1363758.4	-32.6	-
3-carboxy-PROXYL (**19**)	40.0	-1659297.8	498.0	-1659446.3	-35.4	4.4
3-carboxy-PROXYL+	39.3	-1658617.1	481.5	-1658760.6	-212.6	-151.4
3-carboxy-PROXYL-	38.8	-1659360.1	475.2	-1659501.8	-255.4	-
3-carboxy-PROXYLH	39.9	-1660892.2	483.4	-1661036.4	-38.5	-
3,4-dicarboxy-PROXYL (**20**)	47.5	-2153642.8	557.4	-2153809.0	-54.7	-
3,4-dicarboxy-PROXYL+	47.0	-2152952.1	549.6	-2153116.0	-230.8	-
3,4-dicarboxy-PROXYL-	46.7	-2153723.9	541.1	-2153885.2	-264.5	-
3,4-dicarboxy-PROXYLH	47.5	-2155025.3	546.5	-2155188.3	-58.8	-
3-carboxy-2,2,5,5-tetra ethylpyrrolidin-1-lyoxyl	54.1	-2070865.5	603.8	-2071045.5	-10.8	-

(**21**)						
3-carboxy-2,2,5,5-tetra ethylpyrrolidin-1-lyoxyl+	53.7	-2070210.8	595.4	-2070388.3	-173.5	-
3-carboxy-2,2,5,5-tetra ethylpyrrolidin-1-lyoxyl-	52.8	-2070932.9	580.4	-2071105.9	-204.8	-
3-ammonio-PROXYL (**22**)	35.8	-1310766.7	450.8	-1310901.1	-280.5	-
3-ammonio-PROXYL+	35.9	-1309734.2	447.9	-1309867.8	-792.4	-
2,2,5,5-tetramethyl-2,5-dihydro-1*H*-pyrrol-1-yloxy (**23**)	32.1	-1161566.0	423.0	-1161692.1	-8.0	10.3
2,2,5,5-tetramethyl-2,5-dihydro-1*H*-pyrrol-1-yloxy+	31.7	-1160886.9	412.3	-1161009.9	-180.6	-144.5
2,2,5,5-tetramethyl-2,5-dihydro-1*H*-pyrrol-1-yloxy-	30.9	-1161607.3	406.9	-1161728.6	-246.8	-
2,2,5,5-tetramethyl-3-carboxy-2,5-dihydro-1*H*-pyrrol-1-yloxy (**24**)	39.6	-1656130.7	492.3	-1656277.4	-26.9	7.4
2,2,5,5-tetramethyl-3-carboxy-2,5-dihydro-1*H*-pyrrol-1-yloxy+	39.1	-1655440.8	479.6	-1655583.8	-196.8	-143.4
2,2,5,5-tetramethyl-3-carboxy-2,5-dihydro-1*H*-pyrrol-1-yloxy-	39.2	-1656191.4	476.1	-1656333.3	-251.8	-
1-hydroxy-2,2,5,5-tetramethyl-3-carboxy-2,5-dihydro-1*H*-pyrrole	39.6	-1657725.9	478.4	-1657868.5	-33.4	-
2,2,5,5-tetramethyl-3,4-diphenyl-2,5-dihydro-1*H*-pyrrol-1-yloxy (**25**)	56.5	-2371818.1	623.2	-2372004.0	12.8	38.5
2,2,5,5-tetramethyl-3,4-diphenyl-2,5-dihydro-1*H*-pyrrol-1-yloxy+	56.7	-2371158.7	624.5	-2371344.9	-131.8	-91.1
2,2,5,5-tetramethyl-3,4-diphenyl-2,5-dihydro-1*H*-pyrrol-1-yloxy-	55.3	-2371887.6	603.7	-2372067.6	-201.8	-
TMOZO (**26**)	32.3	-1258999.6	432.7	-1259128.7	-13.3	-
TMOZO+	31.8	-1258306.1	418.4	-1258430.8	-191.7	-
TMOZO-	31.2	-1259061.7	412.8	-1259184.8	-247.6	-
TMOZOH	32.2	-1260600.1	419.0	-1260725.1	-20.3	-
TMIO (**27**)	38.8	-1564313.2	478.4	-1564455.8	-3.6	17.3
TMIO+	38.5	-1563640.4	468.6	-1563780.1	-162.2	-125.9
TMIO-	37.5	-1564372.6	458.1	-1564509.1	-225.8	-
TMIOH	38.7	-1565907.3	467.4	-1566046.6	-9.3	-

5-amino-TMIO (**28**)	42.7	-1709365.6	508.8	-1709517.3	-23.7	8.5
5-amino-TMIO+	43.4	-1708705.9	511.0	-1708858.3	-171.2	-125.7
5-amino-TMIO-	41.9	-1709417.3	489.3	-1709563.2	-251.3	-
5-aminomethyl-TMIO (**29**)	46.1	-1812239.1	539.7	-1812400.0	-22.0	-
5-aminomethyl-TMIO+	45.8	-1811578.3	530.3	-1811736.4	-171.9	-
5-aminomethyl-TMIO-	45.5	-1812304.0	525.2	-1812460.6	-237.7	-
5-nitro-TMIO (**30**)	45.6	-2100489.9	544.6	-2100652.2	-12.3	15.3
5-nitro-TMIO+	45.3	-2099787.4	533.8	-2099946.5	-192.7	-144.1
5-nitro-TMIO-	45.0	-2100569.2	522.1	-2100724.9	-183.9	-
5-methoxy-TMIO (**31**)	45.7	-1864392.0	537.6	-1864552.3	-7.3	18.6
5-methoxy-TMIO+	45.5	-1863728.4	528.8	-1863886.1	-158.9	-117.8
5-methoxy-TMIO-	44.7	-1864448.8	515.2	-1864602.4	-228.9	-
5,6-dimethoxy-TMIO (**32**)	52.7	-2164459.4	584.4	-2164633.6	-10.8	19.3
5,6-dimethoxy-TMIO+	52.6	-2163801.2	587.8	-2163976.5	-155.3	-109.4
5,6-dimethoxy-TMIO-	52.3	-2164512.4	573.3	-2164683.4	-228.6	-
5-hydroxy-TMIO (**33**)	42.0	-1761542.0	507.7	-1761693.4	-25.6	8.0
5-hydroxy-TMIO+	41.7	-1760873.7	497.7	-1761022.1	-182.6	-132.7
5-hydroxy-TMIO-	41.1	-1761602.7	484.5	-1761747.1	-246.4	-
5-carboxy-TMIO (**34**)	46.5	-2058662.2	548.9	-2058825.8	-25.9	11.9
5-carboxy-TMIO+	46.2	-2057979.4	538.3	-2058139.9	-189.4	-133.7
5-carboxy-TMIO-	45.8	-2058735.3	526.8	-2058892.4	-231.8	-
5-carboxy-TMIOH	46.3	-2060258.7	530.5	-2060416.9	-32.2	-
4-carboxy-TMIO (**35**)	45.7	-2058651.8	541.7	-2058813.3	-22.6	-
4-carboxy-TMIO+	45.3	-2057985.6	527.2	-2058142.7	-174.5	-
4-carboxy-TMIO-	45.7	-2058702.1	523.8	-2058858.3	-234.6	-
4,7-dicarboxy-TMIO (**36**)	52.7	-2552984.6	591.5	-2553160.9	-41.9	-
4,7-dicarboxy-TMIO+	52.4	-2552324.8	583.0	-2552498.6	-184.9	-
4,7-dicarboxy-TMIO-	53.0	-2553025.4	582.1	-2553198.9	-199.7	-
4,6-dicarboxy-TMIO (**37**)	53.7	-2552997.3	605.1	-2553177.8	-43.3	-
4,6-dicarboxy-TMIO+	53.1	-2552322.6	589.7	-2552498.4	-198.5	-
4,6-dicarboxy-TMIO-	53.6	-2553057.3	589.5	-2553233.1	-239.4	-
4,5-dicarboxy-TMIO (**38**)	53.7	-2552986.7	599.5	-2553165.4	-45.7	-
4,5-dicarboxy-TMIO+	53.1	-2552305.6	587.2	-2552480.7	-203.0	-
4,5-dicarboxy-TMIO-	53.8	-2553053.9	588.7	-2553229.4	-246.4	-
5,6-dicarboxy-TMIO (**39**)	54.4	-2552985.3	614.1	-2553168.5	-43.3	5.8
5,6-dicarboxy-TMIO+	54.1	-2552293.3	603.6	-2552473.3	-215.9	-140.7
5,6-dicarboxy-TMIO-	53.9	-2553070.1	592.9	-2553246.9	-248.2	-

5,6-dicarboxy-TMIOH	54.3	-2554584.3	596.4	-2554762.1	-56.7	-
1,1,3,3-tetraethyl isoindolin-1-yloxyl (**40**)	52.3	-1975889.5	582.0	-1976063.0	18.7	36.9
1,1,3,3-tetraethyl isoindolin-1-yloxyl+	52.2	-1975233.9	570.0	-1975403.9	-126.0	-92.3
1,1,3,3-tetraethyl isoindolin-1-yloxyl-	51.6	-1975942.7	564.0	-1976110.9	-169.6	-
5-carboxy-1,1,3,3-tetra ethylisoindolin-1-yloxyl (**41**)	60.1	-2470239.6	645.9	-2470432.1	-3.6	-
5-carboxy-1,1,3,3-tetra ethylisoindolin-1-yloxyl+	60.0	-2469574.4	639.5	-2469765.1	-151.1	-
5-carboxy-1,1,3,3-tetra ethylisoindolin-1-yloxyl-	59.6	-2470304.2	629.9	-2470492.0	-177.7	-
5,6-dicarboxy-1,1,3,3-tetraethylisoindolin-1-yloxyl (**42**)	67.8	-2964564.5	706.9	-2964775.2	-25.4	26.9
5,6-dicarboxy-1,1,3,3-tetraethylisoindolin-1-yloxyl+	67.9	-2963890.1	698.0	-2964098.2	-175.2	-140.7
5,6-dicarboxy-1,1,3,3-tetraethylisoindolin-1-yloxyl-	67.8	-2964640.9	696.1	-2964848.4	-191.9	-
5-bromo-TMIO (4**3**)	42.8	-8316990.4	526.4	-8317147.4	-2.1	21.1
5-bromo-TMIO+	42.5	-8316307.2	516.1	-8316461.0	-168.6	-126.7
5-bromo-TMIO-	41.9	-8317067.2	503.0	-8317217.1	-209.5	-
5,6-dibromo-TMIO (**44**)	46.8	-15069660.0	559.9	-15069826.9	2.1	25.9
5,6-dibromo-TMIO+	46.4	-15068970.4	549.3	-15069134.1	-168.4	-123.5
5,6-dibromo-TMIO-	45.9	-15069748.9	541.3	-15069910.3	-195.9	-
5-ammonio-TMIO (**45**)	44.2	-1710220.3	547.2	-1710383.5	-269.3	-179.1
5-ammonio-TMIO+	43.5	-1709285.2	520.4	-1709440.3	-685.6	-582.7
5-ammonio-TMIO-	43.7	-1710544.4	505.4	-1710695.1	-208.7	-
1,1,3,3-tetramethyl-2,3-dihydro-1*H*-dibenzo[*e*,*g*] isoindol-1-lyoxyl (**46**)	52.5	-2369110.2	576.8	-2369282.2	0.5	27.4
1,1,3,3-tetramethyl-2,3-dihydro-1*H*-dibenzo[*e*,*g*] isoindol-1-lyoxyl+	52.6	-2368446.2	572.3	-2368616.9	-144.5	-101.3
1,1,3,3-tetramethyl-2,3-dihydro-1*H*-dibenzo[*e*,*g*] isoindol-1-lyoxyl-	51.7	-2369179.9	565.5	-2369348.5	-205.0	-
TMAO (**47**)	43.9	-1966995.2	521.1	-1967150.6	-2.1	-
TMAO+	43.3	-1966383.8	503.2	-1966533.9	-152.9	-
TMAO-	43.1	-1967081.8	501.1	-1967231.2	-213.2	-

4-amino-TMAO (**48**)	47.7	-2112033.7	543.2	-2112195.7	-19.6	-
4-amino-TMAO+	46.8	-2111438.1	525.1	-2111594.6	-162.6	-
4-amino-TMAO-	46.5	-2112124.4	522.1	-2112280.0	-228.7	-
5-amino-TMAO (**49**)	47.8	-2112049.5	548.4	-2112213.0	-22.7	-
5-amino-TMAO+	48.0	-2111447.7	534.2	-2111607.0	-165.6	-
5-amino-TMAO-	47.1	-2112130.8	527.2	-2112287.9	-238.4	-
6-amino-TMAO (**50**)	47.7	-2112047.5	545.4	-2112210.1	-22.0	12.4
6-amino-TMAO+	47.9	-2111453.3	533.6	-2111612.4	-164.4	-116.3
6-amino-TMAO-	46.9	-2112128.2	526.1	-2112285.0	-235.7	-
6-dimethylamino-TMAO (**51**)	54.8	-2317781.6	599.8	-2317960.4	-3.4	24.5
6-dimethylamino-TMAO+	54.3	-2317181.4	581.3	-2317354.7	-139.5	-99.3
6-dimethylamino-TMAO-	54.1	-2317864.7	580.3	-2318037.7	-215.5	-
4-nitro-TMAO (**52**)	50.7	-2503145.3	570.9	-2503315.5	-5.1	-
4-nitro-TMAO+	50.1	-2502517.7	556.9	-2502683.8	-160.7	-
4-nitro-TMAO-	50.2	-2503240.0	556.4	-2503405.9	-195.6	-
5-nitro-TMAO (**53**)	50.8	-2503174.7	576.9	-2503346.7	-10.6	-
5-nitro-TMAO+	50.5	-2502535.2	564.0	-2502703.4	-179.7	-
5-nitro-TMAO-	51.2	-2503213.6	570.0	-2503383.5	-178.6	-
6-nitro-TMAO (**54**)	50.8	-2503156.4	579.2	-2503329.1	-10.6	18.6
6-nitro-TMAO+	50.4	-2502522.1	562.9	-2502689.9	-179.5	-129.3
6-nitro-TMAO-	51.5	-2503179.9	581.3	-2503353.2	-181.1	-
6,7-dinitro-TMAO (**55**)	57.4	-3039307.8	627.8	-3039495.0	-22.4	12.8
6,7-dinitro-TMAO+	57.4	-3038649.5	615.4	-3038833.0	-206.6	-145.1
6,7-dinitro-TMAO-	57.2	-3039419.8	618.0	-3039604.0	-172.4	-
4-carboxy-TMAO (**56**)	51.5	-2461313.3	577.2	-2461485.4	-22.2	-
4-carboxy-TMAO+	50.4	-2460708.2	557.2	-2460874.4	-166.1	-
4-carboxy-TMAO-	51.0	-2461404.1	563.5	-2461572.1	-229.5	-
5-carboxy-TMAO (**57**)	51.6	-2461346.3	581.6	-2461519.7	-24.4	-
5-carboxy-TMAO+	51.2	-2460726.0	568.0	-2460895.4	-176.9	-
5-carboxy-TMAO-	50.9	-2461443.9	562.2	-2461611.5	-219.1	-
6-carboxy-TMAO (**58**)	51.7	-2461331.3	591.3	-2461507.6	-22.8	-
6-carboxy-TMAO+	51.1	-2460714.4	571.7	-2460884.8	-175.4	-
6-carboxy-TMAO-	51.0	-2461431.2	566.3	-2461600.0	-220.2	-
4,5-dicarboxy-TMAO (**59**)	58.6	-2955653.7	628.6	-2955841.1	-44.9	-
4,5-dicarboxy-TMAO+	58.3	-2955043.7	617.5	-2955227.7	-190.7	-
4,5-dicarboxy-TMAO-	58.6	-2955755.2	617.9	-2955939.5	-239.1	-
4,6-dicarboxy-TMAO (**60**)	59.2	-2955646.3	645.0	-2955838.6	-41.8	-

4,6-dicarboxy-TMAO+	58.1	-2955036.8	623.3	-2955222.7	-186.1	-
4,6-dicarboxy-TMAO-	59.0	-2955735.9	628.1	-2955923.1	-235.6	-
4,7-dicarboxy-TMAO (**61**)	59.1	-2955647.9	642.8	-2955839.6	-42.0	-
4,7-dicarboxy-TMAO+	58.2	-2955036.4	625.8	-2955223.0	-188.6	-
4,7-dicarboxy-TMAO-	58.8	-2955706.6	624.8	-2955892.9	-236.5	-
4,8-dicarboxy-TMAO (**62**)	59.2	-2955664.2	640.2	-2955855.1	-43.8	-
4,8-dicarboxy-TMAO+	58.3	-2955049.7	622.0	-2955235.1	-189.7	-
4,8-dicarboxy-TMAO-	58.9	-2955750.2	625.7	-2955936.7	-234.1	-
4,9-dicarboxy-TMAO (**63**)	58.7	-2955625.1	631.3	-2955813.3	-42.6	-
4,9-dicarboxy-TMAO+	58.0	-2955017.2	620.1	-2955202.1	-184.0	-
4,9-dicarboxy-TMAO-	58.8	-2955723.8	625.6	-2955910.3	-247.9	-
5,6-dicarboxy-TMAO (**64**)	59.7	-2955669.1	649.7	-2955862.8	-46.7	-
5,6-dicarboxy-TMAO+	59.1	-2955040.5	630.5	-2955228.5	-200.6	-
5,6-dicarboxy-TMAO-	59.1	-2955773.3	628.6	-2955960.8	-234.2	-
5,7-dicarboxy-TMAO (**65**)	59.7	-2955681.9	661.2	-2955879.1	-43.8	-
5,7-dicarboxy-TMAO+	58.9	-2955055.5	635.3	-2955244.9	-200.0	-
5,7-dicarboxy-TMAO-	59.2	-2955784.7	633.5	-2955973.6	-228.3	-
5,8-dicarboxy-TMAO (**66**)	59.6	-2955694.8	651.2	-2955888.9	-45.1	-
5,8-dicarboxy-TMAO+	59.1	-2955066.3	631.9	-2955254.7	-200.7	-
5,8-dicarboxy-TMAO-	59.1	-2955804.6	629.9	-2955992.4	-228.8	-
6,7-dicarboxy-TMAO (**67**)	59.2	-2955660.2	639.9	-2955851.0	-48.2	-
6,7-dicarboxy-TMAO+	58.9	-2955036.2	626.0	-2955222.9	-203.5	-
6,7-dicarboxy-TMAO-	58.7	-2955769.2	621.1	-2955954.4	-237.2	-
H^+ (experimental)	-	-	-	-26.3	-1107.1	-
O_2	8.7	-394257.7	205.1	-394318.8	3.6	-
$O_2^{-\bullet}$	8.7	-394297.0	203.6	-394357.7	-350.5	-
$HOO^{\bullet}$	10.0	-395770.8	228.9	-395839.0	-34.9	-
H_2O_2	11.0	-397447.4	227.9	-397515.4	-47.2	-

A.1.2 Data for Chapter 5

Table A.3 Contributions to the gas-phase enthalpies (0 K) of species in Chapter 5

Species	Sym.	E^o_{gas}(RMP2) (Hartrees)	E^o_{gas}(G3(MP2) -RAD) (Hartrees)	*ZPE* (Hartrees)	H^o_{gas} (Hartrees)

$^{\bullet}CH_3$	D_{3h}	-39.73168	-39.78520	0.02926	-39.75594
HCH3	T_d	-40.40557	-40.46517	0.04437	-40.42080
$^{\bullet}CH_2CH_3$	C_s	-78.95127	-79.04837	0.05848	-78.98989
HCH_2CH_3	D_{3d}	-79.62006	-79.72315	0.07378	-79.64936
$^{\bullet}CH_2CH_2CH_3$	C_1	-118.16945	-118.30962	0.08701	-118.22261
$HCH_2CH_2CH_3$	C_{2v}	-118.83877	-118.98479	0.10210	-118.88269
$^{\bullet}CH(CH_3)_2$	C_s	-118.17367	-118.31386	0.08690	-118.22696
$HCH(CH_3)_2$	C_{2v}	-118.83877	-118.98479	0.10210	-118.88269
$^{\bullet}C(CH_3)_3$	C_{3v}	-157.39814	-157.58085	0.11499	-157.46586
$HC(CH_3)_3$	C_{3v}	-158.06094	-158.24923	0.12981	-158.11942
$^{\bullet}CH_2OH$	C_1	-114.85342	-114.93575	0.03679	-114.89896
HCH_2OH	C_s	-115.51357	-115.60228	0.05047	-115.55181
$^{\bullet}CH_2F$	C_1	-138.85678	-138.93377	0.02443	-138.90934
HCH_2F	C_{3v}	-139.52494	-139.60822	0.03875	-139.56947
$^{\bullet}CH(CH_3)Cl$	C_1	-538.06689	-538.20675	0.05131	-538.15544
$HCH(CH_3)Cl$	C_s	-538.72985	-538.87584	0.06582	-538.81002
$^{\bullet}CH_2CN$	C_{2v}	-131.82433	-131.92386	0.03061	-131.89325
HCH_2CN	C_{3v}	-132.48540	-132.59073	0.04475	-132.54598
$^{\bullet}CH(CH_3)CN$	C_s	-171.04864	-171.19082	0.05917	-171.13165
$HCH(CH_3)CN$	C_s	-171.70360	-171.85185	0.07336	-171.77849
$^{\bullet}C(CH_3)_2CN$	C_{2v}	-210.27486	-210.45908	0.08701	-210.37208
$HC(CH_3)_2CN$	C_s	-210.92516	-211.11565	0.10117	-211.01448
$^{\bullet}CH_2Ph$	C_{2v}	-270.29188	-270.53737	0.11272	-270.42465
HCH_2Ph	C_s	-270.94455	-271.19286	0.12580	-271.06706
$^{\bullet}CH(CH_3)Ph$	C_s	-309.51471	-309.80227	0.14039	-309.66188
$HCH(CH_3)Ph$	C_s	-310.16471	-310.45515	0.15432	-310.30083
$^{\bullet}C(CH_3)_2Ph$	C_{2v}	-348.73758	-349.06678	0.16818	-348.89861
$HC(CH_3)_2Ph$	C_s	-349.38663	-349.71889	0.18205	-349.53683
$^{\bullet}CH_2COOCH_3$	C_s	-267.23905	-267.41941	0.07519	-267.34423
HCH_2COOCH_3	C_s	-267.90342	-268.08945	0.08853	-268.00092
$^{\bullet}CH(CH_3)COOCH_3$	C_s	-306.46556	-306.68892	0.10326	-306.58565
$HCH(CH_3)COOCH_3$	C_s	-307.12252	-307.35165	0.11681	-307.23484
$^{\bullet}C(CH_3)_2COOCH_3$	C_s	-345.69158	-345.95731	0.13088	-345.82643
$HC(CH_3)_2COOCH_3$	C_1	-346.34382	-346.61512	0.14473	-346.47039
$^{\bullet}CH(CH_3)OCOCH_3$	C_1	-306.46217	-306.68555	0.10194	-306.58361
$HCH(CH_3)OCOCH_3$	C_s	-307.12645	-307.35567	0.11650	-307.23917
$^{\bullet}CH(CH_3)COOH$	C_s	-267.26302	-267.44274	0.07559	-267.36715
$HCH(CH_3)COOH$	C_s	-267.91993	-268.10549	0.08915	-268.01634

$^{\bullet}CH(CH_3)COONH_2$	C_1	-247.39464	-247.58168	0.08724	-247.49444
$HCH(CH_3)COONH_2$	C_1	-248.05178	-248.24440	0.10072	-248.14368
$^{\bullet}C(CH_3)(COOCH_3)CH_2$ $C(CH_3)_2COOCH_3$	C_1	-690.86101	-	0.25781	-690.86894
$HC(CH_3)(COOCH_3)CH_2$ $C(CH_3)_2COOCH_3$	C_1	-691.51557	-	0.27154	-691.51533
$(CH_3)_2NO^{\bullet}$	C_s	-209.31175	-209.47573	0.08281	-209.39292
$(CH_3)_2NO–C(CH_3)_2CN$	C_1	-419.67460	-420.01768	0.17640	-419.84128
$(CH_3)_2NO–CH_2Ph$	C_1	-479.68603	-480.08741	0.20237	-479.88503
$(CH_3)_2NO–CH(CH_3)Ph$	C_1	-518.91530	-519.35821	0.23009	-519.12811
$(CH_3)_2NO–C(CH_3)_2Ph$	C_s	-558.13824	-558.62298	0.25754	-558.36544
$(CH_3)_2NO–CH_2COOCH_3$	C_1	-476.64251	-476.98250	0.16529	-476.81721
$(CH_3)_2NO–CH(CH_3)COOCH_3$	C_1	-515.86924	-516.25140	0.19290	-516.05850
$(CH_3)_2NO–C(CH_3)_2COOCH_3$	C_1	-555.09387	-555.51811	0.22040	-555.29771
$(CH_3)_2NO–CH(CH_3)OCOCH_3$	C_1	-515.88368	-516.26592	0.19231	-516.07362
$(CH_3)_2NO–CH(CH_3)COOH$	C_s	-267.26302	-267.44274	0.07559	-267.36715
$(CH_3)_2NO–CH(CH_3)COONH_2$	C_1	-247.39464	-247.58168	0.08724	-247.49444
DBN (**1**)	C_1	-444.64289	-445.05945	0.24965	-444.80979
DBNH	C_1	-445.25596	-445.68100	0.26131	-445.41969
$DBN–CH_3$	C_1	-484.46023	-484.92842	0.28991	-484.63851
$DBN–CH(CH_3)Ph$	C_1	-754.23115	-	0.39716	-754.27689
$DBN–CH(CH_3)COOCH_3$	C_1	-751.18460	-	0.35977	-751.20698
$DBN–C(CH_3)_2COOCH_3$	C_1	-790.40514	-	0.38660	-790.44278
$DBN–CH(CH_3)COOH$	C_1	-711.98050	-	0.33209	-711.98698
$DBN–CH(CH_3)COONH_2$	C_1	-692.11762	-	0.34441	-692.11910
TEMPO (**2**)	C_s	-482.68700	-483.12856	0.25821	-482.87034
TEMPOH	C_s	-483.30211	-483.75173	0.26984	-483.48190
$TEMPO–CH_3$	C_s	-522.50691	-522.99969	0.29805	-522.70164
$TEMPO–CH_2CH_3$	C_s	-561.73143	-562.26706	0.32615	-561.94091
$TEMPO–CH_2CH_2CH_3$	C_s	-600.95004	-601.52863	0.35403	-601.17460
$TEMPO–CH(CH_3)_2$	C_1	-600.95191	-601.53006	0.35390	-601.17616
$TEMPO–C(CH_3)_3$	C_1	-640.16932	-640.78998	0.38066	-640.40931
$TEMPO–CH_2OH$	C_1	-597.63642	-598.15791	0.30355	-597.85436
$TEMPO–CH_2F$	C_1	-621.64778	-622.16401	0.29126	-621.87275
$TEMPO–CH(CH_3)Cl$	C_1	-1020.84712	-1021.42499	0.31693	-1021.10806
$TEMPO–CH_2CN$	C_s	-614.58697	-615.12535	0.29689	-614.82845
$TEMPO–CH(CH_3)CN$	C_1	-653.81193	-654.39248	0.32412	-654.06836
$TEMPO–C(CH_3)_2CN$	C_1	-693.03228	-	0.35122	-693.02415
$TEMPO–CH_2Ph$	C_1	-753.05541	-	0.37774	-753.39875

TEMPO–CH(CH_3)Ph	C_1	-792.28003	-	0.40519	-792.31776
TEMPO–C(CH_3)$_2$Ph	C_1	-831.49931	-	0.43270	-831.55134
TEMPO–CH_2COOCH_3	C_1	-750.00745	-	0.34008	-750.00735
TEMPO–CH(CH_3)$COOCH_3$	C_1	-789.23233	-	0.36812	-789.24636
TEMPO–C(CH_3)$_2COOCH_3$	C_1	-828.45293	-	0.39505	-828.48212
TEMPO–CH(CH_3)$OCOCH_3$	C_1	-789.24953	-	0.36754	-789.26423
TEMPO–CH(CH_3)COOH	C_1	-750.02822	-	0.34052	-750.02629
TEMPO–CH(CH_3)$CONH_2$	C_1	-730.16571	-	0.35219	-730.15940
4-amino-TEMPO (**3**)	C_1	-537.94553	-538.42297	0.27503	-538.14794
4-amino-TEMPOH	C_1	-538.56101	-539.04644	0.28647	-538.75997
4-amino-TEMPO–CH_3	C_1	-577.76589	-578.29447	0.31459	-577.97988
4-methoxy-TEMPO (**4**)	C_1	-597.01165	-597.52536	0.29016	-597.23520
4-methoxy-TEMPO–CH_3	C_1	-636.83194	-637.39680	0.32976	-637.06704
4-hydroxy-TEMPO (**6**)	C_s	-557.80823	-558.27898	0.26240	-558.01658
4-hydroxy-TEMPOH	C_s	-558.42432	-558.90284	0.27387	-558.62897
4-hydroxy-TEMPO–CH_3	C_s	-597.62918	-598.15086	0.30196	-597.84889
4-carboxy-TEMPO (**8**)	C_1	-670.98919	-671.51277	0.27278	-671.23998
4-carboxy-TEMPO–CH_3	C_1	-710.81030	-711.38484	0.31247	-711.07237
3-carboxy-TEMPO (**9**)	C_1	-670.98643	-671.50990	0.27319	-671.23670
3-carboxy-TEMPOH	C_1	-671.60325	-672.13430	0.28459	-671.84971
3-carboxy-TEMPO–CH_3	C_1	-710.80814	-711.38236	0.31300	-711.06937
3,4-dicarboxy-TEMPO (**10**)	C_1	-859.29033	-	0.28727	-859.52653
3,4-dicarboxy-TEMPOH	C_1	-859.90804	-	0.29919	-860.05848
3,4-dicarboxy-TEMPO–CH_3	C_1	-899.11290	-	0.32722	-899.36022
3,5-dicarboxy-TEMPO (**11**)	C_s	-859.28492	-	0.28795	-859.52044
3,5-dicarboxy-TEMPOH	C_s	-859.90342	-	0.29957	-860.05347
3,5-dicarboxy-TEMPO–CH_3	C_s	-899.10837	-	0.32760	-899.35499
4-carboxy-2,2,6,6-tetraethyl piperidin-1-lyoxyl (**12**)	C_1	-827.86346	-	0.38588	-828.00116
4-carboxy-2,2,6,6-tetraethyl piperidin-1-ol	C_1	-828.47517	-	0.39702	-828.52777
1-methoxy-4-carboxy-2,2,6,6-tetraethylpiperidine	C_1	-867.67743	-	0.42515	-867.82682
PROXYL (**15**)	C_2	-443.47115	-443.86807	0.22889	-443.63917
PROXYLH	C_1	-444.07902	-444.48593	0.24065	-444.24528
PROXYL–CH_3	C_1	-483.28394	-483.73408	0.26847	-483.46561
PROXYL–CH(CH_3)Ph	C_1	-753.06059	-	0.37597	-753.12752
PROXYL–CH(CH_3)$COOCH_3$	C_1	-750.01305	-	0.33887	-750.05634
PROXYL–C(CH_3)$_2COOCH_3$	C_1	-789.23440	-	0.36597	-789.29267

PROXYL–CH(CH_3)COOH	C_1	-710.80947	-	0.31106	-710.83699
PROXYL–CH(CH_3)$COONH_2$	C_1	-690.94544	-	0.32293	-690.96839
3-amino-PROXYL (**16**)	C_1	-498.72919	-499.16208	0.24587	-498.91621
3-amino-PROXYLH	C_1	-499.33806	-499.78062	0.25749	-499.52313
3-amino-PROXYL–CH_3	C_1	-538.54299	-539.02880	0.28520	-538.74360
3-methoxy-PROXYL (**17**)	C_1	-557.79489	-558.26347	0.26122	-558.00225
3-methoxy-PROXYLH	C_1	-558.40389	-558.88282	0.27257	-558.61025
3-methoxy-PROXYL–CH_3	C_1	-597.60879	-598.13096	0.30044	-597.83052
3-hydroxy-PROXYL (**18**)	C_1	-518.59214	-519.01770	0.23323	-518.78448
3-hydroxy-PROXYLH	C_1	-519.20034	-519.63618	0.24474	-519.39144
3-hydroxy-PROXYL–CH_3	C_1	-558.40718	-558.88597	0.27299	-558.61297
3-carboxy-PROXYL (**19**)	C_1	-631.77305	-632.25187	0.24355	-632.00831
3-carboxy-PROXYLH	C_1	-632.38285	-632.87095	0.25539	-632.61557
3-carboxy-PROXYL–CH_3	C_1	-671.58776	-672.11911	0.28318	-671.83593
3,4-dicarboxy-PROXYL (**20**)	C_1	-820.07656	-	0.25818	-820.29720
3,4-dicarboxy-PROXYLH	C_1	-820.68684	-	0.26998	-820.82377
3,4-dicarboxy-PROXYL–CH_3	C_1	-859.89184	-	0.29763	-860.12556
3-carboxy-2,2,5,5-tetraethyl pyrrolidin-1-lyoxyl (**21**)	C_1	-788.64910	-	0.35644	-788.77149
3-carboxy-2,2,5,5-tetraethyl pyrrolidin-1-ol	C_1	-789.25518	-	0.36854	-789.29354
1-methoxy-3-carboxy-2,2,5,5-tetraethylpyrrolidine	C_1	-828.46077	-	0.39620	-828.59591
TMIO (**27**)	C_{2v}	-595.58586	-596.08162	0.25152	-595.83010
TMIOH	C_s	-596.19493	-596.70050	0.26325	-596.43725
TMIO–CH_3	C_s	-635.39966	-635.94846	0.29095	-635.65751
TMIO–CH(CH_3)Ph	C_1	-905.17599	-	0.39821	-905.22069
TMIO–CH(CH_3)$COOCH_3$	C_1	-902.12763	-	0.36111	-902.14868
TMIO–C(CH_3)$_2COOCH_3$	C_1	-941.34954	-	0.38850	-941.38528
TMIO–CH(CH_3)COOH	C_1	-862.92414	-	0.33349	-862.92923
TMIO–CH(CH_3)$COONH_2$	C_1	-843.06105	-	0.34554	-843.06139
5-amino-TMIO (**28**)	C_1	-650.85112	-	0.26772	-651.07916
5-amino-TMIO–CH_3	C_1	-690.66449	-	0.30711	-690.90618
5-methoxy-TMIO (**31**)	C_s	-709.91456	-	0.28359	-710.12673
5-methoxy-TMIO–CH_3	C_1	-749.72800	-	0.32297	-749.95383
5-hydroxy-TMIO (**33**)	C_s	-670.71146	-	0.25537	-670.95185
5-hydroxy-TMIO–CH_3	C_1	-710.52518	-	0.29477	-710.77920
5-carboxy-TMIO (**34**)	C_s	-783.89097	-	0.26613	-784.12060
5-carboxy-TMIOH	C_1	-784.50103	-	0.27795	-784.72864

5-carboxy-TMIO–CH_3	C_1	-823.70584	-	0.30556	-823.94907
4-carboxy-TMIO (**35**)	C_1	-783.88731	-	0.26670	-784.11636
4-carboxy-TMIO–CH_3	C_1	-823.70101	-	0.30596	-823.94385
4,7-dicarboxy-TMIO (**36**)	C_s	-972.18630	-	0.28163	-972.40043
4,7-dicarboxy-TMIO–CH_3	C_s	-1012.00036	-	0.32085	-1012.22831
4,6-dicarboxy-TMIO (**37**)	C_1	-972.19087	-	0.28098	-972.40565
4,6-dicarboxy-TMIO–CH_3	C_1	-1012.00560	-	0.32049	-1012.23390
4,5-dicarboxy-TMIO (**38**)	C_1	-972.18643	-	0.28061	-972.40159
4,5-dicarboxy-TMIO–CH_3	C_1	-1012.00226	-	0.32001	-1012.23105
5,6-dicarboxy-TMIO (**39**)	C_1	-972.18581	-	0.28021	-972.40136
5,6-dicarboxy-TMIOH	C_1	-972.79678	-	0.29201	-973.01034
5,6-dicarboxy-TMIO–CH_3	C_1	-1012.00162	-	0.31967	-1012.23075
TMAO (**47**)	C_s	-748.89162	-749.50439	0.29886	-749.20553
TMAOH	C_s	-749.50578	-750.12728	0.31057	-749.81670
TMAO–CH_3	C_s	-788.71035	-789.37504	0.33857	-789.03647
4-carboxy-TMAO (**56**)	C_1	-937.18489	-	0.31343	-937.48422
4-carboxy-TMAO–CH_3	C_1	-977.00395	-	0.35342	-977.31522
5-carboxy-TMAO (**57**)	C_1	-937.19758	-	0.31351	-937.49684
5-carboxy-TMAO–CH_3	C_1	-977.01727	-	0.35321	-977.32876
6-carboxy-TMAO (**58**)	C_1	-937.19199	-	0.31360	-937.49116
6-carboxy-TMAO–CH_3	C_1	-977.01157	-	0.35351	-977.32276
TIPNO (**68**)	C_1	-675.20285	-	0.32992	-675.24689
TIPNO–CH_3	C_1	-715.01801	-	0.36908	-715.07512
SG1 (**69**)	C_1	-1207.70661	-	0.41486	-1207.80095
SG1H	C_1	-1208.31787	-	0.42602	-1208.40865
SG1–CH_3	C_1	-1247.52158	-	0.45403	-1247.62784
DMINO (**70**)	C_s	-517.13512	-517.55104	0.19708	-517.35395
DMINOH	C_1	-517.75019	-518.17238	0.20866	-517.96372
DMINO–CH_3	C_1	-556.95562	-557.42087	0.23633	-557.18454
2,2-diphenylindolin-1-yloxyl (**71**)	C_1	-899.78486	-	0.30087	-899.89990
2,2-diphenylindolin-1-ol	C_1	-900.40419	-	0.31222	-900.51415
1-methoxy-2,2-diphenyl indoline	C_1	-939.60804	-	0.34013	-939.73316
DPAIO (**72**)	C_1	-1184.38601	-	0.37307	-1184.49330
DPAIOH	C_1	-1185.00544	-	0.38438	-1185.10593

Table A.4 Contributions to the gas-phase free energies (298 K) of species in Chapter 5

Species	T_c (kJmol^{-1})	H_{gas} (kJmol^{-1})	S_{gas} (Jmol^{-1}K^{-1})	G_{gas} (kJmol^{-1})
$^{\bullet}CH_3$	10.6	-104368.6	195.4	-104426.8
$^{\bullet}CH_2CH_3$	12.9	-207375.1	255.7	-207451.3
$^{\bullet}CH_2CH_2CH_3$	15.4	-310378.1	286.6	-310463.5
$^{\bullet}CH(CH_3)_2$	15.9	-310388.9	292.4	-310476.1
$^{\bullet}C(CH_3)_3$	19.2	-413407.4	324.2	-413504.0
$^{\bullet}CH_2OH$	11.1	-301656.1	239.3	-301727.5
$^{\bullet}CH_2F$	10.4	-364696.0	235.3	-364766.2
$^{\bullet}CH(CH_3)Cl$	14.0	-1412913.1	285.8	-1412998.3
$^{\bullet}CH_2CN$	12.0	-346273.8	248.0	-346347.7
$^{\bullet}CH(CH_3)CN$	15.4	-449290.7	296.5	-449379.1
$^{\bullet}C(CH_3)_2CN$	19.4	-552312.5	328.0	-552410.3
$^{\bullet}CH_2Ph$	17.4	-709982.6	313.6	-710076.1
$^{\bullet}CH(CH_3)Ph$	22.1	-812995.2	362.1	-813103.2
$^{\bullet}C(CH_3)_2Ph$	26.1	-916007.2	388.7	-916123.1
$^{\bullet}CH_2COOCH_3$	17.7	-701894.6	316.9	-701989.1
$^{\bullet}CH(CH_3)COOCH_3$	21.8	-804918.8	354.3	-805024.5
$^{\bullet}C(CH_3)_2COOCH_3$	26.2	-907941.1	395.8	-908059.1
$^{\bullet}CH(CH_3)OCOCH_3$	22.7	-804912.6	365.8	-805021.6
$^{\bullet}CH(CH_3)COOH$	17.5	-701954.9	319.0	-701954.9
$^{\bullet}CH(CH_3)COONH_2$	18.8	-649777.9	325.4	-649777.9
$^{\bullet}C(CH_3)(COOCH_3)CH_2C(CH_3)_2COOCH_3$	47.1	-1813829.3	559.8	-1813996.2
$(CH_3)_2NO^{\bullet}$	16.3	-549744.8	302.4	-549835.0
$(CH_3)_2NO–C(CH_3)_2CN$	30.8	-1102262.5	414.1	-1102385.9
$(CH_3)_2NO–CH_2Ph$	31.3	-1259906.8	445.7	-1260039.7
$(CH_3)_2NO–CH(CH_3)Ph$	34.6	-1362936.3	459.5	-1363073.3
$(CH_3)_2NO–C(CH_3)_2Ph$	37.9	-1465950.6	476.7	-1466092.7
$(CH_3)_2NO–CH_2COOCH_3$	30.5	-1251853.1	425.9	-1251980.1
$(CH_3)_2NO–CH(CH_3)COOCH_3$	34.4	-1354877.2	453.7	-1355012.5
$(CH_3)_2NO–C(CH_3)_2COOCH_3$	37.5	-1457896.6	473.4	-1458037.8
$(CH_3)_2NO–CH(CH_3)OCOCH_3$	34.5	-1354916.8	459.9	-1355053.9
$(CH_3)_2NO–CH(CH_3)COOH$	17.5	-701954.9	319.0	-702050.0
$(CH_3)_2NO–CH(CH_3)COONH_2$	18.8	-649777.9	325.4	-649874.9
DBN (**1**)	35.7	-1167812.4	450.4	-1167946.7

DBNH	36.0	-1169413.4	445.6	-1169546.2
DBN–CH_3	38.9	-1272379.5	464.3	-1272517.9
DBN–$CH(CH_3)Ph$	54.1	-1980299.9	590.7	-1980476.0
DBN–$CH(CH_3)COOCH_3$	54.0	-1972239.9	588.1	-1972415.2
DBN–$C(CH_3)_2COOCH_3$	58.1	-2075249.4	614.7	-2075432.7
DBN–$CH(CH_3)COOH$	49.6	-1869272.2	552.8	-1869437.0
DBN–$CH(CH_3)COONH_2$	50.3	-1817108.4	556.7	-1817274.4
TEMPO (**2**)	34.1	-1267742.0	437.7	-1267872.5
TEMPOH	34.5	-1269347.3	429.5	-1269475.3
TEMPO–CH_3	37.7	-1372315.4	455.0	-1372451.1
TEMPO–CH_2CH_3	41.1	-1475334.7	484.2	-1475479.1
TEMPO–$CH_2CH_2CH_3$	45.0	-1578338.9	522.0	-1578494.5
TEMPO–$CH(CH_3)_2$	44.3	-1578343.7	506.1	-1578494.6
TEMPO–$C(CH_3)_3$	48.5	-1681346.1	536.2	-1681506.0
TEMPO–CH_2OH	39.6	-1569627.0	474.2	-1569768.4
TEMPO–CH_2F	39.2	-1632687.7	472.9	-1632828.7
TEMPO–$CH(CH_3)Cl$	43.8	-2680875.4	508.2	-2681026.9
TEMPO–CH_2CN	41.9	-1614190.2	501.9	-1614339.9
TEMPO–$CH(CH_3)CN$	45.8	-1717210.7	523.6	-1717366.8
TEMPO–$C(CH_3)_2CN$	49.5	-1819485.4	543.2	-1819647.3
TEMPO–CH_2Ph	49.5	-1977999.0	570.8	-1978169.1
TEMPO–$CH(CH_3)Ph$	53.1	-2080177.2	583.1	-2080351.1
TEMPO–$C(CH_3)_2Ph$	56.3	-2183181.7	597.3	-2183359.8
TEMPO–CH_2COOCH_3	49.4	-1969094.9	560.6	-1969262.0
TEMPO–$CH(CH_3)COOCH_3$	52.7	-2072113.6	580.3	-2072286.6
TEMPO–$C(CH_3)_2COOCH_3$	56.7	-2175123.1	602.0	-2175302.6
TEMPO–$CH(CH_3)OCOCH_3$	52.8	-2072160.4	585.3	-2072334.9
TEMPO–$CH(CH_3)COOH$	48.3	-1969145.7	546.9	-1969308.7
TEMPO–$CH(CH_3)COONH_2$	49.7	-1916983.8	555.0	-1917149.3
4-amino-TEMPO (**3**)	37.5	-1412869.9	461.7	-1413007.5
4-amino-TEMPOH	38.0	-1414476.3	454.9	-1414611.9
4-amino-TEMPO–CH_3	41.4	-1517444.7	481.1	-1517588.2
4-methoxy-TEMPO (**4**)	41.2	-1567999.8	494.4	-1568147.2
4-methoxy-TEMPO–CH_3	45.1	-1672574.4	513.7	-1672727.6
4-hydroxy-TEMPO (**6**)	37.2	-1465035.4	459.8	-1465172.4
4-hydroxy-TEMPOH	37.7	-1466642.7	452.9	-1466777.7
4-hydroxy-TEMPO–CH_3	41.1	-1569611.2	479.5	-1569754.1
4-carboxy-TEMPO (**8**)	41.8	-1762298.8	506.9	-1762449.9

4-carboxy-TEMPO–CH_3	45.6	-1866874.9	525.4	-1867031.6
3-carboxy-TEMPO (**9**)	41.3	-1762290.7	499.3	-1762439.6
3-carboxy-TEMPOH	41.9	-1763899.5	493.1	-1764046.5
3-carboxy-TEMPO–CH_3	45.0	-1866867.6	516.1	-1867021.5
3,4-dicarboxy-TEMPO (**10**)	49.3	-2256637.6	565.2	-2256806.1
3,4-dicarboxy-TEMPOH	49.4	-2258034.1	553.6	-2258199.2
3,4-dicarboxy-TEMPO–CH_3	52.8	-2361217.5	579.1	-2361390.1
3,5-dicarboxy-TEMPO (**11**)	48.7	-2256622.2	562.7	-2256789.9
3,5-dicarboxy-TEMPOH	49.2	-2258021.2	553.8	-2258186.4
3,5-dicarboxy-TEMPO–CH_3	52.7	-2361203.8	580.9	-2361377.0
4-carboxy-2,2,6,6-tetraethylpiperidin-1-lyoxyl (**12**)	55.9	-2173861.2	615.0	-2174044.5
4-carboxy-2,2,6,6-tetraethylpiperidin-1-ol	56.9	-2175242.8	612.3	-2175425.4
1-methoxy-4-carboxy-2,2,6,6-tetraethyl piperidine	60.5	-2278418.9	639.7	-2278609.6
PROXYL (**15**)	32.6	-1164742.1	426.7	-1164869.3
PROXYLH	32.5	-1166333.5	418.7	-1166458.3
PROXYL–CH_3	36.2	-1269302.7	450.0	-1269436.9
PROXYL–$CH(CH_3)Ph$	51.1	-1977285.2	575.8	-1977456.8
PROXYL–$CH(CH_3)COOCH_3$	50.8	-1969222.1	573.0	-1969392.9
PROXYL–$C(CH_3)_2COOCH_3$	54.4	-2072233.5	588.9	-2072409.1
PROXYL–$CH(CH_3)COOH$	46.5	-1866256.0	538.3	-1866416.5
PROXYL–$CH(CH_3)COONH_2$	47.6	-1814089.9	547.1	-1814253.0
3-amino-PROXYL (**16**)	35.7	-1309868.8	452.8	-1310003.8
3-amino-PROXYLH	35.9	-1311462.1	442.2	-1311593.9
3-amino-PROXYL–CH_3	39.6	-1414431.7	473.0	-1414572.7
3-methoxy-PROXYL (**17**)	38.9	-1464996.0	479.3	-1465138.9
3-methoxy-PROXYLH	39.6	-1466591.6	474.8	-1466733.1
3-methoxy-PROXYL–CH_3	43.3	-1569560.7	505.0	-1569711.3
3-hydroxy-PROXYL (**18**)	35.2	-1362033.4	449.5	-1362167.5
3-hydroxy-PROXYLH	35.7	-1363626.5	442.3	-1363758.4
3-hydroxy-PROXYL–CH_3	38.9	-1466599.4	468.4	-1466739.1
3-carboxy-PROXYL (**19**)	40.0	-1659297.8	498.0	-1659446.3
3-carboxy-PROXYLH	39.9	-1660892.2	483.4	-1661036.4
3-carboxy-PROXYL–CH_3	43.8	-1763861.4	514.6	-1764014.9
3,4-dicarboxy-PROXYL (**20**)	47.5	-2153642.8	557.4	-2153809.0
3,4-dicarboxy-PROXYLH	47.5	-2155025.3	546.5	-2155188.3
3,4-dicarboxy-PROXYL–CH_3	51.4	-2258208.3	577.2	-2258380.3
3-carboxy-2,2,5,5-tetraethylpyrrolidin-1-	54.1	-2070865.5	603.8	-2071045.5

lyoxyl (**21**)				
3-carboxy-2,2,5,5-tetraethylpyrrolidin-1-ol	54.0	-2072236.2	586.9	-2072411.2
1-methoxy-3-carboxy-2,2,5,5-tetraethyl pyrrolidine	57.9	-2175420.6	616.4	-2175604.4
TMIO (**27**)	38.8	-1564313.2	478.4	-1564455.8
TMIOH	38.7	-1565907.3	467.4	-1566046.6
TMIO–CH_3	42.6	-1668876.2	499.0	-1669025.0
TMIO–$CH(CH_3)Ph$	57.8	-2376599.1	631.2	-2376787.3
TMIO–$CH(CH_3)COOCH_3$	57.5	-2368533.9	624.8	-2368720.2
TMIO–$C(CH_3)_2COOCH_3$	60.7	-2471546.4	638.2	-2471736.7
TMIO–$CH(CH_3)COOH$	52.9	-2265567.8	587.6	-2265743.0
TMIO–$CH(CH_3)COONH_2$	53.9	-2213403.8	594.1	-2213580.9
5-amino-TMIO (**28**)	42.7	-1709365.6	508.8	-1709517.3
5-amino-TMIO–CH_3	46.7	-1813927.5	527.7	-1814084.8
5-methoxy-TMIO (**31**)	45.7	-1864392.0	537.6	-1864552.3
5-methoxy-TMIO–CH_3	49.6	-1968954.2	552.9	-1969119.0
5-hydroxy-TMIO (**33**)	42.0	-1761542.0	507.7	-1761693.4
5-hydroxy-TMIO–CH_3	45.9	-1866104.9	523.4	-1866260.9
5-carboxy-TMIO (**34**)	46.5	-2058662.2	548.9	-2058825.8
5-carboxy-TMIOH	46.3	-2060258.7	530.5	-2060416.9
5-carboxy-TMIO–CH_3	50.3	-2163228.0	563.1	-2163395.9
4-carboxy-TMIO (**35**)	45.7	-2058651.8	541.7	-2058813.3
4-carboxy-TMIO–CH_3	49.9	-2163214.7	557.0	-2163380.8
4,7-dicarboxy-TMIO (**36**)	52.7	-2552984.6	591.5	-2553160.9
4,7-dicarboxy-TMIO–CH_3	57.3	-2657548.2	615.0	-2657731.5
4,6-dicarboxy-TMIO (**37**)	53.7	-2552997.3	605.1	-2553177.8
4,6-dicarboxy-TMIO–CH_3	57.7	-2657562.4	620.5	-2657747.4
4,5-dicarboxy-TMIO (**38**)	53.7	-2552986.7	599.5	-2553165.4
4,5-dicarboxy-TMIO–CH_3	57.8	-2657554.9	618.9	-2657739.4
5,6-dicarboxy-TMIO (**39**)	54.4	-2552985.3	614.1	-2553168.5
5,6-dicarboxy-TMIOH	54.3	-2554584.3	596.4	-2554762.1
5,6-dicarboxy-TMIO–CH_3	58.3	-2657553.5	628.9	-2657741.0
TMAO (**47**)	43.9	-1966995.2	521.1	-1967150.6
TMAOH	44.2	-1968599.5	512.3	-1968752.3
TMAO–CH_3	47.9	-2071567.4	548.5	-2071730.9
4-carboxy-TMAO (**56**)	51.5	-2461313.3	577.2	-2461485.4
4-carboxy-TMAO–CH_3	55.2	-2565885.9	596.3	-2566063.7
5-carboxy-TMAO (**57**)	51.6	-2461346.3	581.6	-2461519.7
5-carboxy-TMAO–CH_3	55.6	-2565921.1	605.4	-2566101.6

6-carboxy-TMAO (**58**)	51.7	-2461331.3	591.3	-2461507.6
6-carboxy-TMAO–CH_3	55.5	-2565905.4	609.6	-2566087.2
TIPNO (**68**)	47.9	-1772812.9	558.9	-1772979.5
TIPNO–CH_3	52.0	-1877377.7	574.4	-1877548.9
SG1 (**69**)	67.3	-3171014.1	705.5	-3171224.5
SG1H	67.7	-3172609.3	694.6	-3172816.3
SG1–CH_3	71.3	-3275575.6	723.3	-3275791.3
DMINO (**70**)	30.2	-1358282.6	426.4	-1358409.7
DMINOH	30.6	-1359883.1	412.9	-1360006.2
DMINO–CH_3	34.5	-1462853.5	444.6	-1462986.1
2,2-diphenylindolin-1-yloxyl (**71**)	46.7	-2362640.5	565.4	-2362809.0
2,2-diphenylindolin-1-ol	47.2	-2364252.7	554.7	-2364418.0
1-methoxy-2,2-diphenylindoline	51.1	-2467218.3	583.2	-2467392.2
DPAIO (**72**)	61.6	-3109825.5	687.8	-3110030.6
DPAIOH	62.5	-3111433.2	683.6	-3111637.0

A.1.3 Data for Chapter 6

Table A.5 Contributions to the gas-phase enthalpies (0 K) of species in Chapter 6

Species	Sym.	E^o_{gas}(RMP2) (Hartrees)	E^o_{gas}(G3(MP2) -RAD) (Hartrees)	*ZPE* (Hartrees)	H^o_{gas} (Hartrees)
Scheme 6.2 (R'=CH_3)					
$(CH_3)_2NO$•	C_s	-209.31175	-209.47573	0.08281	-209.39292
TEMPO (**2**)	C_s	-482.68700	-483.12856	0.25821	-482.87034
•$CH(CH_3)_2$	C_s	-118.17367	-118.31386	0.08690	-118.22696
$(CH_3)_2NO–CH(CH_3)_2$	C_1	-327.58928	-327.88822	0.17813	-327.71008
TEMPO–$CH(CH_3)_2$	C_1	-600.95191	-601.53006	0.35390	-601.17616
•$OOCH(CH_3)_2$	C_1	-268.33654	-268.54778	0.09823	-268.44955
TS–Rxn (6.6) (R'=CH_3) core	C_1	-595.90065	-596.39223	0.27568	-596.11654
TS–Rxn (6.6) (R'=CH_3) full	C_1	-869.21683	-	0.45086	-869.25755
$(CH_3)_2N(•OCH(CH_3)_2)OOCH(CH_3)_2$	C_1	-595.90525	-596.41637	0.27524	-596.14113
TEMP(•$OCH(CH_3)_2$)$OOCH(CH_3)_2$ (***A***)	C_1	-869.26551	-	0.45006	-869.32657
TS–Rxn (6.7) (R'=CH_3) core	C_1	-595.85763	-596.38937	0.27651	-596.11286
TS–Rxn (6.7) (R'=CH_3) full	C_1	-869.22548	-	0.45218	-869.30505

$(CH_3)_2N^+(OCH(CH_3)_2)O^-$ $^{\bullet}OCH(CH_3)_2$	C_1	-595.94799	-596.44979	0.27604	-596.17375
$TEMP^+(OCH(CH_3)_2)O^-$ $^{\bullet}OCH(CH_3)_2$ (***B***)	C_1	-869.31288	-	0.45086	-869.36381
$(CH_3)_2CO$	C_{2v}	-192.76802	-192.92630	0.08244	-192.84386
$HOCH(CH_3)_2$	C_s	-193.96145	-194.13616	0.10640	-194.02976
TS–Rxn (6.9) (R'=CH_3) core	C_1	-595.93304	-596.43527	0.27230	-596.16298
TS–Rxn (6.9) (R'=CH_3) full	C_1	-869.29721	-	0.44632	-869.35312
$^{\bullet}OCH(CH_3)_2$	C_s	-193.27734	-193.45381	0.09266	-193.36115
$(CH_3)_2NO–OCH(CH_3)_2$	C_1	-402.62560	-402.95982	0.18068	-402.77914
$TEMPO–OCH(CH_3)_2$	C_1	-676.00427	-676.61006	0.35585	-676.25421
$(CH_3)_2N^+(OCH(CH_3)_2)O^-$	C_s	-402.66270	-402.98469	0.18198	-402.80271
$TEMP^+(OCH(CH_3)_2)O^-$	C_1	-676.02638	-676.62834	0.35756	-676.27078
TS–Rxn (6.13) (R'=CH_3)	C_s	-676.03014	-676.61471	0.35177	-676.26294
$(CH_3)_2NOH$	C_s	-209.93497	-210.10521	0.09461	-210.01060
TEMPOH	C_s	-483.30211	-483.75173	0.26984	-483.48190
PC–Rxn (6.14) (R'=CH_3) core	C_1	-328.11567	-328.42580	0.18329	-328.24251
PC–Rxn (6.14) (R'=CH_3) full	C_1	-601.48454	-	0.35821	-601.43645
TS–Rxn (6.14) (R'=CH_3) core	C_1	-328.10008	-328.40921	0.17933	-328.22987
TS–Rxn (6.14) (R'=CH_3) full	C_1	-601.47151	-	0.35474	-601.42589
PC–Rxn (6.15) (R'=CH_3) core	C_1	-403.22391	-403.57078	0.19019	-403.38060
PC–Rxn (6.15) (R'=CH_3) full	C_1	-676.59343	-	0.36492	-676.57538
TS–Rxn (6.15) (R'=CH_3) core	C_1	-403.21096	-403.55834	0.18683	-403.37151
TS–Rxn (6.15) (R'=CH_3) full	C_1	-676.58890	-	0.36263	-676.57366
PC–Rxn (6.16) (R'=CH_3) core	C_1	-478.27907	-478.66116	0.19445	-478.46672
PC–Rxn (6.16) (R'=CH_3) full	C_1	-751.64778	-	0.36931	-751.66056
TS–Rxn (6.16) (R'=CH_3) core	C_1	-478.25018	-478.64051	0.18997	-478.45054
TS–Rxn (6.16) (R'=CH_3) full	C_1	-751.62512	-	0.36572	-751.64974
$HCH(CH_3)_2$	C_{2v}	-118.83878	-118.98479	0.10210	-118.88269
$HOOCH(CH_3)_2$	C_1	-268.98601	-269.19472	0.10964	-269.08508
Scheme 6.2 (R'=$OCOCH_3$)					
$^{\bullet}CH(CH_3)OCOCH_3$	C_1	-306.46217	-306.68555	0.10194	-306.58361
$(CH_3)_2NO–CH_2OCOH$	C_1	-437.42464	-437.72120	0.13777	-437.58343
$(CH_3)_2NO–CH(CH_3)OCOCH_3$	C_1	-515.88368	-516.26592	0.19231	-516.07362
$TEMPO–CH(CH_3)OCOCH_3$	C_1	-789.24953	-	0.36754	-789.26423
$^{\bullet}OOCH_2OCOH$	C_1	-378.16403	-378.37214	0.05778	-378.31436
$^{\bullet}OOCH(CH_3)OCOCH_3$	C_1	-456.62360	-456.91774	0.11216	-456.80559
TS–Rxn (6.6) (R'=$OCOCH_3$) core	C_1	-815.57490	-816.06117	0.19519	-815.86598

TS–Rxn (6.6) (R'=$OCOCH_3$) full	C_1	-1245.85221	-	0.47950	-1245.85898
$(CH_3)_2N(^{\bullet}OCH(CH_3)OCOCH_3)$ $OOCH(CH_3)OCOCH_3$	C_1	-815.59969	-816.09809	0.19273	-815.90535
TEMP($^{\bullet}OCH(CH_3)OCOCH_3$)O $OCH(CH_3)OCOCH_3$ (***A***)	C_1	-1245.89282	-	0.47673	-1245.91448
TS–Rxn (6.7) (R'=$OCOCH_3$) core	C_1	-815.52695	-816.05660	0.19611	-815.86049
TS–Rxn (6.7) (R'=$OCOCH_3$) full	C_1	-1245.81192	-	0.48051	-1245.86106
$(CH_3)_2N^+(OCH(CH_3)OCOCH_3)$ $O^{-\bullet}OCH(CH_3)OCOCH_3$	C_1	-815.59969	-816.09809	0.19273	-815.90535
$TEMP^+(OCH(CH_3)OCOCH_3)O$ $^{-\bullet}OCH(CH_3)OCOCH_3$ (***B***)	C_1	-1245.91798	-	0.47935	-1245.93702
H(OCOH)CO	C_s	-302.60639	-302.76088	0.04231	-302.71857
$(CH_3)(OCOCH_3)CO$	C_1	-381.06431	-381.30460	0.09723	-381.20737
$HOCH_2(OCOH)$	C_1	-303.80357	-303.97498	0.06704	-303.90794
$HOCH(CH_3)(OCOCH_3)$	C_1	-382.26239	-382.51989	0.12146	-382.39842
TS–Rxn (6.9) (R'=$OCOCH_3$) core	C_1	-815.60767	-816.10376	0.18987	-815.91388
TS–Rxn (6.9) (R'=$OCOCH_3$) full	C_1	-1245.89225	-	0.47440	-1245.91393
$\bullet OCH_2OCOH$	C_1	-303.11529	-303.28877	0.05178	-303.23699
$\bullet OCH(CH_3)OCOCH_3$	C_1	-381.57224	-381.83216	0.10692	-381.72524
$(CH_3)_2NO–OCH_2OCOH$	C_1	-512.46777	-512.79473	0.13987	-512.65487
$(CH_3)_2NO–$ $OCH(CH_3)OCOCH_3$	C_1	-590.92477	-591.30932	0.19452	-591.11480
$TEMPO–OCH(CH_3)OCOCH_3$	C_1	-864.30755	-	0.36977	-864.26475
$(CH_3)_2N^+(OCH_2OCOH)O^-$	C_1	-512.50601	-512.82403	0.14158	-512.68245
$(CH_3)_2N^+(OCH(CH_3)OCOCH_3)$ O^-	C_1	-590.96242	-591.36612	0.19613	-591.16999
$TEMP^+(OCH(CH_3)OCOCH_3)$ O^-	C_1	-864.33258	-	0.37089	-864.27972
TS–Rxn (6.13) (R'=$OCOCH_3$) core	C_1	-591.32462	-591.73896	0.20950	-591.52946
TS–Rxn (6.13) (R'=$OCOCH_3$) full	C_1	-864.70056	-	0.38397	-864.73092
PC–Rxn (6.14) (R'=$OCOCH_3$) core	C_1	-516.40782	-516.80112	0.19827	-516.60285
PC–Rxn (6.14) (R'=$OCOCH_3$) full	C_1	-789.77608	-	0.37339	-789.79600
TS–Rxn (6.14) (R'=$OCOCH_3$) core	C_1	-516.39170	-516.78433	0.19454	-516.58980
TS–Rxn (6.14) (R'=$OCOCH_3$)	C_1	-789.76173	-	0.36927	-789.78508

full					
PC–Rxn (6.16) (R'=$OCOCH_3$) core	C_1	-666.56976	-667.03480	0.20856	-666.82624
PC–Rxn (6.16) (R'=$OCOCH_3$) full	C_1	-939.93569	-	0.38315	-940.01759
TS–Rxn (6.16) (R'=$OCOCH_3$) core	C_1	-666.54440	-667.01624	0.20549	-666.81075
TS–Rxn (6.16) (R'=$OCOCH_3$) full	C_1	-939.92277	-	0.38093	-940.01368
$HCH(CH_3)OCOCH_3$	C_s	-307.12645	-307.35567	0.11655	-307.23912
$HOOCH(CH_3)OCOCH_3$	C_1	-457.28093	-457.57266	0.12461	-457.44806
Scheme 6.3 (R'=CH_3)					
$(CH_3)_2NO–OOCH(CH_3)_2$	C_1	-477.66489	-478.02985	0.18403	-477.84582
$TEMPO–OOCH(CH_3)_2$	C_1	-751.04482	-751.68384	0.35927	-751.32458
$(CH_3)_2NOO^{\bullet}$	C_1	-284.31131	-284.52059	0.08573	-284.43486
$TEMPOO^{\bullet}$	C_s	-557.68110	-558.16767	0.26086	-557.90681
O_2	D_h	-150.12649	-150.18748	0.00371	-150.18377
$(CH_3)_2N^{\bullet}$	C_{2v}	-134.19903	-134.33625	0.07606	-134.26019
$TEMP^{\bullet}$	C_s	-407.56526	-407.98287	0.25248	-407.73038
$(CH_3)_2NO–OO–ONC(CH_3)_2$	C_2	-568.70647	-569.09059	0.17450	-568.91609
TEMPO–OO–(TEMPO)	C_2	-1115.47522	-	0.52536	-1115.33397
$(CH_3)_2NO–OOOCH(CH_3)_2$	C_1	-552.73016	-553.11901	0.18691	-552.93210
$TEMPO–OOOCH(CH_3)_2$	C_1	-826.09157	-	0.36275	-826.11768
TEMPH	C_s	-408.23015	-408.64883	0.26608	-408.38275
$(CH_3)_2N(OO)OCH(CH_3)_2$	C_s	-477.64696	-478.00485	0.18274	-477.82210
$TEMP(OO)OCH(CH_3)_2$ (***C***)	C_1	-751.00241	-	0.35959	-751.00070
Scheme 6.3 (R'=$OCOCH_3$)					
$(CH_3)_2NO–OOCH(CH_3)OCOCH_3$	C_1	-665.96042	-666.40737	0.19832	-666.20905
$TEMPO–OOCH(CH_3)OCOCH_3$	C_1	-939.33976	-	0.37346	-939.41325
$(CH_3)_2NO–OOOCH(CH_3)OCOCH_3$	C_1	-741.03138	-741.50319	0.20090	-741.30229
$TEMPO–OOOCH(CH_3)OCOCH_3$	C_1	-1014.38577	-	0.37647	-1014.48112
$(CH_3)_2N(OO)OCH(CH_3)OCOCH_3$	C_1	-477.64696	-478.08015	0.19756	-477.88259
$TEMP(OO)OCH(CH_3)OCOCH_3$ (***C***)	C_1	-939.30193	-	0.37354	-939.36157
Scheme 6.4 (R'=CH_3)					
$^{-}OOCH(CH_3)_2$	C_s	-268.38123	-268.58825	0.09609	-268.49215

$(CH_3)_2NO^+$	C_2	-209.04178	-209.19869	0.08347	-209.11523
TEMPO+	C_s	-482.43972	-482.87570	0.25948	-482.61623
TS–Rxn (6.29) (R'=CH_3) core	C_1	-671.61960	-672.15454	0.28768	-671.86685
TS–Rxn (6.29) (R'=CH_3) full	C_1	-944.98794	-	0.46342	-945.05946
TS–Rxn (6.30) (R'=CH_3) core	C_1	-671.63601	-672.13820	0.28243	-671.85577
TS–Rxn (6.30) (R'=CH_3) full	C_1	-944.99962	-	0.45899	-945.04282
$TEMP^+(OCH(CH_3)_2)OH$	C_1	-676.39842	-677.00979	0.37006	-676.63973
Scheme 6.4 (R'=$OCOCH_3$)					
$^-OOCH(CH_3)OCOCH_3$	C_1	-456.70968	-456.99481	0.11067	-456.88413
TS–Rxn (6.29) (R'=$OCOCH_3$) core	C_1	-891.30200	-891.83051	0.20652	-891.62399
TS–Rxn (6.29) (R'=$OCOCH_3$) full	C_1	-1321.59642	-	0.49340	-1321.63154
TS–Rxn (6.30) (R'=$OCOCH_3$) core	C_1	-891.28714	-891.78594	0.20064	-891.58530
TS–Rxn (6.30) (R'=$OCOCH_3$) full	C_1	-1321.60055	-	0.48625	-1321.61310
$(CH_3)_2N^+(OCH(CH_3)OCOCH_3)OH$	C_1	-590.96136	-591.35146	0.19024	-591.16122
$TEMP^+(OCH(CH_3)OCOCH_3)OH$	C_1	-864.33267	-	0.36578	-864.35698

Table A.6 Contributions to the gas and solution-phase free energies (298 K) of species in Chapter 6

Species	T_c (kJ mol^{-1})	H_{gas} ($kJmol^{-1}$)	S_{gas} ($Jmol^{-1}K^{-1}$)	G_{gas} ($kJmol^{-1}$)	ΔG_{solv} (water) ($kJmol^{-1}$)
Scheme 6.2 (R'=CH_3)					
TEMPO (**2**)	34.1	-1267742.0	437.7	-1267872.5	-
$^{\bullet}CH(CH_3)_2$	15.9	-310388.9	292.4	-310476.1	-
TEMPO–$CH(CH_3)_2$	44.3	-1578343.7	506.1	-1578494.6	-
$^{\bullet}OOCH(CH_3)_2$	18.8	-704795.5	326.4	-704892.8	-
TS–Rxn (6.6) (R'=CH_3) full system	64.4	-2282171.3	663.2	-2282369.0	-
$TEMP(^{\bullet}OCH(CH_3)_2)OOCH(CH_3)_2$ (***A***)	67.9	-2282349.0	737.1	-2282568.7	-
TS–Rxn (6.7) (R'=CH_3) full system	63.1	-2282297.3	654.8	-2282492.5	-
$TEMP^+(OCH(CH_3)_2)O^{-\bullet}OCH(CH_3)_2$ (***B***)	67.0	-2282447.7	701.7	-2282656.9	-
$(CH_3)_2CO$	16.7	-506294.8	302.3	-506385.0	-14.0
$HOCH(CH_3)_2$	16.7	-509408.4	297.1	-509497.0	-
TS–Rxn (6.9) (R'=CH_3) full system	65.5	-2282421.1	679.9	-2282623.8	-

$^{\bullet}OCH(CH_3)_2$	16.1	-507653.6	299.8	-507743.0	-
$TEMPO–OCH(CH_3)_2$	49.2	-1775456.3	550.5	-1775620.4	-
$TEMP^{+}(OCH(CH_3)_2)O^{-}$	48.0	-1775500.9	532.9	-1775659.8	-
TS–Rxn (6.13) (R'=CH_3)	47.7	-1775480.7	532.6	-1775639.4	-
TEMPOH	34.5	-1269347.3	429.5	-1269475.3	-14.1
PC–Rxn (6.14) (R'=CH_3) full system	52.2	-1579019.2	600.5	-1579198.3	-
TS–Rxn (6.14) (R'=CH_3) full system	48.7	-1578995.0	557.4	-1579161.2	-
PC–Rxn (6.15) (R'=CH_3) full system	52.3	-1776296.3	592.9	-1776473.1	-
TS–Rxn (6.15) (R'=CH_3) full system	51.1	-1776293.1	585.3	-1776467.6	-
PC–Rxn (6.16) (R'=CH_3) full system	56.0	-1973428.8	642.2	-1973620.3	-
TS–Rxn (6.16) (R'=CH_3) full system	53.1	-1973403.2	594.7	-1973580.6	-
$HCH(CH_3)_2$	14.4	-312112.1	268.4	-312192.1	-
$HOOCH(CH_3)_2$	20.0	-706462.8	327.0	-706560.3	-28.9
Scheme 6.2 (R'=$OCOCH_3$)					
$^{\bullet}CH(CH_3)OCOCH_3$	22.7	-804912.6	365.8	-805021.6	-
$TEMPO–CH(CH_3)OCOCH_3$	52.8	-2072160.4	585.3	-2072334.9	-
$^{\bullet}OOCH(CH_3)OCOCH_3$	26.5	-1199316.5	402.5	-1199436.5	-
TS–Rxn (6.6) (R'=$OCOCH_3$) full system	79.8	-3270922.9	797.7	-3271160.8	-
$TEMP(^{\bullet}OCH(CH_3)OCOCH_3)OOCH(CH_3)OCOCH_3$ (***A***)	85.6	-3271062.8	887.3	-3271327.4	-
TS–Rxn (6.7) (R'=$OCOCH_3$) full system	79.0	-3270929.2	788.1	-3271164.2	-
$TEMP^{+}(OCH(CH_3)OCOCH_3)O^{-}$ $^{\bullet}OCH(CH_3)OCOCH_3$ (***B***)	82.5	-3271125.2	844.0	-3271376.8	-
$(CH_3)(OCOCH_3)CO$	23.4	-1000836.6	371.5	-1000947.3	-17.6
$HOCH(CH_3)(OCOCH_3)$	23.5	-1003963.6	365.5	-1004072.5	-
TS–Rxn (6.9) (R'=$OCOCH_3$) full system	80.8	-3271066.2	794.9	-3271303.2	-
$\bullet OCH(CH_3)OCOCH_3$	23.8	-1002195.8	380.5	-1002309.3	-
$TEMPO–OCH(CH_3)OCOCH_3$	57.5	-2269069.6	628.7	-2269257.0	-
$TEMP^{+}(OCH(CH_3)OCOCH_3)O^{-}$	56.4	-2269110.0	608.9	-2269291.6	-
TS–Rxn (6.13) (R'=$OCOCH_3$) full system	55.1	-2270296.0	588.3	-2270471.4	-152.3
PC–Rxn (6.14) (R'=$OCOCH_3$) full system	58.8	-2073550.5	649.2	-2073744.1	-
TS–Rxn (6.14) (R'=$OCOCH_3$) full system	56.3	-2073524.4	623.7	-2073710.4	-
PC–Rxn (6.16) (R'=$OCOCH_3$) full system	63.7	-2467952.4	710.5	-2468164.2	-
TS–Rxn (6.16) (R'=$OCOCH_3$) full system	61.0	-2467944.9	667.6	-2468143.9	-
$HCH(CH_3)OCOCH_3$	21.9	-806634.4	354.7	-806740.2	-

$HOOCH(CH_3)OCOCH_3$	26.3	-1201003.6	390.5	-1201120.0	-24.4
Scheme 6.3 (R'=CH_3)					
$TEMPO–OOCH(CH_3)_2$	52.6	-1972550.1	587.1	-1972725.1	0.0
$TEMPOO^{\bullet}$	37.2	-1464747.1	465.0	-1464885.7	-
O_2	8.7	-394298.8	205.1	-394359.9	-
$TEMP^{\bullet}$	32.1	-1070464.0	422.7	-1070590.1	-
TEMPO–OO–(TEMPO)	75.2	-2928234.2	746.7	-2928456.8	-
$TEMPO–OOOCH(CH_3)_2$	55.3	-2168916.6	600.8	-2169095.8	-
TEMPH	31.6	-1072177.3	411.1	-1072299.8	-
$TEMP(OO)OCH(CH_3)_2$ (***C***)	52.6	-1971699.7	564.6	-1971868.1	-
Scheme 6.3 (R'=$OCOCH_3$)					
$TEMPO–OOCH(CH_3)OCOCH_3$	60.4	-2466369.1	649.8	-2466562.8	-3.6
$TEMPO–OOOCH(CH_3)OCOCH_3$	63.7	-2663456.5	679.0	-2663658.9	-
$TEMP(OO)OCH(CH_3)OCOCH_3$ (***C***)	61.0	-2466232.9	643.7	-2466424.8	-
Scheme 6.4 (R'=CH_3)					
$^{-}OOCH(CH_3)_2$	18.4	-704907.8	314.7	-705001.6	-298.2
TEMPO+	34.0	-1267074.9	432.0	-1267203.7	-184.9
TS–Rxn (6.29) (R'=CH_3) full system	68.9	-2481184.7	710.4	-2481396.5	-
TS–Rxn (6.30) (R'=CH_3) full system	70.9	-2481139.0	735.4	-2481358.3	-
$TEMP^{+}(OCH(CH_3)_2)OH$	48.3	-1776469.3	530.4	-1776627.5	-170.6
Scheme 6.4 (R'=$OCOCH_3$)					
$^{-}OOCH(CH_3)OCOCH_3$	24.2	-1199525.1	367.8	-1199634.7	-289.7
TS–Rxn (6.29) (R'=$OCOCH_3$) full system	83.5	-3469860.1	825.3	-3470106.1	-
TS–Rxn (6.30) (R'=$OCOCH_3$) full system	85.8	-3469809.4	851.1	-3470063.2	-
$TEMP^{+}(OCH(CH_3)OCOCH_3)OH$	55.6	-2269313.7	602.6	-2269493.4	-

A.2 GAUSSIAN archive files

GAUSSIAN archive files containing the B3-LYP/6-31G(d) geometries of principle species in Chapters 4 to 6 are not included in the printed material. Chapters A.2.1, A.2.2 and A.2.3 are available as .pdf files on the accompanying CD-ROM found inside the back cover of this thesis.